UNIVERSITY OF SOUTHAMPTON

FACULTY OF PHYSICAL AND APPLIED SCIENCES

Electronics and Computer Science

Textile Electrode Design and Simulation for Bio-signal Recording

By Zihao Li

Thesis for the degree of Doctor of Philosophy

18 October 2018

ABSTRACT

This thesis describes a skin and skin-electrode model to simulate bio-signal measurements under different conditions targeting human bio-potential measurements. From reviewing different electrode designs, it is clear that the impedance between the skin and an electrode has a significant effect. The skin-electrode impedance is frequently used as a standard to estimate the performance of an electrode in electrode research. During measurements, the impedance of the skin-electrode interface forms a potential divider which reduces the input signal. Hence it is necessary to identify the effect of the skin-electrode impedance. In this thesis, a skin and electrode model was built using COMSOL simulation; and the effect of the skin and external conditions was analysed.

The skin-electrode model here was different from traditional skin electrode circuit models in the way that the different skin layer properties were included as parameters. With these skin parameters, the key factors in the skin-electrode model can be established and optimised. In addition, the relationship between different electrode sizes and the skin-electrode impedance was quantified using this skin-electrode model.

In this skin-electrode model, the skin and electrode have their own significant parameters that affect the total skin-electrode impedance. For the skin, it was found that the dielectric constant of the skin layer is the most significant parameter in determining the total skin-electrode impedance; the skin-electrode impedance difference resulting from the highest and lowest dielectric constant from the literature of the stratum corneum in the skin is over 90 %. For the electrode, when the electrode size was increased from 0.5 cm^2 to 2 cm^2, the skin-electrode impedance was reduced by about 60 %; and when the electrode size was increased from 2 cm^2 to 3 cm^2, the reduction was approximately 13 %. Hence the optimized or efficient electrode size is located between 1.5 cm^2 to 2 cm^2.

Furthermore, a textile electrode implemented by screen printing was selected to test the performance of the skin-electrode model. The electronic textile is a technology which provides a flexible and comfortable platform for sensors and other electronics. If textile electrodes can be shown to provide satisfactory performance, then they may provide an attractive alternative to other more conventional electrodes. For the textile electrode, the electrode is made using two different materials - silver and silicone carbon rubber. Both electrodes have shown that the most efficient electrode size is around 2 cm^2. Moreover, the textile silicone carbon electrode provides an adhesive and soft electrode surface without the need for gel, this reduces the movement between the adhesive and soft surface during measurements and hence results in less impedance noise than a silver textile electrode. Meanwhile, both electrode materials were simulated in the skin-electrode model with the limitations of the skin-electrode model having been identified.

Table of Contents

List of Tables

List of Figures

DECLARATION OF AUTHORSHIP

I, Zihao Li

declare that this thesis and the work presented in it are my own and has been generated by me as the result of my own original research.

Textile Electrode Design and Simulation for Bio-signal Recording

I confirm that:

1. This work was done wholly or mainly while in candidature for a research degree at this University;
2. Where any part of this thesis has previously been submitted for a degree or any other qualification at this University or any other institution, this has been clearly stated;
3. Where I have consulted the published work of others, this is always clearly attributed;
4. Where I have quoted from the work of others, the source is always given. With the exception of such quotations, this thesis is entirely my own work;
5. I have acknowledged all main sources of help;
6. Where the thesis is based on work done by myself jointly with others, I have made clear exactly what was done by others and what I have contributed myself;
7. Parts of this work have been published as:

   Z. Li, R. Torah and J. Tudor, "Modelling the Effects of the Electrode Size and Skin Properties in Bio-Potential Monitoring" in *26th Micromechanics and Microsystems Europe Workshop, Toledo, Spain*, 09/2015

Signed: .....

Date: .....

Acknowledgements

Firstly, I would like to express my gratitude to my supervisors Dr John Tudor and Dr Russel Torah for their supervision and support during my Ph.D. study. Both of them have given me a lot of helps on academic supports and university life.

I would also like to thank all students and staffs in Bay 4 and 5. They have not only supported and encouraged me in my studies but have also made my Ph.D. an incredibly enjoyable experience. I wish to thanks the support from University of Southampton and School of Electronic and Computer Science (ECS), allowing this research to be conducted.

Thanks also to the staffs in the clean room and PEM lab. They have provided the best technical support and training over the past couple of years.

Finally, I would like to thanks to my parents, my girlfriend and the rest of my families. My parents give me this opportunity to study in UK. Meanwhile, without the support from my girlfriend, I cannot finish my Ph.D. study. Thanks for their understanding.

Abbreviations

A/D	Analogue to Digital
AC	Alternating Current
Ag	Silver
AgCl	Silver Chloride
Au	Gold
CMRR	Common Mode Rejection Ratio
DRL	Driven Right Leg
ECG	Electrocardiography
EEG	Electroencephalogram
EMG	Electromyography
FEA	Finite Element Analysis
HYP	Hypodermis and Fat
MEMS	Microelectromechanical Systems
Ni	Nickel
PCB	Printed Circuit Board
PDMS	Polydimethylsiloxane
RC	Resistor-Capacitor
SC	Stratum Corneum
SMD	Surface Mount Devices

Chapter 1: Introduction

1.1 Introduction

Bioelectricity is a broad concept, covering the electric currents associated with life processes, and their bio-potentials. Many applications which record human bio-signals are well known, such as the recording of the bio-signal from the heart (using an ECG) which was introduced by Waller in 1887 (Grimnes and Grottem, 2000). In the field of bioelectricity, researchers and scientists aim to discover information regarding the human body. As more data and information is compiled, the physical condition of the human body can be more easily evaluated. Many body potentials (or bio-signals) are recorded by an electrode based recording system. In hospitals, doctors can know more about their patients and tailor their care accordingly using this information. To measure different bio signals, the electrodes are placed on different parts of the body. The design and manufacturing of the electrode can improve the quality of the bio signals.

However, there is no established method to accurately predict electrode performance before an electrode is made, where most methods consider the skin as a whole part, with the details of the skin being ignored. Most previous research has used equivalent circuits to evaluate the performance of a new electrode or compare it with standard commercial electrodes. If it were possible to simulate or build a model of an electrode before it is implemented, this would lead to considerable savings in time and money.

This chapter introduces the objectives and aims of this research where are related to electrode modelling and the printable electrode. It also describes the research background and the structure of the thesis.

1.2 Aims and scope of the thesis

The aim of this research was to simulate and create a model for different electrodes. Such a model could then be used to develop and implement new electrodes for textile use. Using this new model, the objectives of this research were to:

- Investigate the effects of different skin layers and find the key layers for skin-electrode impedance
- Evaluate and weigh the key properties for the skin layers
- Find the optimal materials and geometries for the relevant electrodes. The optimal geometry of electrode means that the electrode could be used to improve signal quality and reduce the cost of the electrode materials and development.
- Identify the limitations of Finite Element (FE) model when simulating bio-information

1.3 Methodology

This study adopted a quantitative methodology which stresses the mathematical analysis of data collected by experiments (Neuman, 1999). The quantitative methodology was chosen because it has the following advantages:

1. It strives for objective, replicable, and generalizable knowledge.
2. It can manipulate independent variables while controlling for other variables.

In order to simulate and create a model for the skin and electrode, an experimental design based on finite element simulation and printing electrodes was adopted in this thesis. This study was first conducted using software to create a model for simulating the skin and electrode details. The model was used to investigate the effects from the properties of skin and electrode and then identify the key parameters for all the skin layers. After creating the model, a printed silver electrode and silicone-carbon electrode were implemented and experiments used to test the limitations of the model. To test the performance of the model, the research was divided into two parts.

The first part of the project sought to analyse existing electrodes and a model of the skin. These electrodes included conventional gel wet electrodes, dry electrodes and non-contact electrodes. Both dry and non-contact electrodes were applied as foam electrodes or capacitively coupled electrodes in a laboratory environment. There were several standards and growing theories to support them, such as for the effects of clothes and hair. The analysis of the three kinds of electrodes demonstrate the possible directions and methodology for building a model. From this model, the aim was to identify the key parameters for the skin and electrode to affect the skin-electrode impedance.

The second part of the research focused on implementing textile electrodes to test the performance of the model and identify any shortcomings. Because the modelling of the skin and electrodes was based on the parameters of the materials and geometries, it was easy to replace these with new materials and geometries as desired. Some new designs for the electrodes were also tested at this stage. Based on these tests of the new electrodes, the limitations and performance of this skin-electrode model could be identified.

1.4 Statement of novelty

From the reviews about the relevant papers, there is little research between the physical modelling and the skin's structure. Therefore, the study of this thesis bridges the gap between previous researches. The novelty of this report is listed below:

- A model to simulate the physical structure for the skin-electrode interface.
- Evaluation of the effects of skin and electrode properties from the modelling and physical design.
- Implementation of the effect of the skin and electrode properties from simulation and confirmation with the practical designs
- Using the simulation to find the key layers for the skin and the key factors for electrode design.

- Uses a simulation of the skin-electrode model to confirm the effects of the skin and electrode properties on the electrical characteristics
- Provides an optimised formulation of adhesive carbon silicone rubber for dry electrodes
- Undertakes a comparison of textile electrode fabrication between modelling and an experiment device

Publications from this work (Li, R.Torah and Tudor, 2015):

- Z. Li, R. Torah and J. Tudor, 'Modelling the Effects of the Electrode Size and Skin Properties in Bio-Potential Monitoring' in *26th Micromechanics and Microsystems Europe Workshop, Toledo, Spain*, 09/2015.

Planned publication:

- 'A Finite Element Model to determine the Influence of Electrode Design and Skin layers on skin impedance analysis', *PLOS One.*

1.5 Structure of the thesis

This thesis is split into 6 chapters, which includes this introduction, a review of different electrodes, electrode modelling, electrode implementation and a comparison between the model and experimental results. These chapters are summarized as follows:

Chapter 1 provides the introduction to this study and its objectives.

Chapter 2 is the literature review and gives an overview of different types of electrodes in terms of their various functions and implementations. Furthermore, the interference in measurement is reviewed for different types of electrodes with the main sources of interference being identified. Moreover, the skin details and skin-electrode impedance are reviewed using different measuring and simulation methods to evaluate their effects in bio-signal measurement.

Chapter 3 presents the skin-electrode model, where the skin is described in detail and analysed in separate layers. The 2D and 3D simulations were implemented using COMSOL to identify the effects of different outside conditions such as the force applied on the electrode, the thickness of skin, and the geometries and materials of the electrodes.

Chapter 4 describes the fabrication of two electrodes on textiles. The structure of the electrode and the fabrication process are discussed in order to fabricate the silver electrodes on textiles. The differences between the simulated and measured silver electrode are discussed.

Chapter 5 presents a paste that is used to fabricate soft dry electrodes on textiles. The optimal recipe for the paste and fabrication process are discussed. Furthermore, the performance of this electrode which was tested under different conditions to identify its limitations is described. The differences between the simulated and measured soft dry electrodes on textiles are used to demonstrate the performance of the simulation.

Chapter 1

Chapter 6 is the conclusion for this thesis, it gives the overall conclusions from the results and provides a discussion of future work.

Chapter 2: Literature review: Electronic textile based bio-signal recording systems and skin-electrode impedance analysis

2.1 Introduction

A bio-signal recording system should be designed to suit different amplitude ranges, such as the brain signal which has an amplitude from 5 to 400 μV or a heart-pulse signal being from 0.5 to 4 mV. For these different amplitude ranges, the system needs to use different approaches against the noise. The heart-pulse signal, for instance, contains part of the muscle signal when the system is applied to the body. In this way, different designs regarding filtering circuits are applied to different setups. Furthermore, in all recording systems, bio-signals are detected by an electrode. This section focuses on electrodes.

A shown in Figure 2-1, electrodes are described according to their different electrode properties. They can be divided into three categories: conventional (wet) electrodes, dry electrodes, and non-contact electrode. For the wet and dry electrodes, these do not contain any electronic components and are used directly on the skin. When the wet electrode is applied to the patient, conductive gel or solution is applied to the electrode. For the non-contact electrode, the electrode contains some electronic components in the electrode and there is a medium between the electrode and skin. In addition, if an electrode does not contain any electronic components, it is known as a passive electrode. Meanwhile, if the electrode contains some electronic components, it is known as an active electrode.

Depending on the electrode implementation, some electrodes are made on the textile, these are called textile electrodes. The textile electrode types can be classified according to Figure 2-2. In Figure 2-2, the textile electrode can be a wet, dry, or a non-contact electrode. The wet electrode transmits signals using a passive method, the dry electrode is both passive and active, whilst the non-contact electrode must transmit signals using the active method.

In some biomedical papers, non-contact and dry electrodes are both called ‘dry’ electrodes, but the two categories are much more clearly defined in engineering papers. Dry contact electrodes come into contact with the skin surface directly and so cannot measure a signal through clothes. Non-contact electrodes are still dry electrodes but can measure a signal through clothes with a typical separation from the body of around 1.27cm (half an inch) (Chi, Jung and Cauwenberghs, 2010).

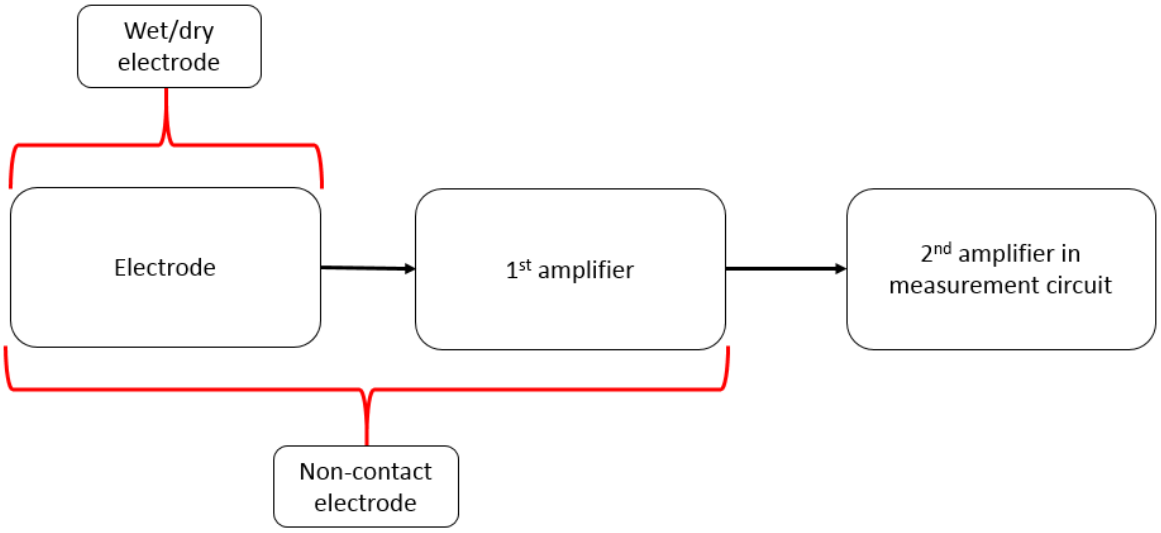

Figure 2-1: Bio-signal recording system and classification for different electrodes.

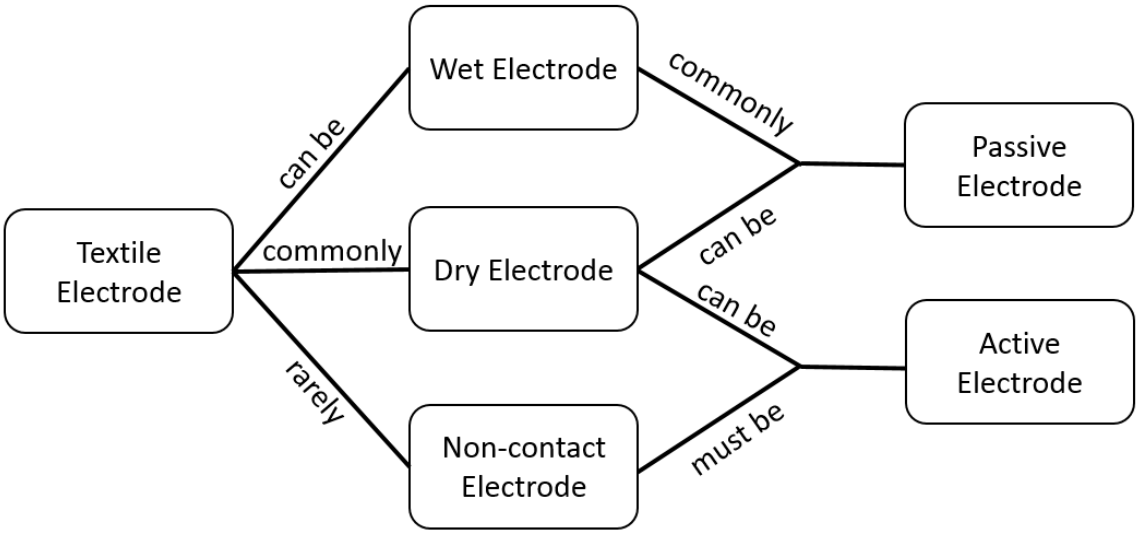

Figure 2-2: Electrode classifications for different usages and applications.

2.2 Bio-potential signal and electrode analysis

Before the detection electrode is introduced further, it is necessary to consider the difference between the different bio-signal sources. Body potential (or bio-signals) can be classified in terms of the different signal types:

- Electroneurogram (ENG): nerve bundle potentials
- Electroretinogram (ERG): retina potentials
- Electrooculogram (EOG): potentials generated by the retina to light stimulus
- Electrogastrogram (EGG): stomach muscle potentials
- Electrocardiography (ECG): bio-signals from the heart pulse
- Electromyography (EMG): signals generated by the muscles
- Electroencephalogram (EEG): potential differences generated by neurons in the brain

Depending on the type of signal, different measurement methods are required. EEG, ECG, EMG, EOG and EGG signals can be directly recorded from the human body using surface electrodes placed in different positions on the body. For instance, the EEG is used for the measurement of brain potentials, and thus, the detecting electrode is placed on the head. All of these electrode measurement methods pick up signals from the skin. On the other hand, ENG and ERG rely on other methods to detect signals. ENG examines the potential differences in nerve bundles, and thus the electrode is a needle. ERG examines retina potentials, and so this electrode is an implanted electrode. ENG also requires detectors to be inserted into the body. This limits the development of ENG and ERG. However, other electrodes have been more widely developed for the purpose of medical and electronic applications or skin surface potential recording (Chi, Jung and Cauwenberghs, 2010). EEG, EMG and ECG continue to be developed for health and clinical applications and this has been the case for several decades (Lymberis *et al.*, 2003; Liao *et al.*, 2012).

Regarding these aforementioned bio-signals, different signals have different frequency ranges, as shown in Table 2-1 and drawn in Figure 2-3. It can be clearly seen that the range of each signal varies in terms of frequency and amplitude. These signals also take different forms depending on a person's movements. For example, the bio-signals will be different depending on whether a person is running or sitting down. The different frequency ranges and amplitudes of the different bio-signals are shown in Figure 2-3.

Bio-signals	**Frequency Range**	**Amplitude**
Electroneurogram (ENG)	0-10000 Hz	0.01- 3mV
Electretonogram (ERG)	0.2-200 Hz	0-900 μV
Electrooculogram (EOG)	0-100 Hz	50-3500 μV
Electrogastrogram (EGG)	0-1 Hz	10-1000 μV
Electrocardiogram (ECG)	0.1-250 Hz	0.5-4 mV
Electromyography (EMG)	0-10000 Hz	0.1-5 mV
Electroeencephalogram (EEG)	δ Waves: 0.5-4 Hz	5-300 μV
	Θ Waves: 4-7.5 Hz	
	α Waves: 7.5-13 Hz	
	β Waves: 13-38 Hz	

Table 2-1: Signal frequencies and amplitudes (Webster, 2006).

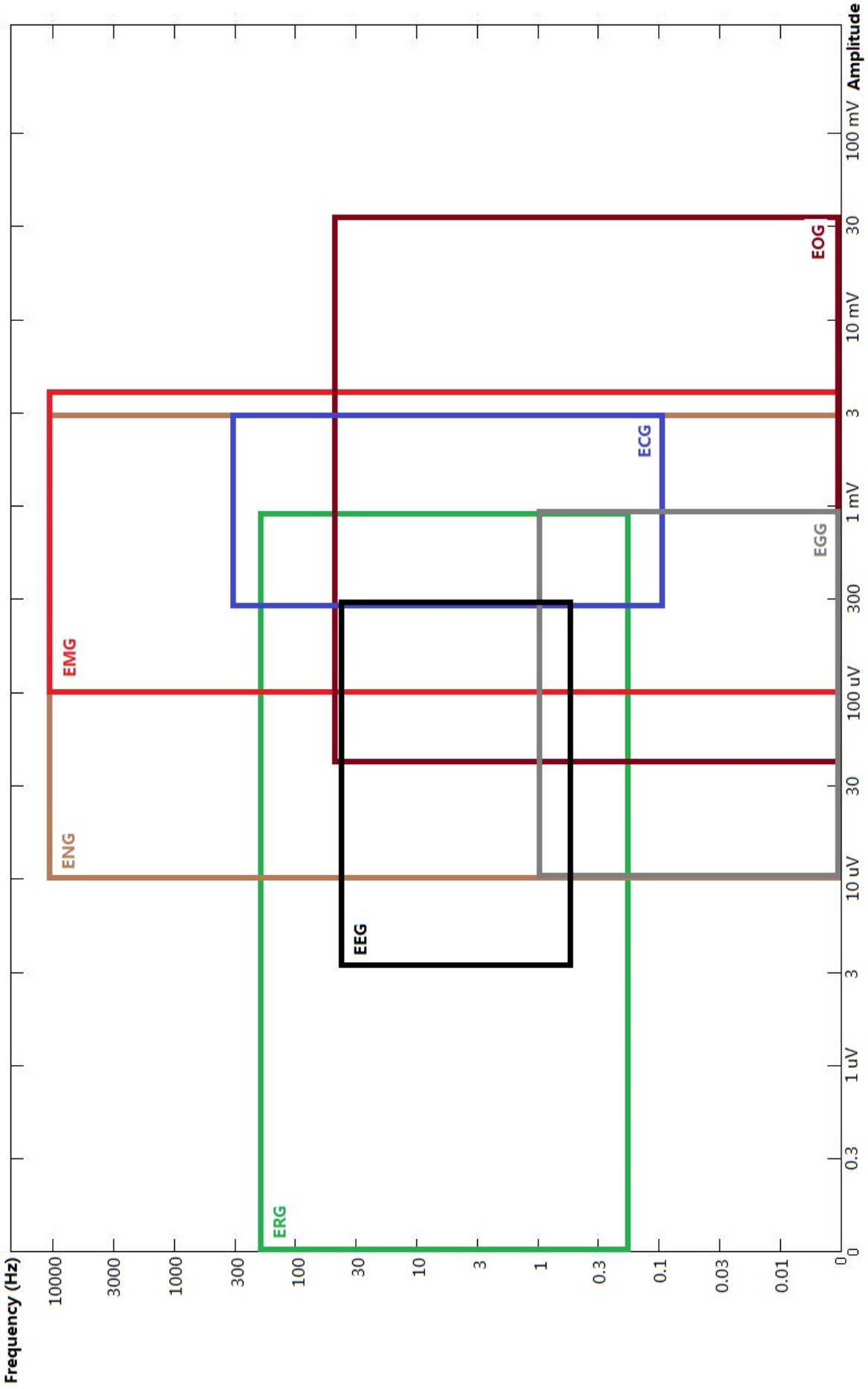

Figure 2-3: Signal frequencies and amplitude ranges (Webster, 2006).

To summarize, because of the small amplitudes (μV to mV range) of the original signals, a signal is easily affected by external noise and interference. Moreover, the amplifying electronics for EEG, EMG and ECG signal measurements need a large gain to amplify small signals.

2.3 Technologies for electrode design and manufacturing

Traditionally, Ag/AgCl surface electrodes with conductive gels are applied to the skin to record EEG, EMG and ECG bio-signals. This method can address most noise problems encountered during this process. These Ag/AgCl electrodes have been studied and developed for about 50 years. They have a standard form and provide excellent results with proper preparation (shaving hair where necessary and applying conductive gel). This preparation reduces the impedance between the skin and electrode providing the optimum measurement conditions, while furthermore, the noise and interference from motion artefacts are decreased by the gel. Thus the recorded signals have acceptable low-frequency noise and drift. However, the shaving step is not convenient for patients. Furthermore, the impedance between the skin and electrodes increases as the gel becomes dry and the skin releases sweat over time. When the gel becomes dry and sweat or oil appears on the skin, the quality of bio-signals will be effected, and the impedance between the skin and electrode will change.

Presently, Ag/AgCl electrodes are still used in hospitals and short-term environments (such as measurements over a couple of hours), but researchers are developing two new types of electrode to overcome the aforementioned problems. These new electrodes are dry contact and dry non-contact electrodes. Dry electrodes record signals without any gel and electrolyte between the skin and electrode. Non-contact electrodes further try to assess the potentials through clothes. Figure 2-4 presents a comparison between the structures of wet, dry and non-contact electrodes. In Figure 2-4, the skin layers and electrode are modelled as capacitors and resistors. For the wet electrode, the skin-electrode interface is one RC circuit (the gel reduces the resistance for the interface), the skin layer is another RC circuit, but the values of the resistor and capacitor are much larger than the interface layer (100 k and 10 nF). For the dry electrode, because there is no gel on the interface, there is only one RC circuit for the skin layer, and the resistance and capacitance of the dry electrode circuit is larger than the resistance and capacitance in the wet electrode circuit. Finally, in addition to the RC circuit for the skin layer, the gap in the non-contact electrode forms a capacitor structure. In this capacitor structure, the skin and electrode forms the two plates for the capacitor, and the gap between electrode and skin (like air or cotton) forms the medium in the capacitor. Typically, the value of the skin impedance is 200 $k\Omega/cm^2$ at 1 Hz and 200 Ω/cm^2 at 1 MHz.

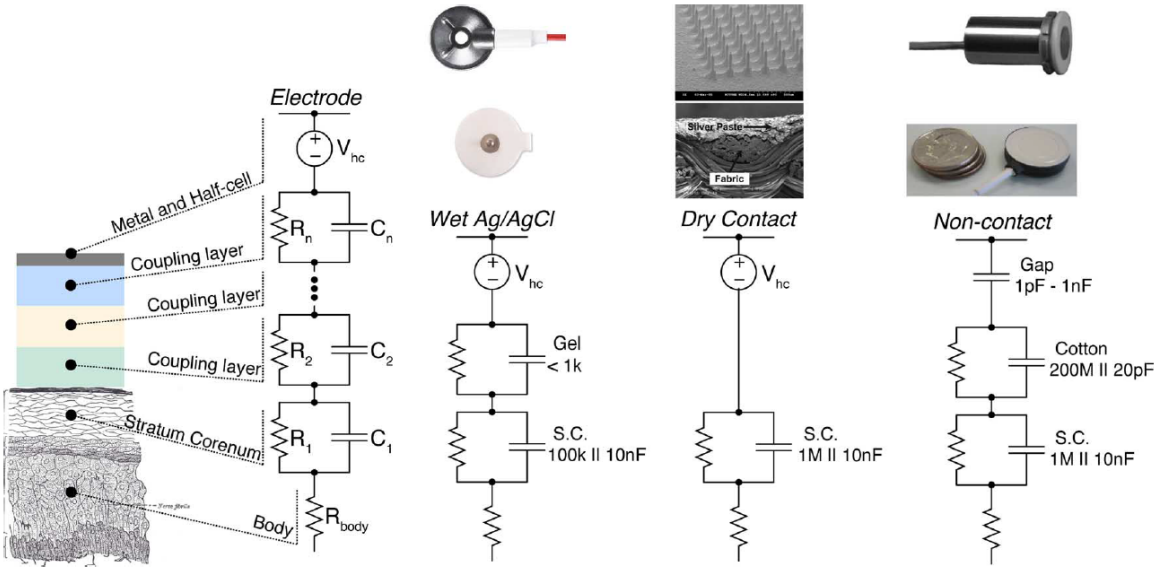

Figure 2-4: Electrical structure of the skin-electrode interface for wet-contact gel-based Ag/AgCl, dry and non-contact metal plate electrodes (Chi, Jung and Cauwenberghs, 2010).

However, wet, dry, and non-contact electrodes have their own advantages and disadvantages as described in Table 2-2.

Electrode type	**Advantages**	**Disadvantages**
Wet	Common and widely used	Gel and electrolyte applied
	Low noise	Impedance changes
	Less motion artefacts	Skin preparation
Dry	No gel or electrolyte applied	Motion artefacts occur when the electrode moves relatives to the skin
	Long-term usage	The impedance changes during long term measurement
Non-contact	No gel and electrolyte applied	High impedance
	No skin preparation required	Motion artefacts from movement
	Long-term usage	The electrode contains electric-components
		Noise interference

Table 2-2: Comparison between wet, dry and non-contact electrodes.

When the electrodes (wet, dry or non-contact) are connected to a recording system, two electrodes form the detecting part of a single channel. A complete channel has three electrodes. The first electrode connects to the detecting point, the second one goes to the reference point and the final electrode is used to cancel the interference signal from the body and the power supply. The human body acts like an antenna, so some noise will be collected from the body and this noise needs to be cancelled. Furthermore, the current flow from the power supply will affect the measurement result. Therefore, the additional electrode is used to cancel out this interference by connecting this electrode to the body. In a conventional bio-potential recording system, the electrode touches the skin directly, and an amplifying circuit amplifies the original signal as shown in Figure 2-5. However, for the non-contact electrode or some dry electrodes, the amplifying circuit is divided into two parts: front-end

and back-end circuits. The front-end circuit contains the electrode and one amplifier, and the back-end circuit contains the two amplifiers, a filter and an analogue to digital (A/D) converter. Finally, a computer interface and signal analysis software is used for data analysis.

In all designs, the back-end circuit has a common form and is based on a simple amplified converter circuit. For some dry electrodes and non-contact electrodes, the front-end circuit contains an electrode and amplifier. In the traditional system, only the electrode connects at the test point, and the electronic circuit of the system is implemented using an external printed circuit board. The advantage of the electrodes in a traditional system is that they are easy to replace. The electrodes do not have any electronic components, and only the electrodes themselves are disposed of and replaced with new electrodes.

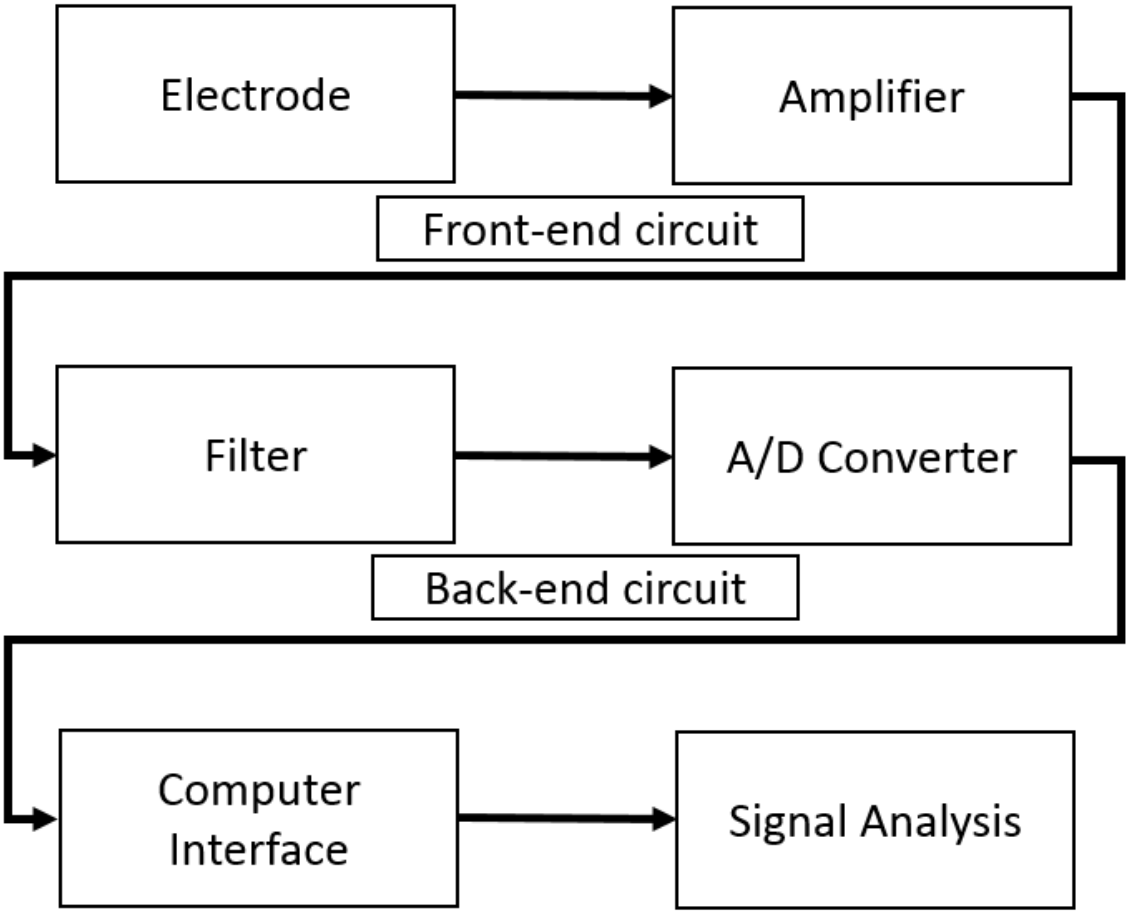

Figure 2-5: Block diagram for the bio-potential measurement.

The electrodes used to measure the bio signals are associated with some unanswered questions such as: which material is better for measurement? What are the best geometries for an electrode? How can the electrode be made more comfortable for the user? And how can the skin affect the measurement? There have been few simulations of the three electrode types: wet, dry, and non-contact electrodes, however the important effects could not be assessed, with limited theoretical support. In response, a model for each electrode type could be used to support and demonstrate what provides the best performance. (Assambo *et al.*, 2007; Chi, Jung and Cauwenberghs, 2010).

In this thesis, the main proposal is to implement the electrode part from Figure 2-5 and apply a simulation model to find the effects from the skin and the most efficient electrode structure to reduce the skin impedance for the bio-potential monitoring system.

2.4 Electrode analysis with the skin-electrode interface

Before the skin and electrodes are modelled, it is necessary to identify how the skin and electrode can be modelled, and what parameters are necessary to assess the performance of an electrode. In Sawan's research (2011), author indicates that cells have the ability to generate electrical signals are called electrongenic cells (such as the brain cells). The electrongenic cells have ion channels, and this ion channel is able to permeate the certain ion (like sodium). In a transient change of the ions, a potential is generated by the ion flux, this potential for the ECG or EMG is the electrical signal in the biological systems. To measure or catch this action potential, the bio-potential electrodes is applied to the biological or bio-signal measurement system to convert the ionic conduction to electronic conduction. In most of the electrode bio-signal measurement system, the skin and body tissues play the role of electrolytic solutions.

With an electrode-electrolyte interface, there are two actions (Sawan, 2011):

- The electrode releases the metallic ions into the electrolytic solution. This action increases the total number of free electrons in the electrode and increase the number of positive cations (or called electric charge) in the electrolytic solution.
- The ions existed in the electrolyte solution are combined with the electrodes. This action decreases the total number of free electrons in the electrode and decrease the number of positive cations in the electrolyte solution.

As a result, a potential difference between the electrode and electrolyte is generated. At the interface between the electrode and electrolyte, the ionic equations are shown below (Neuman, 2000):

$$C <=> C^{n+} + ne^{-} \quad (2\text{-}1)$$

$$A^{m-} <=> A + me^{-} \quad (2\text{-}2)$$

Where C is metallic atom, C^{+} is the Cation, A^{-} is the Anion, n and m are the valences.

In this electrode-electrolyte system, the cations in the solution and the metal of the electrodes are same. Hence the electrode plays the role of cations in the electrolyte and the electrode material gets oxidized, meanwhile, the electrons remain at the electrode and forms the current flow in the bio-potential measurement circuit. Oppositely, If the anion is oxidized at the electrode, the electrons are given to the electrode (Sawan, 2011).

As a result, the reaction is as shown in Figure 2-6:

- Current flow from electrode to electrolyte: Oxidation (loss of e-)
- Current flow from electrolyte to electrode: Reduction (Gain of e-)

For both oxidation and reduction in the electrode-electrolyte interface, there are two parallel layers of oppositely charged ions on the contacting surface between the electrode and electrolyte (like Figure 2-6), which forms an electrode double layer.

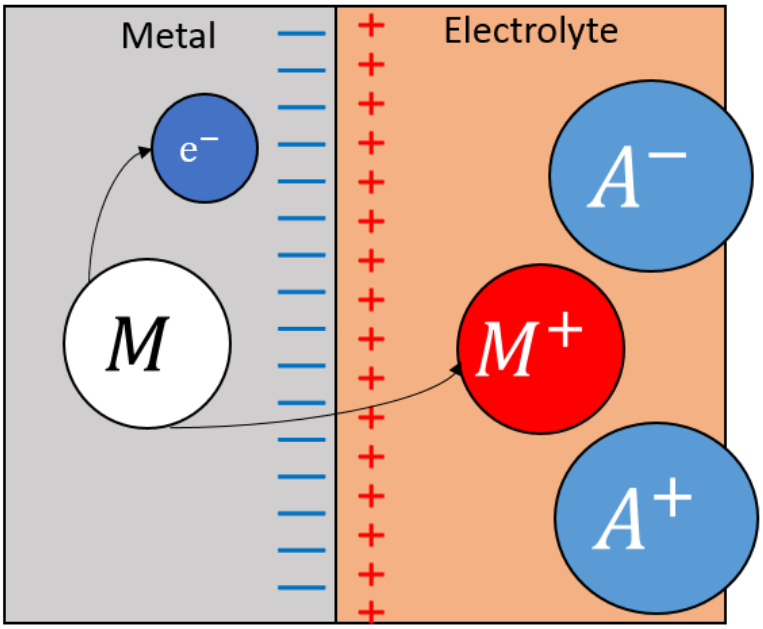

Figure 2-6: Ions gains and losses at the metal-electrode interface. Electrons remain at the electrode. M is the metal, A is anion, e is an electron.

When the potential difference is generated between the electrode and its surrounding electrolyte, the interaction between the electrode material and the solution of ions will change the concentration of the solution ions near the electrode surface. Therefore, the electrolyte solution near the electrode has a different electrical potential to the rest of the electrolyte solution. This potential difference in the electrolyte solution is called half-cell potential (Brinzino, 2000). This half-cell potential depends on the type of metal, the ion concentration in the solution, and the temperature. Furthermore, the oxidation or reduction process at the electrode-electrolyte interface will cause the half-cell potential by the oxidation-reduction reaction.

For the general oxidation-reduction reaction, there is the following equation (Sawan, 2011):

$$aA + bB \leftrightarrow cC + dD + ne^{-} \quad (2\text{-}3)$$

In the equation, a, b, c, d and e are the number of Cations, Anions and electrons.

This particular relationship generates an electric potential, it is known as the Nernst equation:

$$E = \frac{RT}{nF} ln \frac{a_1}{a_2} \quad (2\text{-}4)$$

When a_1 and a_2 are the activities of the ions on the side of the electrode-electrolyte interface (which is shown in Figure 2-7 as the meaning as concentration), R is the universal gas constant, T is the absolute temperature, n is the valence of the ions, and F is the Faraday constant.

Normally, the half-cell potential of the standard hydrogen electrode is zero and is an equilibrium value. When a current flow passes through the electrode-electrolyte interface, the half-cell potential will change. This potential difference (changed half-cell potential difference) between the potential with no current passing and the measured potential with current passing is called the over-potential or over-voltage (Neuman, 2000). Therefore, this potential difference or over-potential is the change in the charge distribution in the interface between the electrode and the electrolyte solution. This over-potential or over-voltage is also known as polarization. The polarization over-potential has three key components: resistance, concentration and the activation over-potentials as shown in Figure 2-7.

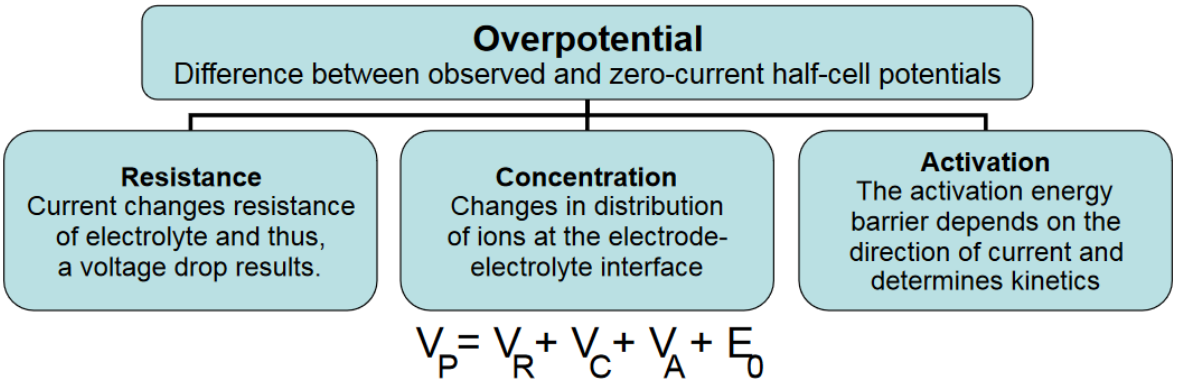

Figure 2-7: Combination of over-potential and their types (Sawan, 2011).

According to Brinzino's (2000) research, Electrodes can be classified as perfect polarizable and non-polarizable:

- Perfect polarizable electrode means that the current pass though the electrode and electrolyte interface by varying the charge distribution around the electrode in the electrolyte solution (Brinzino, 2000). However, when the charge distribution is changed in the perfect polarizable electrodes, no actual DC current can pass through the electrode-electrolyte interface (like the capacitor), there is only a displacement current in the electrode-electrolyte interface. Theoretically, electrodes made from noble metal (like platinum) are more polarizable than other materials.
- Non-polarizable electrode means that the current can pass through the electrode and electrolytic interface without altering the charging distribution around the electrode in the electrolytic solution (Brinzino, 2000). If the electrode is not a perfectly polarizable electrode, some currents can pass through the electrode-electrolyte interface. In practice, the Ag/AgCl electrode is a good example for non-polarizable electrode.

Comparing perfect polarizable with non-polarizable electrodes, the perfect polarizable electrode is like a capacitor and a direct current cannot pass through it. If an electrical potential is applied, there is no actual current or charge (DC current) across the electrode-electrolyte interface. The current across the electrode-electrolyte interface is a displacement current due to the change of charge concentration at electrode surface, therefore, the over-potential will be generated by the change of charge concentration. Furthermore, the perfect polarizable electrode is sensitive to movement. When movement is applied to the polarizable electrode, the charge distribution in the solution near the electrode surface will be changed,

and this gives a voltage change in the electrode measurement, otherwise known as a motion artefact. The motion artefact and its cancellation are introduced in sections 2.4.7 and 2.4.8.

Moreover, the perfectly non-polarizable electrode forms the structure of a resistor and current can easily pass freely through the electrode-electrolyte interface (like Ag/AgCl electrode (wet electrode)). There is no over-potential in the electrode-electrolyte interface.

For a metal electrode (dry or non-contact electrode), which is not a perfectly polarizable or perfectly non-polarizable electrodes, there are two actions at the electrolyte interface (Sawan, 2011):

- A capacitive process: there is no electron exchange between the electrolyte solution and electrode, the charged and polar particles are redistributed by the displacement current.
- A component or resistive effect (or called faradaic process), there is an electron exchange between the electrode and electrolyte solution.

2.4.1 Conventional (wet) electrodes

With the wet electrode, the electrolyte gel is used to enhance the electro-chemical reactions and to reduce the skin-electrode impedance in the non-polarizable electrodes. The Silver/silver chloride (Ag/AgCl) is an ideal non-polarizable electrode. There is no concentration or activation of over-potential through the electrode-electrolyte interface. As a result, the electrodes are very stable for bio-potential recording.

2.4.1.1 Conventional (wet) electrode electrical structure

Silver/silver chloride (Ag/AgCl) with conductive gel is a typical example of a conventional electrode; it provides the best signal quality compared to other electrode types, and is used as a benchmark to evaluate other kinds of electrodes. The Ag/AgCl is an ideal non-polarizable electrode. There is no concentration or activation of over-potential through the electrode-electrolyte interface. As a result, the electrodes are very stable for bio-potential recording. The electrode size can be varied for different usages and the electrode is placed on the body as required where a measurement point is sought. Figure 2-8 gives the circuit that represents the skin-electrode interface for the wet electrode.

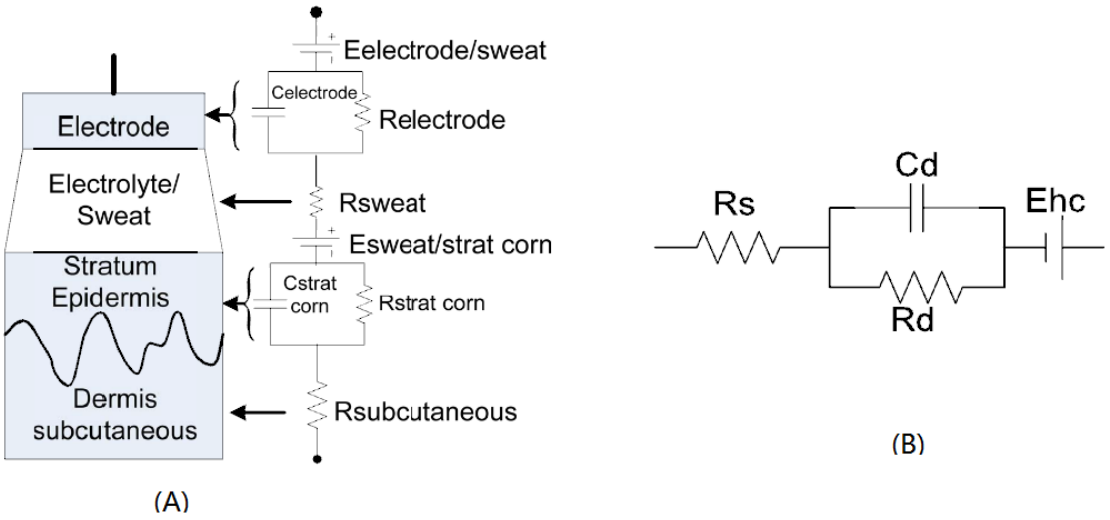

Figure 2-8: (A) Structural and electrical model of a wet electrode. (B) Equivalent circuit between skin and electrode for a wet electrode.

In Figure 2-8 (A), the left part is the structure of a wet skin-electrode and the right part is the equivalent circuit of the model. The structure contains the main layers under the skin such as stratum corneum epidermis, dermis and the subcutaneous layer. If the circuit in Figure 2-8 (A) is simplified based on the Cole equation described later in Section 2.5.1, then the resulting circuit is shown in Figure 2-8 (B). For Figure 2-8 (B), the symbols are described below.

C_d: capacitance of electrode-electrolyte interface

R_d: resistance of electrode-electrolyte interface

R_s: resistance of electrode lead wire

E_{hc}: half-cell potential between electrode and skin

In the simplified equivalent circuit, the skin-electrode impedance of the conventional wet electrode is represented as an RC circuit.

For the capacitance (C_d) of electrode-electrolyte interface, it is the capacitive process: the charged particles are redistributed with no electron exchange between the solution and the electrode. Meanwhile, the resistance (R_d) of electrode-electrolyte interface, it is the faradaic process, and there is an electron exchange between the electrode and solution. Additionally, the E_{hc} (half-cell potential) has been presented at the beginning of section 2.4.

2.4.1.2 Wet electrode manufacturing and fabrication

Figure 2-9 showed the structure of a developed conventional wet electrode; in this case the electrode has been pre-gelled and glued. This electrode was picked up from ECG

measurement in Southampton general hospital. The electrode gel is conductive with low resistance and the glue is used to fix the electrode at the required position.

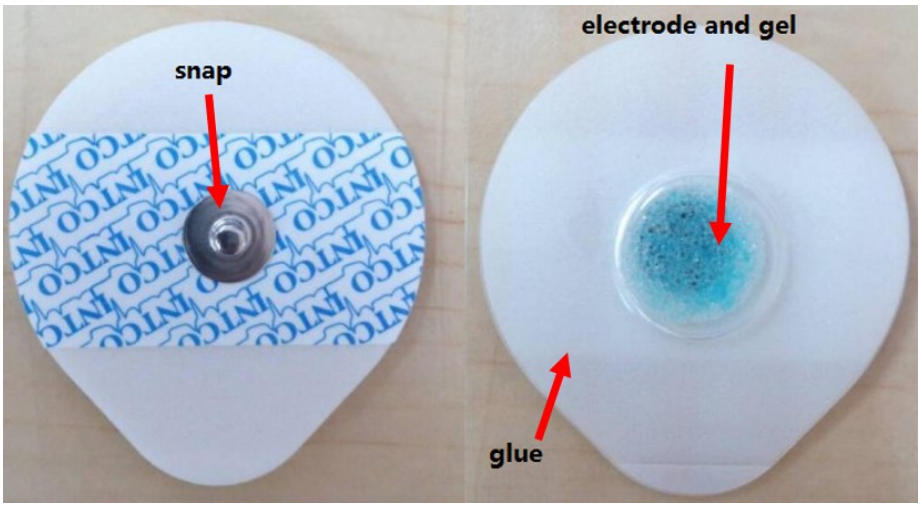

Figure 2-9: The Ag/AgCl coating on the electrode snap prevents the pre-gelled electrode from causing artefacts (Webster, 1984).

2.4.2 Dry electrodes

Comparing with wet electrode, the dry electrodes do not apply any electrolyte gel (like stainless steel electrode) and are classified to polarizable electrodes like the descriptions at the start of section 2.4.

2.4.2.1 Dry electrode structure

Since 1967, literature has been published which focuses on the implementation of dry and insulating electrodes to overcome some of the problems with wet electrodes, such as interference, inconvenience of electrolytes, and the toxicological concerns relating to electrolyte gels (could potentially cause dermatitis). Previous studies from 1971 to 2017 on materials for dry and insulating electrodes are shown in Table 2-3. Since then, further materials have been used to test dry electrode performance (such as PDMS or polyurethane with Cu).

Year	Reference	Construction	Finding
1971	Bergey *et al*	Ag, Au, brass stainless steel	Careful shielding arrangement required
1973	Geddes *et al*	Au	
1979	De Luca *et al*	Stainless steel	
1989	Geddes *et al*	Ag	Effective dielectric thickness changes with dry skin layers and perspiration
1990	Padmadinata *et al*	Ag, stainless steel	
1992	Nishimura *et al*	Stainless steel	
1994	McLaughlin *et al*	Screen printed	
1995	Gondran *et al*	High sodium in conductor	Skin condition is an important parameter
1996	Babak *et al*	Silicon sensor substrate with SF_6O_2	

2000	Searl *et al*	Aluminium, stainless steel, titanium	Impedance decreases exponentially respectively to frequency. Titanium performs best
2001	Griss *et al*	Micro machined (needles) electrode	
2005	Paradiso *et al*	Two stainless steel wires twisted around a textile	Higher noise for dry textile, most reliable behaviour in the conductive fibres
2007	Ju-Yeoul *et al*	Elastomer poly (dimethylsiloxane)	
2007	Gruetzmann *et al*	Dry Ag foil conductive foam (polyester, polyethylene)	Less motion artefact for dry foam, low skin-electrode impedance for dry foam electrode
2008	Baek et al	PDMS, titanium (adhesion layer), gold pattern (centre)	More sensitive to motion artefact, stable ECG signal (1 week), no skin irritation (1 week)
2010	Dias *et al*	Iridium oxide	16 micro-tips in electrode
2010	Chi *et al*	Thin film, cotton dry metal – plate, MEMS Ag/AgCl	Poor settling time, no electrochemical noise for cotton electrode
2012	Salvo *et al*	3D printing	
2014	Bersain *et al*	CB/PDMS electrodes	Underwater
2015	Chlaihawi *et al*	MWCNT (multi-walled carbon nanotube)/PDMS based screen printed dry electrode	
2016	Cunguang L et *al*	Graphene films on polyethylene terephthalate (PET) substrates with graphene paper	Week-long continuous wearable flexible electrode
2017	Andrea et *al*	Screen printing with poly-3,4-ethylenedioxythiophene doped with poly(styrene sulfonate) (PEDOT:PSS) conductive organic polymer.	On textile, easy to clean. Washable and wash up to 20 times

Table 2-3: Summary of publications from 1971 to 2017 on dry and insulating electrodes.

From Table 2-3, it can be seen that dry electrodes have similar problems to wet electrodes, namely interference during movement, and the impedance effects and noise of bodies being near the electrodes. This section introduces the structure of dry electrodes and how to overcome some of these problems.

Dry electrodes can be divided into several categories. The first type of dry electrodes is made from stiff materials and do not use conductive gel. Instead, they rely on the moisture from the skin to enhance the recorded signal. Because of the low cost and good electrical conductivity of stainless steel, many studies have chosen stainless steel for the electrodes. Furthermore, dry electrodes are fabricated using conductive materials such as silver, copper or aluminium. This kind of electrode is tough and not very flexible, which means users will not feel very comfortable. In addition, to improve the performance of this kind of electrodes, researchers have started to apply conductive foam or conductive metal around soft materials, such as polymer. The trend in the material changes can be seen in Table 2-3.

The second type of dry electrode is built with MEMS (micro-electromechanical systems) or thin film structures. The MEMS method is used to reduce the skin/electrode interface

impedance using needles. For MEMS dry electrodes, small needles and nodes are used to design a measurement matrix, and the bio-signal is the result of all the detecting needles.

Electrodes made using conductive metals have the same equivalent circuit as wet electrodes without the gel resistance (R_s in Figure 2-8) as shown in Figure 2-10. Comparing Figure 2-10 with Figure 2-4 (the equivalent circuit for a wet electrode), these two structures are very similar to wet electrodes apart the conductive gel. There are two main improvements for the dry electrodes: the first being the gel in the skin electrode interface has been replaced by the electrode itself, and the second is that the dry electrode allows full contact with the skin as it no longer has a rigid surface.

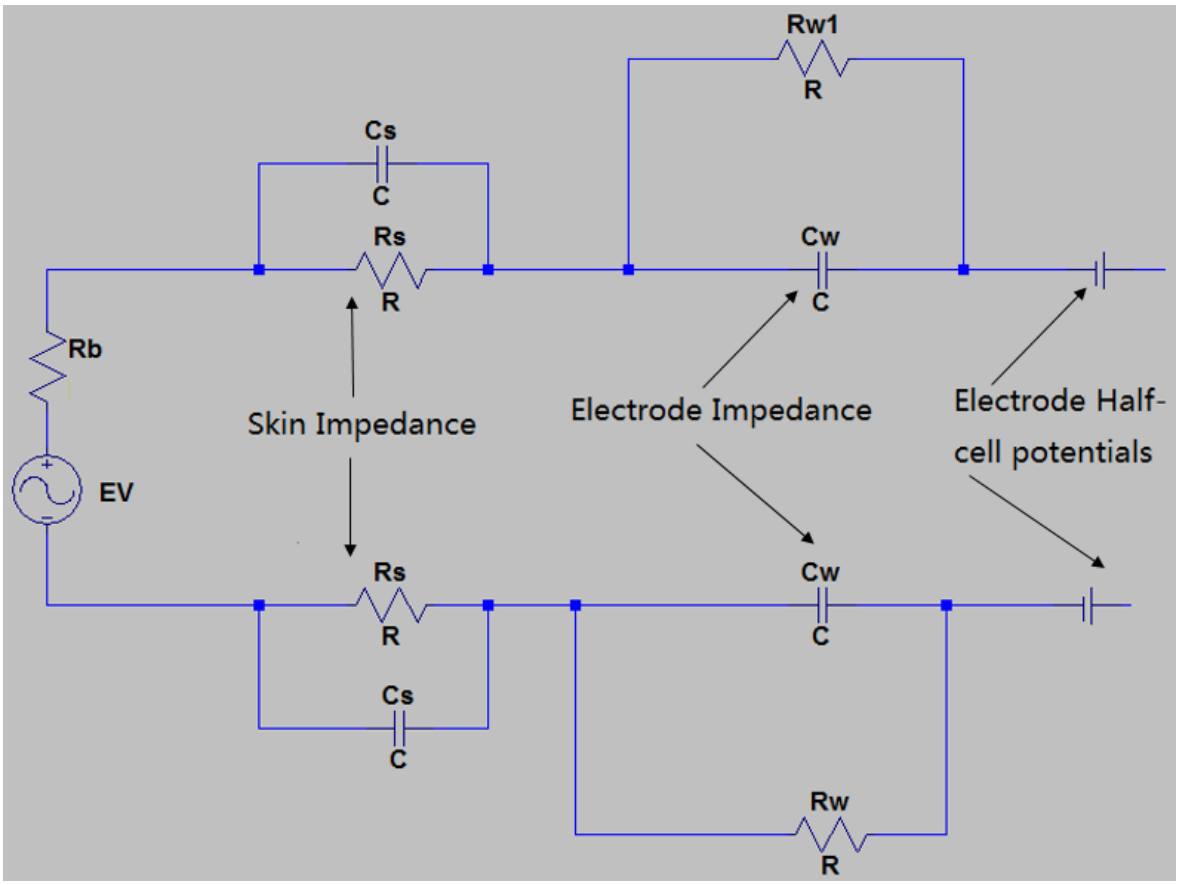

Figure 2-10: Equivalent circuit of metal dry electrodes where E_v is the bio-potential signal inside the body, R_w and C_w are used to build the equivalent circuit for electrode impedance, R_s and C_s are used to describe the skin-impedance. According to different skin and electrodes, their values are different.

2.4.2.2 Manufacturing and fabrication

2.4.2.2.1 Conductive foam dry electrode

In research in 2007 focused on the conductive foam electrode (Gruetzmann, Hansen and Muller, 2007), flexible conductive foam was used to construct the ECG electrode. The soft and flexible material of these electrodes provides a large contact area, which offers comfortable contact and increases the effective recording area. The electrode surface follows the body shape as shown in Figure 2-11. If there is hair present on the body, these hairs can

be pushed down. The shape of the conductive foam means that it always touches the skin. Compared with previous traditional electrodes, the electrode material has been replaced with a soft conductive foam with no need for any skin pre-preparation, but the circuit of the bio-potential measurement remains the same.

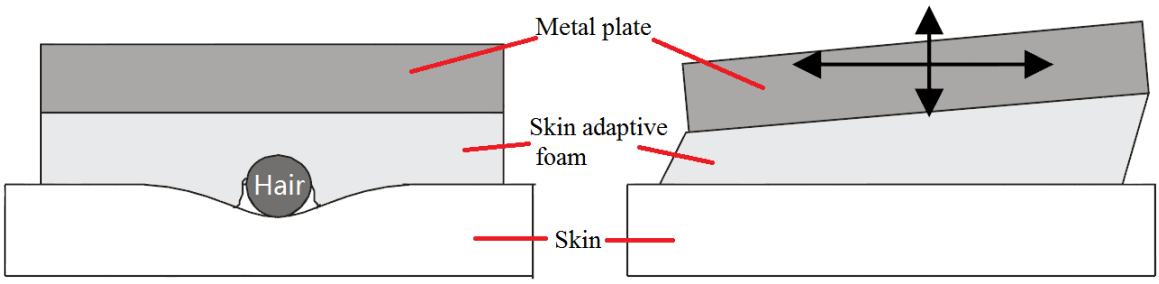

Figure 2-11: Conductive foam increases the contact area and reduces movement problems (Gruetzmann, Hansen and Muller, 2007), the foam covers the hair and allows the electrode movement.

To develop electrodes from a metal dry electrode to a soft electrode, studies by Lin et al (2011) applied the conductive fabric covering all surfaces of a polymer foam with one layer of Cu adhesion layer as shown in Figure 2-12.

The polymer fabric was 0.2 mm thick with a conductivity of 0.07 Ω/ m^2. The size of this dry electrode was 14 mm × 8 mm × 8 mm. The skin-electrode impedance was measured to examine the performance of this dry electrode with two electrodes placed on the forearm. Both electrodes were attached with a distance of 2 to 3 cm separation.

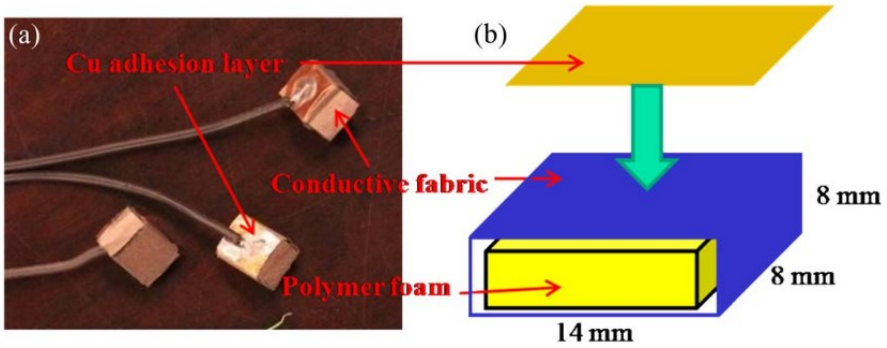

Figure 2-12: (a) top view and (b) detailed views of dry foam electrode from the literature. The foam electrode is covered by the conductive fabric and paste on a Cu layer (Lin *et al.*, 2011).

The measured results of the electrode are shown in Figure 2-13. The results show that the impedance between the skin and dry electrode exhibit a similar trend to conventional wet electrodes with conductive gel. Furthermore, the impedance of the dry electrode on hair is close to that of hairless skin. This means that this dry electrode can provide results that are as stable as those from conventional electrodes and it does not require shaving.

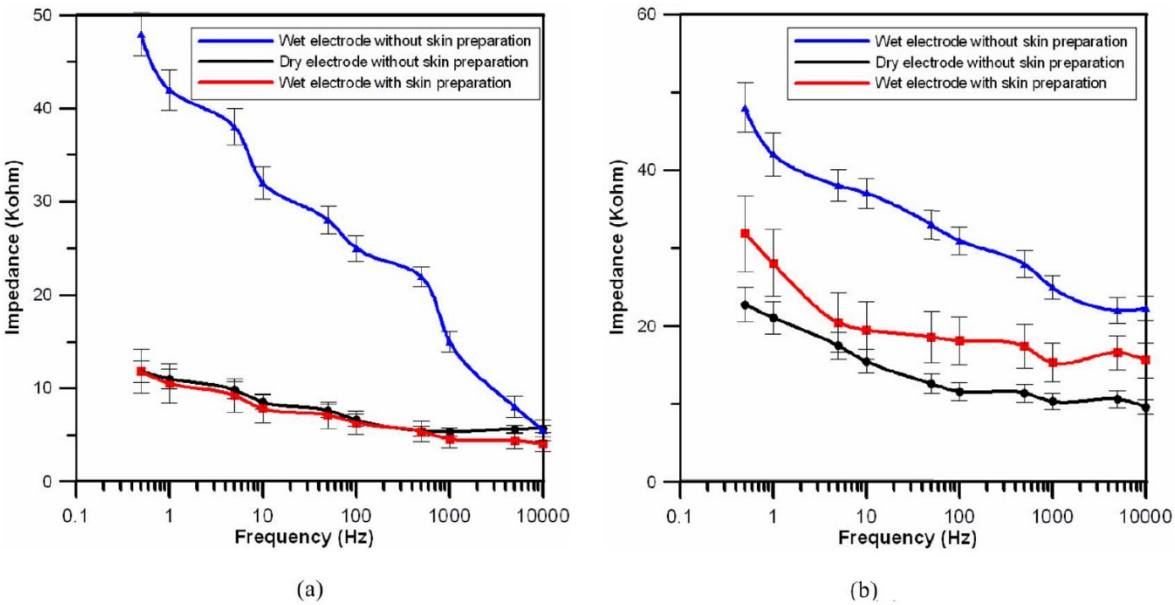

Figure 2-13: Skin-electrode impedance of dry foam electrode on forearm and hairy sites (Lin *et al.*, 2011). Note: The original figure was based on the measurement results from the paper, and as such, the figure quality cannot be changed.

Moreover, Lin et al (2011) provided the averaged values of the long-term impedance variation (5 h) as shown in Figure 2-14. The five-hour impedance variation of the dry electrode without the conductive gel achieved better results and results were relatively consistent. The impedance changed from 47 k to 43 kΩ. Furthermore, the dry foam electrode could provide better stability regarding skin-electrode impedance because it does not need conductive gel.

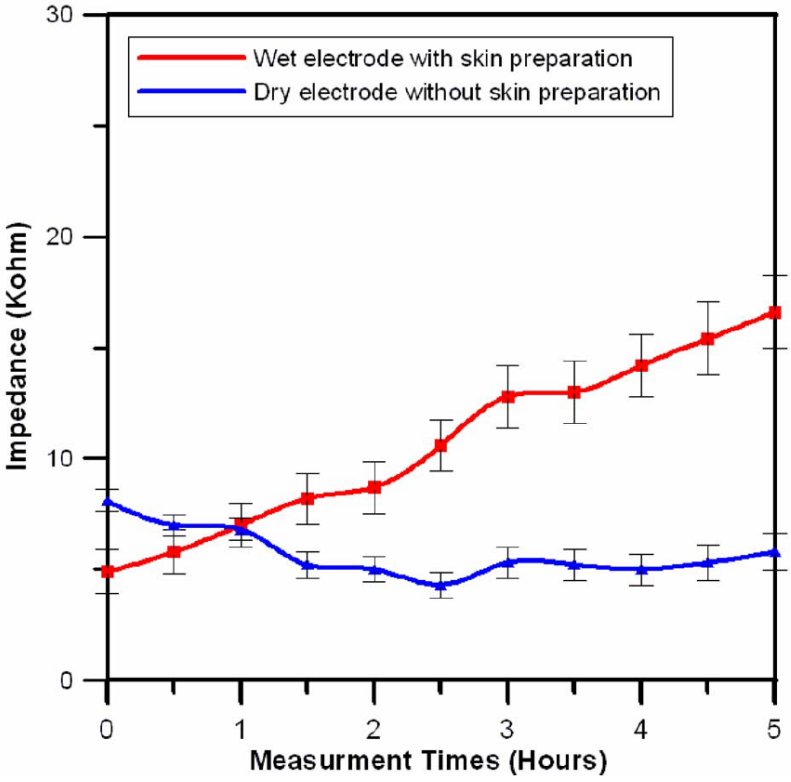

Figure 2-14: Comparison of the impedance variation between wet and dry foam electrodes for measurements over 5 hours (Lin *et al.*, 2011).

Conductive foam is not the only possible conductive material. Elastomeric poly (dimethylsiloxane (PDMS)) with a thin conductive metal in the design by Baek et al (2008) is another possible option as shown in Figure 2-15.

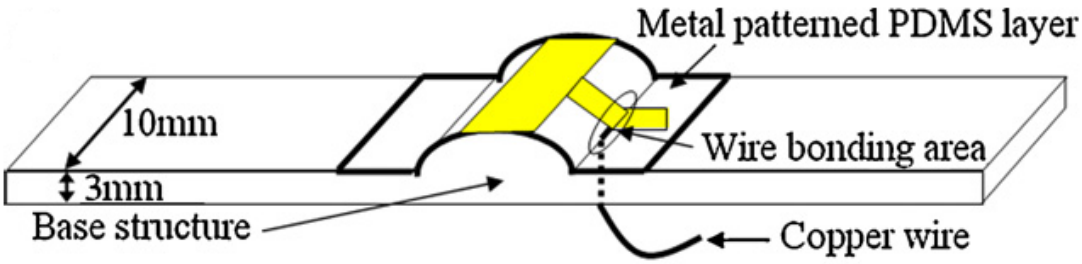

Figure 2-15: Schematic diagram of PDMS dry electrode(J.Y.Baek *et al.*, 2008).

In the design by Baek et al (2008), the substrate material was PDMS. For better contact with the skin, the centre of the design has a convex shape protruding 1.5 mm upward. The titanium and gold pattern was located in the centre. The impedance of the electrode was measured and the results are shown in Figure 2-16 and used to evaluate the electrode performance.

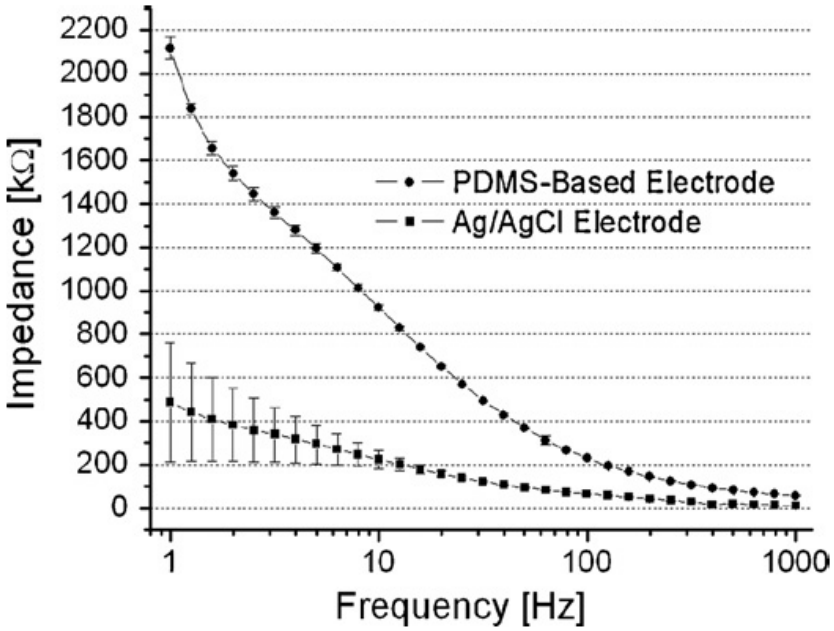

Figure 2-16: Skin-electrode impedance of PDMS electrode on forearm (Baek *et al.*, 2008).

From the results shown in Figure 2-16, the impedance of the PDMS electrode is much higher than that of the Ag/AgCl electrode below 100 Hz. However, the impedance becomes similar above 100 Hz. The impedance changes as time passes and drops quite significantly after 24 hours as shown in Figure 2-17. The test subject in this study also reported that the affected skin was slightly moist when the electrode was removed. Because the electrodes were placed on the skin for a long period (more than 24 hours), the sweat acted as a gel or conductive medium between the electrode and the skin.

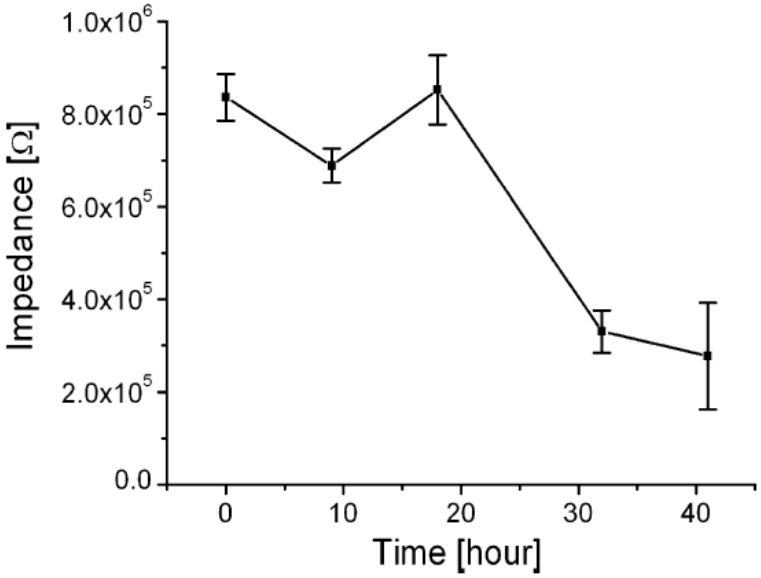

Figure 2-17: Impedance variation of PDMS electrodes in the literature for 40 hours measurement (Baek *et al.*, 2008).

These two dry electrodes described above changed the electrode materials with the aim of improving the performance of the electrodes. Although the dry electrodes do not provide better results than conventional wet electrodes in relation to short-term measurement (2 hours), the dry electrodes show potential for long-term measurement stability (more than 20 hours).

Although there have been numerous different materials used for dry electrodes (see Table 2-3), it is practically impossible to test all materials in great detail. In this thesis, the focus is on dry electrodes with different structures and seeks to demonstrate the differences between them.

2.4.2.2.2 MEMS dry electrode

For the MEMS dry electrode, the mechanical design provides for dry application and does not use any conductive gel. The 1st MEMS electrode was described in 2003 and introduced the array-structure electrode (Mojarradi *et al.*, 2003). Similarly, the Liao et al (2011) offers a simplified design: the electrode contains 17 probes in one electrode and is applied to recording bio-signals as shown in Figure 2-18. Strictly speaking this electrode is not made using MEMS technology but provided inspiration for later designs which do.

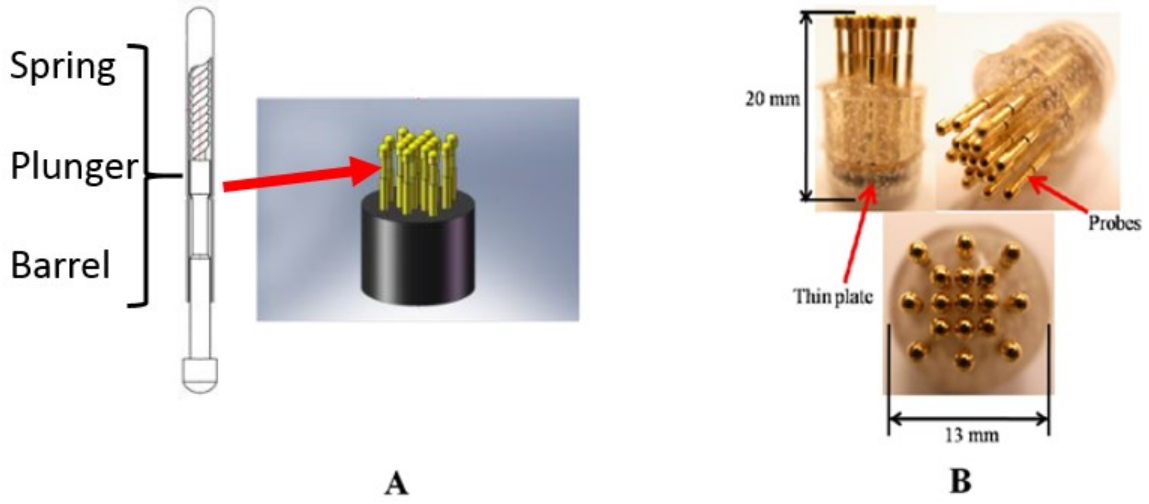

Figure 2-18: Structure of a MEMS dry probe electrode (Liao *et al.*, 2011).

In Liao's design (Liao *et al.*, 2011), the radius of the probe is 1.3 mm and the probes are made of gold (Au) for good conductivity. Furthermore, the probes are made with a mechanical structure inside, with each needle designed as shown in Figure 2-18 (A). With this design, one MEMS electrode provides a set of signals since it collects signals from each probe or needle as shown in Figure 2-18. This allows the recording system to analyse the recorded signals at each needle. Compared with the rigid electrode, this design of the electrode could increase the contact area between the skin and electrode to reduce the impedance. In contrast with the conventional wet electrode shown in Figure 2-19, the probes are used for contact instead of a gel. The equivalent circuit of the conventional wet and MEMS dry electrode indicates that the skin-electrode interface of the MEMS electrode is simplified to a wire without any impedance. This means the skin-electrode interface does not form a RC circuit like the wet electrode. To avoid using a spring and plunger which has a complex mechanical structure, some researchers have built a needle array structure to replace the spring and plunger structure such as that shown in Figure 2-20 (Chiou *et al.*, 2006). The electrode is a silicon needle array formed from a silicon wafer.

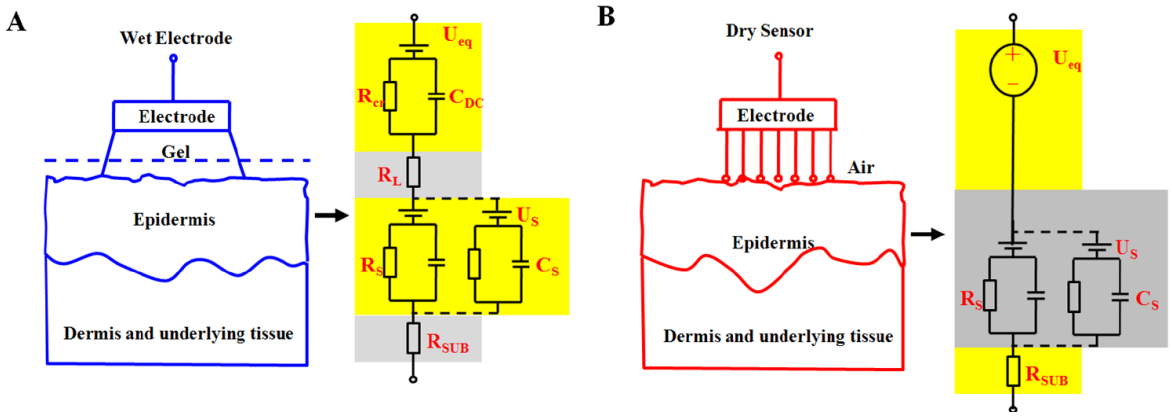

Figure 2-19: Equivalent circuit comparison between the conventional wet electrode and MEMS electrode.

In Figure 2-20, the structure of the silicon probe electrode is similar to the previous dry probe electrode. However, the structure of the MEMS electrode has been simplified. There is no spring and plunger with electrode needles, and the size of each electrode needle is reduced

to 250 µm in height and 35 µm in diameter. With this design, the dry electrode is designed to inject into the skin tissue layer (stratum germinativum (SG)), but not reach the dermis layer to avoid pain or bleeding. To reduce the noise, the probes are coated with titanium/platinum for high conductivity. Therefore, the 20 by 20 needle array is within the size of the 4 mm × 4 mm electrode. The set of probes has a smaller size than previous designs, and each of these probes provide one channel of signal.

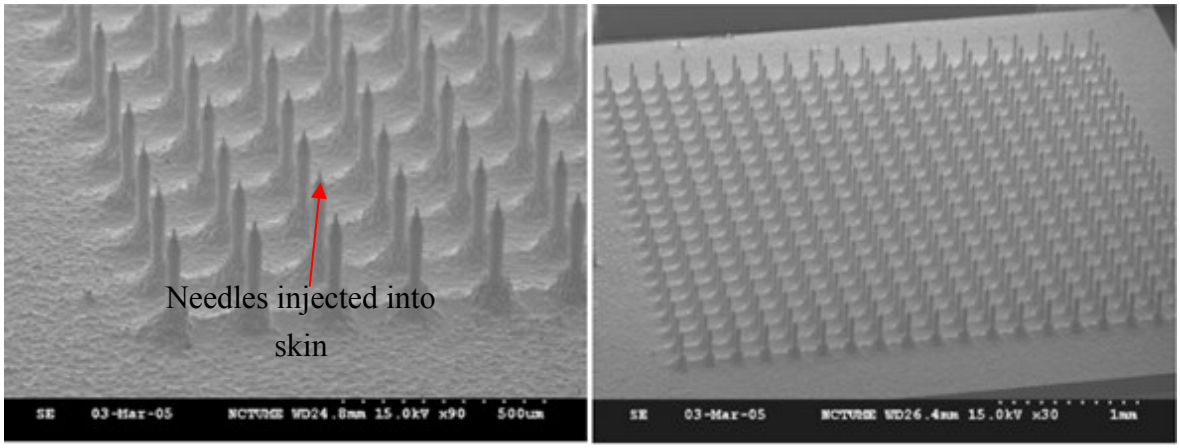

Figure 2-20: Structure of fabricated MEMS dry electrodes, needles are used to inject into the stratum germinativum layer in the skin (Chiou *et al.*, 2006).

In Chiou's design (2006), the authors only show the power spectra between a dry and wet electrode from 0 to 40 Hz as shown in Figure 2-21. The two results are similar at this frequency range. This implementation provides a possible solution for a MEMS electrode. The electrode can also be implemented by 3D printing.

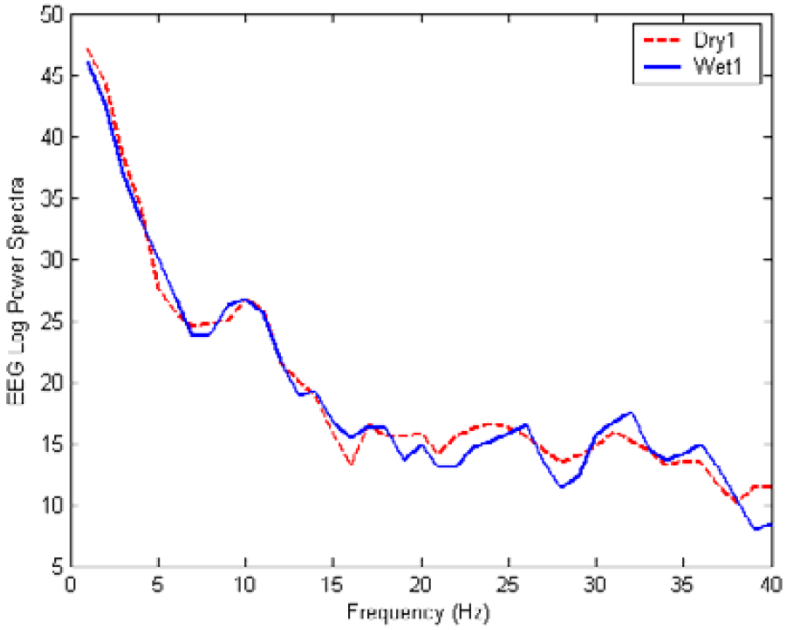

Figure 2-21: Power spectra of a dry MEMS and wet electrode (Chiou *et al.*, 2006).

Although both of the previous two electrodes are called MEMS dry electrodes, different manufacturing procedures have been applied to the electrodes. For the first example, the mechanical structure has been applied to implement the electrode (like a plunger structure).

For the second example, the electrode is made with etching, which is used in microfabrication to fabricate devices using the silicon wafer. However, both of these two MEMS electrodes aim to use a set of bio-signals from a small needle/probe (20 to 30 µm diameter) instead of applying a large surface plate (10 to 20 mm^2) to collect bio-signals.

Hao and Hu (2010) provide an algorithm, which is able to process the signal from each needle. The signal from each needle/probe is different, but the signals contain the same features. This means that those signals can be used to enhance one strong signal, and as a result, the signal is improved. According to Hao and Hu (2010), a compressive algorithm is applied to the signal which is collected by the matrix of probes in one electrode. The spatial sampling structures with Bernoulli coding allow for data loss in the multiple probe electrodes as shown in Figure 2-22. Bernoulli coding is an algorithm which extracts the main feature of the signals and ignores other parts. With this collection system, the signal from one measurement point is divided into 17 parts, then, this combinational algorithm is used to select the main points to reconstruct the signal.

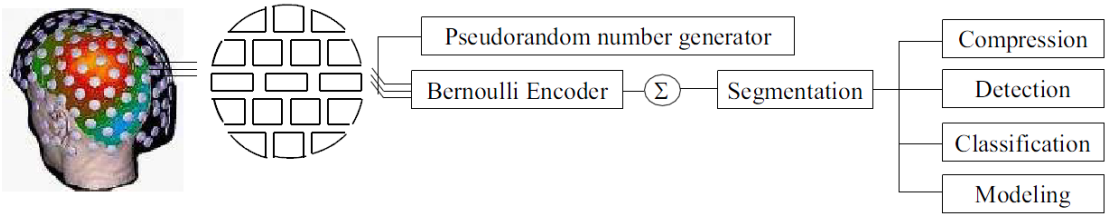

Figure 2-22: Structure of spatial sampling with the encoder (Hao and Hu, 2010).

However, the spatial sampling algorithm can only be used in this specific electrode. If the electrode geometries change, the algorithm will loses its function. Therefore, the spatial sampling algorithm is not appropriate for all uses.

2.4.2.3 Summary of dry electrodes

In the development of dry electrodes, conductive materials such as silver, gold, aluminium, conductive rubber or foam are used, with the aim of making electrodes without the need for conductive gel or electrolyte solution. In addition, MEMS technologies provide a fabrication method. These electrodes solve the problems of lack of comfort, provide large contact area and reduce movement effects. Although the MEMS electrodes contain a set of probes, these probes are slick and flexible, which reduces the discomfort potentially arising from the needles. Compared with wet electrodes, dry electrodes omit the gel used in wet electrodes and hence can improve long term measurement accuracy. Nevertheless, the electrodes still need to directly contact the skin, and hence, the skin and electrode are the significant elements in a bio-signal record.

2.4.3 Non-contact electrodes

The non-contact electrode is developed from the dry electrodes and is applied at a distance from the skin, resulting in a medium between the skin and electrode.

The description of the first non-contact bio-potential electrode was published in 2002 by Harland et al (2002) several years after the development of wet and dry electrodes. The dry

electrode is used to obviate the need for gel and glue whereas the non-contact electrode is used to allow a distance between the electrode and the skin. In the literature, this non-contact electrode is a capacitively-coupled, non-contact electrode for ECG monitoring. This electrode aims to measure the ECG signal through clothing. With wet and dry electrodes, they touch the skin directly and hence do not have a large RC impedance between the electrode and skin. The bio-signals, when using wet and dry electrode, are 'blocked' by the clothes or air separation, meaning any bio signals are below the noise level. Non-contact electrodes are developed to overcome this challenge. In this chapter, the variable non-contact electrode is discussed next, to identify the differences between the wet and dry electrode.

2.4.3.1 Structure of non-contact electrodes

Non-contact electrodes provide a potentially ideal and promising measuring condition that offers measurements for time lengths up to days, and measurements through clothes.

Depending on the measurement method, non-contact electrodes apply conductive materials via an insulating layer (David and Michael, 2005a; Bernat, 2011). Non-contact electrodes use an amplifier inside the electrode to provide large impedance to overcome the problems of high resistance from clothes or hair. It can also overcome the capacitive coupling transfers charge by means of the capacitance between skin and electrode. However, as a result, there will be additional interference caused by the amplifier components and cables (Gargiulo *et al.*, 2010). Furthermore, there are several variables that could affect the capacitance: such as the area, thickness, or permittivity of the material between the skin and the electrode. As the distance from the electrode to the skin increases, the interference arising from movement increases. Protection from interference of the circuit for non-contact electrodes becomes a critical factor.

The most recent designs aim to build non-contact electrodes by using different materials for the contact layer or by using different capacitive circuits. To date, non-contact electrodes are only available in the laboratory, and all need to solve the problems of motion artefacts, friction and thermal noise (Chi, Jung and Cauwenberghs, 2010). Figure 2-23 and Figure 2-24 show the structure of a typical non-contact electrode and its built-in circuit. The R_1, R_2, R_3 and C_f forms the skin circuit. The conductive electrode forms one side of the capacitor, and the skin forms the other plate of the capacitor. The clothes form the dielectric material in the capacitor. The value of C_b is typically from 1nF to 100nF and is inversely proportional to the distance between the electrode and body. C_b is built by the skin and electrode. For the capacitor C_b, the two plates of the capacitor are skin and the electrode. These electrodes are extremely sensitive if the detecting layer of the electrodes is moved 100 μm away from the skin, where the capacitance of C_b changes by a factor of approximately 10 (Kato *et al.*, 2006).

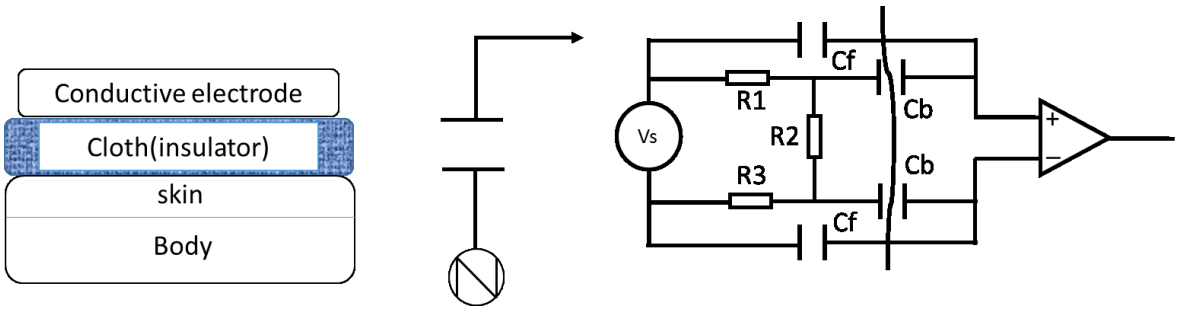

Figure 2-23: Structure and electrical model of the non-contact electrode (Lee *et al.*, 2004; Kato *et al.*, 2006).

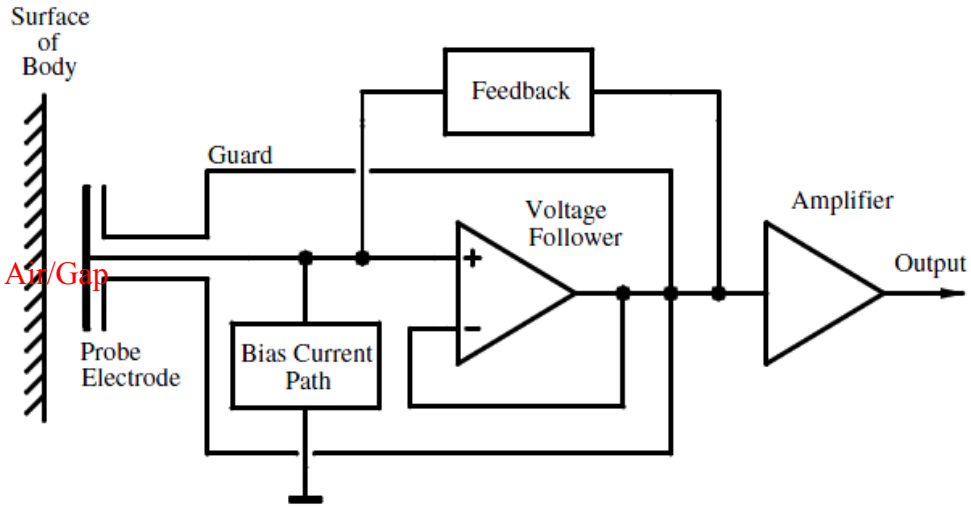

Figure 2-24: Block diagram of an electric potential sensor (or called electrode) displaying the probe electrode, the feedback, guard and the input bias circuits of the electrometer amplifier (Harland, Clark and Prance, 2002).

The following problems are much more serious for non-contact electrodes than for other electrodes (Chi *et al.*, 2010):

- Noise: the intrinsic noise from the built-in circuit. Because of the active design and small values of the signals, the noise from the internal circuit will affect the measurement results.
- Motion artefacts: Any movement will cause capacitance changes, As a result, the potential difference will be varied by the change of capacitance.
- Interference: the electrode is very sensitive at 50/60 Hz resulting from defective cables or lead wires.

Thus the manufacturing and fabrication aim to reduce the effects of these problems and allows the electrode to have a large displacement between the skin and electrode.

2.4.3.2 Manufacturing and fabrication

Recently, non-contact electrodes have been developed and implemented using two different methods. The design of a non-contact electrode is much more complicated than that of other electrodes. With the previous two electrodes, there is no circuit in the electrode. In the

literature, some electrodes are called ‘non-contact electrodes’, but they are in essence dry electrodes.

Sullivan, Deiss and Gauwenberghs (2007) present a non-contact electrode which is shown in Figure 2-25. It uses an instrumentation amplifier built within the electrode to provide large input impedance and buffer the signal. The advantage of this design is that it limits the distance from the electrode to the first amplifier, and amplifies the signal as early as possible, before noise is introduced. This reduces the interference to a minimum. In this design, there is a copper plate at the bottom of the electrode to form the capacitor with the skin. The shield is a ring around the detection plate to protect the electrode from external interference. Therefore, the bio-signal can be modelled as a voltage source coupled into the amplifier circuit through a capacitor (skin and electrode formed capacitor). The capacitance of the first capacitor is calculated as the electrode size divided by the distance between the skin and electrode.

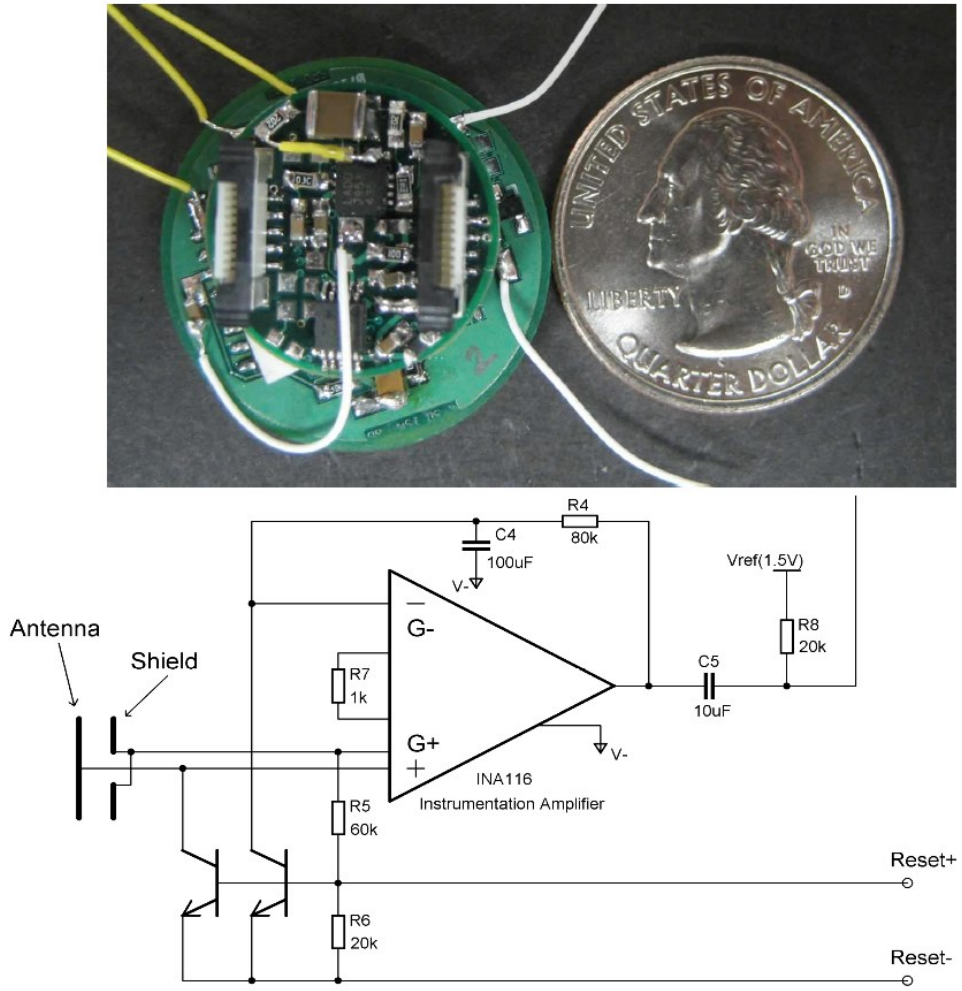

Figure 2-25: Non-contact electrode with instrument amplifier (top) and circuit schematic diagram for the amplifier (bottom) (Sullivan, Deiss and Cauwenberghs, 2007).

According to the design in Figure 2-25 (Sullivan, Deiss and Cauwenberghs, 2007), the researchers investigated the effects of varying the distance between the electrode and the skin. The authors used the overall gain as a measuring standard for the electrodes. The reason for this being that the input impedance is large and tends to infinite, so the impedance of the

skin-electrode interface can be ignored. Therefore, the voltage gain between the sensor and signal generator is measured at the output and is used to assess the effect of the skin-electrode distance. At a distance of 0.2 mm, the gain is 869, whereas at 1.6 mm, it is 539 and 391 at 3.2 mm. Figure 2-26 (Sullivan, Deiss and Cauwenberghs, 2007) shows the theoretical curve of the effect of distance on gain. It can be seen that the gain reduces to less than half the initial value when the distance is increased to 3 mm.

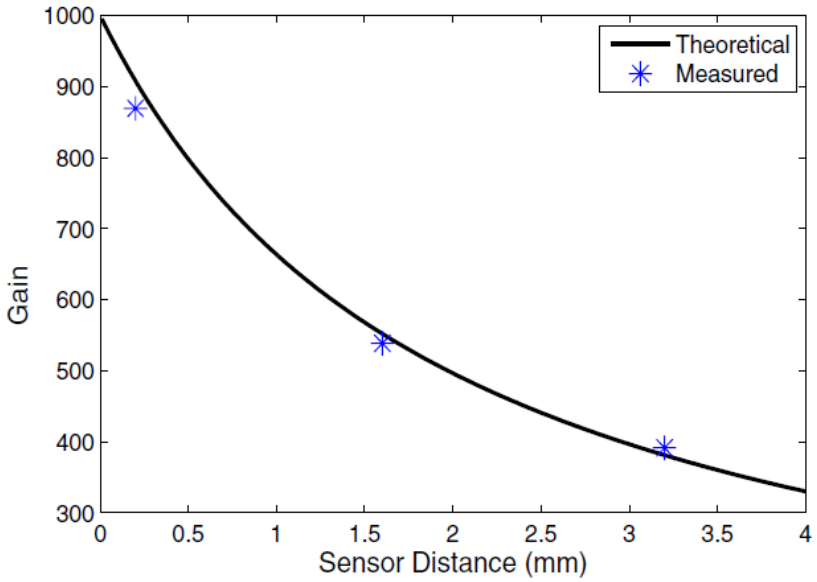

Figure 2-26: Effect of the distance from electrode to skin for the non-contact electrode (Sullivan, Deiss and Cauwenberghs, 2007).

To improve the function of the non-contact electrode, Chi et al (2010) increased the number of amplifiers and capacitor built within the electrode, as shown in Figure 2-27. In this design, there are two amplifiers in the electrode: one provides large input impedance, and the other is a buffer. The 10 nF capacitor and 10 k resistors are used to protect the input of the amplifier and isolate the output of the amplifier from the active shield. Except for the difference in the amplifying and buffer amplifier, the remaining part of the electrode measuring system is the same as Sullivan et al's design (2007).

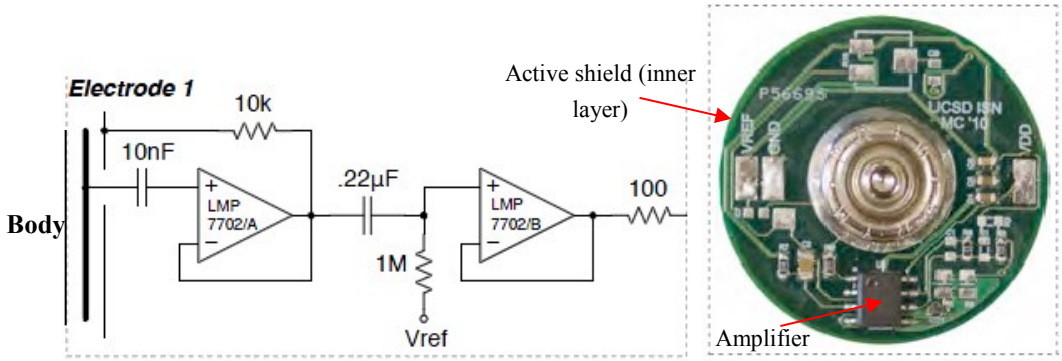

Figure 2-27: Circuit schematics of a non-contact electrode (left) and complete fabricated device (right) (Chi *et al.*, 2010).

Furthermore, Chi et al (2010) compared the non-contact and Ag/AgCl electrode. The non-contact electrode was used to measure the ECG though a cotton shirt (results shown in Figure

2-28). It can be seen that the signals can reach the clinical grade similar to the Ag/AgCl for ECG measurement. However, the electrode is sensitive to motions. This disadvantage precludes using the non-contact electrode long-term or during movement.

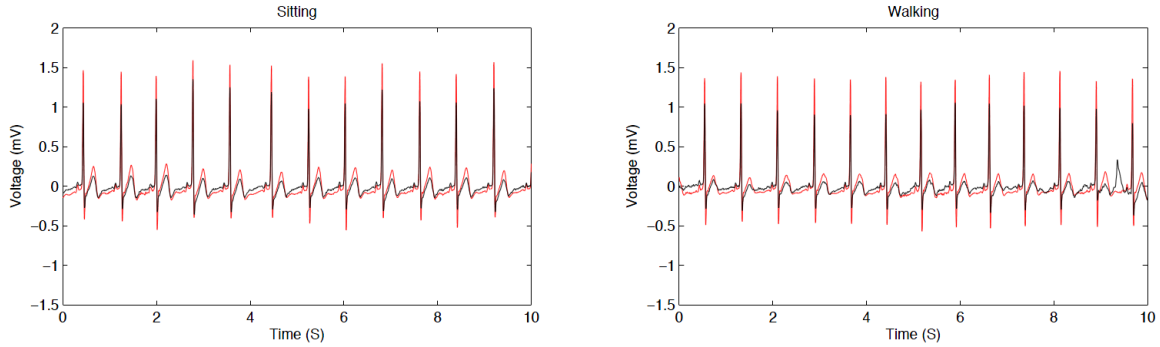

Figure 2-28: Signal comparison between Ag/AgCl (red) and non-contact electrodes (black) during sitting and walking. The non-contact electrode was placed on the chest on top of a cotton shirt.

With the development of the non-contact electrode, a new non-contact electrode developed in 2012 combined the advantages of dry foam and non-contact electrodes (Baek *et al.*, 2012). In Baek's design, the electrode has the benefits from the good contact of a dry electrode and the large input impedance of a non-contact electrode. Baek et al (2012) applied conductive foam to the contact layer of the non-contact electrode to build a new electrode as shown in Figure 2-29. The electrode was combined with an embedded amplifier, shielding block and electrode faced with dry foam. The surface of the electrode was fabricated with Polyolefine covered by polyurethane. The foam was coated with Ni/Cu on all surfaces, employing a similar structure to the dry foam electrode described in Section 2.4.2. The final size for this electrode was 16mm in diameter by 17.7 mm in height.

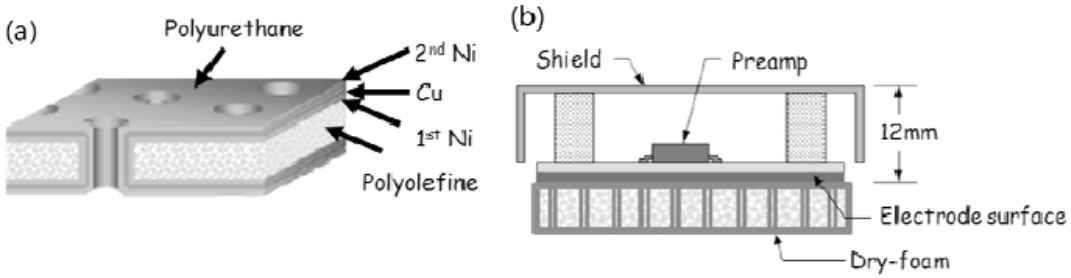

Figure 2-29: (a) the foam material used and (b) the foam surface non-contact electrode (Baek *et al.*, 2012).

The results of Baek's electrodes are shown in Figure 2-30. All the three testing electrodes in Figure 2-30 (A) were under the same conditions: all electrodes were applied with the same constant force and all the sweat was removed before the experiment. From the results, the impedances of the foam non-contact electrodes were lower than the Ag/AgCl electrodes at the hairy sites. It can thus be argued the foam non-contact electrode provides higher performance at hairy sites. In Figure 2-30 (B), the voltage gain of the foam non-contact electrode is about 2dB higher than the rigid electrode in the frequency range 0.1 to 1000 Hz. Furthermore, the electrode provides a stable gain in the frequency range from 4 to 100 Hz.

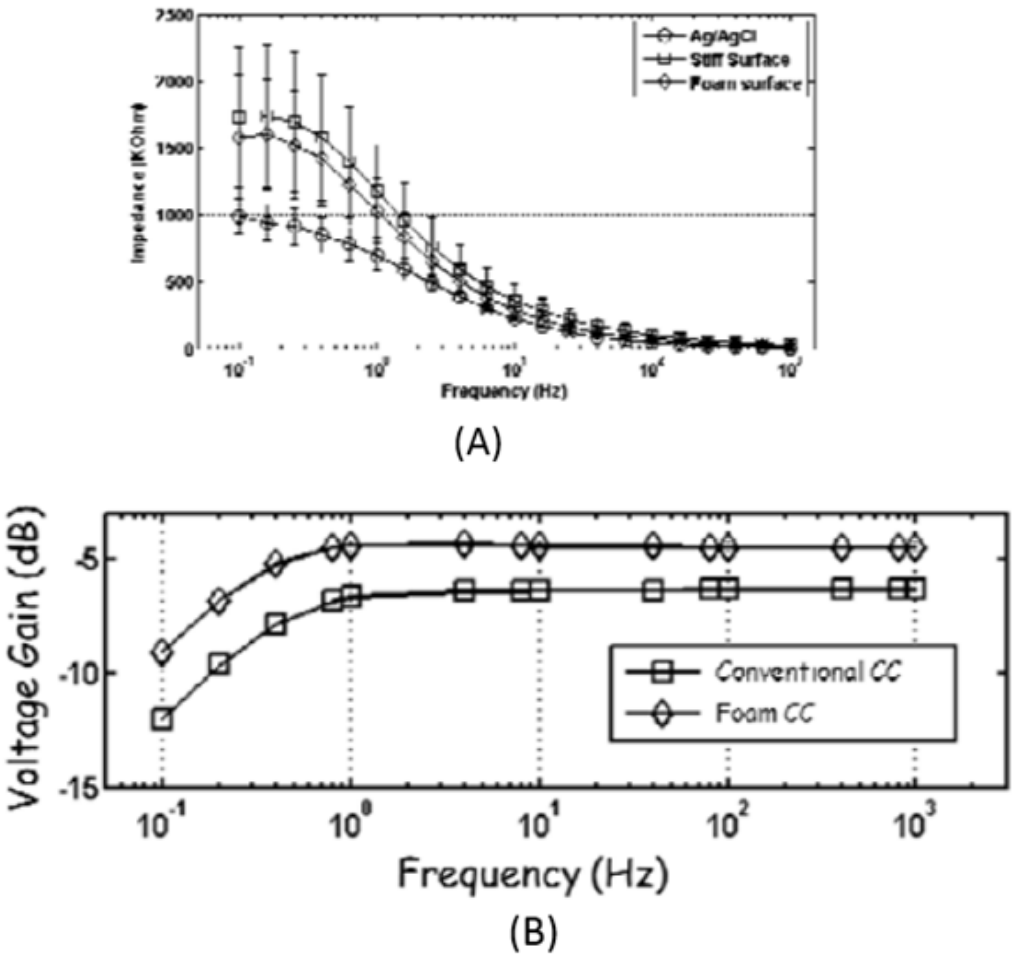

Figure 2-30: (A) Electrode surface-skin interface impedance under different frequencies. (B) Gain of the electrode (Baek *et al.*, 2012), CC means capacitive electrode. Note: Because this result was copied from the literature, the figure quality cannot be improved.

2.4.3.3 Summary of the non-contact electrode

From the review of these three non-contact electrodes it can be seen that only one literature exhibits an impedance variation as a function of frequency. Instead, the results use the power/voltage gain to evaluate the electrode performance. The output gain variation is measured instead of the impedance variation to assess the effect of electrode separation. In the non-contact electrode design, the authors integrated one amplifier circuit into the electrode. When the amplifier is in the electrode, the input impedance is infinity for an ideal amplifier. Moreover, because of the distance between the skin and electrode, if the skin-electrode impedance is used to estimate the performance of the electrode, the median or gap between the electrode and skin needs to be considered as a significant parameter that affects the results. Furthermore, because the non-contact electrode contains an amplifier inside the electrode, if this amplifier is ignored, the existing part of non-contact electrodes have a similar structure to the reviewed two electrodes. The only difference is in the material of the electrodes and the skin's properties. This improvement has the same goal as a dry electrode: finding the best material for the electrode and identifying the most significant parameters for skin layers.

2.4.4 Electrodes on Textile

2.4.4.1 Introduction

The previously described electrode types were based on traditional electronic materials. Although the traditional electrode types are suitable and already available, the electrode on textile potentially improves comfort and long-term usage. In traditional electronics, the circuit is built on a PCB and the electrode is designed using rigid materials such as plastic, or metal. This makes the electrode less comfortable than a textile electrode, which is more flexible.

In the design of electrodes on textile, the theory and analogue design are the same as for dry electrodes but little research has focused on textiles. Although textile-based electrodes are more comfortable for users, the problems of noise and the impedance between the electrode and the skin remain. Moreover, circuits on soft materials are much easier to break than PCB circuits. In particular, the edges of wire connections are easily bent in wearable electrodes. In this section, designs on textile are presented which provide solutions to overcome the problems of the discomfort of other electrode types. All textile electrodes are either dry or non-contact.

As a definition textile electrodes are made from conductive materials and stay on textile. To place the electrode on textile, the method may include weaving or printing.

2.4.4.2 Manufacturing and fabrication

Because the textile electrode can be woven or printed, the difference between these two methods is how to make the electrodes. To weave the electrodes, some conductive yarns are knitted and woven into the textile. The conductive yarns may be made with silver coated yarn or metal filaments. To print the electrodes, conductive materials are used as ink and printed on the textile. The ink may be made from silver or aluminium.

For an electrode made by weaving, aside from conductive yarns made by using different materials, another main difference is the angle between electrode yarns and textile fibres. In Figure 2-31, Pola and Vanhala (2017) listed four different textile electrodes made using different yarns. For Electrode 1, the electrode was knitted and the conductive yarns crossed on the textile. For Electrode 2, the conductive yarns were of the same direction as the textile fibre. For Electrode 3, the conductive yarns followed the warp. Electrode 4 was made by Pola from the literature. The conductive yarns were silver fibres and randomly sewed by a sewing machine. All the electrodes were of a similar size (20 mm × 50 mm).

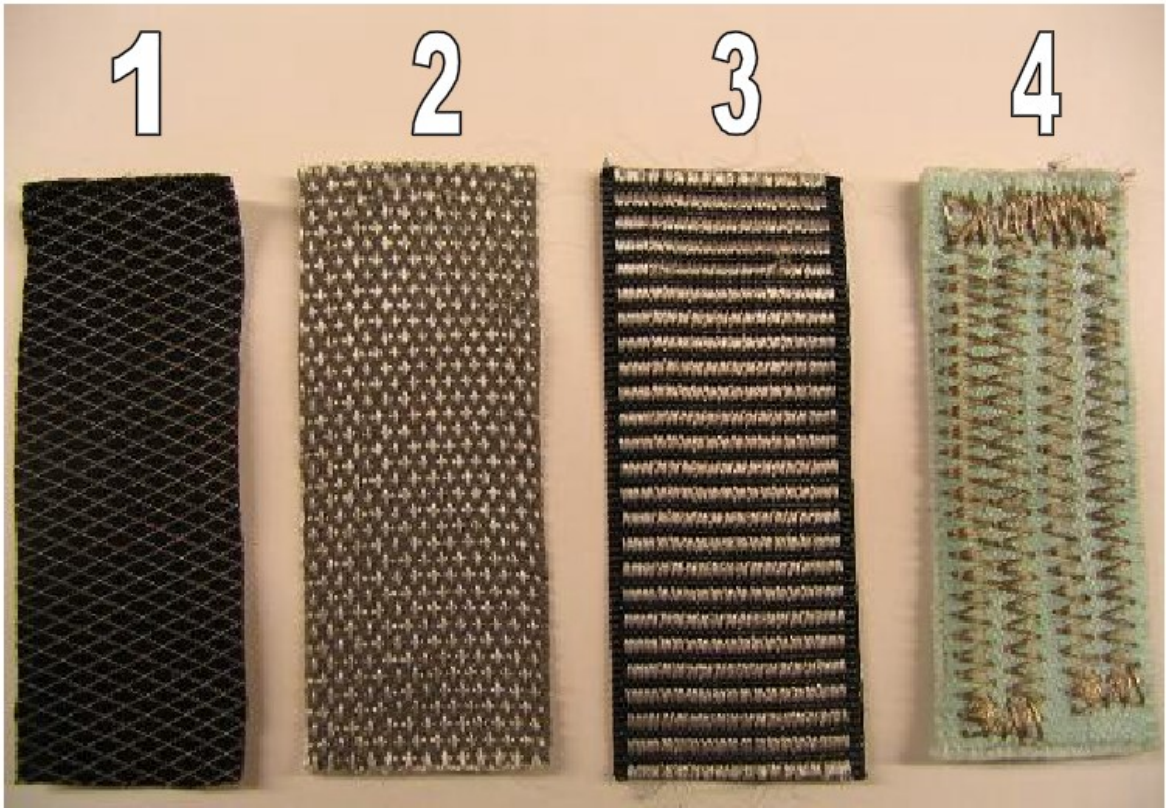

Figure 2-31: Textile electrodes made by different conductive yarns. The conductive yarns form a different angle compared to textile fibres (Pola and Vanhala, 2007).

In order to evaluate the electrode performance, the ECG signals were measured and given different weighting coefficients for the waves in the ECG signals. Table 2-4 shows the weighting coefficients for different waves. QRS-complex, P-wave and T-wave are the main elements measured in the ECG bio-signal. The evaluation was developed on a point base system, where 2 points indicate that these waves were clearly readable, 1 point indicates that the wave involves some noise, otherwise, the wave would be rated as 0 points.

	Basis of evaluation		
	2 point	1 point	0 point
QRS-complex	was found	-	not found
P-wave	was found	-	not found
T-wave	was found	-	not found
Noise level	≤ 0.002 V	0.003 – 0.010 V	≥ 0.01 V
50 Hz interference	≤ 0.002 V	0.003 – 0.010 V	> 0,01 V
Baseline (short time)	did not wander	-	wandered
Baseline (long time)	did not wander	-	wandered
Baseline level	1.6 ± 0.05 V	-	< 1.55 - > 1.65 V
R-wave peak amplitude	> 0,35 V	0.30 – 0.35 V	< 0.30 V
Stabilization time	≤ 10 s	11 - 60 s	> 60 s
R-peak amplitude variation	< 0.05 V	0.05 – 0.1 V	> 0.1 V

Table 2-4: Weighting coefficients for different waves in the ECG signal (Pola and Vanhala, 2007).

Based on the weighting table, the authors gave results for different electrode scores as shown in Table 2-5. The results show that the texture or the angle between the conductive yarns and

the textile yarns did not have an important impact on reading/identifying the signals. Furthermore, in Table 2-5, the ECG signal score of textile electrode is similar to the disposable electrode which is a benchmark or standard electrode. However, this kind of evaluation does not show the electrode performances in detail, although the sewn electrode has a higher score than the others, most of the textile electrodes have similar scores (over 1.3). It is difficult to assert the best solution for making the electrode. Moreover, in research by Pola and Vanhala (2007), the authors aimed to identify the conductive yarns' effects for medical applications but the weighting coefficients could not be used to evaluate the results.

Electrode 1	1.39
Electrode 2	1.31
Electrode 3	1.37
Electrode 4	1.54
Disposable electrodes	1.65

Table 2-5: Calculated mean average scores for all the textile electrodes in Figure 2-31, where a disposable electrode is used as the standard benchmark.

In the same year, Rattfalt, Linden and Hult (2007) aimed to determinate the suitability of three different conductive yarns for ECG electrodes. Figure 2-32 shows these three conductive yarns. Each yarn was fabricated using different methods (100 % stainless steel and knitted to the textile; 20 % stainless steel and 80 % polyester stable fibre and knitted; core pf polyester and a single twined silver plated cooper wire). To evaluate the performance of the electrode made by different yarns, the skin-electrode impedance was measured by the method in Figure 2-33 for the electrodes. In the measurements, sinusoidal signals were applied to the skin from a signal generator and provided a testing signal at 1, 10, 100, 1000 and 10 kHz. The results were measured by a Universal Impedance Bridge.

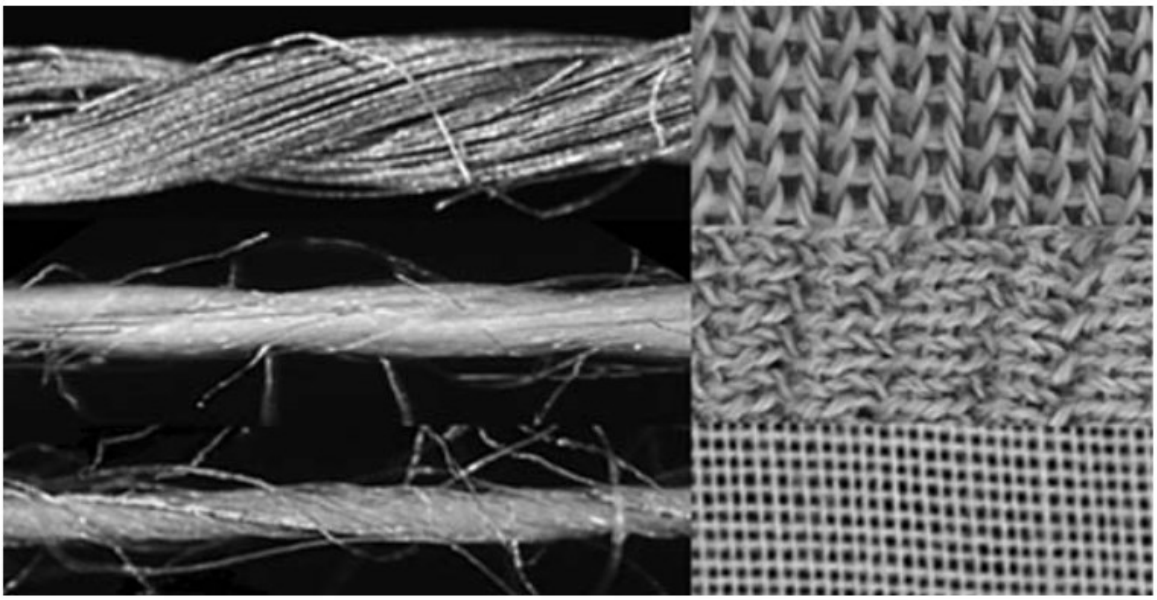

Figure 2-32: Three electrodes made by different conductive yarns. Top: 100 % stainless steel and knitted to the textile. Middle: 20 % stainless steel and 80 % polyester stable fibre. The electrode was knitted as well. Bottom: core polyester and a single twined silver plated cooper wire. The electrode was woven fabric.

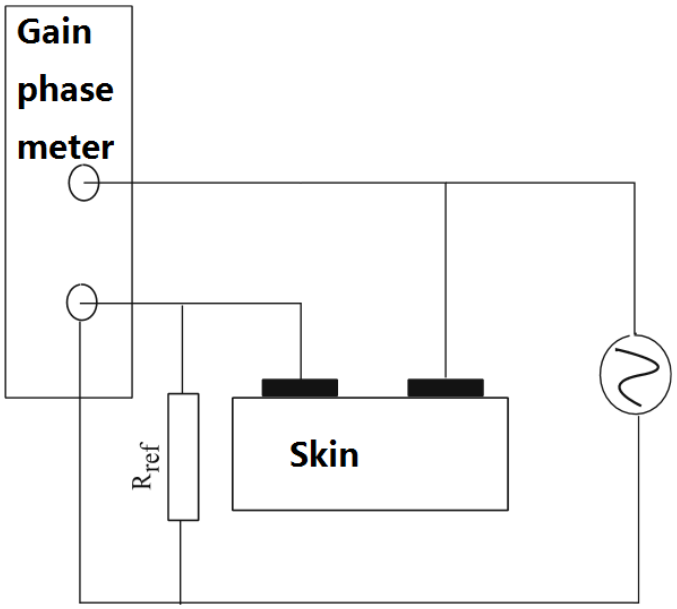

Figure 2-33: Indication of the electrode impedance measurement.

The results of skin-electrode impedances for different conductive yarns are shown in Figure 2-34, where the magnitude is used to assess the performance of the electrodes, and the phase is used to assess the stability under increasing frequency. The phase shift is generated by the charged tissue or the surface at the transition between the electrode and the electrolyte. When the phase difference of the electrode changes less as a function of frequency, the electrode has a higher stability. For all four skin-electrode impedances, Electrode B had a similar phase shift to the reference electrode and had the second lowest skin-electrode impedance under increasing frequencies. Comparing all three textile electrodes, the conductive yarns made by 20 % stainless steel and 80 % polyester staple fibres and knitted with the textile, exhibited better performance than the other two conductive yarns. Comparing the results in Figure 2-34 and Table 2-5, the performance of the different conductive yarns are shown by different methods. However, the method of measuring the skin-electrode impedance is more obvious than the weighting scores for the electrode, and the electrodes were measured in different places. Compared with the findings of previous research (Pola and Vanhala, 2007), if the electrodes are not used for the ECG measurement, the weighting score system of evaluation will miss most of its function.

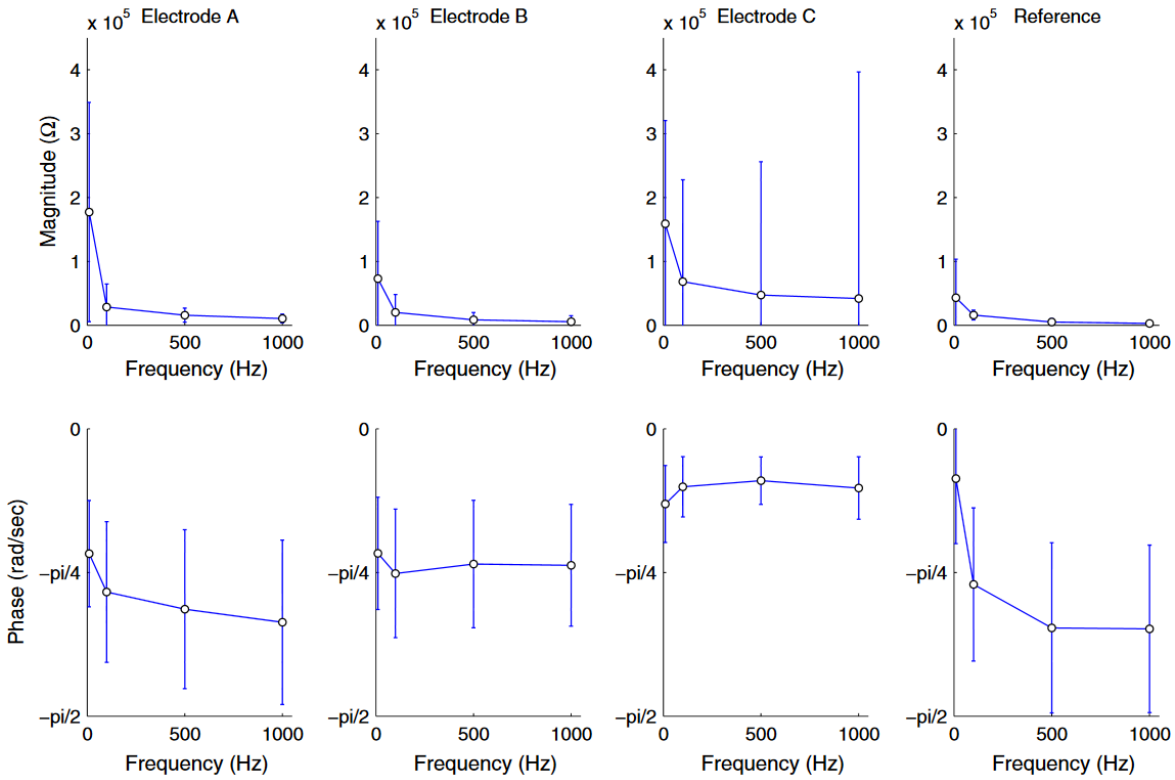

Figure 2-34: Skin-electrode impedance and phase shift for the textile electrodes with different conductive yarns. The median value ± standard deviation of each electrode is based on 10 measurements.

Moreover, aside from weaving conductive yarns to the textile, printing a conductive pattern on the textile is another method for making a textile electrode. For printing an electrode, one of the most popular methods is screen printing. Because these electrodes use screen-printing technology, the materials used in the printing procedure play the role of ink. The ink is forced through a mesh polymer with a typical image (like a circuit or patterns), and the image will stay on the textile (as in Figure 2-35). Furthermore, according to different printers, the screen mesh will be varied (e.g. the holes in the mesh will be of different sizes), hence creating variabilities in the viscosities of the ink.

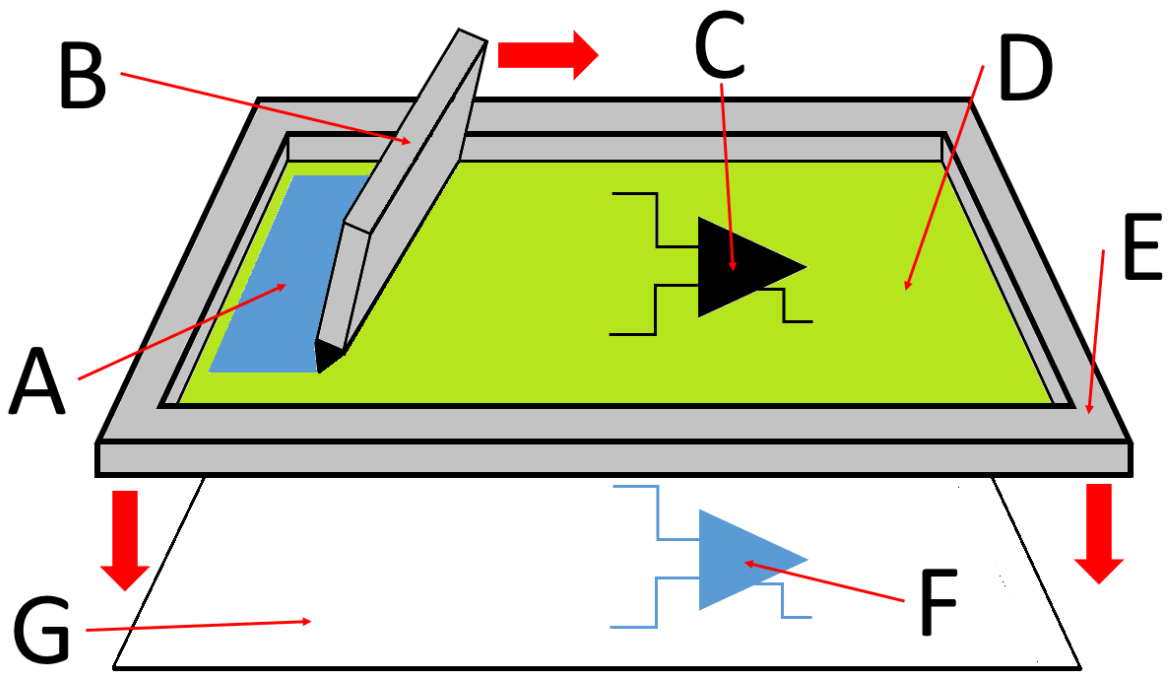

Figure 2-35: Screen printing indication: A: Ink; B: Squeegee; C: Image (circuit or patterns); D: Mesh polyester; E: Screen frame; F: Image (circuit or patterns) on the textile and G: Textile.

One of the samples shown in Kang, Merritt and Grant (2008) is a design of a textile electrode for an ECG and is reproduced in Figure 2-36. The textile electrodes favour building the front-end circuit of the electrode on the textile and using conductive silver. This design screen prints the circuit onto a textile and uses surface mount devices (SMD) for the textile circuit. This means that the electrode circuit is printed on the textile. This design contains the following layers: electrode, circuit, coating and conductive adhesive paste to attach the electrical components, as shown in Figure 2-36. The electrode layer is first printed with an Ag/AgCl ink, then, the circuit pattern is printed using Ag/AgCl ink on the other side of the textile. Next, a 1mm hole is punched to connect the electrode side to the circuit pattern side. After this, SMD components are attached to the circuit using conductive epoxy paste and coated with a dielectric material which serves as an insulating coating to prevent short circuits.

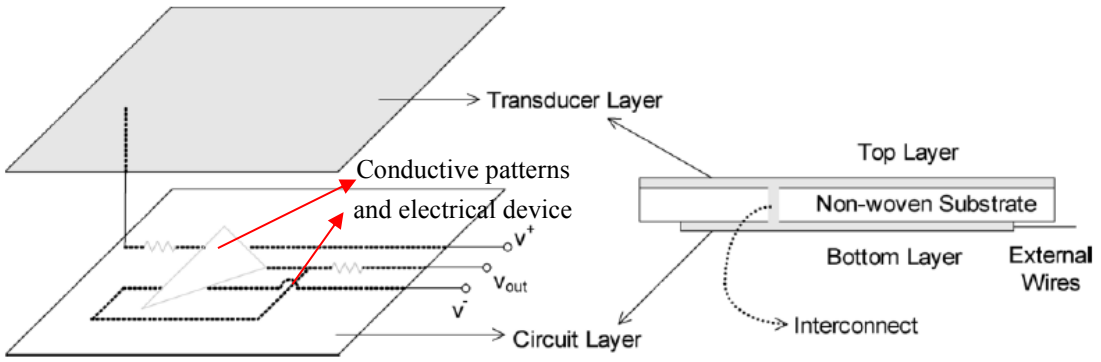

Figure 2-36: Two layer textile electrode. A hole is used to interconnect both layers (Kang, Merritt and Grant, 2008).

Figure 2-37 shows the textile electrode device made by screen printing. Screen printing is applied to print the conductive pattern on the textiles. The electrode size is 2.5 × 2.5 cm and the conductor pattern is 1.0 mm wide. The paste material is Creative Material 112-15. The thickness of the conductive pattern is 40 µm on the circuit side and 30 µm on the electrode side.

The paper's author did not make any comparison between the textile electrode skin impedance and a standard Ag/AgCl wet electrode. There is only a comparison of the ECG signal between sitting and jogging, as shown in Figure 2-37. In the application, the author only uses the ECG signal from sitting and jogging to assess the performance of the electrode, as shown in Figure 2-38. In this screen printed electrode, all the circuit patterns are printed on the textile. Comparing the design of a textile electrode with a dry electrode, it can be seen that the circuit pattern on the textile is replaced with the PCB design on the dry electrode, and the circuit becomes more flexible.

Figure 2-37: Physical structure of the electrode on textile (Kang, Merritt and Grant, 2008): (a) Circuit layer; (b) Electrode layer; and (c) Circuit layer with external wires and encapsulation.

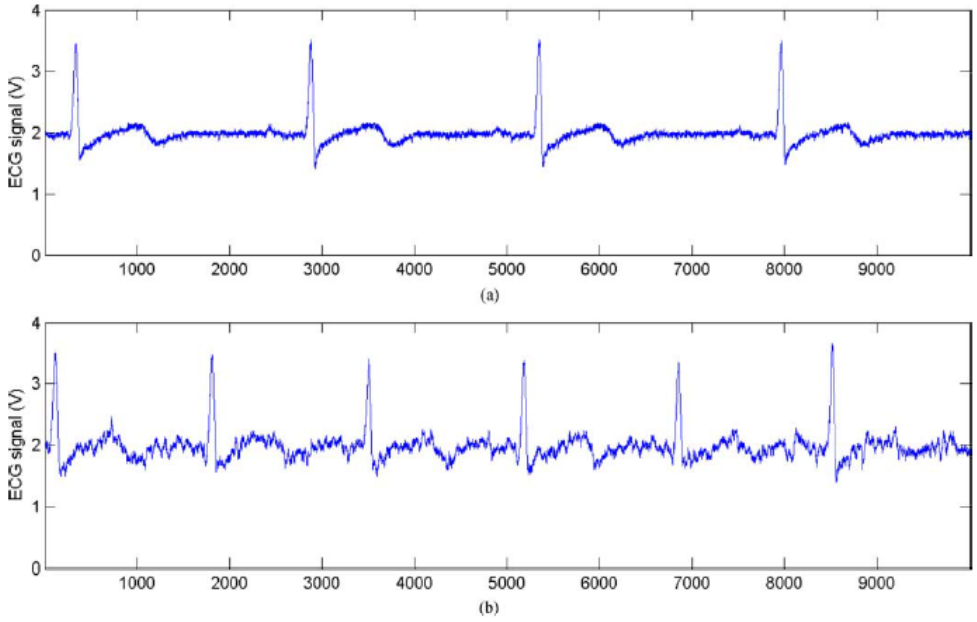

Figure 2-38: ECG signals meausred by textile electrode during: (a) jogging and (b) sitting, where the x-axis shows the sampling index with the sampling rate at 250

samples/s, that means the heart-beats is about 8 seconds in the measurement, which is a little bitter higher than the normal 6 seconds heart-beats.

Another example of a screen printed electrode is the fabric electrode array in Yang's design (Yang *et al.*, 2014). The electrodes are also printed on the textile as shown in Figure 2-39, but the main function is to apply electrical stimulation to the arm. The design of this fabric array is similar to the previous electrode, the difference is that the electrode and circuit are on the same side, so it contains multiple electrodes on one piece of textile and the external circuit will connect to the end of electrode array.

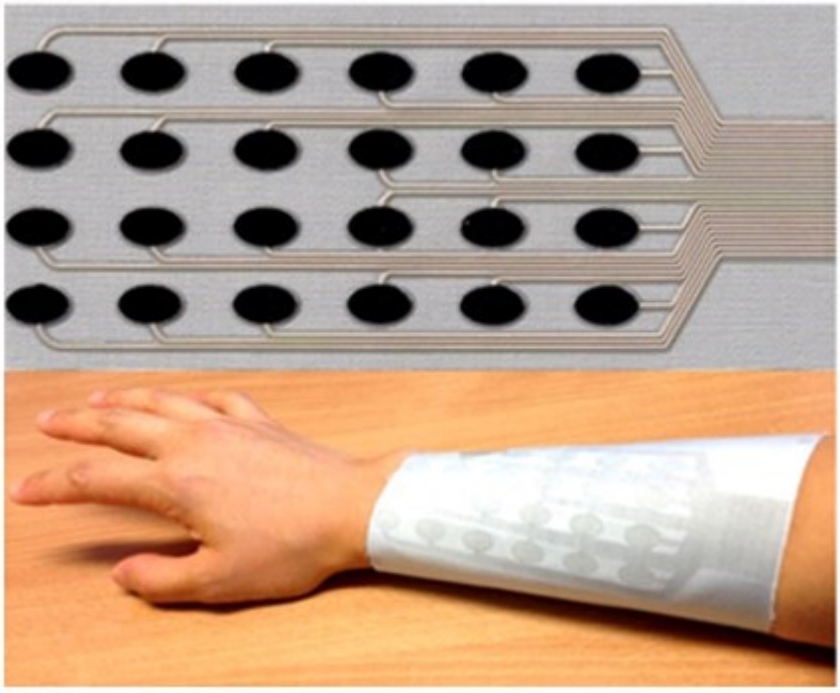

Figure 2-39: Electrode array on textile and the PCB patterns (Yang *et al.*, 2014).

Comparing the printing procedure of an electrode array with the previous single electrode, the electrode array contains more layers than the single electrode. In Figure 2-40, all the layers are printed in a sequence. With the previous single electrode, the silver is printed on the textile directly. There is no layer to provide a smooth surface like the interface layer in Figure 2-40. Moreover, because of the interface layer, the patterns on the electrode array are much finer than the single electrode as shown in Figure 2-37. The gap between the silver patterns for the electrode array can reach 0.4 mm. Hence the interface layer can help to achieve finer printing results in the screen printing procedure.

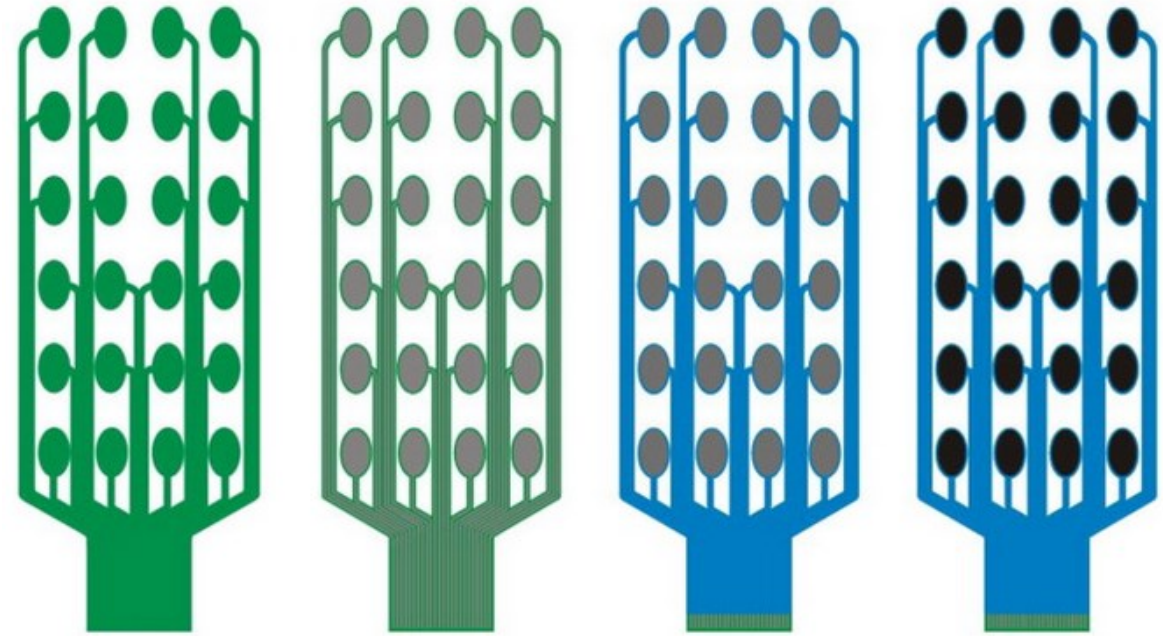

Figure 2-40: Printing of each layer from left to right: interface layer, conductive layer, encapsulation layer and carbon silicone rubber layer.

Furthermore, Yang et al (2014) measured the resistivity for the patterns on different materials (Kapton and textile) with results being shown in Figure 2-41. Kapton is a flexible polyimide film with a smooth surface. From the results, the resistances of the silver patterns on the textile with an interface are 49 mΩ/sq and the resistances of silver patterns on Kapton are 55 mΩ/sq. In the literature, mΩ/sq is used to describe the resistivity for a uniform sheet thickness. When the resistivity unit (Ω.m) divided by the sheet thickness (m), the unit becomes Ω/sq. These comparisons shows the advantages of the interface layer.

However, there was no clear evaluation of the performance for the electrode itself in this paper. The performance of the electrode was seen in terms of the comparison between an electrode array circuit and a flexible PCB array with the same electrode array design. The electrode arrays were used to measure the movement of the joint angles for hand and wrist movement. The average accuracy for the electrode array on textile was approximately 97% and the average accuracy of the PCB electrode array was approximately 98%. Thus, the textile electrode array can reach a similar accuracy to the flexible PCB electrode array.

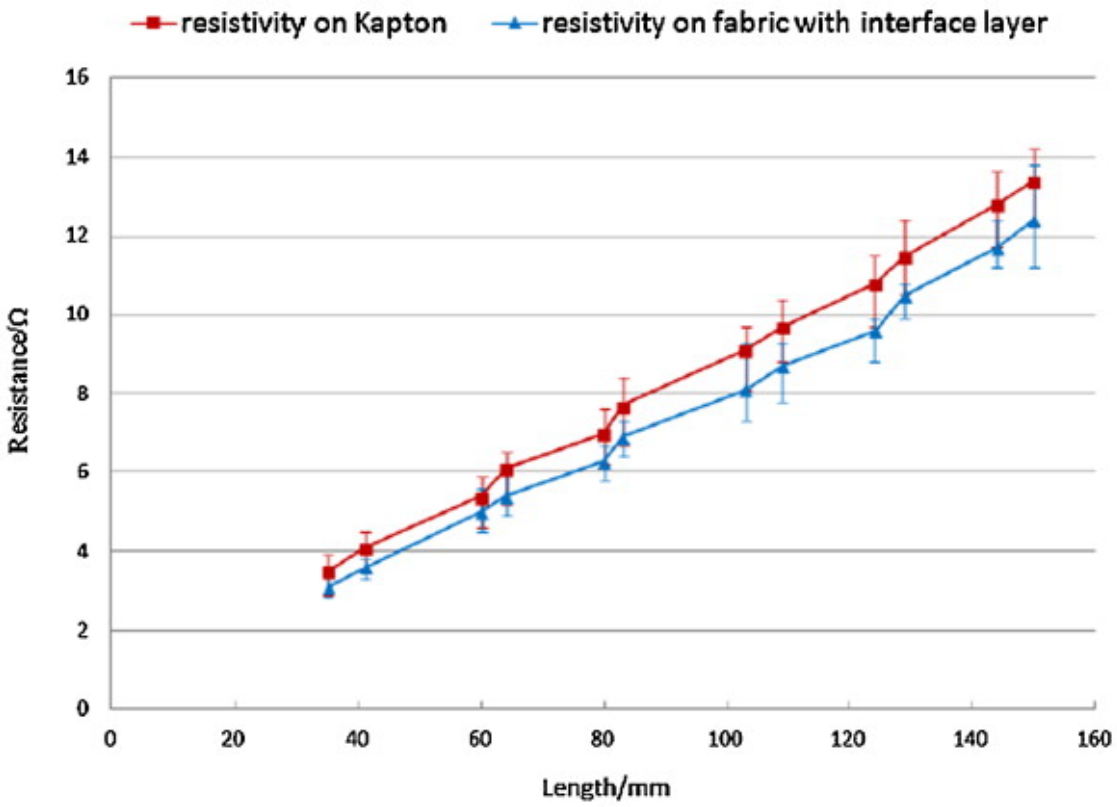

Figure 2-41: Silver circuit patterns printed on different soft materials. Note: Because this result was copied from the literature, the figure quality cannot be improved.

Although the screen printed electrodes and their circuits can reach the level of flexible PCB circuit design, there has been no comparison between electrodes on textile and traditional hard PCB circuit design.

Some designs aim to sew the PCB into the electrode to improve the design of the electrode. For example, Merritt developed an improved textile device (Merritt, Nagle and Grant, 2009). This electrode is still printed on the textile, however, the electrode circuit is built on an interposer PCB as shown in Figure 2-42. All the SMD components in the previous textile electrode are transferred to the interposer. Because the interposer is a PCB, the gap between the electrical circuit patterns is 0.4 mm. Furthermore, the same circuit on the interposer can be connected with various electrode designs with different materials or electrode sizes. Another benefit of this interposer is simplifying the textile. Therefore, the chance of circuit failure between the textile and the SMD circuit is reduced.

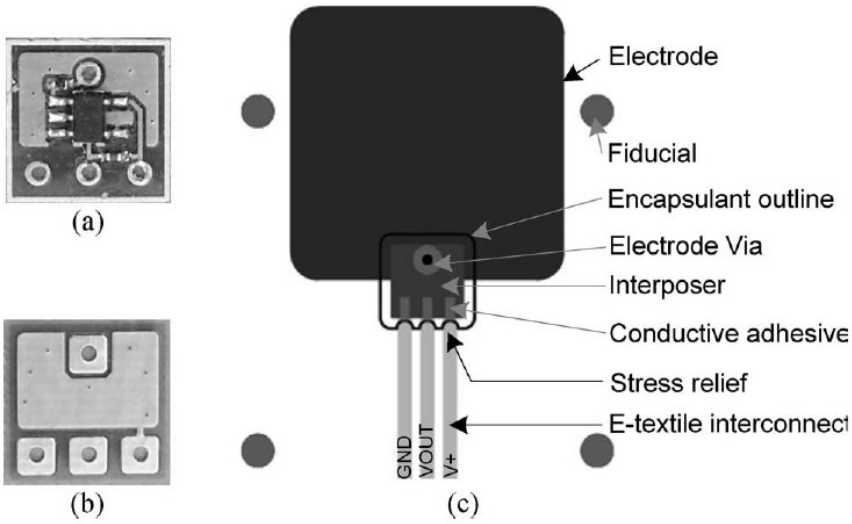

Figure 2-42: Overview of the interposer textile electrode design: (a) Top view; (b) Bottom view; and (c) Interposer implementation on a textile electrode (Merritt, Nagle and Grant, 2009).

Figure 2-43 demonstrates the fabrication of the interposer-based electrode. The dimensions of the interposer are 6.5 mm × 6.5 mm and the size of the electrode is 400 mm^2. After the encapsulation, the size of the encapsulated interposer is 11.6 mm × 11.6 mm. The interposer-based electrode is compared with the previous textile electrode, carbon rubber electrode and Ag/AgCl electrode.

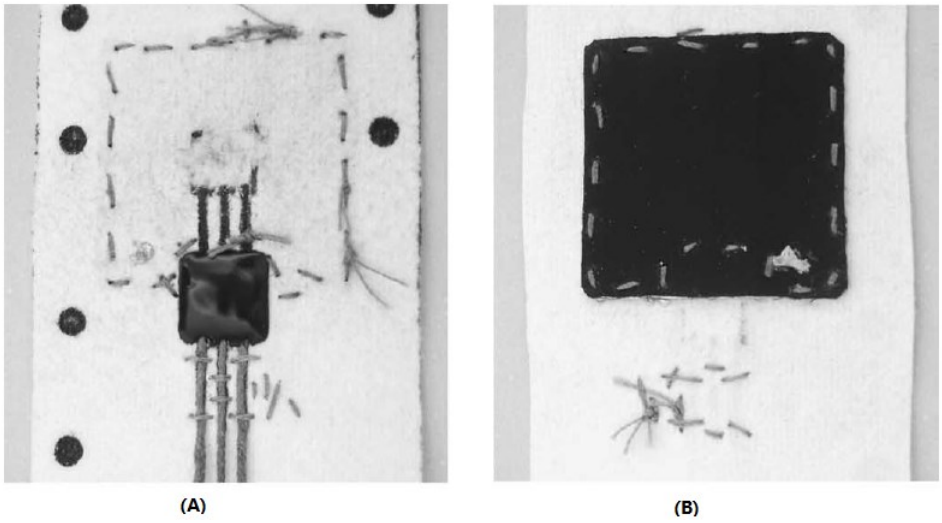

Figure 2-43: Fabrication of interposer textile electrode (a) interposer with glob top encapsulation (top view) and (b) the electrode side (bottom view) (Merritt, Nagle and Grant, 2009).

In this study, without measuring bio-signals, Merritt used power spectral density under different frequencies to demonstrate electrode performance. This method is used to present a similar function as the skin-electrode impedance under different frequencies, in wet or dry electrodes. The results are shown in Figure 2-44 and Figure 2-45. From the results, all four electrodes show similar changes from 0 Hz to 200 Hz. The interposer electrode can equal the performance of the Ag/AgCl electrode while sitting. Moreover, the author carried out a

comparison of the interposer electrode before and after washing. There is a signal comparison before and after 5 cycles of washing showing there are no major differences before and after washing. From these solutions, it can be seen that washing properties are another factor with which to evaluate textile performance.

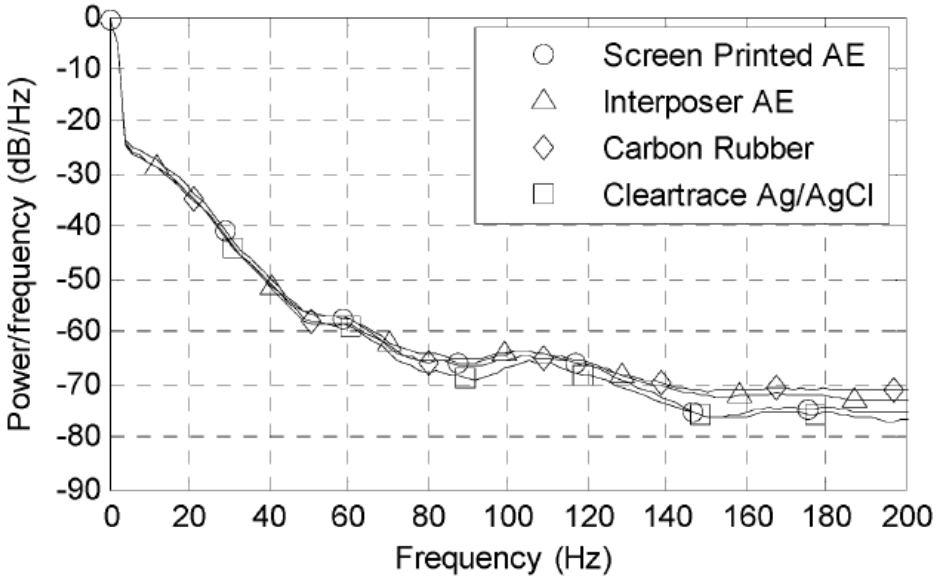

Figure 2-44: Power spectral density estimation for sitting by four types electrodes in (Merritt, Nagle and Grant, 2009).

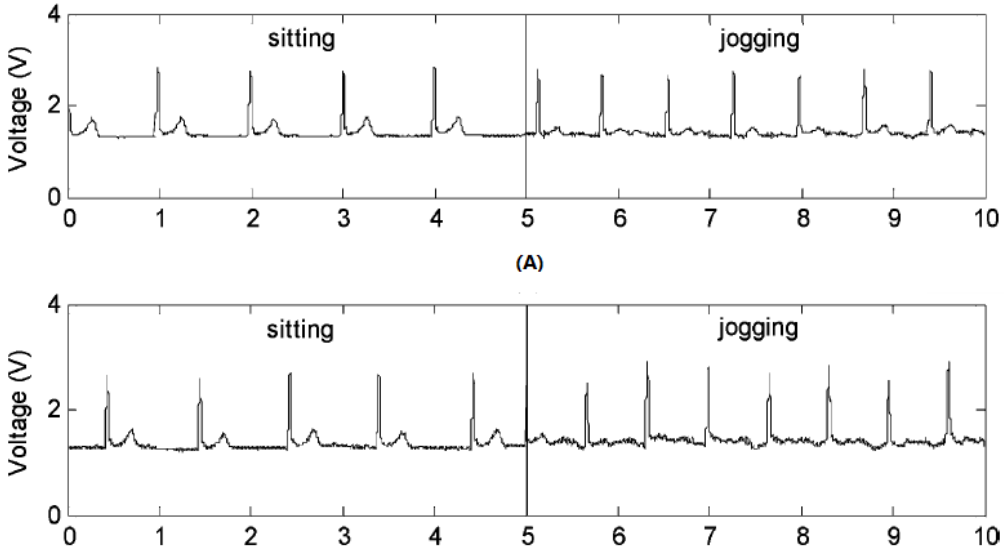

Figure 2-45: ECG recordings during sitting and jogging for 5 seconds (A) before washing and (B) after 5 circle washing (Merritt, Nagle and Grant, 2009).

2.4.4.3 Summary of textile electrodes

From the reviews of these textile electrodes, it can be seen that the only comparison has been from the signal quality during measurement. All the textile electrodes seem to exhibit a similar performance to dry electrodes. Furthermore, the skin-electrode interface shows similar measurement conditions as a dry electrode. Compared with dry electrodes, textile

electrodes are potentially suitable for long-term measurement due to their comfort and potential for integration into standard clothing.

2.4.5 Summary of electrode types

For all electrode types, different electrodes use different standards to assess electrode performance. The most common method is to place the electrode on the measurement positon, such as the EEG on the head, and then compare the signal with an Ag/AgCl electrode at the same position. In general, the Ag/AgCl electrode is used as a benchmark to identify the difference in signal quality between the two electrodes. However, different electrodes have applied other standards to assess electrode performance. For example, for dry electrodes, the skin-electrode impedance is measured across different frequencies to make a comparison with an Ag/AgCl electrode.

Table 2-6 shows the skin-electrode impedance at 100 Hz for different electrodes. It clearly shows that the wet Ag/AgCl electrode has the lowest impedance and the MEMS electrode impedance has the 2nd lowest, however, its fabrication procedure is more complex than for the other electrodes. The dry electrode provides acceptable results for electrode impedance and can be realised as a textile electrode to improve electrode efficiency. Finally, the non-contact electrode impedance is measured through cloth and cotton. It therefore has the highest impedance and capacitance.

Electrode type	Impedance
Wet Ag/AgCl	5 k ‖ 25 nF
Dry/ metal plate	1.3 M ‖ 12nF
Non-contact	305M ‖ 34 pF
MEMS	650k ‖ ---

Table 2-6: Measured skin-electrode impedances for typical electrodes (Chi, Jung and Cauwenberghs, 2010).

To summarise, if the electrode contacts the skin, the skin-electrode impedance under different frequencies is a key factor to describe electrode performance. If the electrode does not contact the skin, the skin-electrode impedance cannot be used to assess the electrode performance. If the electrode does not contain any electrical components inside the electrode, for example the wet/ dry electrode, the skin-electrode impedance can be measured directly and reflects the electrode performance. If the electrode is an active electrode, for example the non-contact electrode, the skin-electrode impedance is difficult to measure. From the signal transmission viewpoint described at the start of chapter 2, an electrode without electrical components is referred to as having a passive electrode structure; while an electrode with electrical components is called an active electrode.

2.4.6 Passive/Active electrode signal transmission

Passive electrode structure transmission has been discussed and analysed over the past 50 or 60 years and is already used in practice. A good example is the current ECG or EMG bio-signal collecting system in a hospital. The electrodes do not contain any electrical

components and are connected to the measured equipment. For the active electrode, the electrode contains an amplifier and buffer circuit inside the electrode. For clarification, the passive or active electrode are the structures used to transmit signals.

2.4.6.1 Structure of Passive/Active electrode

As described in the previous Sections 2.4.1 and 2.4.2, both conventional and dry electrodes use the passive transmission method, which means there is no circuit on the electrode. An electrode at the front-end part is a single transducer and only contains conductive material with or without conduction gel and without any electronic components. Other parts of the system, including the amplifier or filters, are on a PCB connected by wires.

As there is no electronic component in these electrodes, they do not require a power supply. In this case, the contact between the electrode and head or scalp plays the pivotal role. If the contact between the head and skin is perfect, the resistance between them can be assumed to be zero. The potential difference is amplified directly without any interference. Hence the impedance of skin-electrode interface needs to be identified as a standard to evaluate an electrode.

However, a zero-impedance contact cannot be achieved. When the electrode contacts with the skin, there will always be a finite impedance between the electrode and the skin. Furthermore, when further activities in the measurement such as movement or sweat will change the impedance between two measurement electrodes, this impedance change will cause the changes of potential difference on the skin. Furthermore, these movements may change the resistance between the scalp and electrode. Although passive electrodes are used in normal hospital equipment and daily life, all of these disadvantages limit further development and it is therefore a mature technology.

On the other hand, active electrodes contain electronic components (such the amplifier inside the electrode) which require a power supply. The feature of this kind of electrode is that it has high input and low output impedance. This property of an active electrode can lead to a reduction of interference from the connecting wires. For conventional electrodes, the noise will increase as the distance increases from the electrode to the first amplifier. This is because the connecting wire is like an antenna and will pick up outside signal electrical noise. However, if the electrode connects to the first amplifier immediately after recording, the interference from the wire will be minimised. Furthermore, for the active electrode, the amplifier is like a buffer to pass the signal to the rest of the circuit.

2.4.6.2 Manufacturing and fabrication

From the literature review, all current non-contact electrodes must have an active design in terms of the collection system. Also, some dry electrodes use the active structure to reduce noise. Figure 2-46 shows the difference between the passive and active electrode structure.

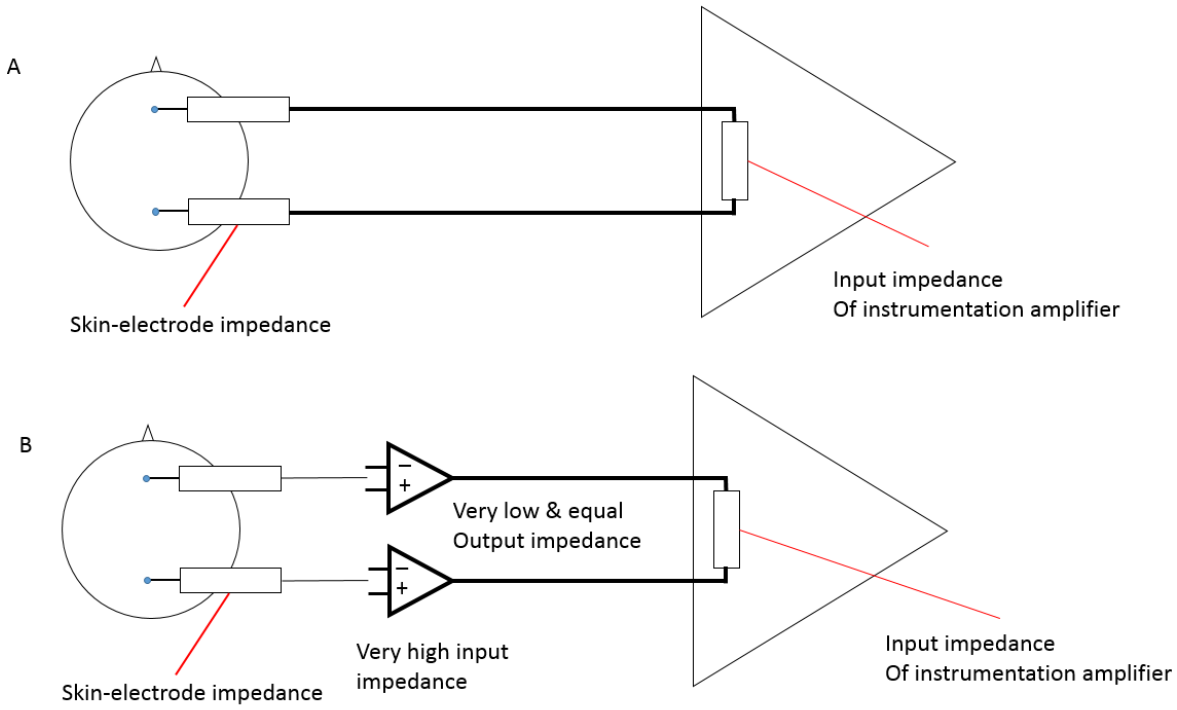

Figure 2-46: Structure of the bio-potential monitoring system using: (A) passive electrodes and (B) active electrode.

The active structure of a non-contact electrode is shown in Figure 2-47. Although different electrodes have different circuit designs, the general schematic is similar. There must be a guard or shield to reduce the noise and to protect the central elements from other electronic components such as the powered amplifiers or cables (Panek, 2013). Inside the shielding box, a buffer amplifier with a feedback loop is applied to improve the input impedance.

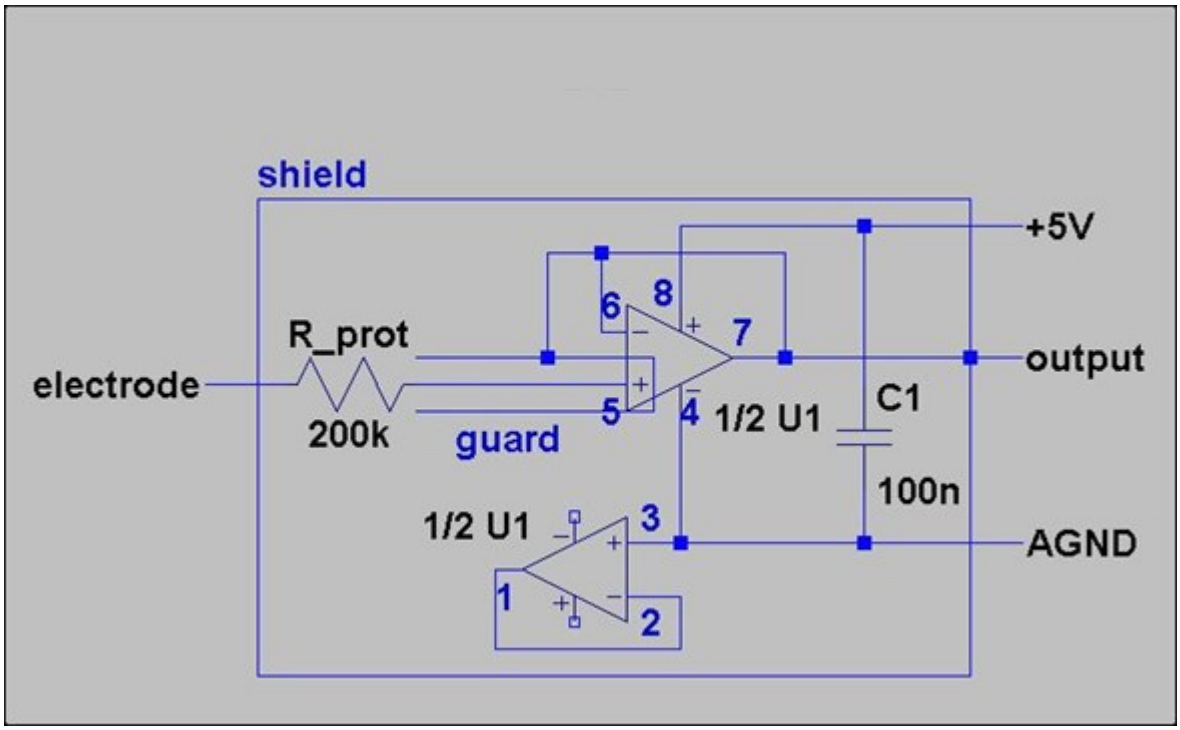

Figure 2-47: Active electrode schematic (Merritt, Nagle and Grant, 2009; Chi *et al.*, 2010).

Compared with passive electrodes, the disadvantage of active electrodes is the interference from the active components such as the buffer amplifier as shown in Figure 2-47. When the current flows to the earth, it will generate a different voltage from the body. This potential difference will result in interference with the recording signal. To overcome this interference problem, the active electrode design introduces an active shield to protect the signal from this interference. Another disadvantage is the cost and complexity of making one single electrode. Each single electrode contains one or two amplifiers and protection. This means the active electrode involves more cost and procedures than a passive electrode. However, there is no evidence that an active electrode has a longer life cycle than a passive electrode, so an active electrode does not offer any distinct advantages as a replacement.

2.4.7 Interference and interference cancellation

For all bio-potential transmission, interference is the key effect on the measured results. The interference is divided into several components, such as from the external environment (surrounding signals from cable), when the different bio-potentials are overlapped or movement during measurement. In this section, interference and interference cancellation are introduced.

2.4.7.1 Motion artefacts

The movement induced artefact is a common occurrence, when the electrode moves with respect to the electrolyte (or skin and other body tissue), the distribution of the charge on polarizable electrode interface changes. This changes the half-cell potential temporarily. Therefore, this potential difference appears on the electrodes is called motion artefact. In general, the non-polarizable electrode (like Ag/AgCl) has less motion artefact. The reason is that the non-polarizable electrode forms the structure of a resistor and current can easily pass freely through the electrode-electrolyte interface (Sawan, 2011). When movement is applied to the non-polarizable electrode, the charge distribution in the solution near the electrode surface will not be changed, therefore the effect from motion artefacts is much less than the polarizable electrode.

2.4.7.2 50/ 60Hz AC interference

This artefact occurs as a result of poor electrode contact, poor skin preparation, dried electrode gel, or defective cables and lead wires. Normally, this 50/60 Hz AC interference can be reduced by a common mode rejection/signal. More details about common-mode signal rejection are discussed when considering interference cancellation in section 2.4.7.4.2. In the one amplifying circuit, if the signal is transferred as a differential voltage or source, the common-mode signal is the half-sum of the voltages which form the following equation:

$$V_{CM} = \frac{V_1 + V_2}{2} \text{ (2-5)}$$

In the bio-signal measurement, V_1= voltage crossing the impedance of the electrode, V_2= is the voltage crossing the internal impedance between the measuring electrode and the reference electrode.

2.4.7.3 Other interference

There are another two ways for electric and magnetic interference to couple with bio-signal recording systems (Basic & Emerging Systems Technology, 1976; Heuer and Fuhrhop, 2015):

1) Variable magnetic fields
2) Capacitive coupling to electrode leads

The magnetic fields generate a voltage via the electrode leads and inside a person's body. The intensity of the magnetic fields is large enough to affect the differential voltage even if the electrode leads are short or the leads are twisted when they are long. The capacitive coupling of the electrode leads and a person's body is caused by the electrical fields flowing through the patient to the earth. However, the most significant interferences are motion artefacts and 50/60 AC interference.

2.4.7.4 Interference cancellation

From the previous two subsections, interference or noise is from the electrode itself and the environment. To deal with these two problems, one solution is to improve the design of the electrode, which could act against the interference; additional methods are impedance matching and a Driven Right Leg (DRL) circuit.

2.4.7.4.1 Impedance Matching

As the name implies, the aim is to make the two impedances (skin impedance and electrode impedance) match. The reason for this is that the maximum power-transfer theorem states that to transfer the maximum amount of power from a source to a load, the load impedance should match the source impedances (Todorow, 2009). Furthermore, the signal reflection can be minimized by the impedance matching. The signal reflection occurs when the signal is transmitted through a transmission medium (like cooper cable). Some of the source signal may be reflected back to the original rather than being carried by the transmission cable. This concept could be used to explain the bio-signal transmission.

For an AC source, the internal impedance (Z_g), cable impedance (Zo) and driven load impedance (Z_L) are shown in Figure 2-48.

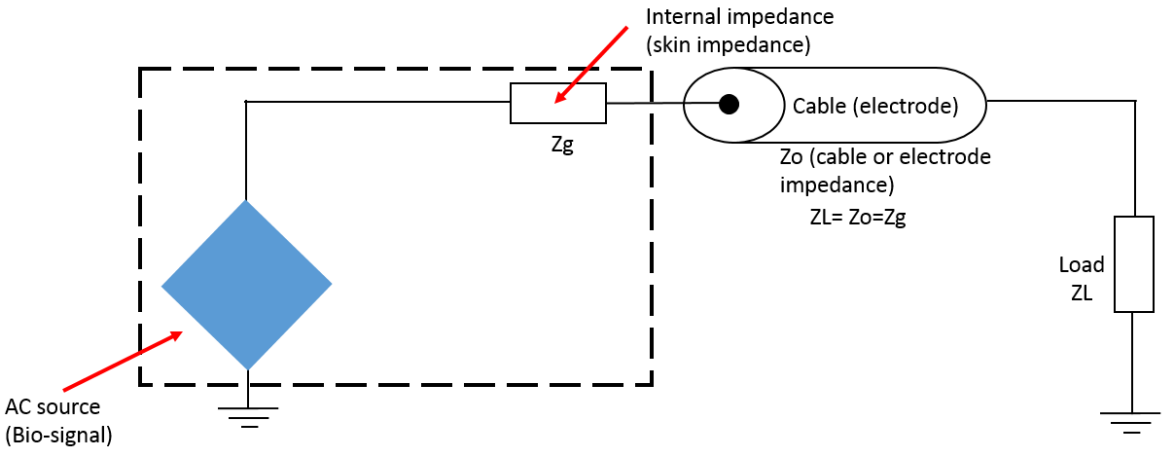

Figure 2-48: Indication of source, transmission line (electrode) and load impedance analysis.

The transmission line (electrode) has the impedance (Zo) that's a function of the line's (electrode's) inductance (L) and capacitance (C):

$$Z_o = \sqrt{L/C} \quad (2\text{-}6)$$

When the transmision impedance matching the internal impedance, the transmission power will achieve the maxium power as shown in Figure 2-49.

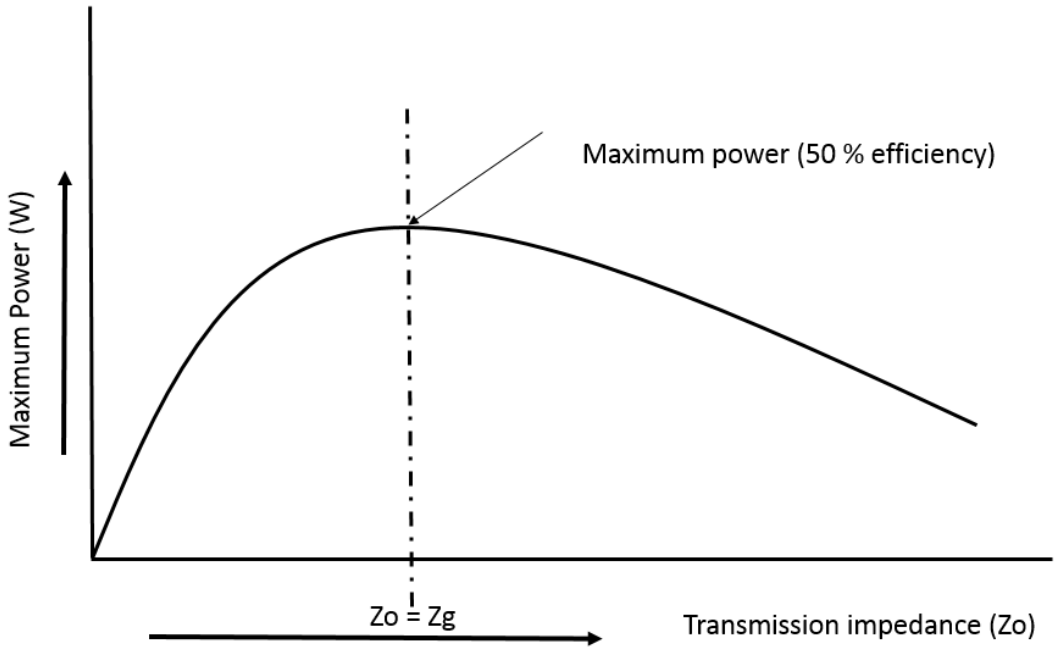

Figure 2-49: How impedance match works. The maximum power to the transmission line is approached by matching the transmission line impedance and source impedance.

Therefore, to achieve the maximum power transfer over the transmission line (electrode), the line (electrode) impedance must match the source and load impedances. Alternatively, if the transmission line (electrode) has zero impedance, the load impedance only needs to

match the internal impedance (skin impedance), meanwhile, the maximum power can be reached by matching internal and load impedance.

If the impedance cannot be matched, the maximum power will not be delivered. Therefore, the load doesn't absorb all the signals sent by the line.

2.4.7.4.2 Driven Right Leg (DRL) circuit

For a bio-signal recording system, a common ground for the whole system is required. However, the body of the patient cannot be used as a ground for the recording system due to internal body potentials. It is necessary to associate the reference circuit (human body) with the recording system, which is the purpose of a DRL circuit, The DRL circuit was introduced in 1983 (Miklavcic *et al.*, 2006) and is implemented in all modern bio-signal recording systems. Because of the small magnitude of bio-signals, the DRL circuit reduces the magnitude of the common-mode voltage by driving the AC voltage of the patient close to the electrical cable of the amplifier.

Figure 2-50 shows the basic electronic circuit required for a bio-potential recording system (Clapers *et al.*, 2011). According to the circuit, if the voltage on each recording electrode (V_{e1} and V_{e2}) and the common-mode input impedance (Z_{c1} and Z_{c2}) of the input terminal of the differential amplifier are unbalanced, there will be a common-mode voltage causing a voltage difference at the two inputs of the amplifier (Z_{c1} and Z_{c2}). In the instrumentation amplifier, the Z_{e1} and Z_{c1} or Z_{e2} and Z_{c2} form the ratio of the common mode rejection ratio (CMRR), which depends on the manufacturer of the amplifier and the external electrode impedance. As the CMRR increases, the circuit will have less common-mode voltage. On the other hand, reducing the impedance of Z_{e3} will allow the power-line current to pass through the reference electrode. This is another method to reduce the common-mode voltage.

If the DRL circuit is added, current flow will pass through the output side of the DRL amplifier due to the low input impendence. Also, the common voltage will go from the input side of the DRL amplifier, which means the voltage, will pass and be added to the body. Because the differential potential between two points is to be measured, the additional noise signal will be cancelled. Figure 2-51 is an example explaining the common-mode voltage in a DRL circuit.

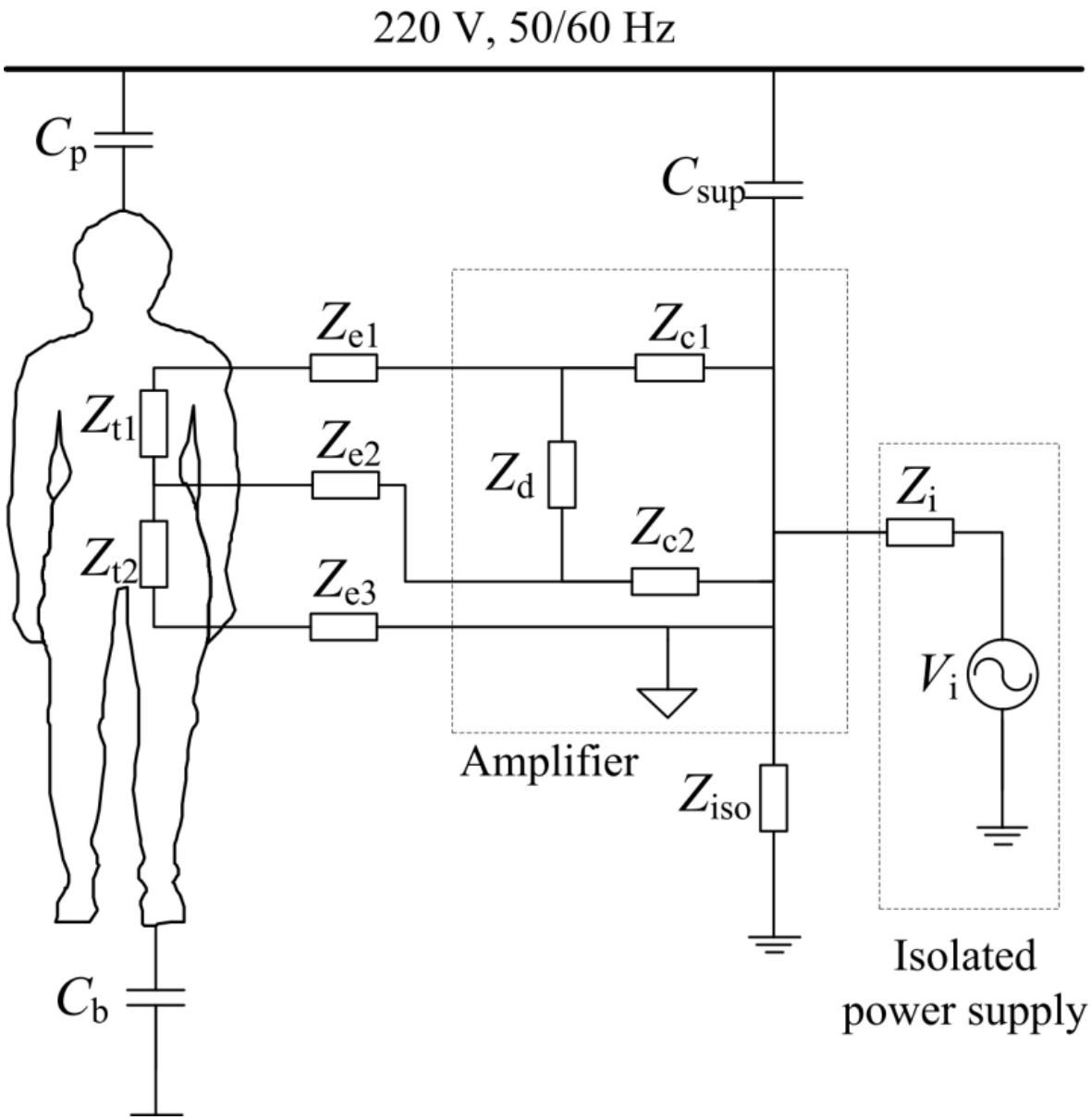

Figure 2-50: Circuit model for interference coupling in bio-potential amplying circuits (Clapers *et al.*, 2011).

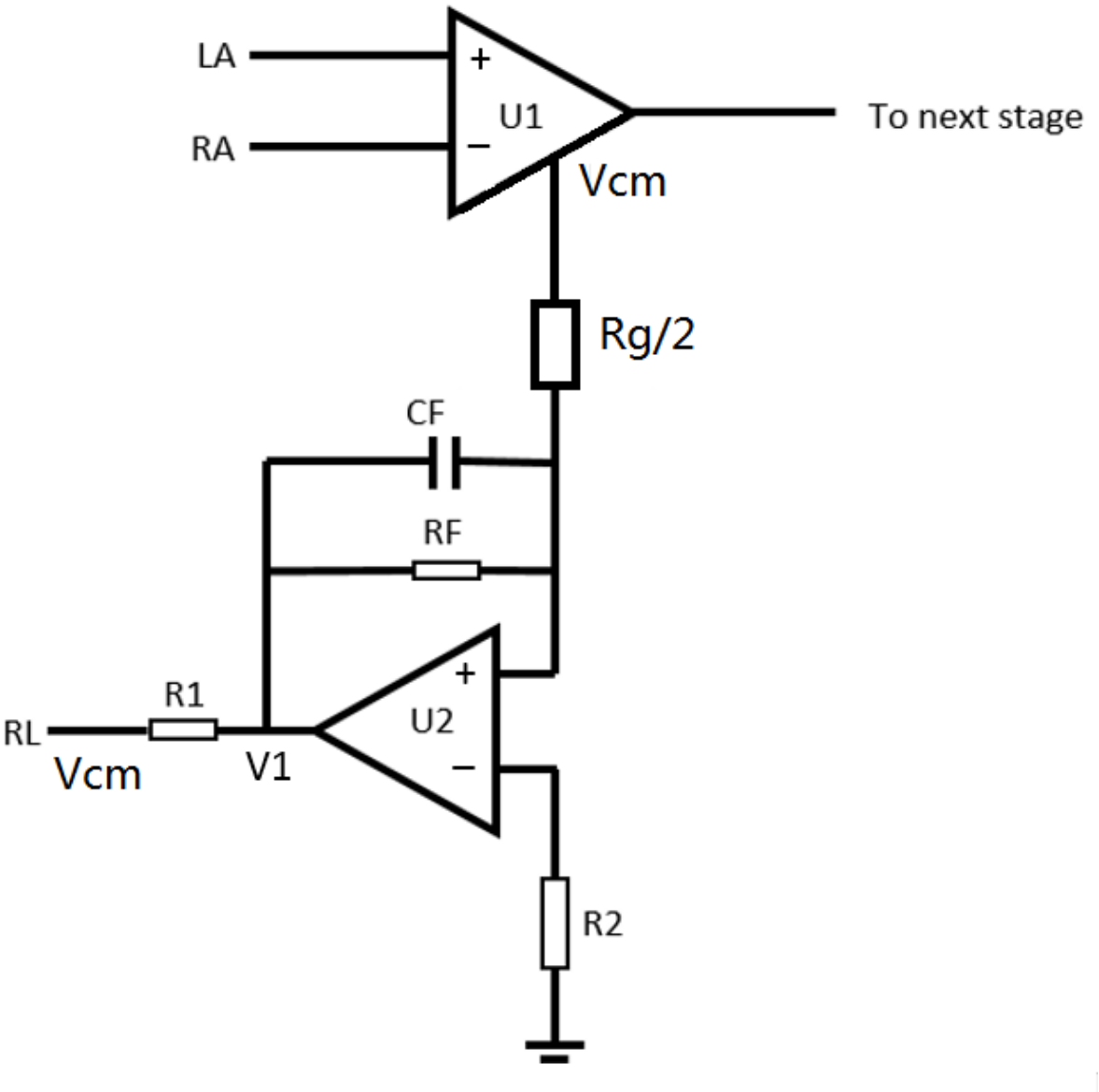

Figure 2-51: Driven right leg (DRL) circuit, where RL is the driven electrode and R1 is the impedance of the electrode (Yang *et al.*, 2012).

In Figure 2-51 the common-mode voltage (V_{CM}) is sensed by a calculated resistor $\frac{Rg}{2}$ (where Rg is the internal resistor in the operational amplifier (U1)) and an amplifier and is connected to the right leg of the body being monitored (David and Michael, 2005). This negative feedback limits the common-mode voltage between the amplifier and the body to zero. In Figure 2-51, the current passed through $\frac{Rg}{2}$ has the following equation:

$$i_{CM} = \frac{2V_{CM}}{Rg} \quad (2\text{-}7)$$

Furthermore, the current passed through R_F has the following equation:

$$i_F = \frac{-V_1}{R_F} \quad (2\text{-}8)$$

According to KCL (Kirchhoff's Current Law), $I_{CM} = I_F$, the equation becomes:

$$V_1 = \frac{-2R_F}{R_g} V_{CM} \text{ (2-9)}$$

Also, the voltage at RL is V_{CM}, so we have the following equation:

$$V_{CM} = V_1 + i_{RL} R_1 \text{ (2-10)}$$

$$\rightarrow V_{CM} = \frac{-2R_F}{R_g} V_{CM} + i_{RL} R_1$$

$$\rightarrow V_{CM} = \left(\frac{R_1}{1 + \frac{2R_F}{R_g}} \right) \cdot i_{RL} \text{ (2-11)}$$

The V_{CM} is affected by the $(\frac{R_1}{1+\frac{2R_F}{R_g}})$. If the R_F is much larger than R_g, the common model voltage will go to zero. The DRL circuit effectively improves the CMRR of the circuit.

From these two interference cancellation methods, researchers aims to use the additional and external circuit to reduce the effect from noise. However, the skin conditions is another variable in the measurement. Hence the next section discusses the skin and skin-electrode interface in the bio-signal recording.

2.5 Skin and skin-electrode impedance analysis

From the review of different electrode types and bio-signal recording procedure, the skin and skin-electrode interface are the significant parameters which affect the measurement results. For example, the electrical properties of skin (like conductivity or dielectric constant etc.) may be different for different persons or the applied force on the electrode may generate different measurement results. If the electrode contacts the skin, the skin-electrode impedance is the key factor used to evaluate the performance of the electrode. Analysing the skin impedance and making the results optimal for skin impedance are the key factors in the implementation of an electrode. The skin impedance is different from one person to another. The value of the impedance between two skin surface electrodes is usually used to describe and evaluate the performance of an electrode. The skin impedance is negligible if:

- The applied voltage is high enough for skin electrical breakdown
- The skin is completely wet
- The effective skin contact area is very large
- The applied signal frequency is very low or very high

Thus it is important to understand the effects of skin layers, and identify which part will be the most important during the skin impedance measurement. From the top to the bottom of the skin, there is the following structure: stratum corneum (SC), epidermis (E), dermis (D), hypodermis (HYP) and muscle (M). All the details of the skin are shown in Table 2-7.

.

Skin layer	Properties of skin layers					
	Thickness (mm)	**Young's Modulus (MPa)**	**Conductivity (S/m)**	**Density (kg/m^3)**	**Poisson ratio**	**Dielectric Constant/Relative permittivity**
Stratum Corneum(SC)	0.019-0.022	1.99-3.2	0.000125 - 0.000455	1050	0.43∓0.12	1140 - 6600 (averaged SC from 1000 Hz to 10 Hz) 10×10^4 (2 Hz) to 10×10^7(2 Hz include lowing layers)
Epidermis (E)	0.05 - 0.15	0.134-1.0	0.55 ± 0.2	1020	0.48	1.14×10^3
Dermis (D)	1.2 - 2	0.02 - 0.08	2.9 ± 0.33	1900	0.48	1.14×10^3
Hypodermis and fat (HYP)	4 - 6	0.2-2	0.02-0.04	1800	0.48	1.2×10^7 (at 10 Hz) 3.3×10^5 (100 Hz) 1.2×10^4 (1000 Hz)
Muscle (M)	10 - 40	1.33-2.21	0.04-0.8	1120	0.45∓0.1	2.5×10^7 (at 10 Hz) 9.3×10^6 (100 Hz) 4.32×10^4 (1000 Hz)

Table 2-7: Different mechanical and electrical properties of the skin layers for the stratum corneum (SC), epidermis (E), dermis (D), hypodermis and fat (HYP) and muscle (M) (Agache *et al.*, 1980; Tavernier, Dierickx and Hinsenkamp, 1992; Chen *et al.*, 1996; Hendriks, 2001; Flynn and McCormack, 2008; Geerligs, 2009; Bazzazi and Sadr, 2010; Huclova, Erni and Fröhlich, 2012; Hara *et al.*, 2013; Gabriel, Gabriely and Corthout, 1996).

- **Stratum Corneum (SC)**

The Stratum Corneum (SC) is the outermost layer of skin, which is used to protect the skin from the harmful environment (Ponec *et al*, 2003). The thickness of the stratum corneum (SC) is approximately 10 μm (0.01 mm) to 1 mm or more depending on the person and location on the body. The thickest SC only occurs at the soles of feet or the palms of hands. The typical SC thickness relevant for ECG or EMG at the typical measuring place such as the chest or forearm is 0.019 to 0.022 mm as shown in Table 2-7.

- **Epidermis (E)**

The epidermis contains 4 or 5 layers according the region of skin to be measured, which are the stratum lucidum (only in palms and soles), stratum granulosum, stratum spinosum and stratum Basale/Germinativum (Marks and Miller, 2006).

- **Dermis (D)**

The dermis is the skin layer between the epidermis and the hypodermis layer, it contains the connective tissue and is used to protect the body from the stress and strain (James *et al*, 2005).

- **Hypodermis (HYP)**

This skin layer is located under the dermis layer immediately and is used to storage people's fat. Furthermore, this layer contains more blood vessels and nerves than other layers (Kita, 2019).

For different people or measuring equipment, these skin layers will decide the skin impedance. Furthermore, because the interference from high frequency (over 1000 Hz) has been removed by the low-pass filter in the measurement circuit, the skin-electrode impedance and interference impedance are only important at low frequency.

2.5.1 Electrical model of the skin and skin-electrode interface

For skin impedance analysis electrical bio-impedance measurement is often used. Because biological tissue (like skin) contains cells and the cells are encircled by conductive fluids, biological tissue can be represented by an electrical circuit with resistors, capacitors and inductors. In most of the relevant literature, the electrical properties of human skin have been modelled using Cole-Cole equations. Using the Cole equations (see below), the skin details are represented 4 parameters: R_0, R_∞ , α and τ.

$$Z(\omega) = R_\infty + \frac{R_0 - R_\infty}{1 + (j\omega\tau)^\alpha} \quad (2\text{-}12)$$

This equation represents the cell shown in Figure 2-52. In Figure 2-52, the cell membranes become the capacitors. When the frequency is zero, the circuit becomes an open circuit, and the current flow will pass through the space between each cell. The impedance of the equation becomes R_0. When the frequency is very high (over 100 kHz), the circuit is short-circuited, and the current will pass through the cell. The impedance of the equation becomes R_∞. Figure 2-53 shows the the Cole diagram.

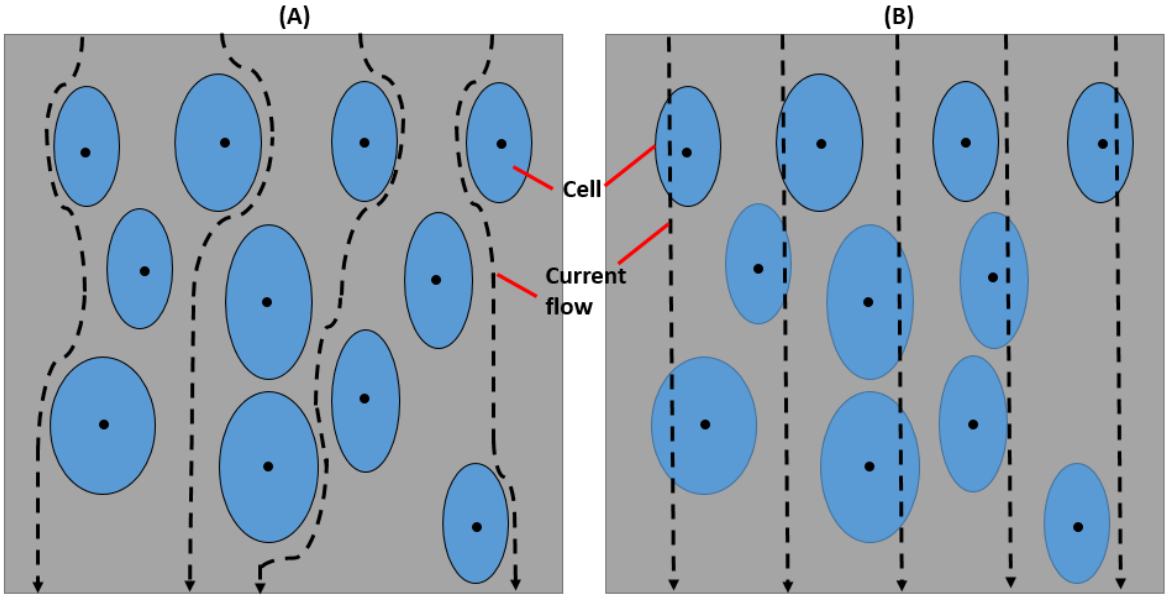

Figure 2-52: Current in the bio-logical tissue at different frequencies: (A) current flow at low frequency and (B) current flow at high frequency (López, 2011).

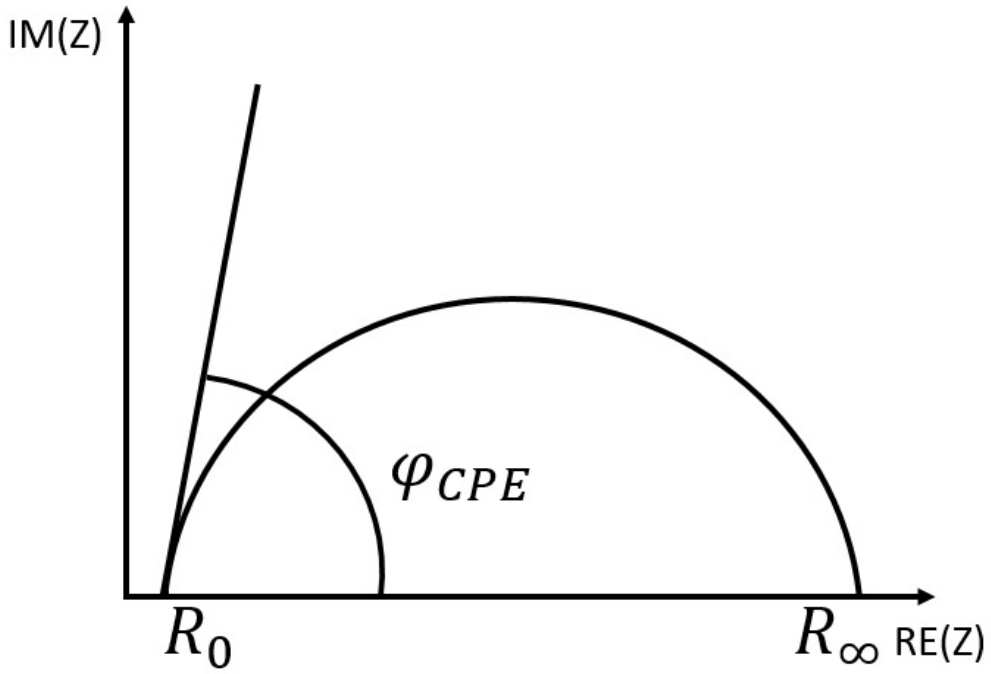

Figure 2-53: Cole diagram used to determine the 4 parameters for equivalent skin impedance (R_0, R_∞ , α and τ).

In Figure 2-53, the φ_{CPE} is the constant phase element, which forms a fractional capacitor (the phase angle between 0° to -90° and the circuit remains constant with frequency), and its impedance has the follow function:

$$Z_{CPE} = \frac{1}{(j\omega C)^{\alpha}} \quad (2\text{-}13)$$

Where, C is the capacitance, and α is the exponential value between 0 and 1.

Furthermore, in the Cole diagram shown in Figure 2-53, the φ_{CPE} has the following equation, which is used to determinate α.

$$\varphi_{CPE} = \alpha \frac{\pi}{2} \quad (2\text{-}14)$$

Moreover, when the IM (Z) is at its maximum, the frequency is maximal and equal to 1/ τ.

Based on the Cole equations, the skin and skin-electrode impedance can be described using the mathematical equations, and these equations can be used to simulate the skin and skin-electrode interface and are able to support the simulation for the skin and skin-electrode impedance. Furthermore, in these skin equations, the impedance is defined and calculated from the electrical properties of the skin or skin cell (like dielectric constant or conductivity). If the skin's electrical properties are measured or calculated for different people, this will provide a more accurate estimate of the skin's impedance.

2.5.2 Measurement of the electrode model of skin impedance

Because the skin impedance can be represented by electrical components, some measurement methods, called the two or four electrode measurement, are used to identify the parameters (R_0, R_∞ , α and τ).

In the two-electrode measurement shown in Figure 2-54, a single frequency impedance measurement is applied to obtain the impedance of the skin. An ideal differential amplifier is used to measure the potential differences caused by the current through the biological tissues and the electrodes. In the measurement, Z_m is the total impedance of the tissue impedance (Z_{TUS}) and the impedance between the skin and electrodes (Z_{ep}). The total impedance (Z_m) can be calculated by the following equations.

$$Z_m = \frac{V_m}{I_m} \quad (2\text{-}15)$$

$$V_{ep} = I_{ep} Z_{ep} \quad (2\text{-}16)$$

$$V_m = V_{ep} \times 2 + V_{TUS} \quad (2\text{-}17)$$

$$\rightarrow Z_m = \frac{V_{TUS} + 2V_{ep}}{I_m} = Z_{TUS} + 2Z_{ep} \quad (2\text{-}18)$$

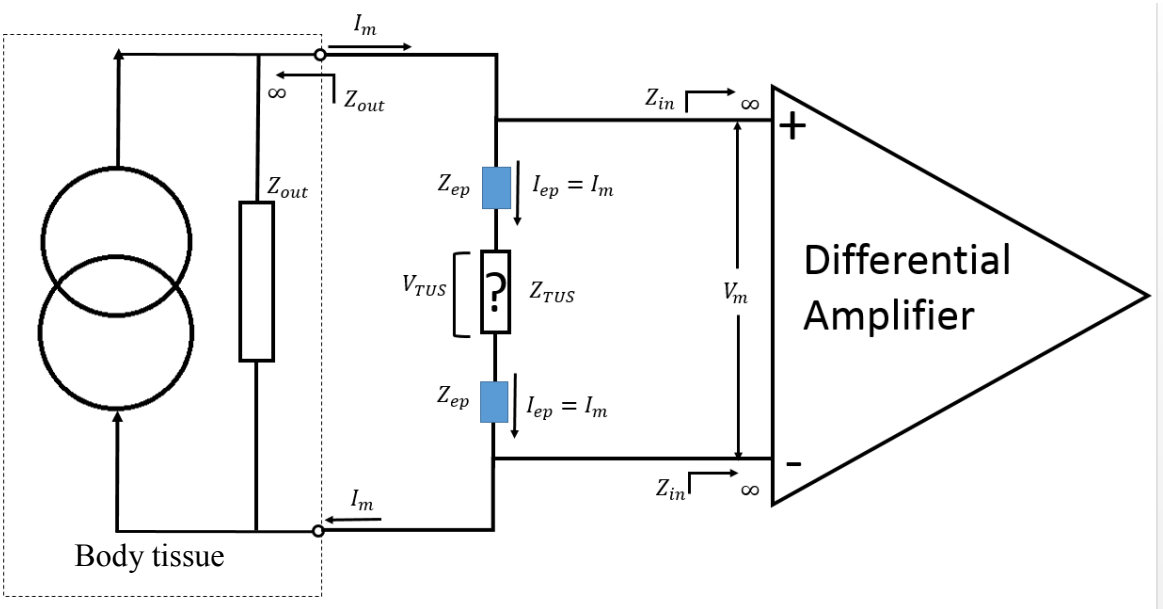

Figure 2-54: Two-electrode measurement for skin impedance (López, 2011).

However, the two-electrode measurement cannot identify the impedance from the skin-electrode interface or the impedance from tissue. Hence, the four-electrode measurement shown in Figure 2-55 is another method to measure the skin impedance. This method seeks to identify the tissue impedance and the skin-electrode impedance.

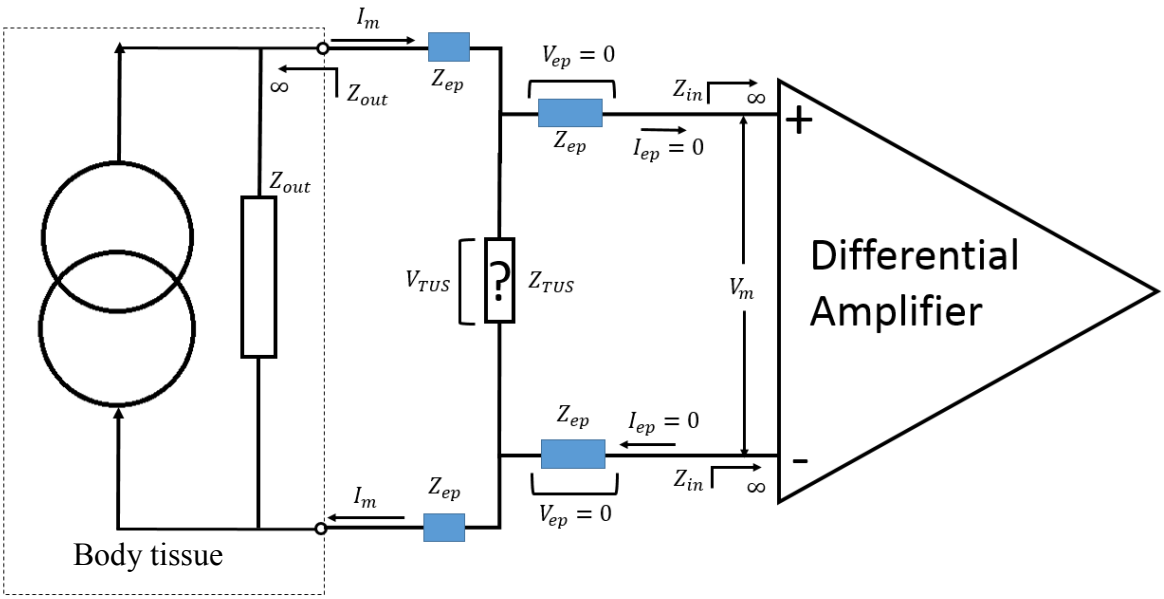

Figure 2-55: Four-electrode measurement for skin impedance (López, 2011).

In the four-electrode measurement, if the electrode impedance (Z_{ep}) is much smaller than the input impedance of the detected electrode, and the impedance of amplifier is larger enough to ignore the electrode current (I_{ep}), then V_{ep} becomes zero, and $Z_m = Z_{TUS,}$ the sum impedance will be the skin tissue impedance and have the following equation:

$$Z_m = \frac{V_{TUS} + 2V_{ep}}{I_m} = Z_{TUS} \quad (2\text{-}19)$$

However, the four-electrode measurement cannot cancel the parasitic capacitance that exists between the electrode and amplifier.

The two-electrode and four-electrode measurements have their own advantages and disadvantages and so are used for different purposes. For example, if the aim of the measurement is to analyse the electrode's effects (like different materials or measuring conditions), a two-electrode measurement is the better option, because a two-electrode measurement circuit is simple. If the measurement involves multi-frequency sources, four-electrode measurements will be the better choice. This is because a four-electrode measurement is able to identify the impedance from tissue or the electrode.

Moreover, a high electrode impedance may cause the potential artefacts. In the skin impedance recording system, the skin potentials were present between the inside and the outside of the skin. This impedance will depend on the skin thickness, sweat glands or hair follicles. When bio-potentials are recorded by a two-electrode or four-electrode system on the surface of skin, any differences in the impedance of the skin under these two electrodes will generate a different offset potential from each electrode, which is called the motion artefact described in section 2.4.7.1. This potential will change over time if the impedance of the skin under one electrode is varies differently from the impedance of the skin under the other electrode. However, if the electrode impedance is low enough and the skin impedance is high it will render the electrode impedance negligible, and the electrode impedance will not affect the final measurement results.

Further, if the skin-electrode impedance is equal to the impedance from the amplifier in the bio-signal recording system, the signal will be transferred by with the maximum power and less signal reduction as described in section 2.4.7.4.1. Therefore, it is necessary to keep the electrode impedance low and identify the skin-electrode impedance to improve the signal quality and transmission.

2.5.3 Finite element analysis (FEA) model for skin and skin-electrode interface

From 2000, finite element analysis started to be used to model the skin (Bischoff, Arruda and Grosh, 2000). This modelling included the mechanical properties of the skin, the skin's conductivity under different temperatures, and electrical changes for different muscle structures. Compared with the skin electrical equivalent circuit model, the FEA model simulates the complex properties of the skin. Furthermore, as the development of FEA simulation software, this method is able to analyse the skin properties in more detail.

In 2017, research (Teklemariam *et al.*, 2017) using a finite element model was presented to ascertain the influence of electrode design and muscle architecture on a EMG signal. In this study, the biological tissues applied a quasi-static assumption that ignores capacitive and inductive effects in the simulation. Under this assumption, the tissue can be considered as resistance. Furthermore, a recorded EMG signal taken from one healthy male was imported as the muscle signal in this model. The inter-electrode distance and the electrode orientation were considered to affect the EMG measurements. In this simulation, the following governing equations were applied to analyse the current and potential during the simulation:

$$\nabla \cdot D = \rho \text{ (gauss law) (2-20)}$$

$$\nabla \cdot \mathrm{J} = \frac{\partial \rho}{\partial \mathrm{t}} \text{ (charge continuity equation) (2-21)}$$

$$\mathrm{D} = \varepsilon_0 \varepsilon_r \mathrm{E} \text{ (2-22)}$$

$$\mathrm{J} = \sigma\, \mathrm{E} \text{ (2-23)}$$

Where ρ = charge density, D= electric displacement, J= current density, E= electric field, ε_0=vacuum permittivity, ε_r= dielectric constant/relative permittivity and σ = electrical conductivity.

Combining equations (2-21 to 2-23) and $\varepsilon=\varepsilon_0\varepsilon_r$,

$$\nabla \cdot \left(\frac{\partial \varepsilon \mathrm{E}}{\partial \mathrm{t}} - \sigma\, \mathrm{E} \right) = 0 \text{ (2-24)}$$

The electric potential has the following quasi-static equation:

$\mathrm{E} = -\nabla \mathrm{V}$ and combined with previous equation (2-24):

$$-\nabla \cdot \left(\frac{\partial \varepsilon \nabla \mathrm{V}}{\partial \mathrm{t}} - \sigma \nabla \mathrm{V} \right) = 0 \text{ (2-25)}$$

Which is the governing equation for the electric current and potential.

This final equation was used for the time-dependant electric current in the model and is used to indicate the model building in this thesis.

Figure 2-56 shows the FEM simulation for the bio-signals collected by two electrodes. The skin model has been divided into three layers: the skin (2 mm thickness), fat (3 mm thickness) and muscle (30 mm thickness).

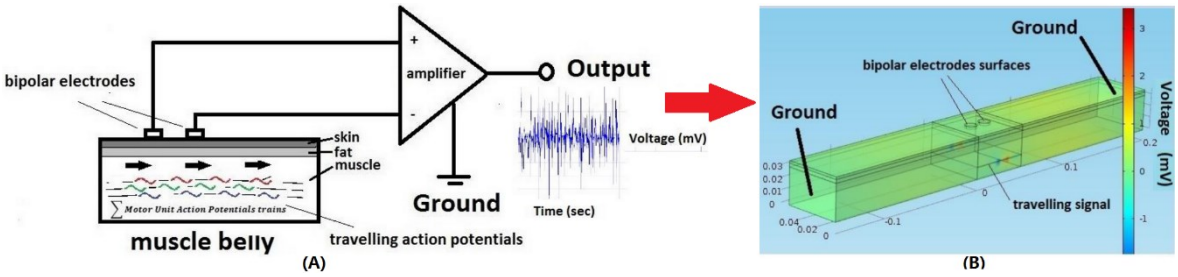

Figure 2-56: (A) bio-signal measurement by two electrodes and (B) three layers COMSOL FE model for muscle tissue (Teklemariam *et al.*, 2017) .

In the model shown in Figure 2-57, three parameters (inter-electrode distance, electrode orientation and muscle angle) were used to simulate their effects.

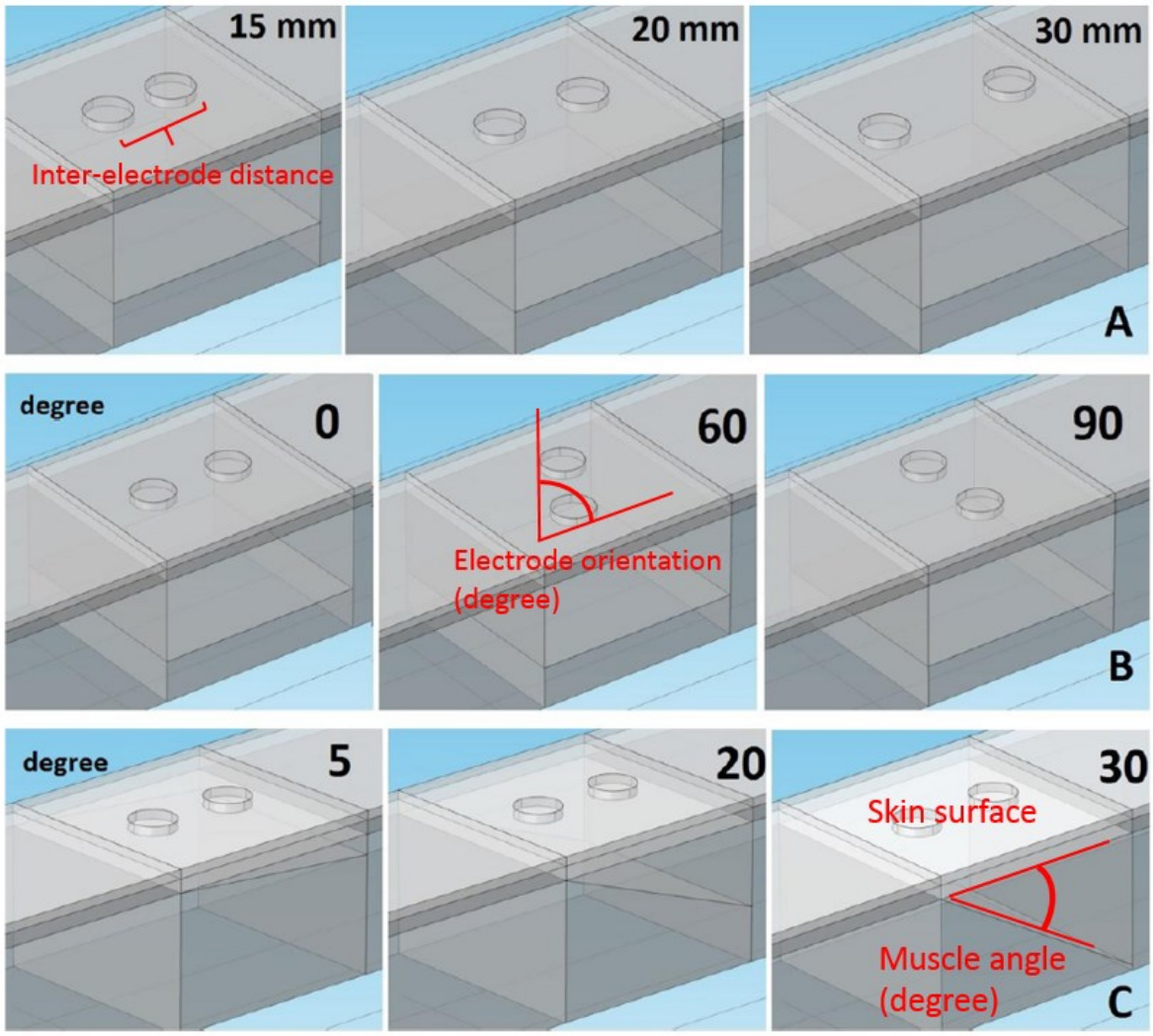

Figure 2-57: (A) inter-electrode distance (mm); (B) electrode orientation (degree); and (C) muscle angle (degree), where the bio-signal is applied on the plane of the bottom muscle (Teklemariam *et al.*, 2017).

In all three simulations, both the electrode orientation and inter-electrode distance have less effect on the input signal when compared with the impact of the muscle angle. When varying the inter-electrode distance, the difference in the signal detected by two electrodes between the lowest distance (15 mm) and highest distance (30 mm) was just 3 %. When the electrode orientation was varied, the change from 0° to 90° was only 2 %. For the impact of muscle angle (from 5° to 30°), the muscle angle reduced the input signal by approximately 13 %.

Comparing the inter-electrode distance and electrode orientation, the muscle in the muscle-angle simulation forms a low pass filter as shown in Figure 2-57. The muscle angle shown in Figure 2-57 is the angle between the skin surface and the layer under the skin surface. If the frequencies in the simulation are lower than 170 Hz, the signal will be retained. Furthermore, if the muscle is parallel to the horizon direction (muscle angle = 0°), the muscle tissue plays the role of band-stop filter (attenuating the frequency range between 92 - 542 Hz). When the muscle angle increases, if the muscle angle is greater than 20°, over 50 % of the input signal is reduced. However, if the inter-electrode distance is increased to 25 mm when the muscle angle is greater than 20°, the input signal will be enhanced by approximately 120 %. Thus, it could be asserted that adjusting the input signal on the muscle angle could be used to affect the results regarding the inter-electrode distance. From this simulation, a possible method and result is shown in relation to the evaluation of the combination of electrode distance and muscle angle.

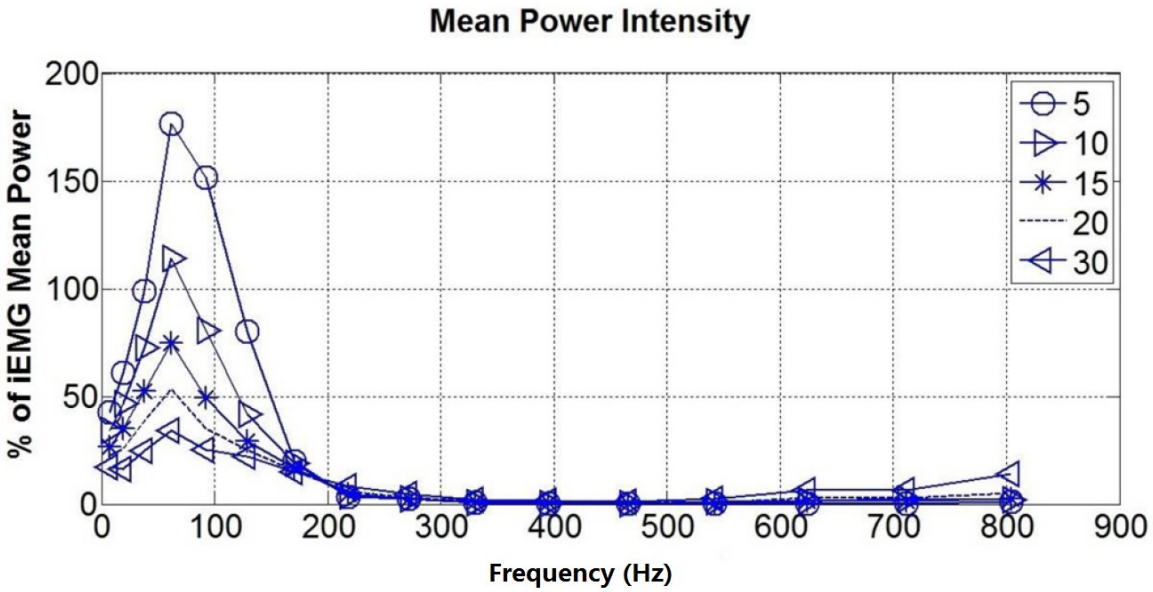

Figure 2-58: The effects from different muscle angles, the mean power is used to evluate the performance (Teklemariam *et al.*, 2017).

Aside from the simulation based on the FE model, other researchers have undertaken FEA calculations with SPICE simulations. In research by Boone and Holder (1996), the researchers used a FEA model based on WOO (which is an old FEA tool from the 1990s) to identify the effect of skin impedance. To measure the skin impedance, the researchers incorporated the following settings in the FEA and SPICE simulation as shown in Figure 2-59. In this setting, the FEA simulation result was used to generate a voltage for skin impedance using the SPICE model. The FEA simulation result was connected into a simulation of common-mode voltage, and the common-mode voltage was used to generate

a fixed common-mode error. After the common-mode voltage, an RC circuit (R_{er} and C_{er}) was used to simulate the skin-electrode impedance. Finally, an amplifier in the simulation was connected with a resistance 1 MΩ and capacitor with 40 pF, which was used to simulate the effects of the patient cables and multiplexers. The common-mode rejection error was limited between 80 dB at 10 Hz and 60 dB at 50 kHz.

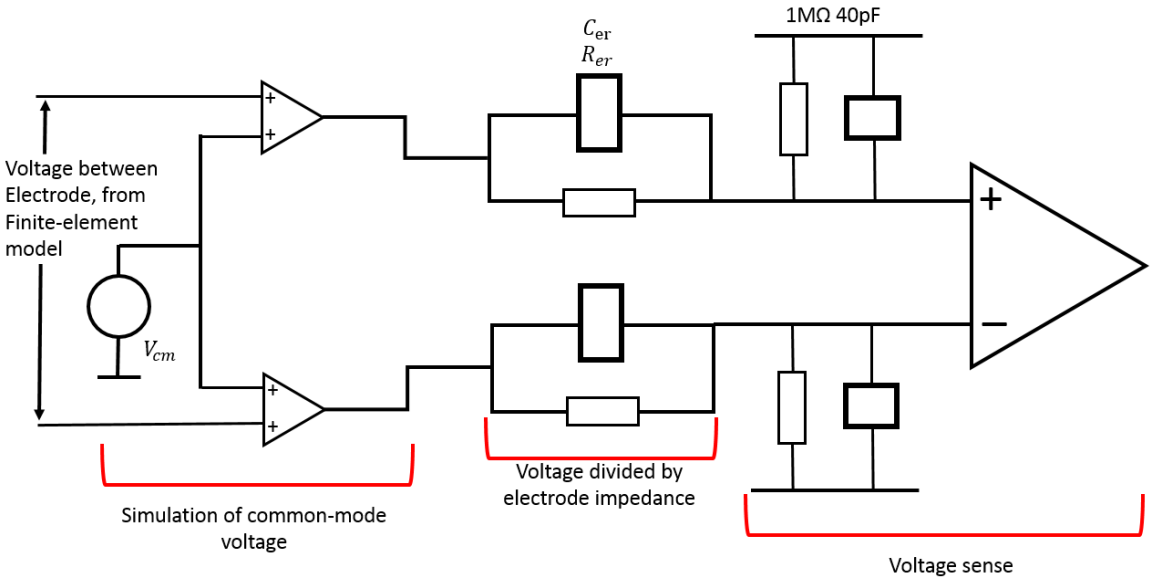

Figure 2-59: Simulation of the skin and skin-electrode measurement circuit with Finite-element model (Boone and Holder, 1996).

Based on this FE analysis and circuit model, if the skin impedance changes between different measurement frames, the skin-electrode impedance will show artefacts in different images as shown in Figure 2-60. The skin impedance image could be seen clearly under different impedance values. In Figure 2-60, the skin-electrode impedances were approximately constant and similar of 2 kΩ; however, when the skin-electrode impedance was increased to 5 kΩ, the impedance image changes. Therefore, the skin impedance of 2 kΩ was a threshold and chosen as the maximum acceptable value.

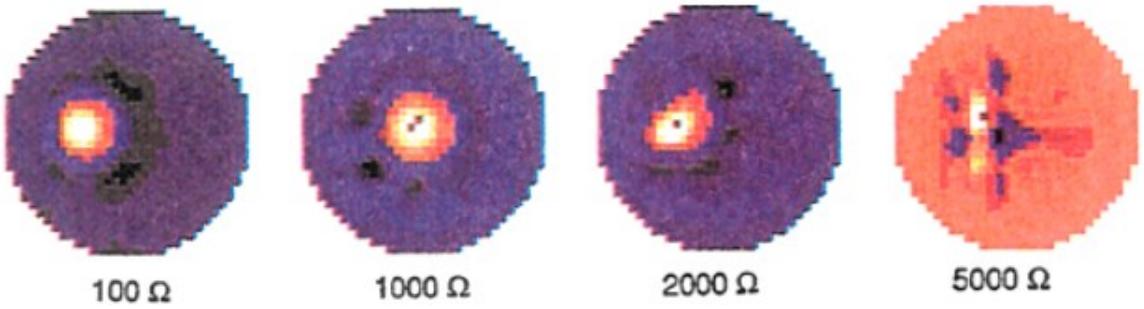

Figure 2-60: Skin impedance images, the samples were randomly chosen from a set of 60 available at 50 kHz (Boone and Holder, 1996). Note: The original figure was based on the measurement results from the paper, and as such, the figure quality cannot be changed.

In this study, it does not provide details of the FEA model, however, it provides a method to combine the FEA model into the SPICE simulation. Furthermore, this method could be used as evidence to show the connection between the FEA model and SPICE circuit simulation.

From the previous two FEA examples and the FEA combined with SPICE simulation, it is seen that the FE model takes account of more parameters and uses more realistic details for the simulation of skin-electrode architectures and properties. Furthermore, the FE model has the ability to be combined with a SPICE model to incorporate circuit elements. Comparing the FE model with an electrical circuit model for skin-electrode impedance, the FE model focuses more on the skin and the electrodes themselves, whilst the circuit simulation is used to simulate the whole measurement and skin-electrode system.

2.6 Conclusions

In this chapter, different electrodes have been introduced with reference to different bio-potential applications. Because the bio-signal results of wet electrodes in short-term measurements (couple of hours) have higher quality than those from a dry and non-contact electrode, the wet electrode is always chosen as the benchmark for bio-signal recording.

However, a dry electrode typically provides more comfortable usage and more of the electrode area will be in contact than with a wet electrode. Because the dry electrode does not have the electrolyte gel, there is no irritability for the skin. As the electrode is dry, it will not become dry. Moreover, because the wet electrode uses the gel, the wet electrode will remove the skin or hair cause the contamination. Furthermore, the dry electrode aims to increase the measurement time from hours to days and reaches the same measuring level as a wet electrode.

For the recently developed non-contact electrodes which, in contrast to the wet and dry electrode, these do not need to measure the signal by contacting with the skin and are able to measure the bio-signal through cloth. However, the non-contact electrode provides the worst signal quality of all the three electrode types.

From these three type electrodes, the dry electrode has been selected for further research. This is because the dry electrode has the widest combinations with other electrode types. For example, if the dry electrode is made by textile, it becomes textile dry electrode (Yang *et al.*, 2014); if the electrode contains an amplifier inside the electrode, it may have the function of non-contact measurement (Baek *et al.*, 2012). Nevertheless, if the dry electrode is applied electrolyte gel, it may have the same measuring results as wet electrode. Therefore, the research of dry electrode will provide more possibility than other electrode types. Moreover, for the dry electrode implementation shown in Figure 2-2 and described in Table 2-3, the dry electrode can potentially utilise a huge selection of materials (PDMS, conductive foam, etc.) and manufacturing procedures (MEMS, printing, coating, etc.). Furthermore, all the preamplifier electrodes can utilize a similar circuit, so the problem becomes that of identifying the best performing skin and skin-electrode interface properties based on the parameters of the skin, electrode geometries, or the external applied force to the electrode. Therefore, the focus of the research in this thesis is on analysing the electrode design and simulation from a skin and electrode viewpoint.

From the review of the textile electrodes, the textile electrode is the most comfortable when conducting measurements, so the electrode design and simulation incorporating textile properties are an important target for any new electrode design. In this thesis, screen printing is used to implement all the new electrode designs since screen printing provides the most suitable method of varying the electrode properties. Inkjet and stencil printing are used to assist the screen print.

Chapter 3: Development of a skin-electrode simulation

3.1 Introduction

From Chapter 2, it is clear that any circuit analysis must consider the relationship between the skin and the electrodes. The conventional wet electrode employs conductive gel to provide the optimum measuring conditions. The dry electrode is applied directly to the skin without gel and uses different materials such as those in Table 2-3 to provide the optimum measuring results. The non-contact electrode measures the bio-potential through the clothes and this method is the most unstable. For all electrodes, the skin-electrode interface can be simulated by a capacitor and resistor circuit, but the skin-electrode model and impedance analysis described in the literature has been limited by the variable properties of the skin. There are several studies (Taji *et al.*, 2013; Hyem and Mokhtar, 2013) that have focused on identifying the changes of the impedance between an electrode and the skin from force or different electrode materials (Ag, AgCl or Aluminium). However, all of them have focused on a particular situation and there is no standard system to show the relationship between these parameters (such as force, electrode materials or the geometries of electrodes) and skin-electrode impedance in a numerical model. Thus it is worth examining if these properties of the skin and the electrode give different results.

3.2 Skin and body model using software simulation

From the reviews in section 2.4.1 and the studies (Pursiainen, Lucka and Wolters, 2011; Taji *et al.*, 2013), a skin-electrode structure model can be built using several resistors and capacitors as shown in Figure 3-1(A). Thus the impedance variation of the skin-electrode interface can be estimated by the resistors and capacitors in Figure 3-1(B).

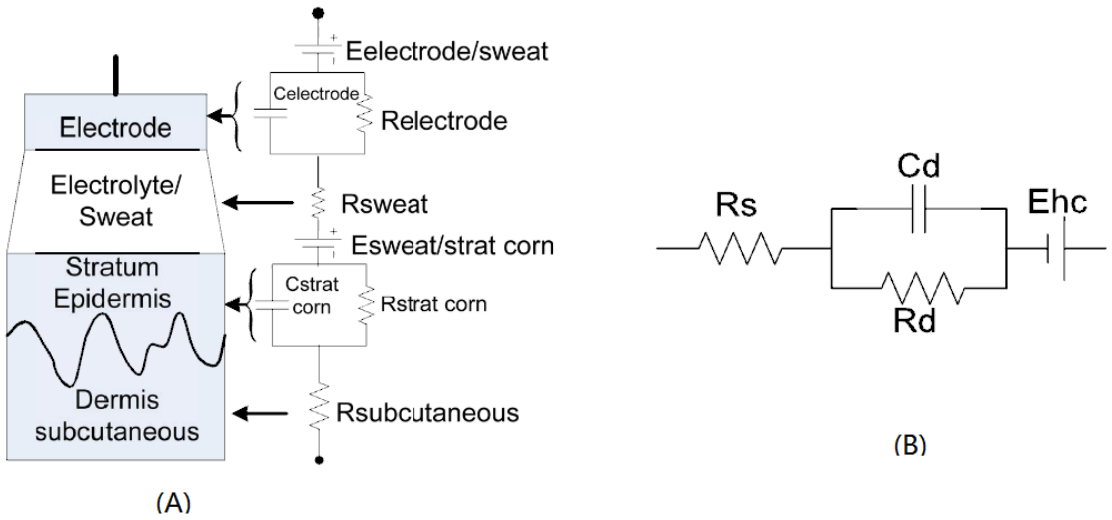

Figure 3-1: Electrode and skin model (A) Skin-electrode interface and equivalent circuit and (B) impedance of the skin-electrode interface equivalent circuit, where R_s is the R_{sweat}, C_d is $C_{electrode}$, Rd is $R_{electrode}$ and E_{hc} is half-cell potential.

This method shown in Figure 3-1 allows the effects of different skin properties to be analysed using electrical simulation software (LTSpice or PSpice). Furthermore, the study provided details regarding the effect of skin capacitance, impedance, electrolyte gel and sweat on the skin-electrode impedance. Thus the impedance variation of the skin-electrode interface can be estimated by the equivalent resistor and capacitor circuit, as shown in Figure 3-1(B). The half-cell potential (E_{hc}) in Figure 3-1 (B) shows the potential difference between the skin or electrolyte (gel or moisture) and the electrode or the ion concentration between the electrode and skin. R_s is the resistance of the electrolyte gel and moisture; C_d is the capacitance between the electrode and the top skin layers; R_d is the electrical resistance between the electrode and the top skin layers. This circuit structure means that the electrode and skin forms a RC circuit. Although the circuit simulation method can show the effects of the measurement conditions, such as the applied force or electrode size on the skin impedance, and is used to make a comparison between the ideal value and measured results, there is no consideration of the distance between the electrode and the skin or the influence of sweat. In the measurement, the skin's stretch will be different under different pressures and this is another parameter that the circuit simulation cannot represent. When the electrode is under differing pressures, the skin will stretch differently and this may cause different measurement results.

Furthermore, if different electrode materials, geometries or measuring environments are applied, it is difficult to evaluate the performance of the electrode. The properties and structure of the skin includes different layers and tissues, where the thickness of the skin layers varies and tissues are variable due to different conditions. For example, because of fat, some people may have thicker skin than others, so the equivalent circuit model does not show all aspects of the skin. As a result, the equivalent circuit limits some boundaries of the measuring conditions. Thus, another finite element analysis (FEA) software package, COMSOL, is used to simulate micro changes in the skin conditions. The details of each layer of skin and electrode are used in COMSOL as closely as possible, such as the stratum corneum layer, tissue or skin. Any changes in the skin can be mapped into the COMSOL model. Due to the FEA simulation using the physical details of skin (such as the permittivity of different materials, different layers of liquids) to build the model, the electrical properties are more accurate than an equivalent circuit simulation. When the COMSOL model is built, it can generate data about impedance versus frequency. Meanwhile, the SPICE model can import the impedance data as the input data to simulate the further amplifying circuit. Hence, the model made by COMSOL provides a platform to link the physical structure with electrical properties like Figure 3-2. In Figure 3 2, the block diagrams are grouped by their functions and software. The interface between the electrode and skin is listed separately.

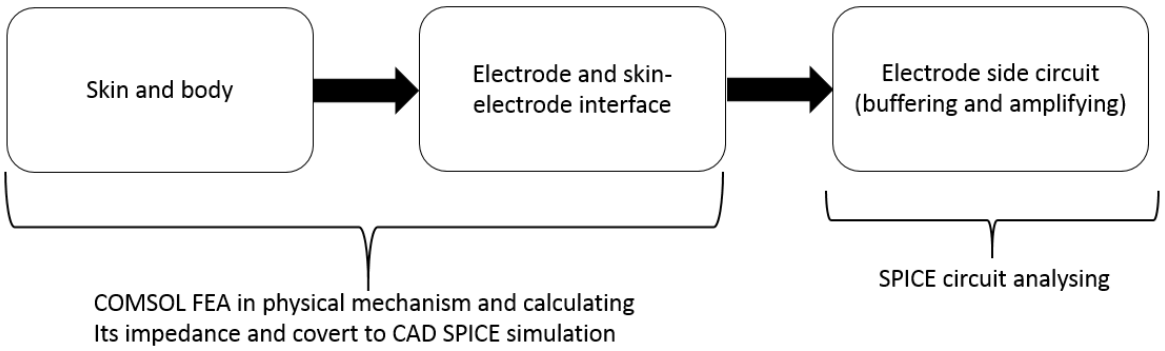

Figure 3-2: Block diagram of the steps to achieve a skin-electrode model in software.

Comparing with the schematic of the equivalent circuit model, there are a number of reasons why FE model is necessary.

FE model can improve the efficiency of making an electrode. Although the skin-electrode model can be simulated by schematic circuit simulation software; the values of the components in Figure 3-1(B) can only be estimated by using experimental results. Then, the estimated values in Figure 3-1(B) are used to calculate the simulation results to compare with the experimental results. Therefore, FE analysis could obtain approximate results before implementing the device, which means a skin-electrode model can improve the efficiency of the future electrode designs and the process.

Moreover, when the FE model is created, it could be used to calculate the impedance or voltage from the skin and the skin-electrode interface. When the impedance or voltage is calculated, the data set of the impedance or voltage can then be added into the SPICE simulation for further modelling.

3.3 Simulation software tool selection

In relation to the above descriptions, this section discusses the reasons for the selection of the software for all of the modelling.

Regarding the research and the functions that we want to implement, the key point is to link the simulation between the physical models and the SPICE model. For example, the modelling software is used to generate a set of data describing impedance vs frequency, and this set of data is converted into the SPICE software. Thus, the functions of different software and program possibilities are compared. Potential software includes: MATLAB, ANSYS and COMSOL. Different software has differing potential to deal with different problems.

- MATLAB deals with data and system logic problems, which makes it suitable for solving data analysis and control theory problems. MATLAB also provides an interface with SPICE. The block structure in Simulink has been used to simulate the different mathematical functions. However, MATLAB does not provide a suitable interface for building the physical structure, which means MATLAB cannot be used to build the skin-electrode model. However, because MATLAB is good at handling data and analysing the data set results, the data obtained from the physical structure analysis can be analysed using MATLAB.

- ANSYS is FEA software for electrostatics, electro mechanical and electronic and electrical analysis. FEA means models are built as complete 2D/3D model structures, then, each structure is divided into a discrete number of elements for analysis. The boundary conditions and environment changes are drawn into the models.
- Furthermore, all the material properties can be edited in the software. This means the FE model can be built relating to the physical skin model which will allow the skin model to be built in detail. Hence the disadvantages of MATLAB are covered by ANSYS and provide another possible way to solve the skin-electrode model. In addition, ANSYS provides an equation editor, and thus, some parameters such as movement or flexibility can be included via the equations. This means that the model will feature more dynamic detail than MATLAB. However, ANSYS does not provide an interface to the SPICE software. And because the model needs to be further implemented into SPICE software to provide a suitable model for the subsequent circuit, ANSYS is therefore not a good choice.
- COMSOL has similar functions as ANSYS, i.e. FEA. In addition, COMSOL includes the essential interface between the modelling software and a SPICE model. Furthermore, COMSOL possesses similar libraries to ANSYS, which include electrostatics for capacitor structure, and MEMS structures and electro mechanical structures to analyse movement in the electrode-skin model. The challenge with COMSOL is to build the link between the actual electrodes, modelling simulation, and the SPICE model. From the measurement of the electrode samples, the circuit can be estimated as in Figure 3-1 (B) and from the structure of the actual electrodes, the simulations can also be derived. Of all the software considered, COMSOL is the only one that provides a link between the physical model and the SPICE circuit simulation. Hence, COMSOL was selected her as the software to implement the electrode model in this thesis.

3.4 Parameters of the skin-electrode model

According to Figure 3-1, when the electrode comes into contact with the skin, it forms a circuit containing resistors and capacitors depending on the skin, electrode type, the medium between the skin and electrode, and the external conditions (temperature, moisture capacity or pressure). Under these external conditions, some parameters may cause a change of capacitance, resistance, and electrical field. These are:

Material and geometries (size or thickness) of the electrodes

- Because electrodes are made using different materials and geometries (such as the different dry electrodes described in Chapter 2), these differences will cause different results when the skin-electrode model is built. To determine which parameter will have the greatest impact on the results, the geometry is tested as the 1st variable in the simulation. However, if the electrode material is decided, the geometries of the electrodes are used to balance the efficiency between the material and measuring results. For example, the electrode is placed on various body positions, and according to skin's different thicknesses or electric properties, the electrode may be designed to different geometries to match the different measurement conditions.

Electrode conformability

- When the electrode is applied to the skin, if the electrode is a soft and flexible, such as polyurethane or silicone rubber, the electrode will conform to the skin surface and provide more comfortable contact for the user. The example in Figure 2-29 showed electrode conformability as described in the literature.

Pressure and movement of the skin and electrode

- When pressure is applied to the electrode, a deformation of the skin is generated and the contact area will be increased as shown in Figure 3-3(a) and (b). Furthermore, the distance and impedance of skin tissue will be reduced by this pressure as shown in Albulbul and Chan's research (2012). The result in Albulbul and Chan's research (2012) showed that the force would increase the capacitance (C_b) and reduce the resistance (R_d and R_s) as shown in Figure 3-1 (B). This conclusion can be used in this thesis to assess the results from the simulation. Hence the deformation of the electrode geometry during pressure becomes another factor that affects the skin-electrode impedance.

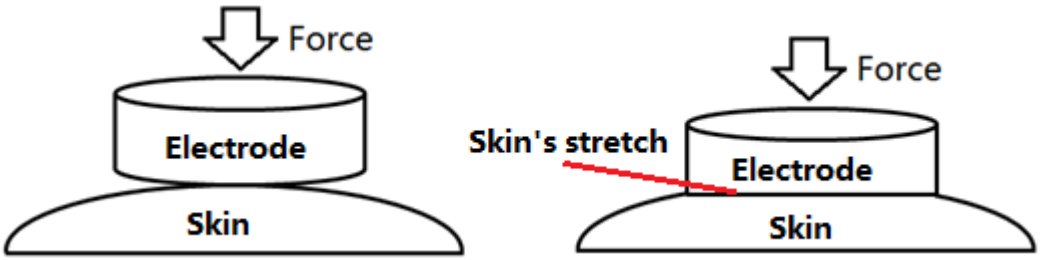

Figure 3-3: Force applied to the electrode (before application and immediately after).

Skin properties

- Because the skin contains different layers and each layer has different thickness and material properties, if the outside conditions in the above like pressure or movement are varied and applied to the skin, the bio-potential measurement will be different. To identify the key layer of the skin in different position is critical to the model.

For the work in this thesis, we assume that the electrodes contact the skin directly. Therefore, the skin's properties, electrode materials, electrode size, electrode conformability, electrode movement and pressure on the electrode are all considered. If the parameters with the most significant impact on electrical performance can be identified, the optimal electrode can be designed and implemented. All of these physical parameters lead to a complicated analysis, but can present an optimal electrical result for the electrode design.

3.5 Skin-electrode model created by COMSOL

Depending on the properties described in Section 3.4 and the existing skin structure, the simplest skin model can be built in the frequency domain. In the model, the software was COMSOL Multiphysics (version 5.2a, Cambridge, UK).

In Figure 3-4, the structure of the skin-electrode model is shown, which uses the layer from Table 2-7. The skin layers from top to bottom are the stratum corneum (SC), epidermis (E), dermis (D), hypodermis, fat (HYP), and muscle (M).

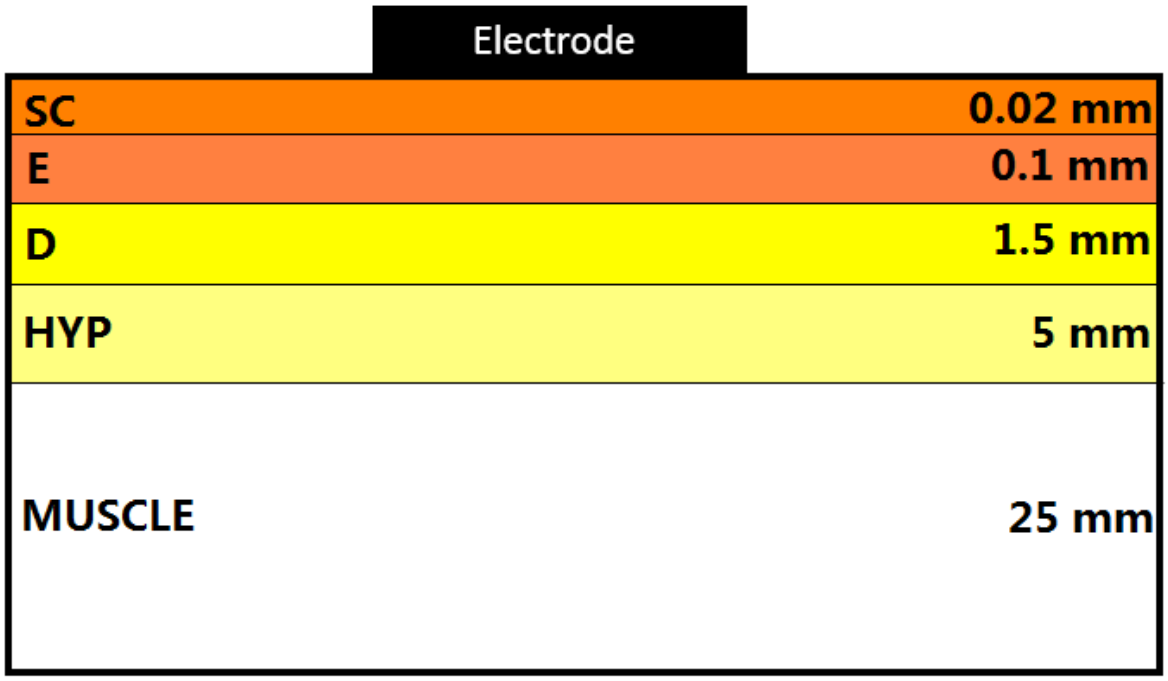

Figure 3-4: Construction of skin-electrode model.

The bottom two layers of the model are the thickest two layers, which are muscle and the hypodermis. In all the simulations, these two layers were the least effected by pressure or other outside environmental conditions. The stratum corneum is the outermost layer of skin which contacts with the electrode or conductive gel or sweat. The interface between the skin and the electrode may be air or the conductive gel (such as polyoxethylene). Furthermore, the bio-signal is mainly from the muscle, so the top layer of muscle is considered as the signal source. In Figure 3-4, there is no medium between the skin and the electrode, which means the electrode contacts the skin directly and forms a dry electrode structure.

3.5.1 2D COMSOL cross-section skin-electrode model

For the simulation, the skin-electrode model was simulated in 2D and 3D. Because the model is symmetric, a 2D model is used to represent the 3D structure, thus reducing complexity. Furthermore, if the 2D cannot fully present the skin-electrode model, the structure of 3D model is able to be built based on the 2D model. Hence the skin parameters (such as Young's Modulus, dielectric constant, electrical conductivity or layers' thickness) in the 2D model were applied using average values to test the simulation performance, where the average values were calculated from the literature summaries described in Table 2-7 and shown in Table 3-1: Because the dielectric constant of skin varies with frequency and most of the bio signals are at very low frequencies as shown in Figure 2-3, therefore, the frequency range is set from 0.1 to 10 Hz and the dielectric constant of skin layer at 10 Hz was selected. Furthermore, the electric properties of skin will not change at lower frequency (10 Hz) or higher frequency (1000 Hz), for example, if the dielectric constant of SC layer skin layer gives more impact on skin-electrode impedance at low frequency than other layers, the SC layer will change the skin-electrode impedance more than other skin layers at high frequency. Meanwhile, the dielectric constant of silver (Ag) was set to 1. The reason is that a metal has

a lattice structure and its ions can be polarized (Lourtioz *et al.*, 2005). However, due to the existence of a sea of conducting electrons, the notable effects of conductivity far surpass any effect of polarization. In this process, the metallic ions are polarizable. Therefore, the AC dielectric constant for metals is close to 1.

Electrode and skin	**Thickness (mm)**	**Young's Modulus (MPa)**	**Conductivity (S/m)**	**Poisson ratio**	**Density (kg/m^3)**	**Dielectric Constant/ Relative Permittivity**
Electrode (Ag)	1	8.3	61.6×10^6	0.37	10500	1
Stratum Corneum(SC)	0.02	2.6	0.0003	0.43	1050	6600
Epidermis(E)	0.1	0.5	0.55	0.48	1020	1.14×10^3
Dermis(D)	1.7	0.06	2.9	0.48	1900	1.14×10^3
Hypodermis and fat (HYP)	5	0.28	0.03	0.48	1800	1.2×10^7
Muscle(M)	25	1.77	0.42	0.45	1120	2.5×10^7

Table 3-1: Different mechanical and electrical properties of the skin layers; the value of each layer was calculated as an average value from Table 2-7.

Using the skin layer electrical and mechanical properties described Table 3-1: (like the thickness, Young's Modulus, conductivity etc.), the 2D single electrode model is built in Figure 3-5 with each layer labelled. Because this is still an initial test stage, the electrode material was silver and the silver properties were chosen from data in the simulated software itself to avoid the variation in the silver used in the literature. In Chapters 4 and 5, the actual material properties of the electrodes are measured and included in the simulation. In the 2D simulation, the model has the 'Model width' and 'Model depth' (or called thickness in COMSOL) as shown in Figure 3-5 for converting the 2D structure to 3D structure.

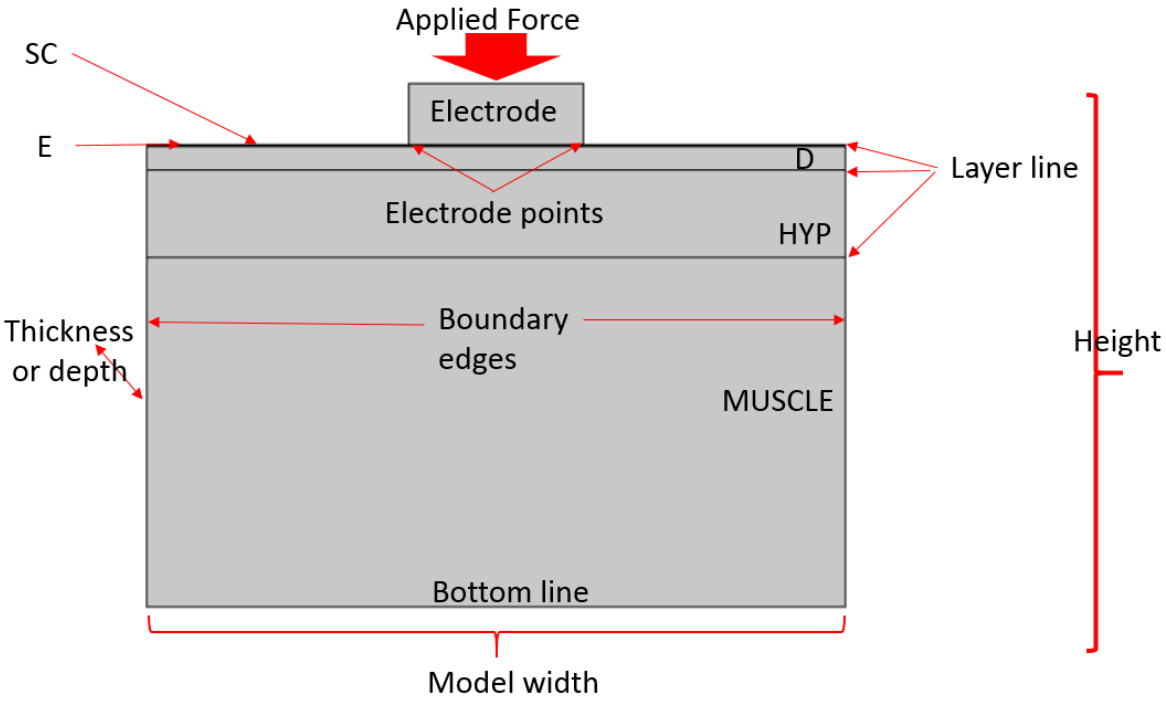

Figure 3-5: Cross section of simplified single skin-electrode model, each layer is labelled and Dermis layer contains multiple layers.

In the literature (Mohanty *et al.*, 2013), the average forearm length for young people (aged 18-25 years) was between 20 cm to 25 cm. Therefore, the width of the model was set to 225

mm (middle number between 20 and 25 cm) and the electrode was placed at the centre of forearm. Furthermore, because the electrode size is controlled by 'model thickness', to have a 1 cm^2 electrode (the most commonly used from literature), the model thickness was set to 10 mm for initial test.

Each model material layer was labelled in Figure 3-5. Because the dermis layer contains varying multiple layers inside, the line between E and D layer in Figure 3-5 was thicker than others since it contains the multiple dermis layers. The muscle layer was used as the base layer under all the skin layers and provided the bio-signal source.

In the simulation, because the SC layer and E layer were thinner than other three layers (about 200 times and 50 times thinner than the HYP layer), the mesh and element size of these two layers were set to 'finer domain' from COMSOL. In 'finer' setting, the maximum element size was 0.549 mm and the minimum element size was 0.000206 mm.

The mesh and element size of other thicker layer (like D, HYP, muscle and electrode layer) were set to 'coarse domain'. In 'coarse' setting, the maximum element size was 2.75 mm and the minimum element size was 0.0549 mm. Because thick and thin layers have different settings (finer and coarse), COMSOL would handle more mesh elements on 'finer domain' and less mesh elements on 'coarse domain'. If all domains were applied 'normal', COMSOL would not identify domain importance and the simulating results would be averaged.

For the mechanical simulation, the 'Solid Mechanics' provided by COMSOL was used to simulate the model. All the materials in the model were chosen as linear elastic materials and the solid model was isotropic, which means the movement of model will be effected by Young's modulus, material density and Poisson's ratio of the materials. The materials included the silver electrode and all the skin layers.

Furthermore, the electrode was placed on top of the skin layer and a 5 N force was applied to the top surface of the electrode. This applied force was based on the literature (Albulbul and Chan, 2012). In the literature, Albulbul (2012) applied a force of 8.8 N as an effective force to reduce the skin-electrode impedance. Because the current model is much smaller than a forearm, therefore, a smaller force 5 N was applied to the top of electrode and was used to identify the change of electrode centre and skin-electrode impedance.

Moreover, the bottom line as shown in Figure 3-5 and both sides (boundary edges in Figure 3-5) of the model have been set to 'fixed constraint', which means the model will not move downward and to both the left and right directions at different forces. Meanwhile, the 'layer lines' labelled in Figure 3-5 were defined as 'prescribed displacement in y direction', the function provided by COMSOL, these layers can only be moved in the vertical direction (y-axes), which was the direction of the applied force. Furthermore, the 'Electrode points' labelled in Figure 3-5 were defined as 'Prescribed Point in y direction', these points can only be moved in y direction.

In 'Solid Mechanics', the following constitutive equations are calculated in COMSOL:

$$0 = \nabla \cdot \mathrm{FS} + \mathrm{Fv} \quad (3\text{-}1)$$

$$\mathrm{F} = \mathrm{I} + \nabla \boldsymbol{u} \quad (3\text{-}2)$$

$$\mathrm{S} = S_{ad} + \mathbf{C}{:}\,\epsilon_{el} \quad (3\text{-}3)$$

$$\text{Where } S_{ad} = S_0 + S_{ext} + S_q \text{ and } \epsilon_{el} = \epsilon - \epsilon_{inel}$$

$$\epsilon = \frac{1}{2}[(\nabla \mathbf{u})^{\mathrm{T}} + \nabla \mathbf{u} + (\nabla \mathbf{u})^{T} \nabla \mathbf{u}] \quad (3\text{-}4)$$

$$\mathbf{C} = \mathbf{C}\,(E, v) \quad (3\text{-}5)$$

In the equations, F = deformation, v = volume, S= stress (2nd Piola-Kirchhoff stress), I= unit tensor (of order two), **u**= displacement. **C** is the fourth-order stiffness tensor, v is Poisson's ratio, ϵ= tensor, E= Young's Modulus.

Because the ϵ_{inel} inelastic tensor is zero, therefore, ϵ_{el}= ϵ.

Combining equation (3-3) to (3-5),

$$S = S_{ad} + \mathbf{C}{:}\frac{1}{2}[(\nabla \mathbf{u})^{\mathrm{T}} + \nabla \mathbf{u} + (\nabla \mathbf{u})^{T} \nabla \mathbf{u}] \quad (3\text{-}6)$$

For the force applied to the top of the electrode, it has the following equations:

$$S_{ad} = S_{ext} = \frac{F_{total}}{A} \quad (3\text{-}7)$$

A is the electrode area.

If S_{ad} is substitute into (3-6),

$$S = \frac{F_{total}}{A} + \mathbf{C}{:}\frac{1}{2}[(\nabla \mathbf{u})^{\mathrm{T}} + \nabla \mathbf{u} + (\nabla \mathbf{u})^{T} \nabla \mathbf{u}] \quad (3\text{-}8)$$

Therefore, combing equation (3-7),(3-1),(3-2) with zero initial tensor and deformation, the final displacement of defamation is:

$$0 = \nabla \cdot \nabla \boldsymbol{u}\,\{\frac{F_{total}}{A} + \mathbf{C}{:}\frac{1}{2}[(\nabla \mathbf{u})^{\mathrm{T}} + \nabla \mathbf{u} + (\nabla \mathbf{u})^{T} \nabla \mathbf{u}]\} \quad (3\text{-}9)$$

For the electrical simulation, the 'Electrical Current' provided by COMSOL was used to simulate the model.

All the materials in the model (included the skin and electrode) were chosen as 'Current Conservation' provided by COMSOL, which means the impedance of the model will be effected by electrical conductivity and dielectric constant. The virtual 'Ground' is set to the 'Bottom line' and the 'Boundary edges' are set to electrical insulation (electric potential V is zero: Dirichlet boundary condition, the boundary equation is a constant voltage).

Meanwhile, the applied potential was 0.391 mV with 'Harmonic Perturbation' at the top of electrode. The convergence was calculated by the root mean square of the total impedance from the electrode to ground, since this value represents the impedance variance at the electrode and the impedance kept constant. The function of 'Harmonic Perturbation' was used to provide a periodic potential. The impedance was calculated from the 'bottom line' to the top of the electrode. Moreover, in COMSOL AC model, the software used the inverse of the absolute value of real and imaginary part of the total admittance as the impedance.

In addition, the electrical governing constitutive equations involved in COMSOL are the following equations:

$$\nabla \cdot \boldsymbol{D} = \rho \text{ (gauss law) (3-10)}$$
$$\nabla \cdot \mathbf{E} = \frac{\rho}{\varepsilon 0} \text{ (gauss law) (3-11)}$$
$$\mathbf{D} = \varepsilon_0 \varepsilon_r \mathbf{E} \text{ (constitutive relation) (3-12)}$$
$$\nabla \cdot \mathbf{J} = j\omega\rho \text{ (3-13)}$$
$$\mathbf{J} = \sigma \mathbf{E} + j\omega \mathbf{D} + \mathbf{J_e} \text{ (3-14)}$$

Which ρ = charge density, $\boldsymbol{D}$ = electric displacement, $\boldsymbol{J}$= current density, $\boldsymbol{J_e}$=initial current density, $\mathbf{E}$ = electric field, $\omega = 2\pi \times$ frequency, ε_0=vacuum permittivity, ε_r= dielectric constant or relative permittivity and σ = electrical conductivity.

Combining equations (3-12), (3-13) ,(3-14) with zero initial current density and $\varepsilon = \varepsilon_0 \varepsilon_r$,

$$\mathbf{J} = (\sigma + j\omega\varepsilon_0\varepsilon_r)\mathbf{E} \text{ (3-15)}$$
$$\nabla \cdot (j\omega\varepsilon\mathbf{E} - \sigma \mathbf{E} - j\omega\mathbf{D}) = 0 \text{ (3-16)}$$

The electric potential has the following quasi-static equation:

$$\mathbf{E} = -\nabla V$$

and combined with previous equation:

$$-\nabla \cdot (j\omega\varepsilon\nabla V + \sigma \nabla V - j\omega\boldsymbol{D}) = 0 \text{ (3-17)}$$

Which is the governing equation for the electric potential.

Nevertheless, the 'Deformed Geometry' provided by COMSOL is used to couple the 'Solid Mechanics' with 'Electrical Current' in COMSOL.

When the COMSOL start to simulate the model, there are three steps, the sequence is shown in the following order:

1. 'Step 1: Stationary' calculates the changes of geometry (deformation) from 'Solid Mechanics', and saves the deformation to 'Deformed Geometry'.
2. Loading the changes of geometry from 'Deformed Geometry'.
3. 'Step 2: Frequency-domain Perturbation' for 'Electric current' and 'Deformed Geometry', this step is used to calculate the impedance in frequency domain.

In this simulation, the total number of elements calculated by COMSOL is 88764.

3.5.1.1 2D single skin-electrode modelling

In this section, the 2D single electrode is simulated as Figure 3-5 and applied all the boundary conditions to see how the skin changes.

3.5.1.1.1 2D single electrode modelling conditions test - 2D model thickness (or depth) and width

In the simulation, although this is called 2D model, the 2D model is a 2D cross-sectional view of a 3D geometry (like Figure 3-6), hence the effects from 'model thickness' (or depth)

and 'model width' in Figure 3-6 needs to be identified. In the simulation, the electrode width and height keep the same (width: 10 mm and height: 1 mm).

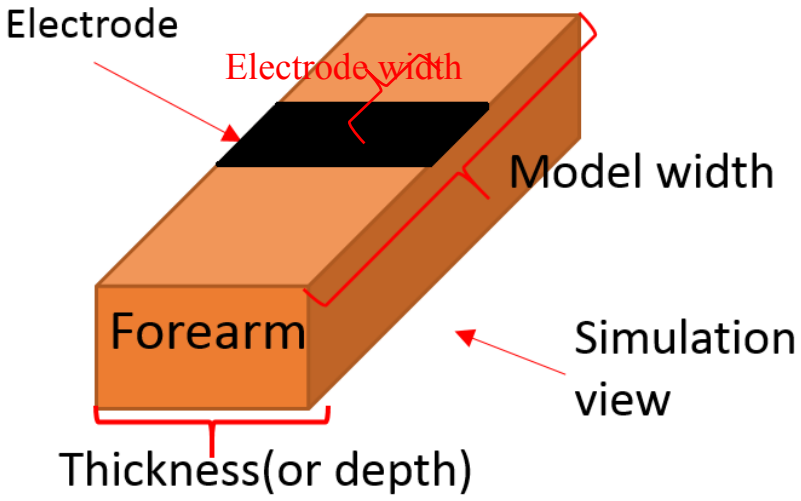

Figure 3-6: Representation of 2D cross-section single-electrode skin simulation.

Figure 3-7 and Table 3-2 show the deformation of centre movement and centre movement trend.

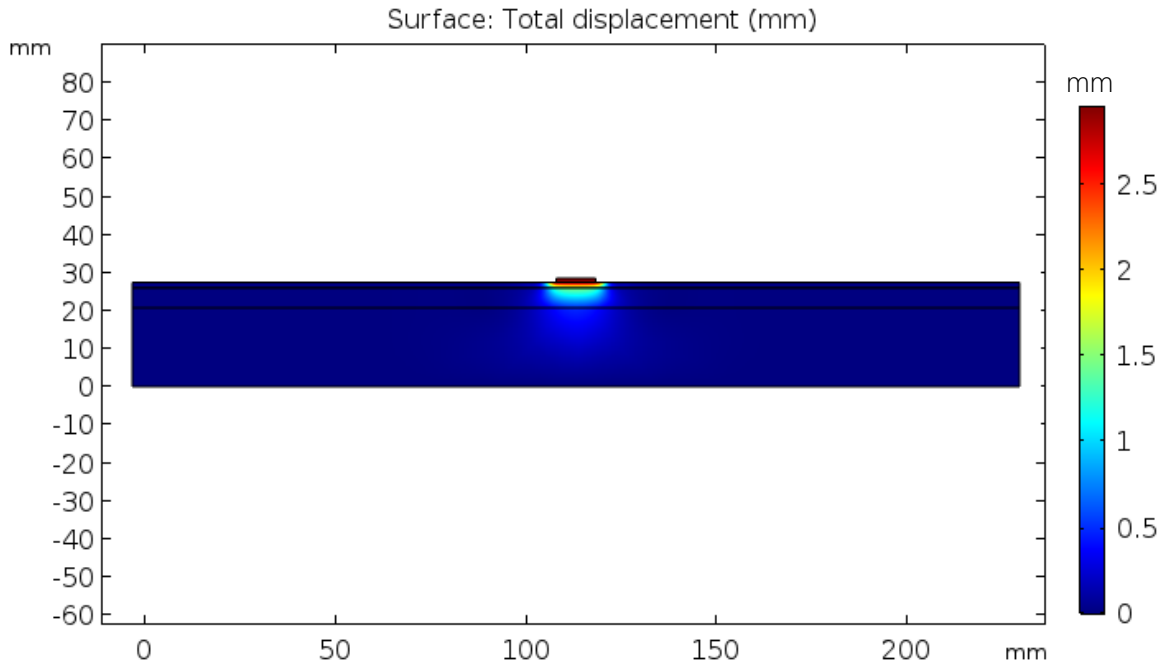

Figure 3-7: Deformation of 2D single electrode model, the applied force is 5 N and the model thickness is 10 mm.

Model thickness (mm)	Electrode centre movement at 5 N applied force (mm)
10	2.85
20	1.42
30	0.95
40	0.71
50	0.57
80	0.36
100	0.28

Table 3-2: Electrode centre movement at different 2D model thickness changes, the thickness increased from 10 to 100 mm.

In Table 3-2, when the model thickness was increased from 10 to 20 mm, the movement of electrode centre was reduced from 2.85 to 1.42 mm (about 50 %, comparing to the movement of 10 mm thickness). Moreover, if the thickness of the model was increased to 40 mm, the movement of electrode centre had been reduced 50 % again (from 1.42 mm to 0.71 mm). Subsequently, when the model thickness was increased from 40 to 80 mm, the movement of electrode centre was reduced from 0.71 mm to 0.36 mm (50 %). Therefore, it could be concluded that the electrode centre movement is reduced 50 % as model thickness doubled. Because this is a 2D model, the electrode size keeps increasing as the whole model thickness increases. This is a limitation of the 2D model, which is the electrode size changes with a change of model thickness or depth. When the model thickness is doubled, the electrode area is doubled. Meanwhile, the applied force is constant (5 N), therefore, the pressure on the skin is reduced by 50 %. Because the pressure is reduced by 50 %, the electrode centre movement is reduced by 50 %. From this result, it could be concluded that if the applied force on electrode is constant, the skin deformation is relevant to electrode size.

3.5.1.1.2 Single electrode electrical property simulation test

To test the electrical property of 2D single electrode model, a periodic signal is applied to the model to identify the skin-electrode impedance. In the simulation, the frequency is changed from 0.1 Hz to 10 Hz with steps of 0.1 Hz. The impedance is measured from the top of electrode to the bottom of the skin. The model thickness is fixed to 10 mm and the width is set to 225 mm. This model thickness gives a 10 mm × 10 mm electrode. Figure 3-8 plot the skin-electrode impedance for single electrode model at low frequencies (from 0.1 to 10 Hz).

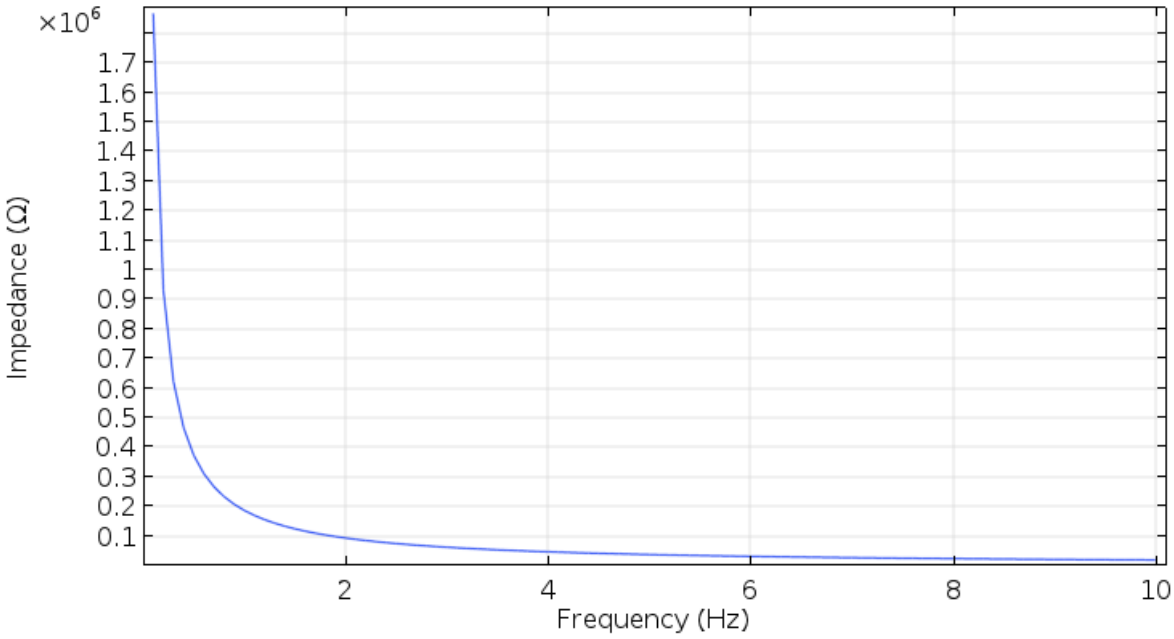

Figure 3-8: 2D single skin-electrode model impedance varying low frequencies (0.1 to 10 Hz), the electrode size is 10 mm × 10 mm, where 10 mm is the model thickness.

In Figure 3-8, the highest simulated impedance value was much higher than results produced by Saadi and Attri (2013) or Alper and Jari (2014). From the literature, when the frequency was under 10 Hz, the skin-electrode impedance of silver should be around 10^4 to 10^5 Ω. However, when the frequency is increased to 10 Hz in 2D single electrode model, the simulated impedance is reduced from 1.9×10^6 Ω to 19117 Ω. The simulated results become closer to the literature results. This may come from the following reasons:

- In the literature, the skin-electrode impedance was measured by two-electrode or four-electrode measurement as shown in section 2.5.2. In this simulation, there was only one electrode on the skin, meanwhile, the impedance was simulated from the top of electrode to bottom of muscle. Comparing with two-electrode measurements, the simulation has only half of the measuring structure that is it only measures the skin-electrode impedance under one electrode. If the two-electrode measurement is applied to the model, the simulated results may be reduced at this frequency range.
- In addition, the simulated conditions for the single electrode are limited by the 2D thickness or depth. In this 2D simulation, only the skin under two electrodes and the skin between two electrodes are simulated and the resistive or capacitive effects from surrounding skin are limited by this 2D simulation.

Therefore, another simulation was implemented to find if the model width would affect the skin-electrode impedance, the simulated results are shown in Figure 3-9.

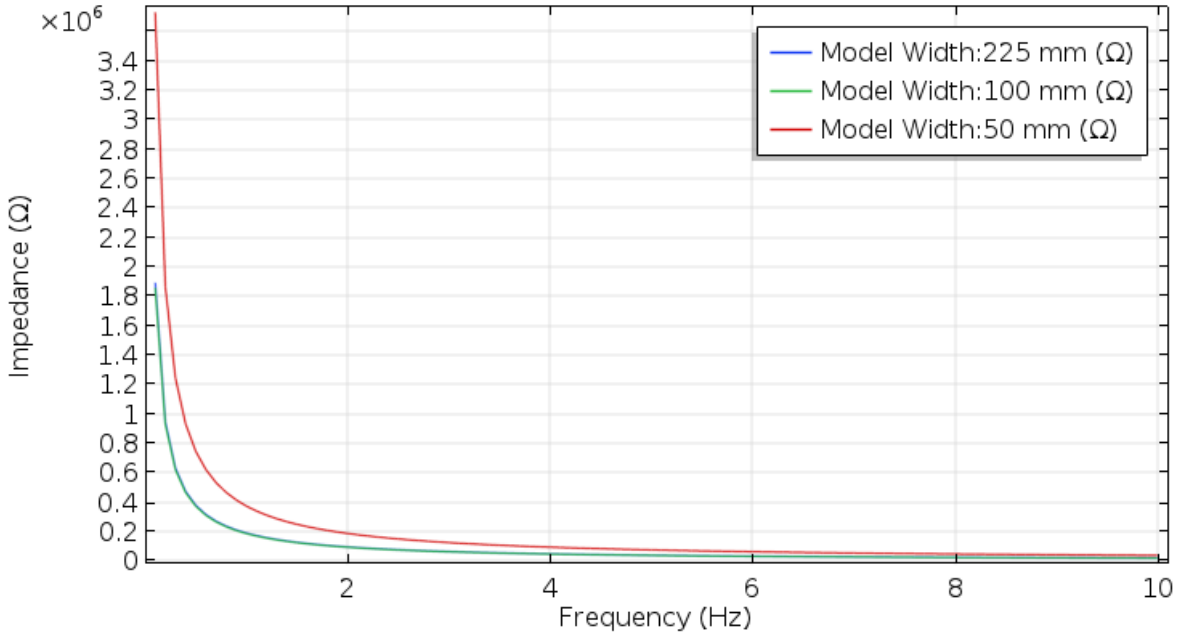

Figure 3-9: 2D single skin-electrode impedance change of model width at low frequencies (0.1 Hz to 10 Hz) with 3 different model width (225 mm, 100 mm, 50 mm), the applied force is 5 N and the model thickness (or depth) is 10 mm. The 225 mm and 100 mm model width are overlapped, so cannot be separated in the figure.

In Figure 3-9, when the model width was reduced from 225 mm to 100 mm, the skin-electrode impedance at 0.1 Hz is increased from 1.86×10^6 Ω to 1.89×10^6 Ω (approximately 1.7 %), these two simulations were almost the same. Although the model width was reduced 50 %, the total skin-electrode impedance kept almost the same. However, when the model

width was decreased from 100 mm to 50 mm, the single skin-electrode impedance at 0.1 Hz was increased from 1.89×10^6 Ω to 3.72×10^6 Ω (about 100 %). This impedance change means the forearm length has produced the significant impact like model thickness in Table 3-2. If the simulated forearm length is less than 100 mm, the forearm length becomes a significant parameter. Therefore, for further single electrode model design, the forearm length could be shorten to 100 mm and the skin-electrode impedance will not been effected too much. In next section, the 2D dual electrode model is implemented to approach two-electrode measurement and test if the results may be closer to the literature results.

3.5.1.2 2D dual electrodes skin electrode model

If the single electrode model is expanded to contain an additional electrode, i.e. a dual electrode model, the simulation can be used to identify the skin-electrode impedance between the two electrodes. In the dual electrode simulation, the same boundary conditions as the single electrode were applied to the model. For example, the 'Layer lines' in Figure 3-10 were defined as 'prescribed displacement in y direction' and the 'Electrode points' labelled in Figure 3-10 were defined as 'Prescribed Point in y direction', these layers and points could only be moved in y-axes direction. Furthermore, the two electrodes at the top of the skin receives the same force of 5 N. For the width of the 2D dual electrodes model, the width is set to 225 mm, which is the same as single-electrode model. The two electrodes has a 50 mm displacement between each other (calculating from the electrode centre). This displacement is selected based on the literature (Simper, 2005; Alper and Jari, 2014). For the thickness of this 2D dual electrodes model, it has the thickness of 10 mm, this thickness gives two 10 mm × 10 mm electrodes. In addition, other skin parameters are shown in Table 3-3.

Electrode and skin	**Thickness (mm)**	**Young's Modulus (MPa)**	**Conductivity (S/m)**	**Poisson ratio**	**Density (kg/m^3)**	**Dielectric Constant/ Relative Permittivity**
Electrode (Ag)	1	8.3	61.6×10^6	0.37	10500	1
Stratum Corneum(SC)	0.02	2.6	0.0003	0.43	1050	6600
Epidermis(E)	0.1	0.5	0.55	0.48	1020	1.14×10^3
Dermis(D)	1.7	0.06	2.9	0.48	1900	1.14×10^3
Hypodermis and fat (HYP)	5	0.28	0.03	0.48	1800	1.2×10^7
Muscle(M)	25	1.77	0.42	0.45	1120	2.5×10^7

Table 3-3: Different mechanical and electrical properties of the skin layers; the value of each layer was calculated as an average value from Table 2-7.

Moreover, there were several different boundary conditions for 'Electric Current'. In the 'Electric Current', the ground became two side boundaries (electric potential V was zero: Dirichlet boundary condition, the boundary equation was a constant voltage). Meanwhile, the 'bottom line' has the potential of 3 mV (as averaged bio-signal potential (Kareem *et al.*, 2017)). The impedance is calculated from one electrode top surface to another by COMSOL. The potentials applied to two electrodes are about 0.89 mV and 0.91 mV with the function of 'Harmonic Perturbation'. These potentials were converged potentials and calculated from simulation. The converged potential is found by using the integral of the rms (root mean square) of the potential on the electrode and find the constant value of the skin-electrode impedance. The parameter used to calculate the convergence was the root mean square of

the total impedance from the electrode to ground, since this value represented the impedance variance at the electrode and the impedance kept constant. The function of 'Harmonic Perturbation' was used to provide a periodic potential. The impedance was calculated from the 'bottom line' to the top of the electrode. Moreover, in COMSOL AC model, the software used the inverse of the absolute value of real and imaginary part of the total admittance as the impedance.

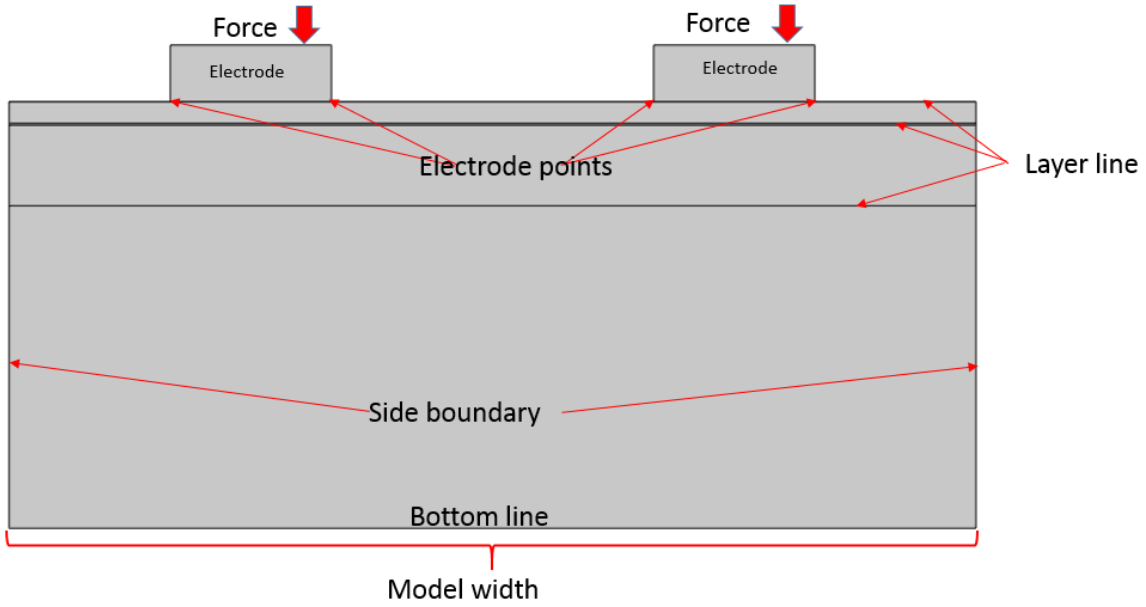

Figure 3-10: Cross section of simplified dual skin-electrode model, each edge is labelled for introduction.

In Figure 3-11, when the applied force (5 N) was applied to both electrodes, each single electrode centre has the similar movement as single electrode shown in Table 3-2, the electrode centre has been moved 2.8 mm for 10 mm model thickness.

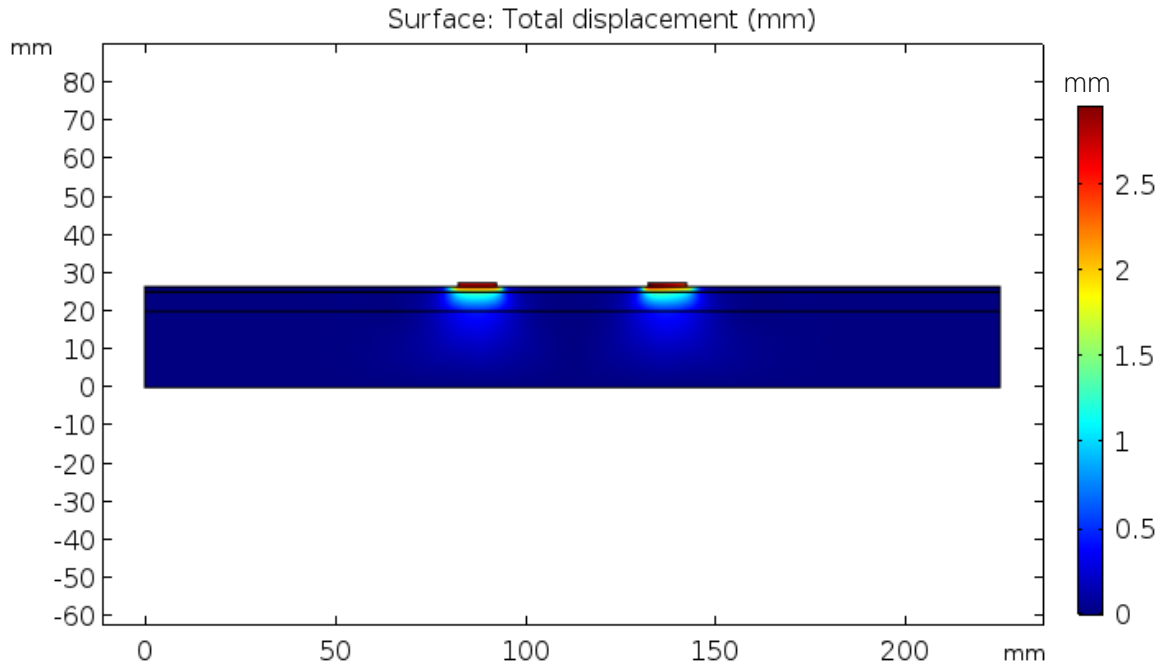

Figure 3-11: Cross section of movement of dual skin-electrode model, a 5 N force is applied to both electrodes.

Comparing with 2D single skin-electrode model, the 2D dual skin-electrode model can be used to estimate the skin impedance between two electrodes, which is close to the two-electrode measurement shown in section 2.5.2 or section 2.5.3. Figure 3-12 shows the impedance change of the dual electrodes versus input signal frequency for two electrodes with 5 N applied force. The frequency values were chosen to see their effect at low frequencies (0.1 to 10 Hz). The electrode size was 10 mm × 10 mm.

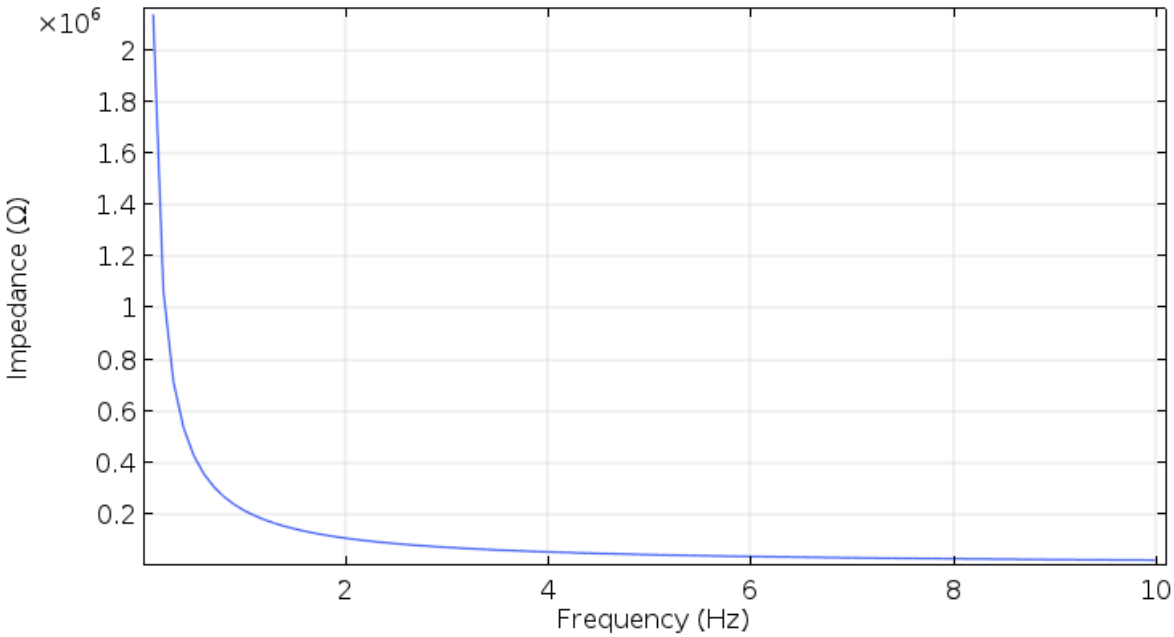

Figure 3-12: 2D dual skin-electrode model impedance varying different frequencies, the electrode size is 10 mm × 10 mm, where the 10 mm is model thickness.

The impedance curve of dual skin-electrode model in Figure 3-12 had the similar problem as the single electrode model. When the frequency was increased from 0.1 Hz to 10 Hz, the skin-electrode impedance between two electrodes was reduced from 2.1×10^6 Ω to 2.2×10^4 Ω. The impedance value at 0.1 Hz was much higher than the literature results (about 10^4 or 10^5 Ω). However, when the frequency was reduced to 10 Hz, the skin-electrode impedance becomes close to the literature results. The problem may arise from the following reasons:

- In this 2D dual electrode model, although it had the structure of two-electrode measurements for skin-electrode impedance, the skin and electrode area were still limited by the 2D model. Because this is the 2D simulation, the model thickness (or depth) increases the skin and electrode area together, and the skin and other tissue as shown in Figure 3-13 cannot be simulated by the 2D model. Conversely, although the skin and other tissue in Figure 3-13 were not measured by the two-electrode measurement directly, the skin and other tissue parts are included in the measurement. Therefore, the literature measurements have this difference from the 2D simulation.
- Moreover, the averaged skin materials may be the second reason to produce this difference between simulation and measurements. To the current simulation, all the skin materials were selected as the average values. However, the material properties at different frequencies were varied. For example, the dielectric constant of HYP layer is different at 10 Hz, 100 Hz and 1000 Hz. When the frequency increased from 10 Hz to 1000 Hz, the dielectric constant of HYP layer changed from 1.2×10^7 to 1.2×10^4, the difference is over 99 %. Therefore, the averaged value of skin materials may limit the accuracy of the simulation.

Because the 2D simulation cannot overcome the model thickness (or depth) problem, to improve the simulation results and analyse the effects of skin materials, a 3D model is built and discussed in next chapter.

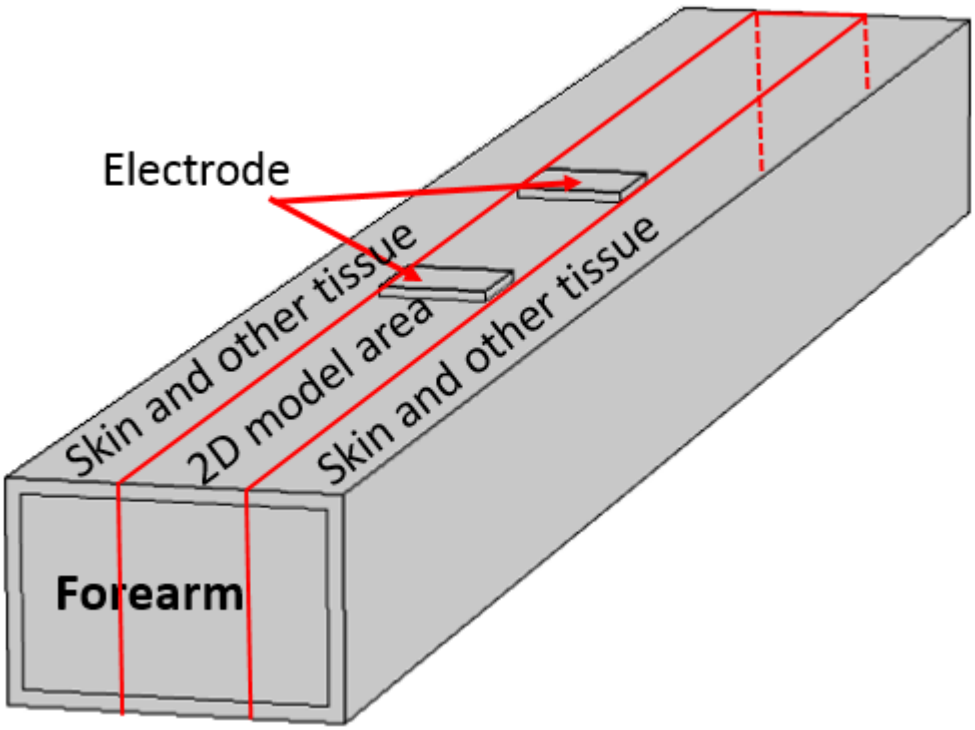

Figure 3-13: Representation of 2D dual-electrode skin simulation, the 2D dual-electrode modelled area and other skin areas are separated by red lines.

3.5.2 3D Skin-electrode model built by COMSOL

The previous section demonstrates that the movement and applied force between the electrode and the skin can change the electric capacitance, and therefore the skin-electrode impedance. However, this was in a 2D model which does not reflect the full properties of the skin and electrodes. Hence it was necessary to create a 3D model to provide a more comprehensive skin electrode model.

The model is shown in Figure 3-14 (a) and (b), the skin layers have the same details as before and include the stratum corneum (SC), epidermis (E), dermis (D), hypodermis (HYP) and muscle (M). Because the dermis consists of multiple layers of different densities it was divided into four sub-layers. The top square is the electrode and the thickness of each layer is shown in Figure 3-14 (a). Figure 3-14 provides the definition of each part of the 3D model.

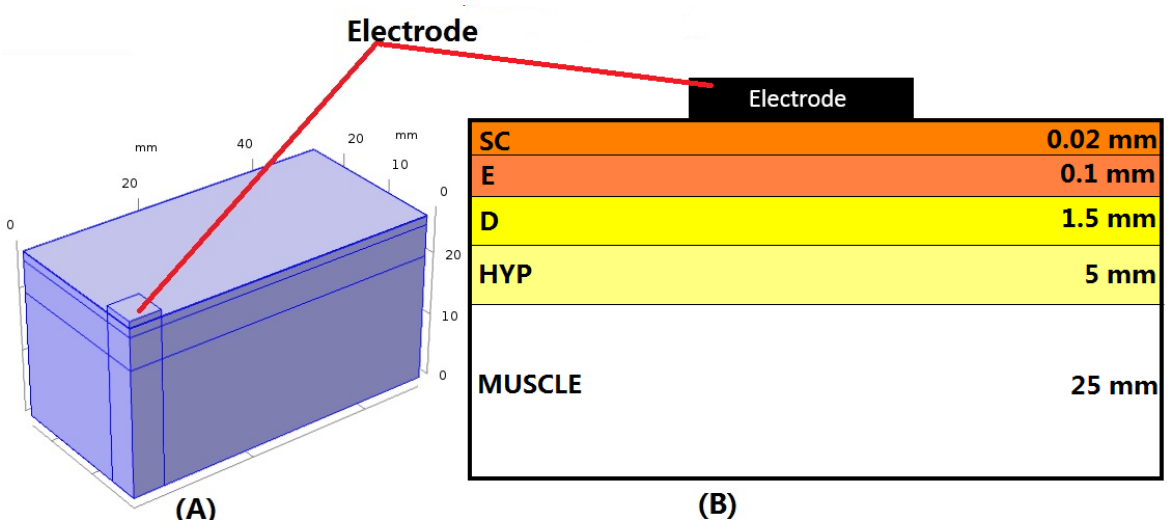

Figure 3-14: (A) 3D COMSOL simulated skin layers, where each layer is projected into the COMSOL model and (B)The different skin layers from top to bottom (electrode, stratum corneum (SC), epidermis (E), dermis (D), hypodermis (HYP), and muscle (M)).

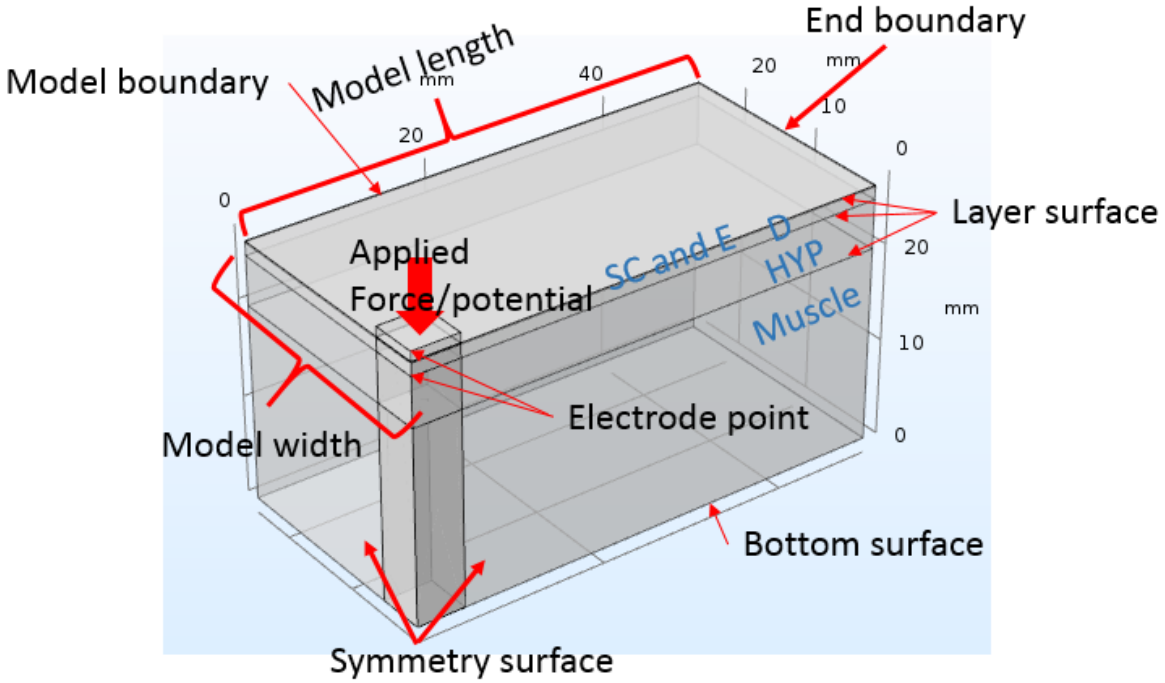

Figure 3-15: Simulated model including the applied signal and symbols/definition for the surfaces, edges and points.

Based on the 2D model, the simulation of 3D model is still built by 'Solid Mechanics' and 'Electric Current'.

Therefore, the materials are still linear elastic and isotropic for 'Solid Mechanics' and 'Current Conservation' for 'Electric Current'. In addition, the skin thickness and the properties of materials are shown in Table 3-4. Although the Young's Modulus, Conductivity, Dielectric constants are taken as averaged value, all of them will be discussed in this chapter.

Electrode and skin	Thickness (mm)	Young's Modulus (MPa)	Conductivity (S/m)	Poisson ratio	Density (kg/m^3)	Dielectric Constant/ Relative Permittivity
Electrode (Ag)	1	8.3	61.6×10^6	0.37	10500	1
Stratum Corneum(SC)	0.02	2.6	0.0003	0.43	1050	6600
Epidermis(E)	0.1	0.5	0.55	0.48	1020	1.14×10^3
Dermis(D)	1.7	0.06	2.9	0.48	1900	1.14×10^3
Hypodermis and fat (HYP)	5	0.28	0.03	0.48	1800	1.2×10^7
Muscle(M)	25	1.77	0.42	0.45	1120	2.5×10^7

Table 3-4: Different mechanical and electrical properties of the skin layers; the value of each layer was calculated as an average value from Table 2-7.

However, compared to the previous simulation in 2D model, the 'lines' in 2D have moved to surfaces in 3D. To summarize, some new boundary conditions are added to the model:

- Added the projection part under the electrode. The projection part allows the COMSOL to use intensive mesh to analyse the skin under electrode.
- In 'Solid Mechanics', 'Model boundaries' surface in Figure 3-15 were set to 'fixed constraints'. There would be no movement on that surfaces. When the force was applied to the model, if there were no fixed constants to limit the model movement, the whole model will be pushed under the applied force. In the real-life situation, the far end of the skin (the end of the arm) has less movement as well, the model width which decided the position of 'Model boundaries' will be discussed in section 3.5.2.1.1.
- 'Electrode points' on the centre line and 'Layer surface' in Figure 3-15 were set to 'Prescribed Displacement in z-axes direction ', these points and surfaces can only move in the z direction.
- 5 N force was applied, as before, to the top surface of electrode, which was the same as 2D model.
- The electrodes could be variable shapes in practice (e.g. circular or rectangle), but in the simulation, the 1cm^2 square electrode was used to represent the electrode as 2D model.
- The 'symmetry surfaces' in Figure 3-15 were set to 'Symmetry', a function provided by COMSOL to make a symmetrical structure, so only a quarter of an electrode was needed in Figure 3-15.
- Because this 3D model was set to 'Symmetry', the 'Model length' was set to 50 mm to approve 100 mm forearm length. This forearm length has the similar skin-electrode impedance as the full forearm length (about 1.5 % difference) and has been shown in section 3.5.1.2.
- In 'Electric Current', the 'Model boundary' surface was set to 'electric insulation', which is same as 2D model.
- The ground was applied to the 'End boundary' (electric potential V was zero: Dirichlet boundary condition, the boundary equation was a constant voltage).
- A potential of 3 mV representing the averaged forearm bio-signal potential (Kareem *et al.*, 2017)) is applied to the 'Bottom surface'. A potential of 9.6 mV

was applied to the top of electrode surface with 'Harmonic Perturbation', which was calculated using the same method as in section 3.5.1.1.1.

- The impedance was calculated from this bottom surface to top of the electrode.

Furthermore, a variable mesh for different layers has been added to improve the mesh calculation:

- In the mesh, the D, HYP and muscle layers in COMSOL were defined to 'Coarse', because they are much thicker than the SC or E layer. For the 'Coarse', the maximum element size was set to 15 mm and the minimum element size was set to 2.7 mm.
- For the thin layer (SC and E), 'swept function' in COMSOL was applied to build the mesh for them. The 'swept mesh' was especially useful for the thin geometries. Because other meshes (like 'coarse') create more elements than necessary to account for the skewed dimension that exist within a thin geometry. The swept mesh creates hexahedral (default) mesh elements. This mesh function can handle the disproportional dimension size with less elements.
- For the electrode layer, the initial testing dimension is 10 mm (width) × 10 mm (length) × 1 mm (thickness), although the testing thickness was thicker than SC and E layer, the area (width × length) of electrode was much smaller than other layers. Therefore, the 'swept mesh' was applied to the electrode.
- The 'Solid Mechanics' and 'Electric Current' were still coupled by 'Deformed Geometry' function, which is the same as 2D model.
- The simulating sequence was same as section 3.5.1 (page 73).
- The total number of elements to solve was 54378.

In the 3D model, the governing equations in COMSOL for the solid mechanics are same as 2D model, therefore, the governing equation for displacement is:

$$0 = \nabla \cdot \nabla \boldsymbol{u} \{\frac{F_{total}}{A} + \mathbf{C}:\frac{1}{2}[(\nabla \mathbf{u})^{\mathrm{T}} + \nabla \mathbf{u} + (\nabla \mathbf{u})^{T} \nabla \mathbf{u}]\} \quad (3\text{-}18)$$

Where **u** is the displacement and F_{total} is the force applied to the electrode, A is the electrode area, **C** is the fourth-order stiffness tensor.

For the electrode potential, it has the same governing equation as 2D single-electrode model in frequency domain:

$$-\nabla \cdot (\mathrm{j}\omega\varepsilon\nabla \mathrm{V} + \sigma \nabla \mathrm{V} - \mathrm{j}\omega \boldsymbol{D}) = 0 \quad (3\text{-}19)$$

Which is the governing equation for the potential in frequency domain.

3.5.2.1 3D single skin-electrode COMSOL model

3.5.2.1.1 3D simulation condition – model width effects

Compared with the 2D simulation, the 3D simulation had better control of the sizes of electrode, and the skin-layers could be meshed in more realistic structure than the 2D simulation. In the single electrode structure, the model width has been tested to see its effects. In the 3D model, the model width was defined in Figure 3-14. Because the simulation was a

quart of an electrode, and the 'model width' was half of the forearm width. The electrode size has been chosen as 10 mm × 10 mm, which is the most commonly used from literature. The model width is increased from 5 mm to be the same size as the electrode. This step is used to find the effects from the model width which represents the forearm width. The electrode centre is moved as the model width changes.

Model width in Figure 3-14 (mm)	**Electrode centre movement (mm)**
5	6.5
7	5
10	4.1
20	3.5
25	3.4
30	3.4

Table 3-5: Electrode centre movements under different 3D model widths.

In the simulation, when the model width was increased from 5 mm to 30 mm (see Table 3-5), the electrode centre movement is reduced from 6.5 to 3.4 mm. Because the model width change did not give a significant effect on the electrode centre movement after 20 mm, if the model width is greater than 20 mm, the electrode movement would not be affected by the applied force. From the literature, the average forearm girth for young people (aged 20 to 30) was between 23 to 30 cm (Hume *et al.*, 2009; Abe and Loenneke, 2015). From the forearm girth, the estimated radius of forearm is between 3.6 to 4.8 cm. If the radius of forearm is converted into model width, because the model width is half of the forearm width, the model width should have the same range as the radius of forearm (between 3.6 to 4.8 cm). To see the effects from model width, the skin-electrode impedances for different model widths are simulated and shown in Figure 3-16.

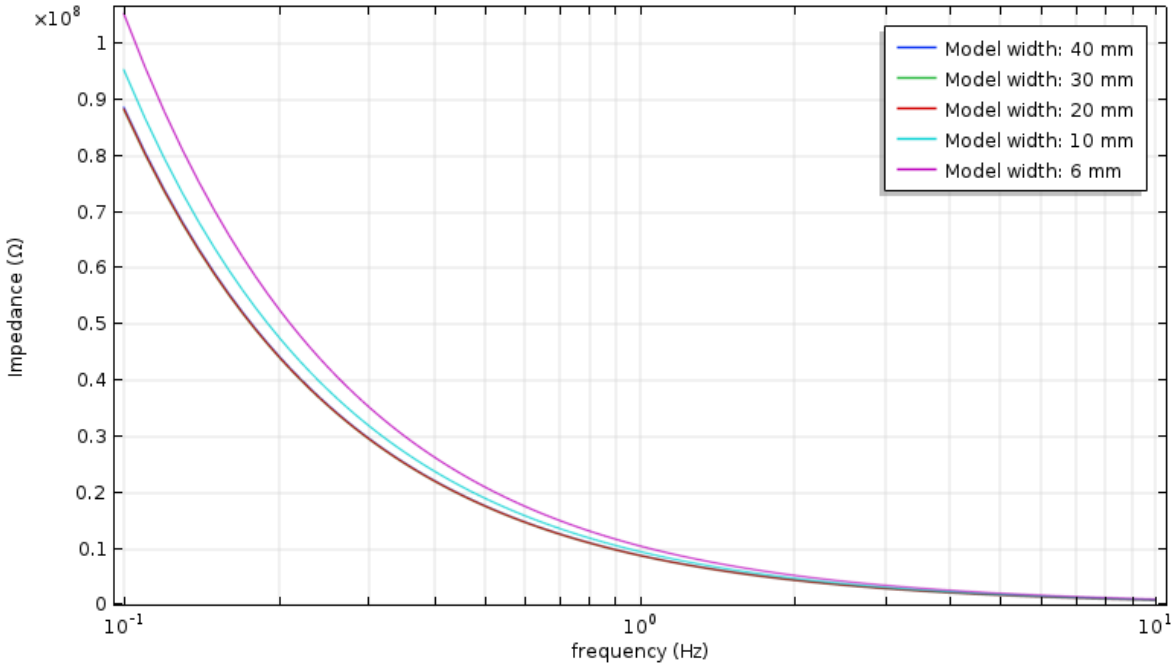

Figure 3-16: 3D Skin-electrode impedance change of model width at low frequencies (0.1 Hz to 10 Hz) with 5 different width (40 mm, 30mm, 20 mm, 10 mm and 6 mm), the applied force is 5 N, the model widths of 20, 30 and 40 mm overlap so cannot be identified in the figure.

In Figure 3-16, when the model width was increased to 20 mm or more, the skin-electrode impedances are almost the same. When the model width was increased from 20 mm to 40 mm, the impedance at 0.1 Hz was reduced from $8.88 \times 10^7\ \Omega$ to $8.84 \times 10^7\ \Omega$ (Approximately 0.5 %). However, when the model width was increased from 7 mm to 20 mm, the impedance at 0.1 Hz was reduced from $10.5 \times 10^7\ \Omega$ to $8.9 \times 10^7\ \Omega$ (about 20 %). From the changes of impedance for different model widths, it could conclude that if the model width is more than 20 mm for 1 cm^2 electrode model, the skin-electrode impedance will not be affected by the model width. Therefore, the model width is set to 30 mm to identify the effects from skin layer in following sections. Furthermore, 30 mm model width can provide some space to identity the effects from electrode sizes.

3.5.2.1.2 COMSOL analysis for skin layer effects in 3D model

In this subsection, because the 3D model was implemented, the 3D model was used to analyse the skin layers' properties under different input stimuli to identify which parameter has the key impact. The simulation model was used to observe the effect on the skin-electrode combination of the various skin and electrode parameters (e.g. Young's modulus, dielectric constant, conductivity or electrode sizes). The simulation as a function of pressure is shown in Figure 3-17. The dark red indicated increased deformation due to pressure with the dark blue showing less deformation. From previous sub-sections, the electrode would be moved by the applied force, so the skin's Young's Modulus was tested as the first effective parameter. In all the simulation of skin layers' effects, the applied force on the electrode is constant force (5 N).

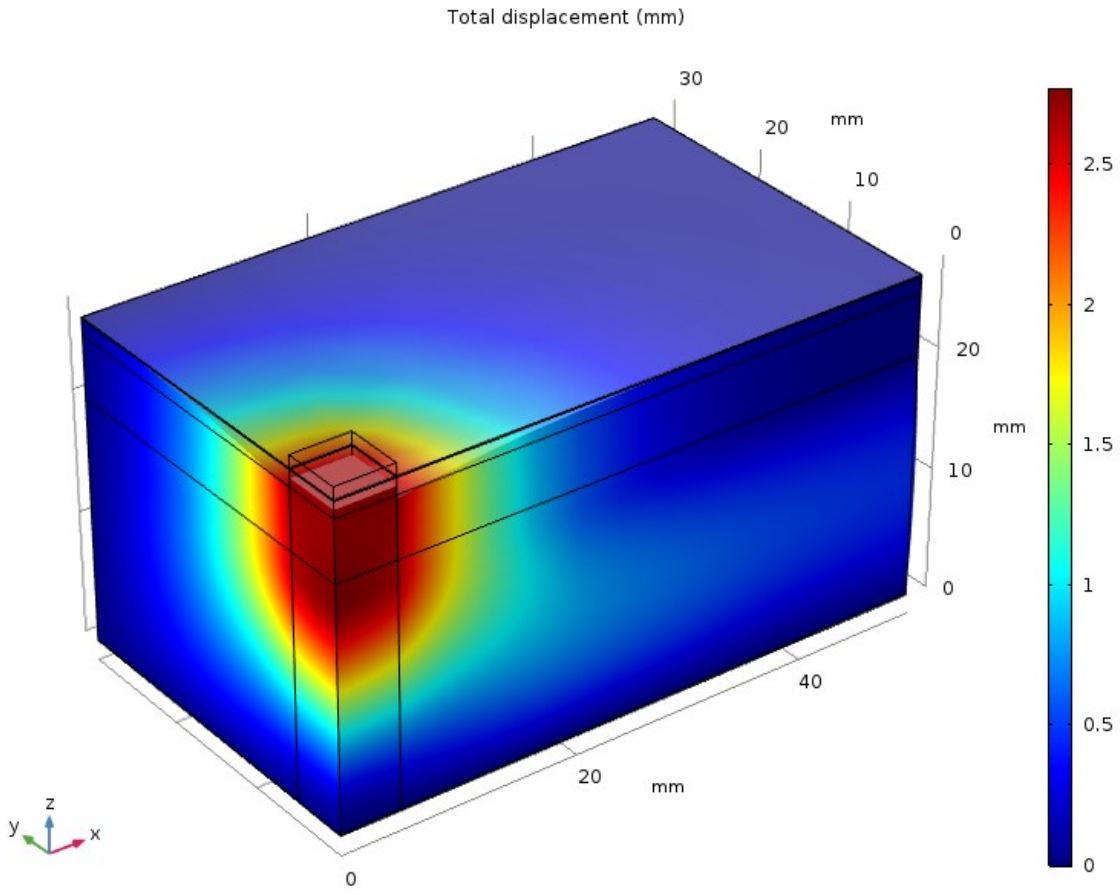

Figure 3-17: Simulation of the pressure applied on the electrode and the deformation.

3.5.2.1.2.1 Young's Modulus of different skin layers

In the simulation, the effects of Young's Modulus on different skin layers were simulated and the results presented in Figure 3-18 to Figure 3-21. The stratum corneum, epidermis, dermis and will hypodermis and fat affect the EMG measurement results more than muscle. From the literature, each layer was varied in different intervals as shown in Table 3-6. Therefore, the Young's Modulus of each layer was increased from the minimum to maximum value to identify its effects for different skin layers. To analyse the Young's Modulus of each layer, 4 data points have been selected to analyse: the first quartile, the median, the third quartile and the upper limit of each Young's Modulus. In addition, the whole muscle layer is the source of the bio-signal and the applied force will not change the bio-potential on the muscle layer, so the change of Young's Modulus of the muscle is not considered.

Skin layer	Stratum Corneum (SC)	Epidermis(E)	Dermis(D)	Hypodermis and fat (HYP)	Muscle(M)
Young's Modulus (MPa)	1.99 - 3.2	0.134 - 1.0	0.02 - 0.08	0.2 - 2	1.33 - 2.21

Table 3-6: The range of Young's Modulus of Stratum Corneum (SC), Epidermis(E), Dermis(D) Hypodermis and fat (HYP) and Muscle(M) from the literature (Agache *et al.*, 1980; Chen *et al.*, 1996; Hendriks, 2001; Flynn and McCormack, 2008; Gerligs, 2009; Bazzazi and Sadr, 2010; Hara, 2013)

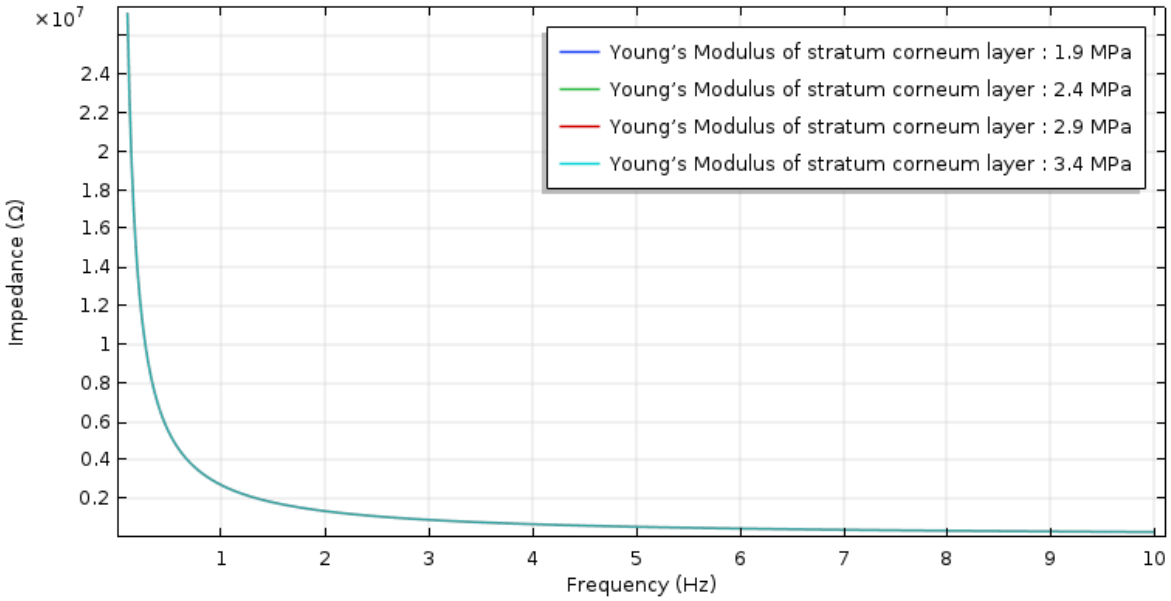

Figure 3-18: Impedance change of the stratum corneum layer under frequencies (0.1 Hz to 10 Hz) with 4 different Young's Modulus of stratum corneum layers (1.9 MPa, 2.4 MPa, 2.9 MPa and 3.4 MPa), the applied force was 5 N.

Figure 3-18 showed the effects of different values of Young's Modulus of the stratum corneum at a constant applied force. When the force is applied to the electrode, Young's Modulus is the key factor which affects the distance between the electrode and the skin and therefore the impedance. From the simulation results, when the frequency was increased from 0.1 Hz to 10 Hz, the impedance decreased from $2.72 \times 10^7\ \Omega$ to $2.74\times 10^5\ \Omega$ with SC Young's Modulus at 1.9 MPa. Comparing this with the impedance under the same frequency range but with a Young's Modulus of 3.4 MPa, the impedance for the skin-electrode model increased by 0.9 %, which indicates there was no significant effect on the impedance as a result of varying the stratum corneum's Young's Modulus using the literature values (from 1.9 – 3.4 MPa).

After analysis of the Stratum Corneum layer, the results for the epidermis and dermis layer with different Young's Modulus from the literature are shown in Figure 3-19 and Figure 3-20.

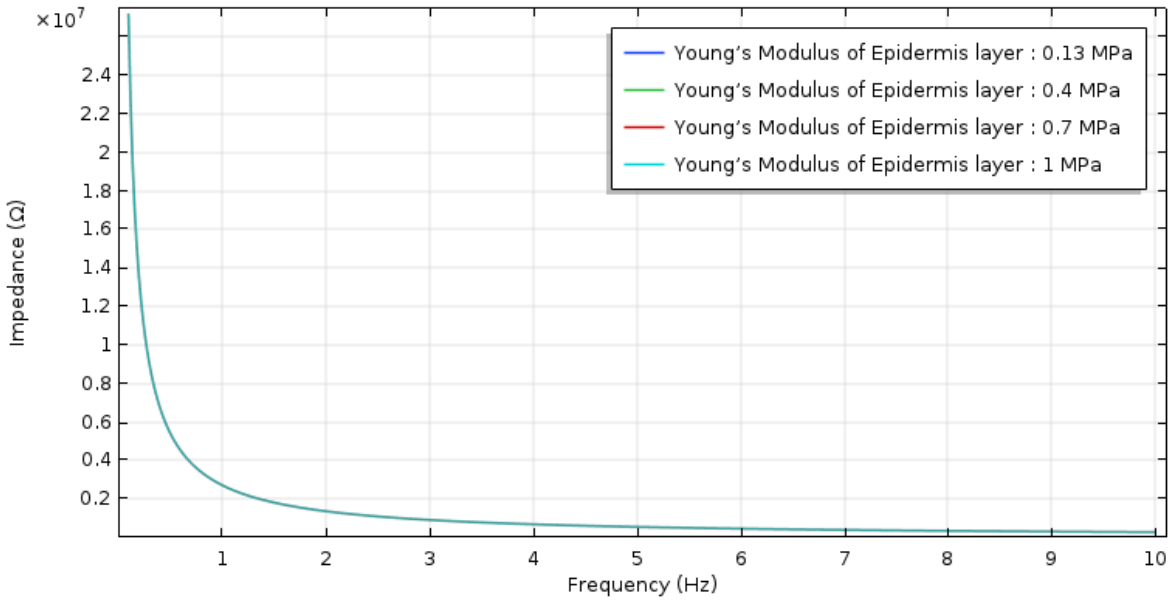

Figure 3-19: Impedance change of the epidermis layer under low frequency (0.1 to 10 Hz) with 4 different Young's Modulus for the epidermis layers (0.134 MPa, 0.4 MPa, 0.7 MPa and 1 MPa), the applied force was 5 N.

Figure 3-19 showed the impedance change for the epidermis layers with 4 different Young's Modulus values taken from the literature and described in Table 2-7 and with a 5 N applied force. When the frequency was increased from 0.1 Hz to 10 Hz, the impedance decreased from $2.7 \times 10^7\ \Omega$ to $2.7 \times 10^5\ \Omega$ with the Young's Modulus for the epidermis at 0.13 MPa. Comparing the highest and lowest impedance values under different Young's Modulus values, the impedance for skin-electrode model increased by approximately 0.3 %.

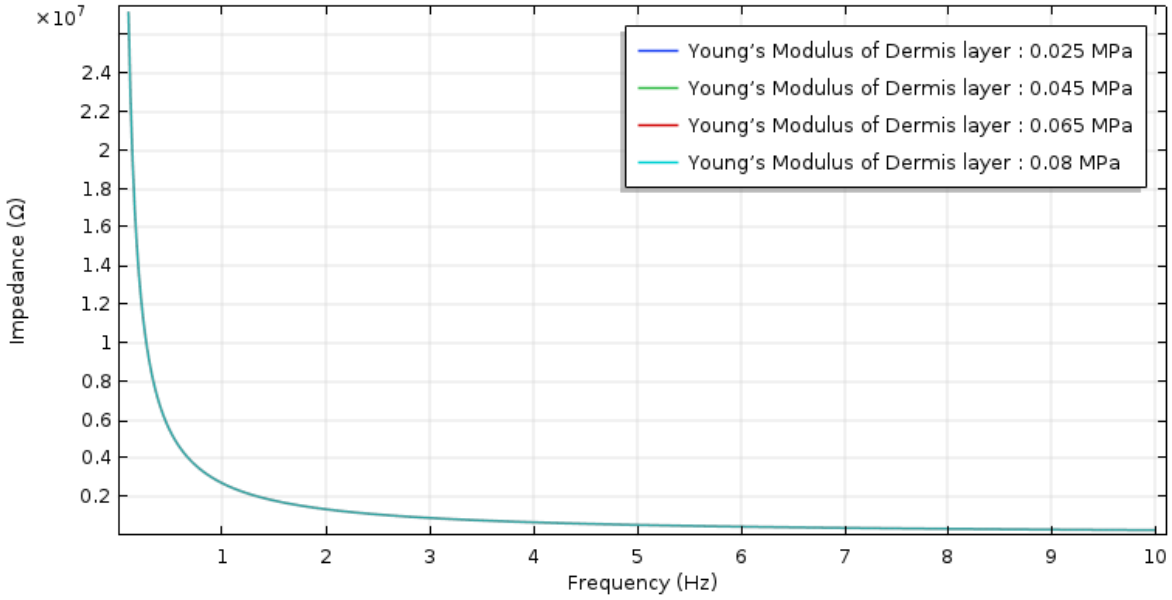

Figure 3-20: Impedance change of the dermis layer with 4 different Young's Modulus values under low frequencies (0.1 to 10 Hz) of the dermis layer (0.025 MPa, 0.045 MPa, 0.065 MPa and 0.08 MPa), where the applied force was 5 N.

The results in Figure 3-20 showed that the largest impedance was $2.71 \times 10^7 \Omega$. When the Young's Modulus of the Dermis was equal to 0.08 MPa and the applied force was 5 N under 0.1 Hz, then the Young's modulus of the dermis layer increased from 0.025 MPa, and the highest impedance increased by approximately 0.6 %.

Finally, Figure 3-21 showed the effect of the Young's modulus of the HYP layer with 4 different values taken from the literature and shown in Table 2-7.

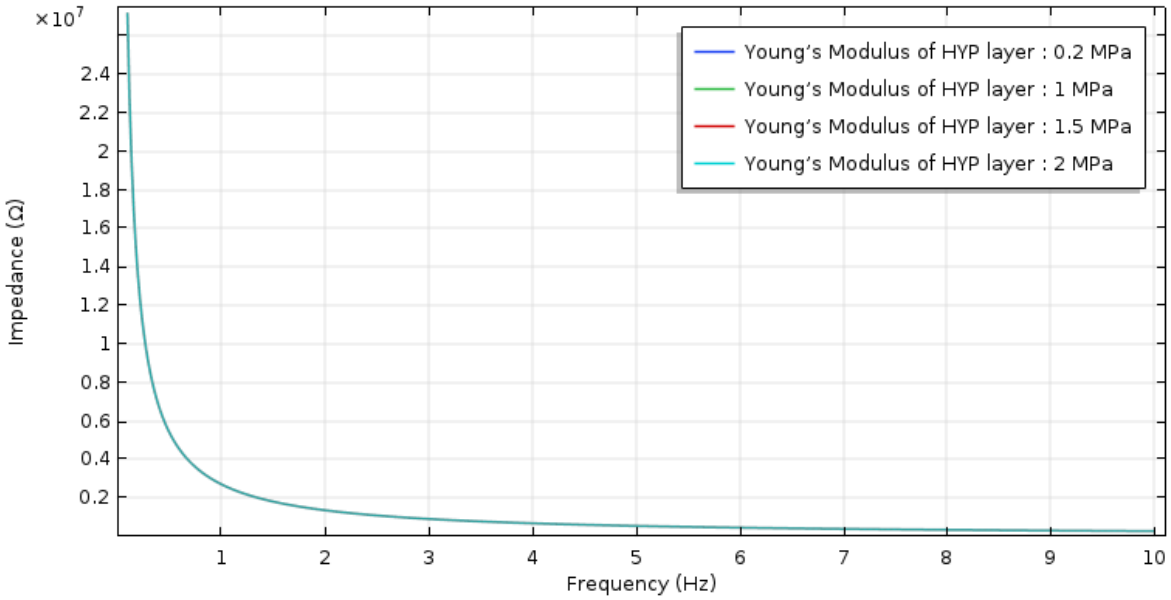

Figure 3-21: Impedance change of the HYP layer with 4 different Young's Modulus values under low frequencies (0.1 to 10 Hz) of the HYP layer (0.2 MPa, 1 MPa, 1.5 MPa and 2 MPa), where the applied force was 5 N.

The results in Figure 3-21, the highest impedance is $2.72 \times 10^7 \Omega$ with the HYP Young's Modulus at 2 MPa and 0.1 Hz. If the frequency is kept at 0.1 Hz, the simulated impedance decreases to $2.58 \times 10^7 \Omega$, so the impedance has been changed by about 5 %.

The results show that all the four layers (stratum corneum, epidermis, dermis and hypodermis) have little effects (less than 5 %) arising from different values of Young's Modulus. Young's Modulus for different variables did not provide significant effects. Meanwhile, in the simulation of Young's Modulus for the skin, the HYP is the thickest layer of all 4 layers, so the Young's Modulus range of HYP had the largest difference compared to the other three layers, of approximately 5 %. Therefore, in the further simulation, the averaged Young's Modulus for each layer will be used.

3.5.2.1.2.2 Conductivity of different layers

In the skin layer, the conductivity is another parameter that impacts on the skin-electrode impedance in the measurements. From the literature, each layer has a different range of conductivity as shown in Table 3-7. Therefore, the conductivity of each layer is increased from the minimum to maximum value to identify its effects for different skin layers. (stratum corneum, epidermis, dermis and hypodermis). To analyse the conductivity of each layer, 4 data points have been selected to analyse: the first quartile, the median, the third quartile and the upper limit of each conductivity.

Skin layer	Stratum Corneum (SC)	Epidermis(E)	Dermis(D)	Hypodermis and fat (HYP)	Muscle(M)
Conductivity (S/m)	0.000125 - 0.000455	0.55 ± 0.2	2.9 ± 0.33	0.02-0.04	0.04-0.8

Table 3-7: The range of conductivity of Stratum Corneum (SC), Epidermis (E), Dermis (D) Hypodermis and fat (HYP) and Muscle (M) from the literature (Huclova, Erni and Fröhlich, 2012; Dierickx and Hinsenkamp, 1992; Gabriel, Gabriely and Corthout, 1996; Miklavcic, Pavselj and Hart , 2006).

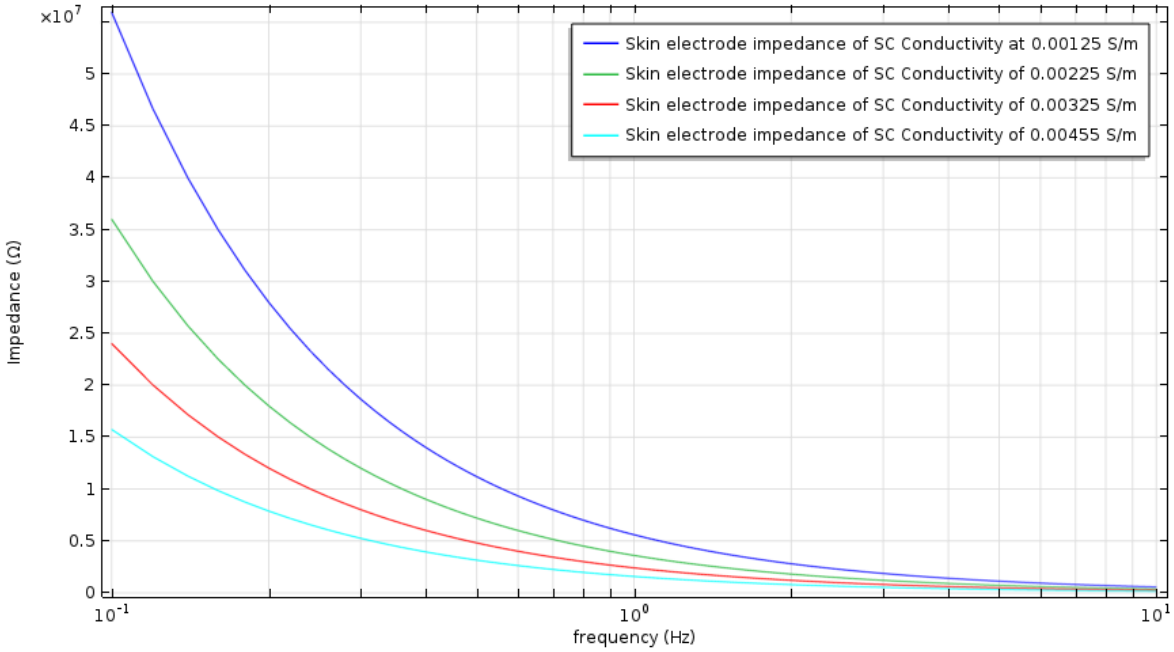

Figure 3-22: Impedance change of the SC layer with 4 different conductivities (0.000125 S/m, 0.000225 S/m, 0.000325 S/m and 0.000445 S/m) under low frequencies (0.1 to 10 Hz).

In Figure 3-22, the skin-electrode impedance of SC reduced as the conductivities increased. When the conductivity increased from 0.000125 S/m to 0.000445 S/m, the impedance at 0.1 Hz decreased from 5.6×10^7 Ω to 1.6×10^7 Ω, which is approximately 71 %. Furthermore, the reduction of the impedance was proportional to the decrement of the SC's conductivities, when the conductivity reduced every 0.0001 S/m, the impedance reduced by approximately 33 %.

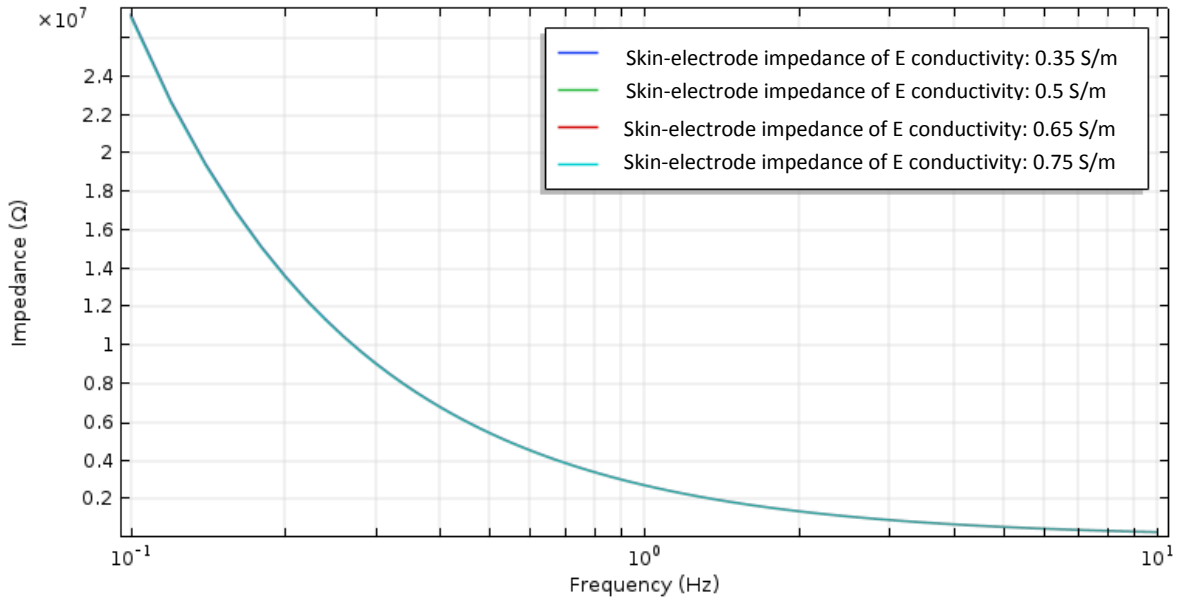

Figure 3-23: Impedance change of the E layer with 4 different conductivities (0.35 S/m, 0.50 S/m, 0.65 S/m and 0.75 S/m) under low frequencies (0.1 to 10 Hz).

For the impedance change of the E layer, there was no obvious changes as shown in Figure 3-23 during the change in conductivity. When the conductivity of E increased from 0.35 to 0.75 S/m, the skin-electrode impedance increased by only 4 %, which is much less than the changes in the SC layer and the conductivity of E layer cannot give the impact on the simulation. Therefore, all 4 conductivities could be used in the simulation, and 0.5 S/m is selected for further simulation. After analysing the effect from the E layer, the conductivity of D the layer is shown in Figure 3-24.

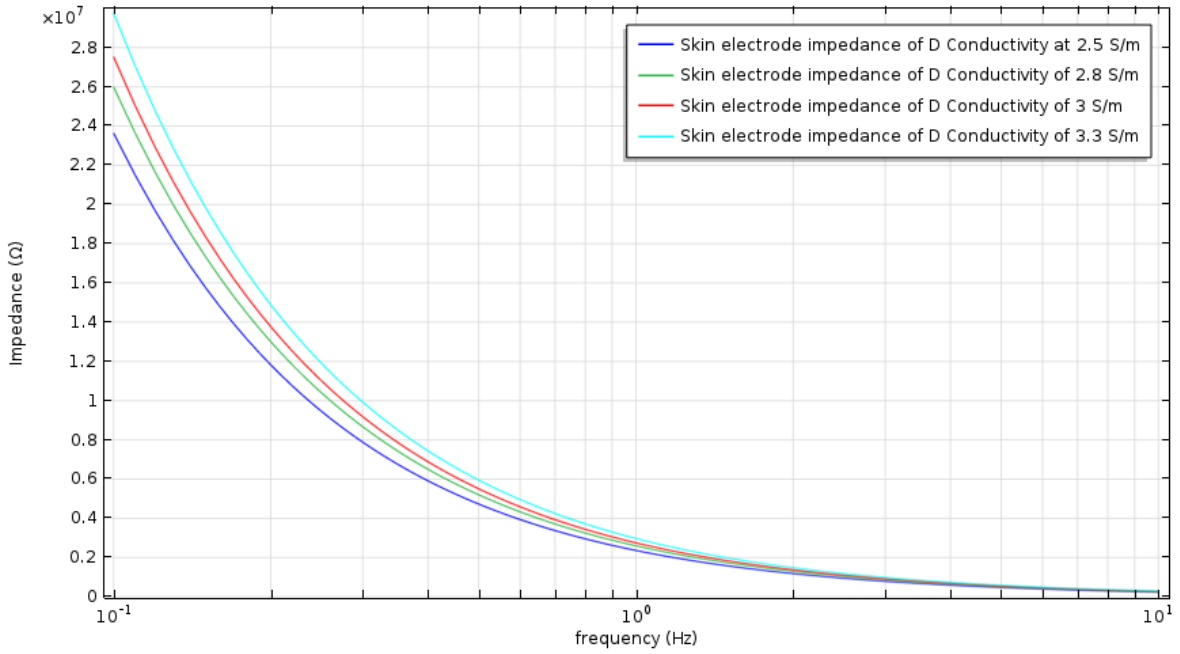

Figure 3-24: Impedance change of the D layer with 4 different conductivities (2.5 S/m, 2.8 S/m, 3.0 S/m and 3.3 S/m) under low frequencies (0.1 to 10 Hz).

Figure 3-24 showed the impedance change for the D layer, when the conductivity increased from 2.5 to 3.3 S/m. The impedance at 0.1 Hz increased from 2.4 × 10^7 Ω to 3 × 10^7 Ω, which is approximately 25 %. Although the D layer had an effect on the skin-electrode impedance, the impedance difference between the lowest and highest values was still smaller than the conductivity change of SC. Furthermore, the conductivity of D layer was in very small interval, the difference between the highest and lowest conductivity was only about 30 %. Therefore the median number of the conductivity of D layer (3 S/m) could be used for further simulation. After analysing the conductivity of S layer, a further comparison, the impedance simulation of HYP conductivity is shown in Figure 3-25.

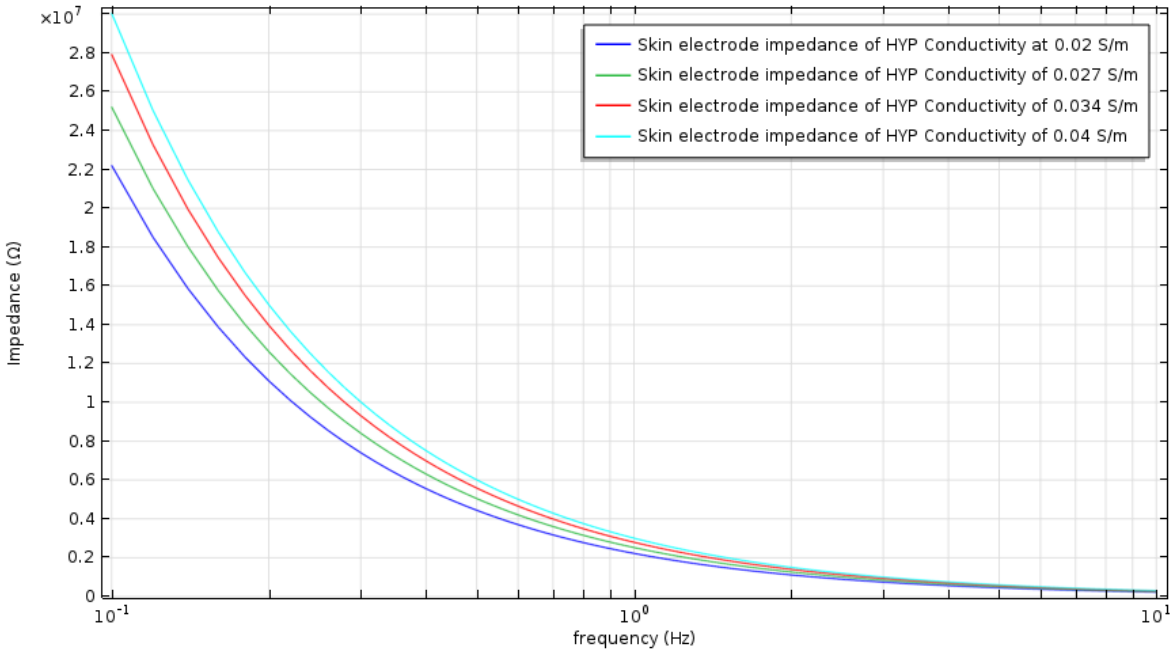

Figure 3-25: Impedance change of the HYP layer with 4 different conductivities (0.02 S/m, 0.027 S/m, 0.034 S/m and 0.04 S/m) under low frequencies (0.1 to 10 Hz).

When the conductivity of HYP layer changed from 0.02 to 0.04 S/m, the skin-electrode impedance increased from 2.2 × 10^7 Ω to 3.1 × 10^7 Ω, a change of approximately 41 %. This is a significant change and represented the second highest impact on the overall impedance after the SC layer.

Comparing these two impedance changes during the change of dielectric constant of SC and HYP, for the SC layer, the impedance decreased during when the dielectric constant of SC increased. In contrast, for the HYP layer, the impedance increased when the dielectric constant of HYP also increased. This phenomenon can be explained by the following equations representing the linear electric model. To obtain more accurate results, the non-linear electric model should be used but the following reasons mean that the non-linear model cannot apply to the simulation.

- In the simulation and literature, the linear character of conductivity or dielectric constant is able to cover most of the situations at a fixed frequency. If we would like to analyse some external factors (such as electrode size, applied force etc), the result can be calculated by this linear skin-electrode model. Comparing with non-linear dielectric constant or conductivity, both of dielectric constant and conductivity varies

as frequency, it means that each dielectric constant and conductivity has its own value at a fix frequency, therefore, if the dielectric constant and conductivity at the fixed frequency is known, the difference between linear and non-linear simulated result will not have a huge difference. Further, in some of the literature (Camelia *et al.*, 1996), the dielectric constant and conductivity are given only at certain frequencies; for example under 1000Hz, there were only 4 given dielectric constants and conductivities. So this limited number of points are not sufficient for a non-linear model. Therefore, the linear electric model is applied to the model. Furthermore, In all the literature, the dielectric constant and conductivities for low frequency were measured at several discrete frequencies such ass 10 Hz, 100 Hz, 1000 Hz. However, most of the data were focused on the high frequency range (higher than 10^7 Hz), therefore, there were no enough data to support the non-linear simulation.

- There is no existing equipment to measure data of dielectric constants and conductivities varied with frequencies at University of Southampton.

Therefore, the linear electric model is applied to analyse the simulation.

For an AC source, permittivity can be written as:

$$\varepsilon = \varepsilon_r \varepsilon_0 + j\frac{\sigma}{\omega} \quad (3\text{-}20)$$

In the equation, ε is the permittivity of the material, $\varepsilon_r$is dielectric constant, ε_0 is electric constant, σ is the conductivity and ω is the angular velocity (relative to frequency). Moreover, the impedance in the simulation can be presented as:

$$Z = R + j\frac{1}{\omega C} \quad (3\text{-}21)$$

Where Z is the impedance, R is the series resistance and not parallel with the capacitor and C is the capacitance.

Furthermore, for the capacitance and resistance, their relationship can be presented as:

$$C = \varepsilon\frac{A}{d} \quad (3\text{-}22)$$

Where A is the area of the overlap of the two plates of the capacitor and d is the separation between two plates.

If all the equations are combined together, the impedance can be presented as:

$$Z = R + j\frac{1}{\omega\left(\varepsilon_r\,\varepsilon_0 + j\frac{\sigma}{\omega}\right)\frac{A}{d}} \quad (3\text{-}23)$$

In the equation, the R, d and A are constant values, they will not be changed at different frequencies, so the equation can be shortened to:

$$Z_{variable} = j\frac{1}{\omega\left(\varepsilon_r\,\varepsilon_0 + j\frac{\sigma}{\omega}\right)} \quad (3\text{-}24)$$

$$\rightarrow \frac{1}{Z_{variable}} = \frac{\sigma}{\omega} - j\omega\varepsilon \quad (3\text{-}25)$$

From the above equations, it can be seen that the impedance is related to the conductivity, permittivity, and frequency (angular velocity), Conductivity dominates the real part and permittivity dominates the imaginary part. In the simulation of SC conductivity, the value of SC conductivity was applied between 0.000125 S/m to 0.000455 S/m and the SC permittivity was approximately 9×10^{-9} F/m, the permittivity and frequency in the imaginary part of the impedance drive the impedance results. So the impedance keeps decreasing as the SC conductivity increases. In contrast, in the simulation of HYP conductivity, the value of HYP conductivity was applied between 0.02 S/m to 0.04 S/m and the HYP permittivity was approximately 3×10^{-6} F/m, the conductivity in the real part of the impedance drives the impedance result. So the impedance continues to increase as the HYP conductivity increases.

Therefore, to consider about the real part of the impedance and drive the impedance results, the highest conductivity of HYP (0.04 S/m) is chosen for the further simulation.

Although the SC and HYP show opposing trends to the impedance change, the SC and HYP layers had the greatest impact in the simulation. For the SC and HYP layers, the difference between the lowest and highest values was approximately 70 % and 40 %, which are much higher than other layers. Both of these two layers have lower values of conductivity (the scales are 0.0001 and 0.01 S/m), and the conductivity (S/m) is a reciprocal of the resistivity (Ω.m), so any small impedance change in SC and HYP are higher than the impedance change in the E and D layers. For all the skin layers, the SC layer is the outermost layer and decided by the age of the person. For example, older people have looser skin than the young. If the simulation is used to model older people, the SC layer's conductivity needs to be considered as one of the key parameters. Moreover, the HYP layer was the second most important layer in the simulation of skin's conductivity, as fat is contained in the HYP layer. If the simulation is used to identify people with high weight, the HYP layer needs to be considered as one of the most important effects.

Moreover, by analysing the trend of the impedance change, it was found that the permittivity is another key parameter that impacts on the skin electrode impedance, so the dielectric constant, which is the parameter used to calculate the permittivity of a single material, is analysed in the next subsection.

3.5.2.1.2.3 Dielectric constant of different layers

The dielectric constant/relative permittivity of the skin layers is another factor that affected the simulation results. In the literature, it has been shown that the dielectric constant of tissue under the skin varies with frequency. If the frequency is 2 Hz, the dielectric constants of some tissues may reach 10^7 (like HYP or SC in Table 3-8) (Gabriel, Gabriely and Corthout, 1996). However, when the frequency increases to 10 Hz, the dielectric constant of SC reduces to 7000. Therefore, it is necessary to analyse the effects of dielectric constant variation for the skin layers. Based on Table 2-7 and Table 3-8 , except for the muscle layer (signal source), the dielectric constant of SC layer was varied from 1000 to 10×10^7, if the frequency of SC was changed from 2 to 1000 Hz. Meanwhile, the HYP had 3 dielectric constant values at different frequencies (10 Hz, 100 Hz and 1000 Hz). In the simulation, the dielectric constants at different frequencies were substituted into the same frequency range to see the effect of dielectric constant. The reason was that the impedance in the simulation

showed the same effects at low or high frequency, if the impedance was low at lower frequency, the impedance would be low at high frequency. Furthermore, this step can be used to see if one dielectric constant could cover different frequency ranges.

Skin layer	Stratum Corneum (SC)	Hypodermis and fat (HYP)
Dielectric constant	6600 to 1140 (averaged SC from 10 Hz to 1000 Hz) 10×10^4 (2 Hz) 10×10^7(2 Hz include lowing layers)	$1.2\times1\ 0^7$ (at 10 Hz) $3.3\times\ 10^5$ (100 Hz) 1.2×10^4 (1000 Hz)

Table 3-8: Dielectric constant of Stratum Corneum (SC) and Hypodermis and fat (HYP) at different frequencies from the literature (Huclova, Erni and Fröhlich, 2012; Gabriel, Gabriely and Corthout, 1996; Miklavcic, Pavselj and Hart, 2006).

Hence the dielectric constant of the SC layer was analysed first under 10 Hz.

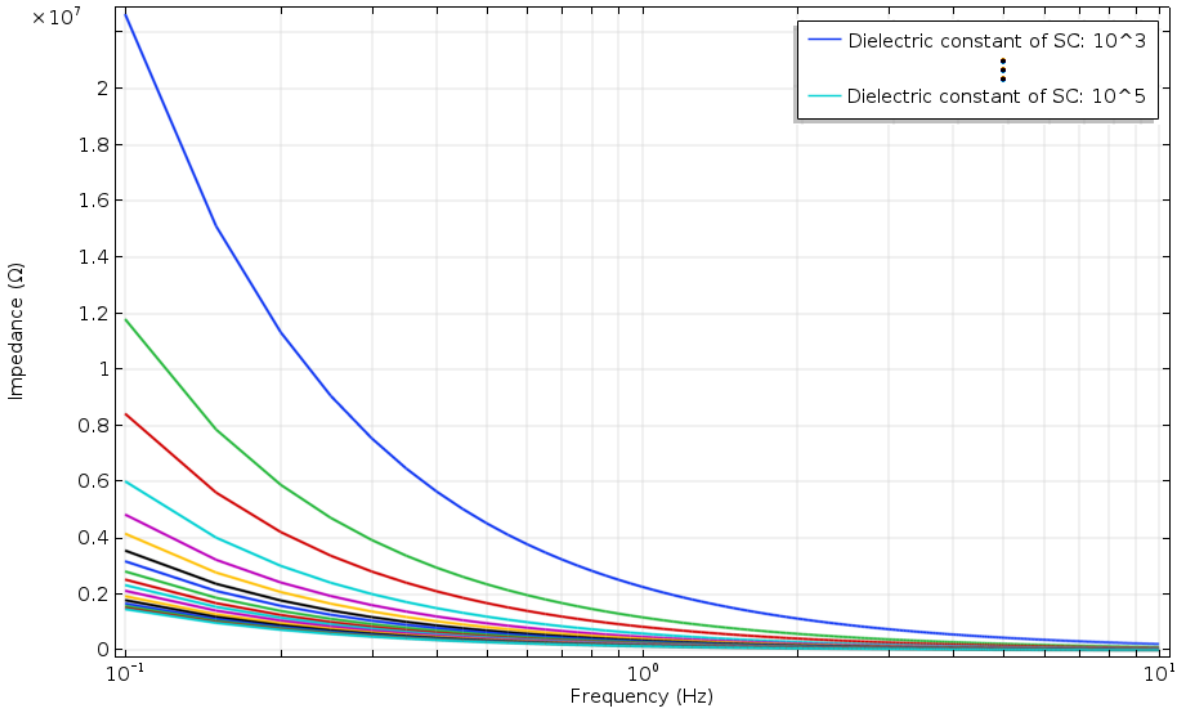

Figure 3-26: Impedance changes under low frequencies (from 0.1 to 10 Hz). The dielectric constant of SC was increased from 1×10^3 to 100×10^3 in steps of 20. The blue is the starting dielectric constant (1×10^3).

Figure 3-26 showed the different dielectric constants under varied frequencies. Because the dielectric constant is different at different frequencies, the change of the dielectric constants (from 1×10^3 to 100×10^3) covered the average dielectric constants at different frequencies. When the dielectric constant of SC increased from 1×10^3 to 100×10^3 at the lowest frequency (0.1 Hz), the skin-electrode impedance reduced from $2.5\times10^7\ \Omega$ to $1.2\times10^6\ \Omega$, which means the impedance reduced by approximately 95 %. When the dielectric constant increased from 1×10^3 to 100×10^3 at the highest frequency (10 Hz), the skin-electrode impedance reduced from $2.4\times10^5\ \Omega$ to $1.2\times10^4\ \Omega$ (about 95 %).

Meanwhile, if the dielectric constant of SC increases from 10^7 to above this corresponds to the dielectric constant at a very low frequency of less than 2 Hz and which includes some tissue under the SC layer (Miklavcic *et al.*, 2006).The skin-electrode impedance curves were shown in Figure 3-27 with different impedance curves as the dielectric constant increases.

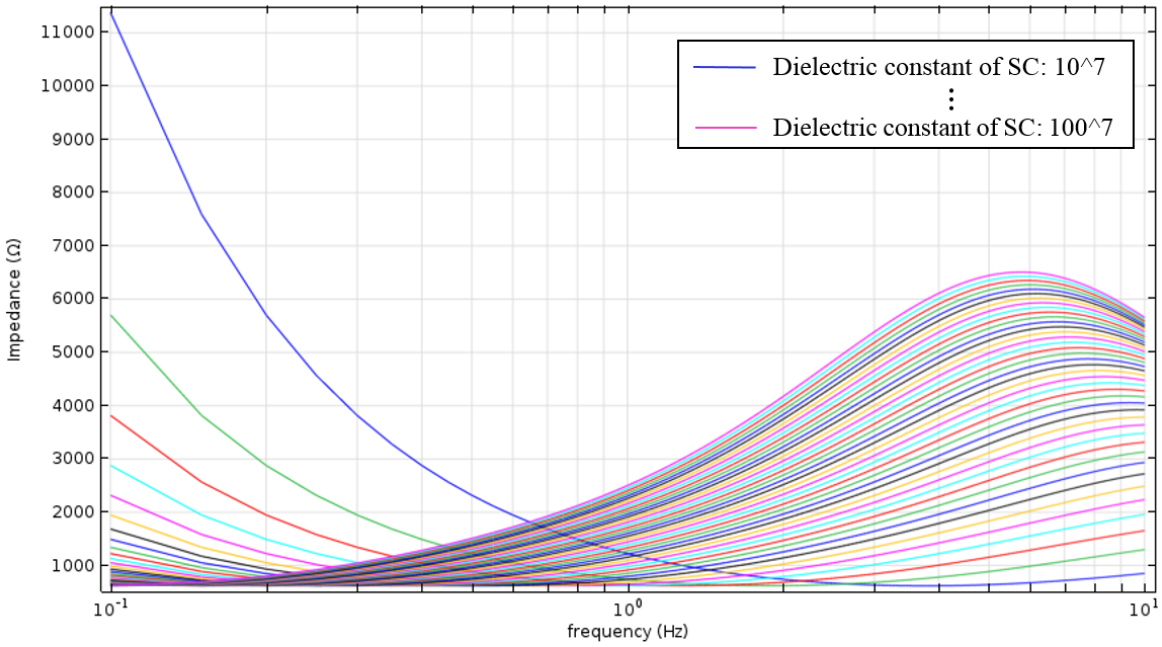

Figure 3-27: Skin-electrode impedance changes at low frequency from 0.1 to 10 Hz. Where the dielectric constant of SC increased from 10^7 to 10^9.

At 0.1 Hz, the skin-electrode impedance decreases from 1.1×10^4 to 621 Ω. However, the impedance was not reduced to zero when the dielectric constant increased. When the dielectric constant of the SC was increased to 38×10^7, the impedance started to increase. At very low frequency (less than 1 or 2 Hz), the impedance continued increasing and started to reduce at a specific frequency which depended on the dielectric constant of all the skin layers. The reason could be analysed using equation (3-26):

$$Z_{variable} = j\frac{1}{\omega\left(\varepsilon_r\,\varepsilon_0 + j\frac{\sigma}{\omega}\right)} \quad (3\text{-}26)$$

Where ε is the permittivity of the material, ε_r is the dielectric constant, ε_0 is the electric constant, σ is the conductivity and ω is the angular velocity (relative to frequency).

Therefore, the impedance is calculated from the following equation:

$$Z_{variable} = \frac{1}{\omega\varepsilon_r\,\varepsilon_0 + j\sigma} \;and\; \varepsilon = \varepsilon_r\,\varepsilon_0 \quad (3\text{-}27)$$

$$=>\; Z_{variable} = \frac{\omega\varepsilon - j\sigma}{\omega^2\varepsilon^2 - \sigma^2} \quad (3\text{-}26)$$

$$=>\; Z_{variable} = \frac{\omega\varepsilon}{\omega^2\varepsilon^2 - \sigma^2} - j\frac{\sigma}{\omega^2\varepsilon^2 - \sigma^2} \quad (3-28)$$

Equation (3-28) showed that if the dielectric constant kept increasing, the real part of the equation would dominate the final result ($Z_{variable}$), the total equation would become small and tend zero. However, this equation calculated $Z_{variable}$ is the imaginary part of equation (3-23). When this imaginary part ($Z_{variable}$) becomes zero, the real part of the equation (2-23) would dominated the total impedance. That is why the impedance in Figure 3-27 starts to increase at a certain frequency.

Moreover, to identify the effects of dielectric constant at high frequency (higher than 100 Hz) and wide frequency range (10 Hz to 1000 Hz), 3 certain dielectric constant from the literature were selected (6600 (10 Hz), 3300 (100Hz) and 1140 (1000 Hz)) and substituted into the frequency range from 10 to 1000 Hz and shown in Figure 3-28.

Figure 3-28 shows that the dielectric constant of SC at 100 Hz was close to the dielectric constant of SC at 1000 Hz. When the dielectric constant was changed from 6600 (10 Hz) to 3000 (100 Hz), the impedance at 1 Hz increased from 1.7×10^6 Ω to 5.1×10^6 Ω, which is approximately 200 %. Meanwhile, when the dielectric constant changed from 3000 (at 100 Hz) to 1140 (at 1000 Hz), the impedance at 1 Hz increased from 5.1×10^6 Ω to 9×10^6 Ω, which is about 76 %. To avoid the mismatch between different data for the SC layer, the average dielectric constant of dry skin (1140 covers the 10 to 1000 Hz (IT IS Foundation, 2018)) was applied to the SC to simulate the skin electrode model.

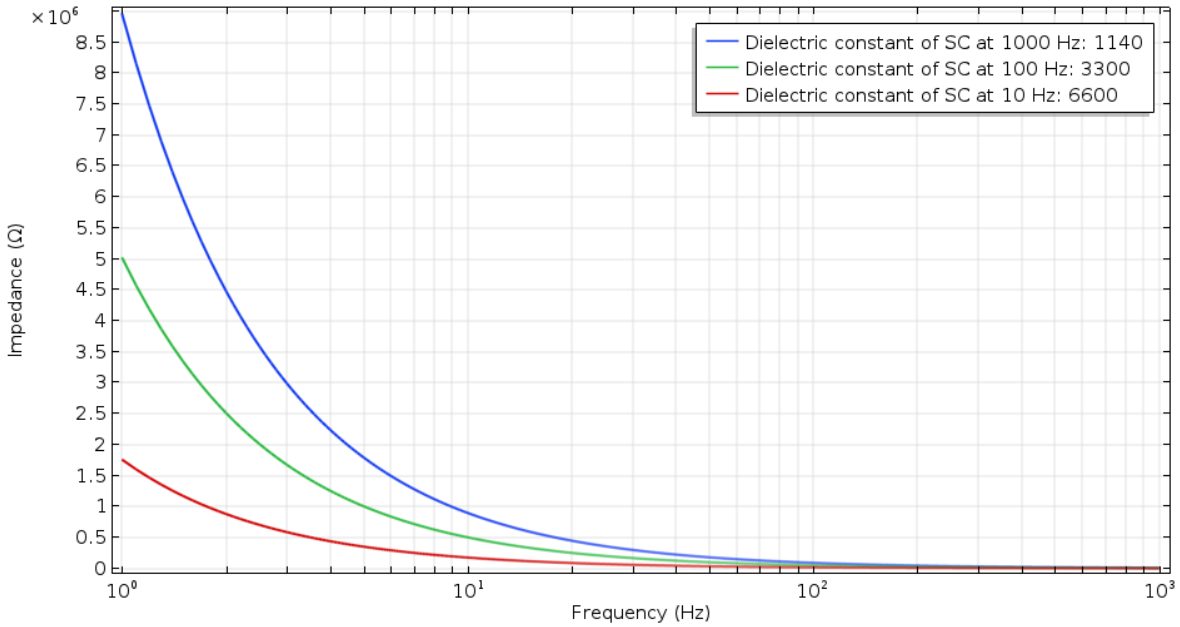

Figure 3-28: Impedance changes of the SC layer at varied frequencies (from 1 to 1000 Hz). The dielectric constants of SC were set to 6600 (at 10 Hz), 3000 (at 100 Hz) and 1140 (at 1000 Hz).

In the skin model, the HYP layer had a significant impact on conductivity, furthermore, the dielectric constant of HYP also has different values under different frequency ranges as shown in Table 2-7. To show the effects from different dielectric constants of the HYP layer, the value of the dielectric constant at 10 Hz, 100 Hz and 1000 Hz were simulated at the frequency range from 1 to 1000 Hz with the results shown in Figure 3-29.

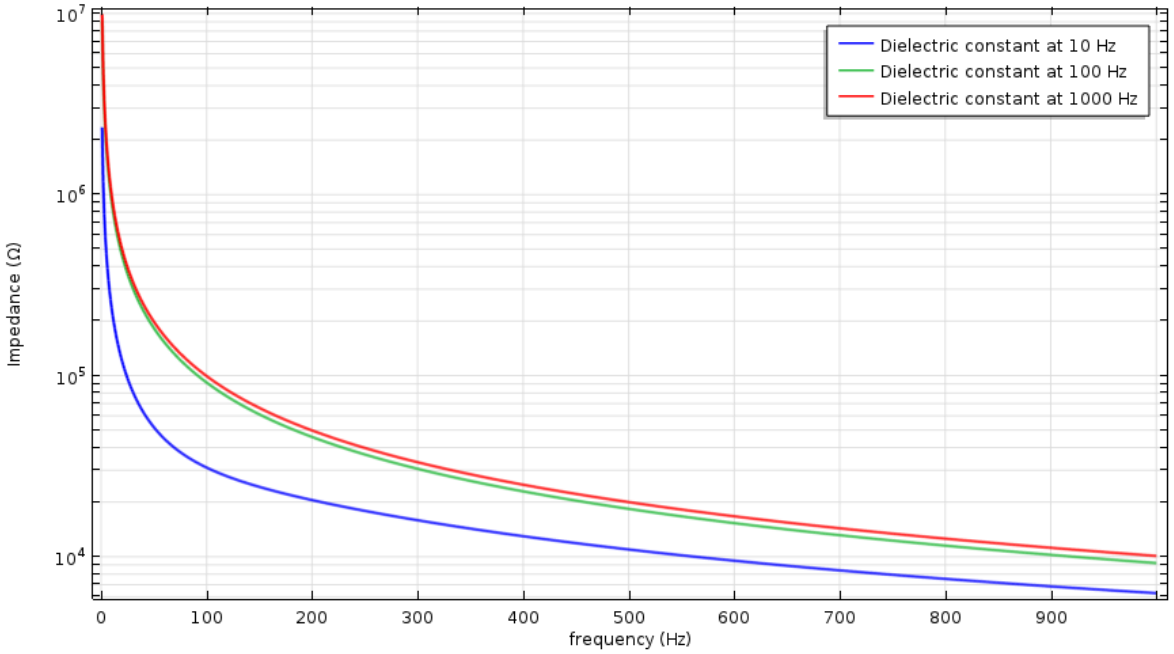

Figure 3-29: Impedance changes of the HYP layer at frequencies (from 1 to 1000 Hz). The dielectric constants of HYP were set to 1.2×10^7 (at 10 Hz), 3.3×10^5 (at 100 Hz) and 1.2×10^4 (at 1000 Hz).

From Figure 3-29, the impedance curves using the dielectric constant of HYP at 100 Hz and 1000 Hz were similar, when the dielectric constant was changed from 3.3×10^5 (at 100 Hz) to 1.2×10^4 (at 1000 Hz), the impedance at 1 Hz was increased from 9×10^6 Ω to 9.7×10^6 Ω, only approximately 8 %. However, when the dielectric constant was changed from 1.2×10^7 (at 10 Hz) to 3.3×10^5 (at 100 Hz), the impedance at 1 Hz increased from 2.7×10^6 Ω to 9×10^6 Ω, a difference of approximately 233 %, which is over 2 times. This is also the problem of the varied dielectric constant of HYP layer at different frequencies. From the literature, there is no average dielectric constant for the HYP layer, and the dielectric constant is non-linearly proportional to the frequency, so if the skin impedance is analysed around or less than 10 Hz, the dielectric constant of HYP used is 1.2×10^7. For a frequency higher or around 100 Hz, the dielectric constant of HYP layer could be chosen as 3.3×10^5, a value that generates similar results to the frequency at 1000 Hz.

Moreover, from the existing literature Cardu (2012) applied COMSOL to assess the impedance for a 1 cm^2 electrode, however the results showed some different conclusions. Figure 3-30 presents this model. In the Cardu model, the skin layer contained two layers (SC (0.03 mm) and the remaining layer (0.6 cm)) and two electrodes were placed at the top end of the model and placed 5 cm apart. From this simulation in the literature, the skin-electrode impedance was 4.2×10^4 Ω at 20 Hz. However, the simulation of skin-electrode impedance in this thesis was 4.5×10^5 Ω at 20 Hz, which was 10 times higher than the impedance in the literature. However, this mismatch between the simulation in this thesis and the simulation in the literature may come from the following reasons.

1. In the literature, the dielectric constant of the SC layer was set to 1.1×10^5. However, in this thesis, the average dielectric constant of SC was set to 1140 which represent an average value for dielectric constant. In section 3.5.1.2.3, the effect of dielectric

constant of the SC layer has been discussed, the total skin-electrode impedance would reduce as the dielectric constant increases. Therefore, if the dielectric constant of SC was set to 1.1×10^5 in our model, the total skin-electrode impedance is about $2.8 \times 10^4\ \Omega$, which is about 33 % less than the skin-electrode impedance in Cardu's research. Furthermore, in Cardu's research, the author did not give the details for the remaining part of the skin. Therefore, we cannot assess the effect from the remaining part of the skin. From this simulation comparison between the literature and thesis, it could see that the selection of dielectric constants will determine the final simulation results.

2. Although the model built in the literature was partly similar to the model in this thesis, the measured skin in the literature (skin under the electrodes and the skin between the two electrodes) was less than the simulated skin in this thesis. In section 3.5.1.2 and 3.5.2.1, the limitations of this method had been discussed. If the only simulated the electrode and the skin under the electrode, some information around the skin would be missed. The literature (Cardu *et al.*, 2012) author also mentioned that if there were applied force, the model in the literature would vary the depth of electrode.

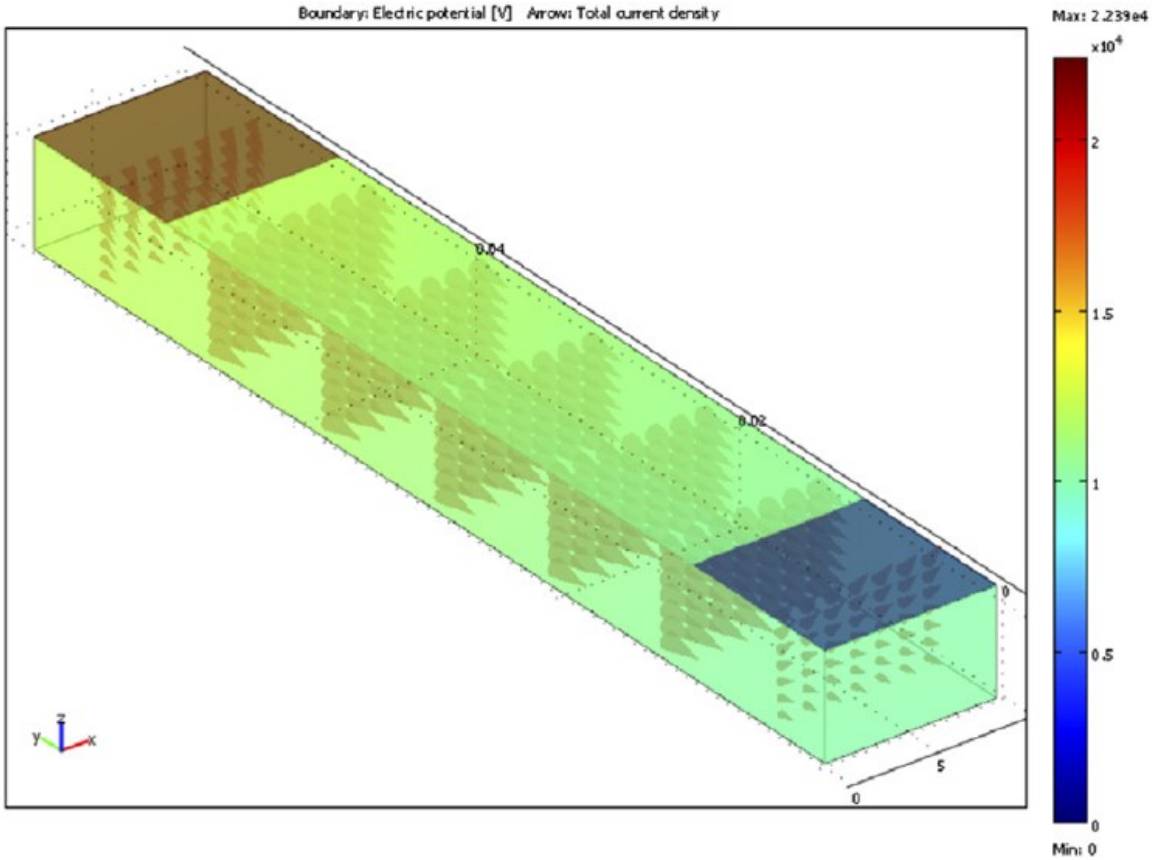

Figure 3-30: the original 3D two-electrode simulation in the literature (Cardu *et al.*, 2012), the red is the applied potential and the blue is ground. Meanwhile, the arrows present the current flow under the skin. Note: The original figure was based on the measurement results from the paper, and as such, the figure quality cannot be changed.

From this comparison between the simulation in literature and the simulation in this thesis, the dielectric constant is the most influential factor in the simulation. As mentioned in section 3.5.2.1.3, if the simulation is to be more accurate, the dielectric constant need to be defined

as a non-linear parameter for the model. In the current simulation, the dielectric constant was a constant value. However, the dielectric constant varied with frequency, therefore, the model in this thesis cannot apply well for the full frequency range. Moreover, having conducted a search, there was no database or literature that provides the needed data. Hence, the non-linear parameters of the dielectric constant cannot be added to the simulation. Nevertheless, if the simulation of the skin-electrode impedance is at a fixed frequency, the model in the thesis has the potential to simulate and provide acceptable results.

3.5.2.1.3 Summary of skin effects

In the simulation, the impedance between the electrode and the body was used to describe the electrical properties of the model. The effects of Young's Modulus, conductivity and dielectric constant on the electrical properties of the main skin layers, stratum corneum, epidermis, dermis and hypodermis, were modelled.

For the Young's Modulus of these four skin layers from the literature values, the impedances were calculated for the highest and lowest values of Young's Modulus. The HYP layer gave the highest impedance change of approximately 5 %. The HYP is the thickest of all four layers, so it has the greatest impact on the results. The averaged Young's modulus for each layer is applied in the simulation.

For the conductivity of these four layers (SC, E, D and HYP), the SC and HYP layers provided the greatest impact on the skin-electrode impedance; the calculated impedance difference between the highest and lowest conductivity was approximately 70 % for the SC layer and 40 % for HYP layer. Therefore, the mean value from the literature of the SC layer (0.0003 S/m) is set for the simulation. Meanwhile, because the conductivity of HYP dominates the real part of the impedance (shown in section 3.5.2.1.2.2), to maximize the effect of the conductivity of HYP layer, the highest conductivity of HYP (0.4 S/m) is selected. Furthermore, because the E and D layer do not give a huge impact on the simulation, any value of E and D layers in the their ranges (see Table 3-7) will provide an acceptable results. Therefore, the median number of E (0.5 S/m) and D (3 S/m) 0.5 S/m are used in the simulation.

For the dielectric constants of these four layers, the dielectric constant of SC showed a significant impedance difference (over 95 %). Because the dielectric constant of SC at low frequency (less than 10 Hz) is varied and forms a non-linear relationship with the frequency, there is no constant value for the dielectric constant. Furthermore, a comparison was made between the dielectric constant of SC at 10 Hz, 100 Hz and 1000 Hz, the impedance difference increased approximately 200 % (10 Hz to 100 Hz) and 76 % (100 Hz to 1000 Hz). The difference between 100 Hz and 1000 Hz was much smaller than the difference between 10 Hz and 100 Hz. Therefore, if the simulation was used for very low frequency (less or around 10 Hz), the dielectric constant of SC would be 6.6×10^3, for other situations, the dielectric constant of dry skin (1.14×10^3) would be applied to the simulation.

Meanwhile, because the dielectric constant varies with frequency, the dielectric constant of HYP was simulated at 3 different frequencies (10 Hz, 100 Hz and 1000 Hz). The skin-electrode impedance difference in the simulation between 100 Hz and 1000 Hz was much

small, approximately 8 %. However, the difference between 10 Hz to 100 and 1000 Hz was much larger than the difference between 100 and 1000 Hz, approximately 233 %. Because the simulation is expected to cover the frequency range from low to high, and the dielectric constant at low frequency has huge change, the dielectric constant of HYP (3.3×10^5 at 100 Hz) will be used in the simulation.

From the simulation of the dielectric constant of SC and HYP, it can be seen that the change in the dielectric constants at low frequency (less than 10 Hz) had the most impact on the skin impedance. However, the dielectric at low frequency varied over a large interval. For example, when the frequency was increased from 10 Hz to 100 Hz, the dielectric constant of HYP reduced from 1.2×10^7 to 3.3×10^5. If the simulation requires more accurate results, the dielectric constant at each frequency step (like 1 Hz) is needed. However, having conducted a search, there is no database or literature that provides these data. So the dielectric constant using an average dielectric constant (like SC layer) or at certain frequency (100 Hz, like HYP layer) were chosen for the simulation.

Compared with the standard circuit-based skin-electrode model, the FE simulation provided more detail about the effects inside the skin. In the simulation, this has shown that the dielectric constant or conductivity of skin may change the skin-electrode impedance by over 70 %. When the electrode is going to implemented, the skin's effects need to be considered carefully when designing an electrode.

3.5.2.2 3D duel skin-electrode model built by COMSOL

From previous sections, a 3D skin-electrode model was built and the skin's properties simulated using the model. In the single electrode simulation, the skin-electrode is like a capacitor, with the electrode and bottom tissue as two plates of the capacitor. If the dual skin-electrode model is applied, the model is like two electrodes connected in series (like Figure 3-31). Therefore, the 3D dual skin-electrode electrode was analysed in more complex measuring situations.

3.5.2.2.1 3D dual skin-electrode simulation model structure and functions

In the current simulation model, the bio-signal and skin properties were combined together to generate the impedance between two electrodes. For the measurement situation, the measuring circuit is shown in Figure 3-31. The skin-electrode impedance between the two electrodes was measured using an impedance analyser.

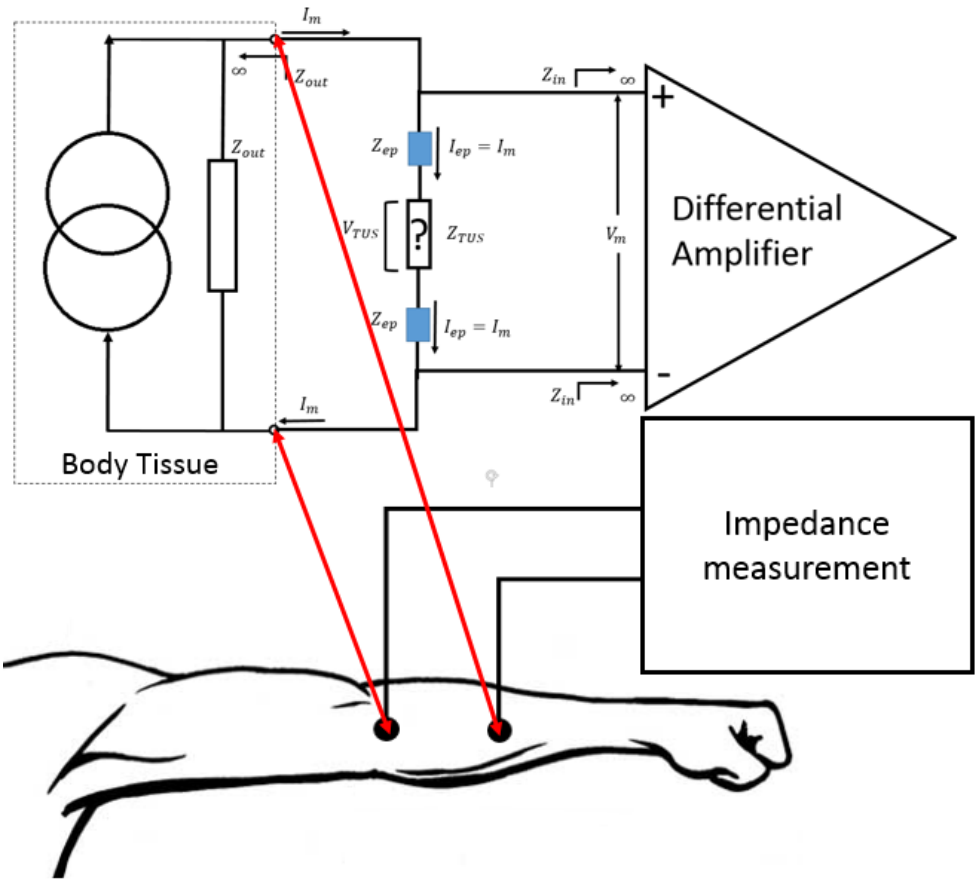

Figure 3-31: Illustration of the impedance measurement system of the skin-electrode interface.

The skin-electrode impedance measured in Figure 3-31 was used to evaluate the performance of the electrodes. As the skin properties or outside measuring conditions were changed (e.g. applied force or electrode size), the impedance varied. In the simulation, the aim was to reflect the measuring conditions as much as possible. Figure 3-32 shows the dual electrode structure model of the skin-electrode impedance in Figure 3-31.

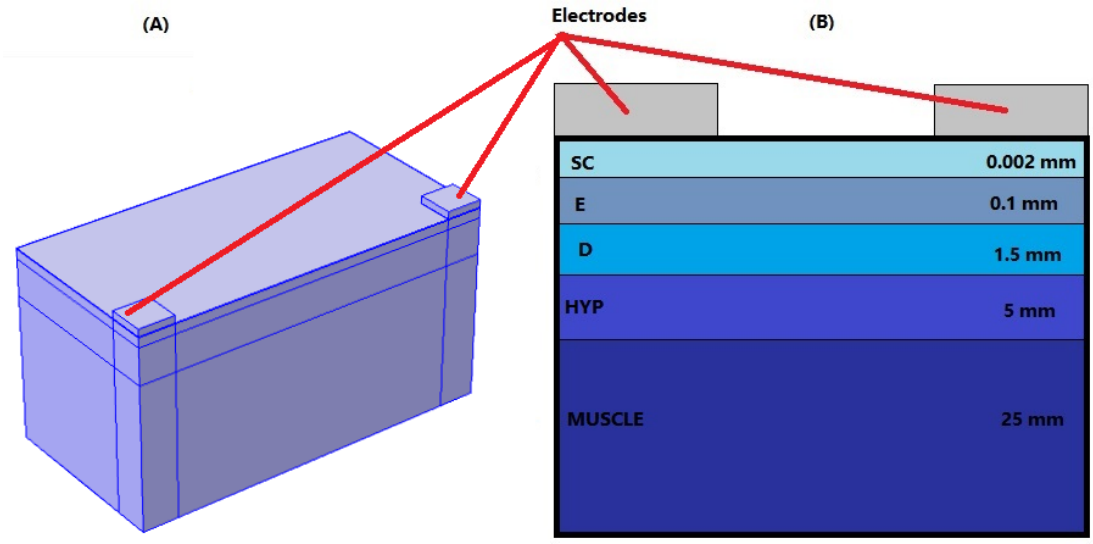

Figure 3-32: Skin-electrode impedance model: (A) COMSOL modelling the skin layers and electrode put on the skin; and (B) the accurate skin layers and electrode put on the skin.

In this simulation, some conditions are applied to update 3D single electrode model:

- The 'Model length' was set to 225 mm, which is the average forearm length from literature.
- The 'Model width' was set to 30 mm. The 'model width' has been proved in section 3.5.2.1. For 1 cm^2 electrode, model width of 20 mm cannot affect the results. The model width set to 30 mm allowed the change of electrode size.
- The model was symmetric from 'symmetry surface'.
- Two electrodes had a 50 mm separation between each other (calculating from the electrode centre). In the literature (Simper, 2005; C.Alper and Jari, 2014), this separation was between 5 to 7 cm.
- In the 'Solid Mechanics', the 'End boundary' was set to 'Fixed Constraint'. There was no any movement at this boundary (Dirichlet boundary condition, the boundary equation is zero movement).
- The bottom surface was fixed.
- In the 'Electric Current', The 'End boundary' was set to ground (electric potential V was zero: Dirichlet boundary condition, the boundary equation was a constant voltage).
- The total number of elements was 45156.
- The skin thickness and the properties of materials are shown in Table 3-9. The Young's Modulus, Conductivity, Dielectric constants were analysed from previous section 3.5.2.1.

Electrode and skin	**Thickness (mm)**	**Young's Modulus (MPa)**	**Conductivity (S/m)**	**Poisson ratio**	**Density (kg/m^3)**	**Dielectric Constant/ Relative Permittivity**
Electrode (Ag)	1	8.3	61.6×10^6	0.37	10500	1
Stratum Corneum(SC)	0.02	2.6	0.0003	0.43	1050	1140
Epidermis(E)	0.1	0.5	0.5	0.48	1020	1.14×10^3
Dermis(D)	1.7	0.06	3	0.48	1900	1.14×10^3
Hypodermis and fat (HYP)	5	0.28	0.4	0.48	1800	3.5×10^5
Muscle(M)	25	1.77	0.42	0.45	1120	2.5×10^7

Table 3-9 Different mechanical and electrical properties of the skin layers and electrode.

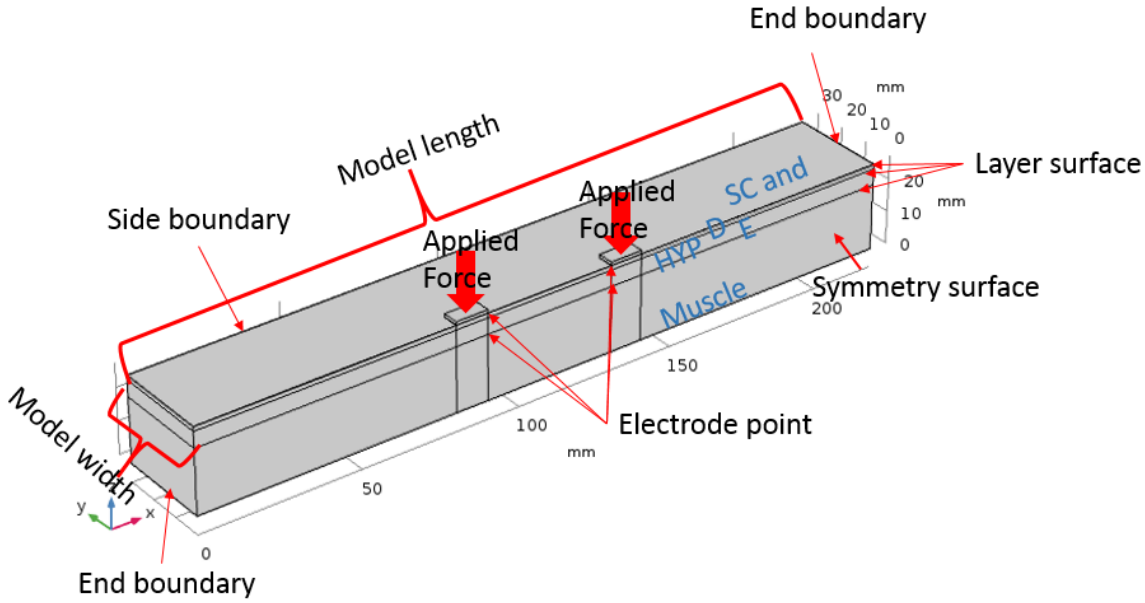

Figure 3-33: Simulated model included the applied force and symbols/definition for each surfaces and edges.

3.5.2.2.2 3D dual electrode simulation results for skin-electrode

Figure 3-34 shows the deformation of the dual electrodes at 5 N applied force. From Figure 3-34, it can be clearly seen that the deformation is applied to all the tissues under the skin.

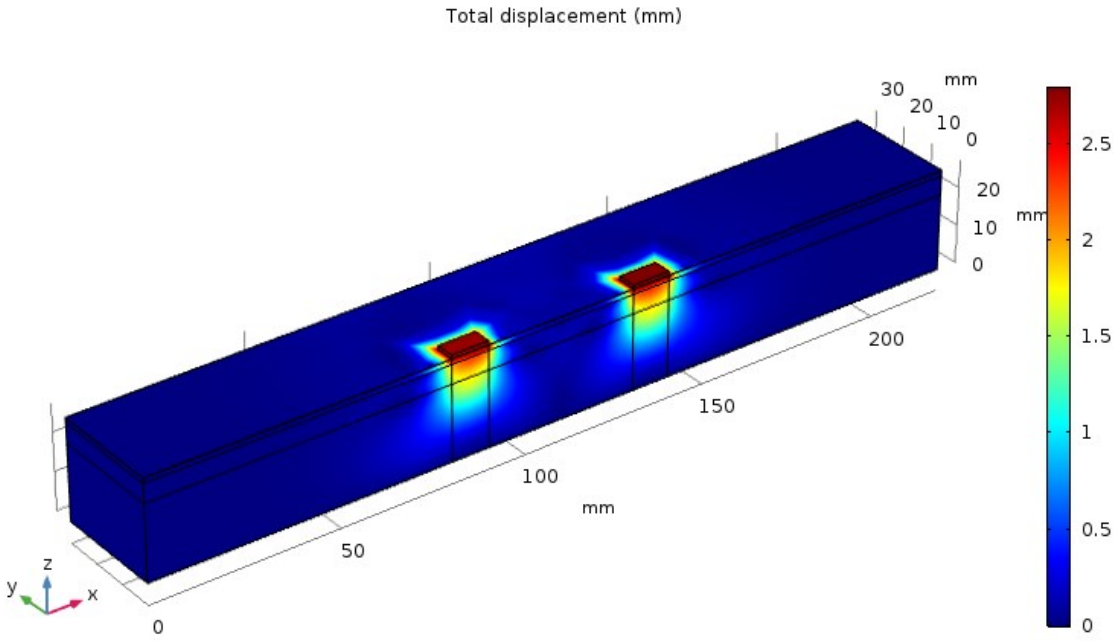

Figure 3-34: Simulation of the 5 N force applied on the dual electrodes (1 cm^2) and the deformations.

From the previous 3D single skin-electrode model, the effects of the skin's properties were fully analysed. The aim of this dual electrode model was to identify the effect from different electrode sizes, because the skin under electrode and skin between two electrodes were was changed at different electrode sizes.

If the size of electrode was changed from 0.5 to 3 cm^2 and the displacement between two electrode centre is 50 mm, the impedance was varied and shown in Figure 3-35 (frequency: 10 Hz to 1000 Hz). In this simulation, the frequency range was expanded to 10 Hz to 1000 Hz, and this makes it easier to see the effect of the electrode size from low to high frequency.

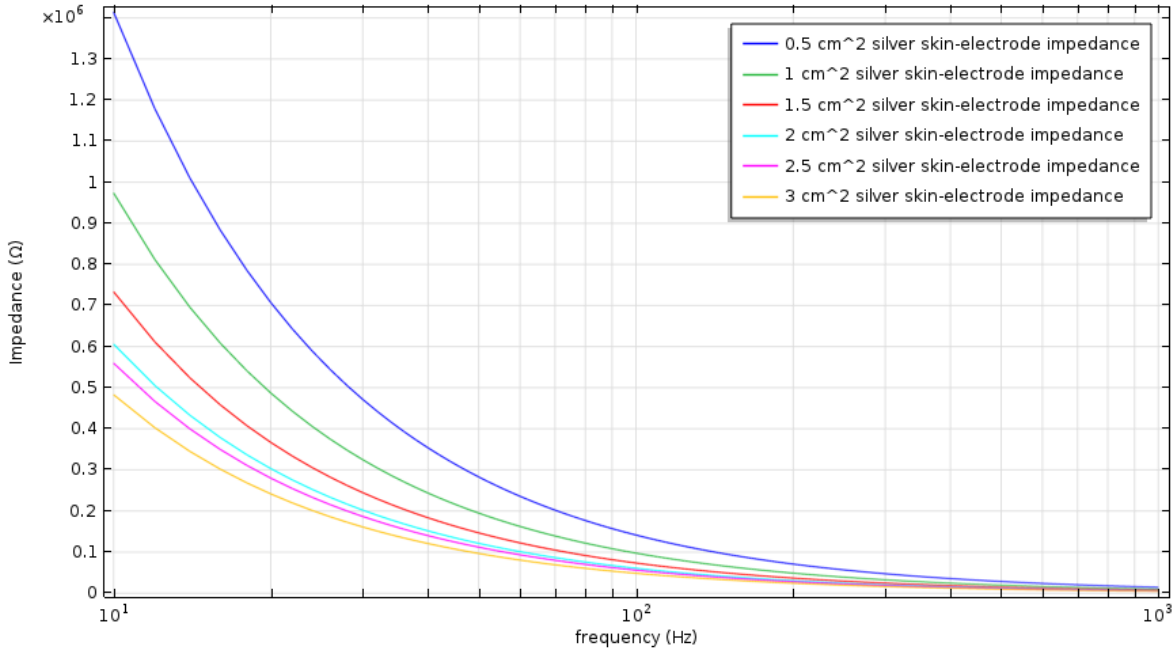

Figure 3-35: Impedance change as a function of different frequencies (10 Hz to 1000 Hz) and electrode sizes (electrode size changed from 1 cm^2 to 3.5 cm^2).

From Figure 3-35, it can be seen that the skin-electrode impedance keeps decreasing as the size of electrode increases, the 0.5 cm^2 electrode at 10 Hz having the highest impedance, which was 1.4×10^6 Ω. When the electrode size was changed to 3 cm^2, the highest impedance decreased approximately 67 % at 10 Hz. However, when the electrode size increased from 0.5 cm^2 to 2 cm^2, the skin-electrode impedance exhibits the most change (reduced by approximately 60 %). When the electrode size increased from 2 cm^2 to 3 cm^2, the skin-electrode impedance decreased by around 14 %. Because the properties of the skin are variable, the simulation results were chosen from the average values**.** It was found that increasing the electrode size from 0.5 cm^2 to 2 cm^2, reduces the skin-electrode impedance dramatically (by over 60 %). If the skin-electrode impedance was reduced further by increasing the electrode size from 2 cm^2 to 3 cm^2, the change was not as large and did not bring significant improvement to the results. Therefore 2 cm^2 electrodes were chosen as the optimal electrode size and the threshold for designing the electrode.

If the frequency was applied as a constant value (e.g. 100 Hz), the skin-electrode impedance results depending on the electrode size are shown in Figure 3-36. From this figure, the highest change in the skin-electrode impedance (about 60 %) occurred when the electrode size was changed from 0.5 cm^2 to 2 cm^2. This means the impedance will be significantly affected by the electrode size between 0.5 cm^2 and 2 cm^2. Therefore, the 2 cm^2 could be the threshold for the electrode design and the optimal size of the electrode.

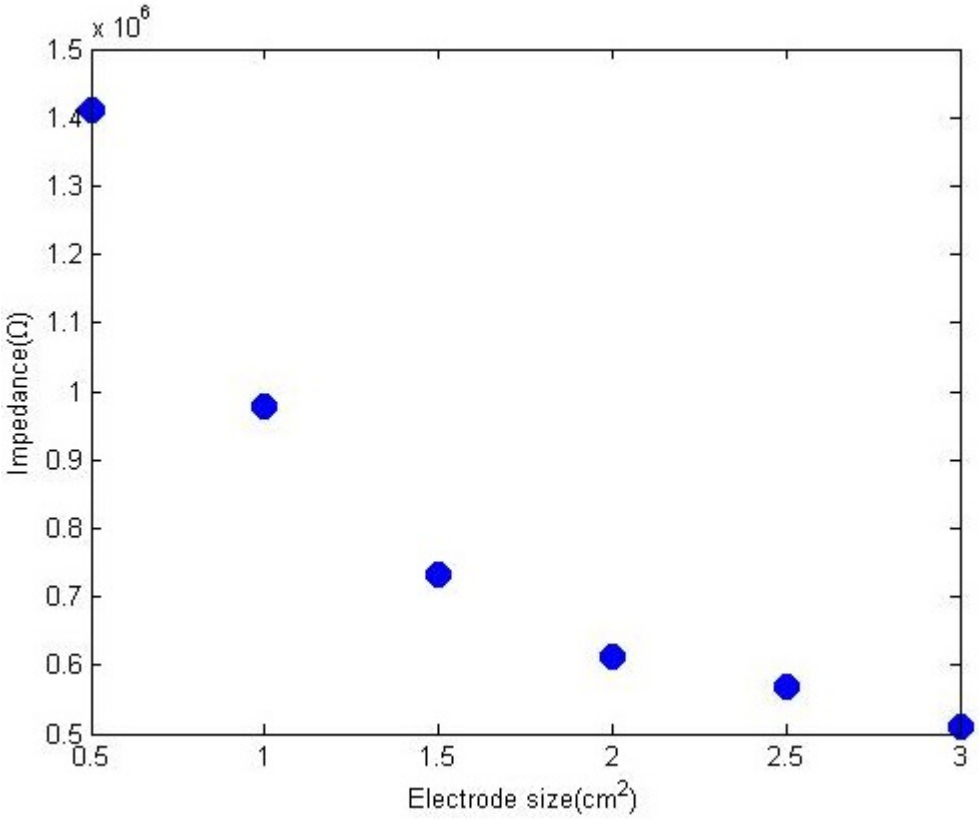

Figure 3-36: Impedance changes with variations in the size of electrode at 10 Hz, where the electrode size was increased from 0.5 cm^2 to 3 cm^2.

Moreover, Figure 3-36 shows the skin-electrode impedance changes in the low frequency range (0.1 to 10 Hz). In this frequency range, the skin's dielectric constants has been changed the value at low frequency.

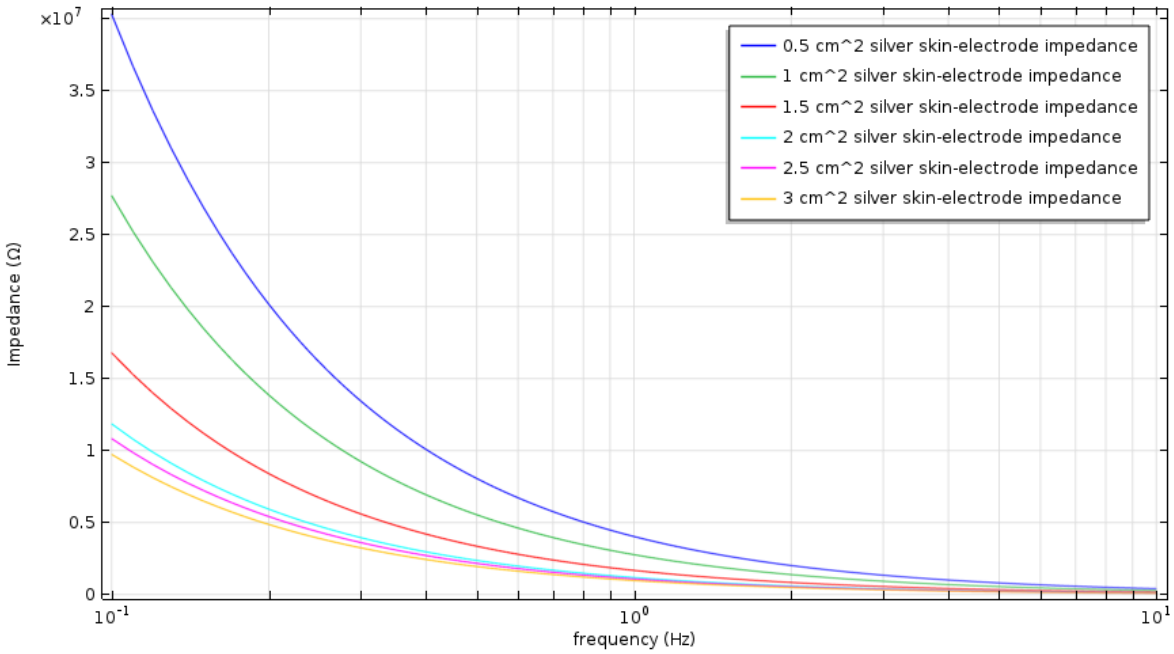

Figure 3-37: Impedance change as a function of frequency (0.1 to 10 Hz) and electrode size (0.5 cm^2 to 3 cm^2).

In Figure 3-37, if a frequency of 2 Hz was chosen, which is the defined low frequency from the literature, it can be used to analyse the change of skin-electrode impedance. At 2 Hz, the highest impedance was 2×10^6 Ω at 0.5 cm^2 and was 308 % higher than the value of the 3 cm^2 electrode impedance. When the electrode size was decreased from 0.5 cm^2 to 2 cm^2, the skin-electrode impedance has the highest decrement (from 2×10^6 to 5.9×10^5 Ω, about 70 %). After this, when the electrode size was increased from 2 to 3 cm^2, the skin-electrode impedance is reduced from 5.4×10^5 Ω to 4.9×10^5 Ω (about 9 %). The results are similar to the impedance in the 100 Hz range. Based on the cost of material and the improvement in the electrode efficiency, 2 cm^2 electrodes were chosen as the optimum electrode size.

Nevertheless, the change of electrode size from the skin-electrode model in this thesis is also able to be compared with the literature. In the literature, Bosnjak (Bosnjak *et al.*, 2017) showed the relationship between the electrode size (defined as electrode contact area in his paper) and the skin-electrode impedance. Bosnjak used a stainless steel electrode and showed the relationship between the electrode size and the skin-electrode impedance. The electrode size in Bosnjak's research was selected as 100, 200, 320, 672 and 960 mm^2. When the electrode size was increased from 100 to 200 mm^2, the skin-electrode impedance at 10 Hz had the highest impedance reduction (from 9×10^5 Ω to 1.5×10^5 Ω, about 80 %). If the electrode size is further increased to 320 mm^2, the skin-electrode impedance at 10 Hz was only reduced by about 30 % (from 1.5×10^5 Ω to 1×10^5 Ω). Furthermore, when the electrode was further increased from 320 to 672 mm^2 (electrode size had been doubled), the skin-electrode impedance at 10 Hz was reduced by only about 40 %. Further, from Bosnjak's results, the total skin-electrode impedance of 672 mm^2 and 960 mm^2 were almost same. The results showed the skin-electrode impedance may not further reduce after 672 mm^2.

The relationship between the stainless steel electrode size and skin-electrode impedance (Bosnjak *et al.*, 2017), it compares with the conclusions in this thesis. When the electrode size or contact area was less or equal to 2 cm^2, the change of electrode size has more impact on the skin-electrode impedance. However, when the electrode size or contact area was greater than 2 cm^2, the effect from electrode size is less. Therefore, the 2 cm^2 is the threshold for designing electrode.

3.6 Conclusion

In this chapter, COMSOL was identified as the optimum FE modelling software to produce a skin/electrode model. The simulation model was developed step by step, from a 2D single electrode to a 3D dual electrode skin-electrode model. The FE model allows analysis of the electrode and the effects of the skin.

The 2D simulation model was sufficient to analyse the electrode's movement and the electrode force's effects. Because the 2D model is a cross-section of the electrode and skin, it showed that the electrode moves downward and the edge of the electrode is squashed under the applied force. But the 2D simulation cannot be used to simulate the skin-electrode impedance. In the 2D simulation, the model is based on a cross-sectional model, which means the 2D model is limited by its structure. Furthermore, the skin-electrode impedance

needs to consider the electrode and the skin around the electrode, so the 2D skin-electrode simulation is less accurate than a 3D simulation.

In the 3D simulation, the importance of four skin layers (SC, D, E and HYP) was analysed. Firstly, from the simulation of Young's Modulus, because the HYP is the thickest layer across all four layers, the HYP layer provided the most significant effect on the skin-electrode impedance (about 5 %) based on an interval chosen from the literature (0.2 to 2 MPa) for the variation in Young's Modulus.

Secondly, in the simulation of the skin layers' conductivities, the SC and HYP layers had the greatest impact on the skin-electrode impedance. For the SC layer which has the largest effect, when the conductivity of SC was increased from 0.000125 S/m to 0.000455 S/m (about 256%, based on the interval chosen from the literature), the impedance reduced by 70 %.

The second most significant layer is the HYP layer. When the conductivity of HYP layer was increased in an interval from 0.02 S/m to 0.04 S/m (increased 100 %), the overall impedance increased by about 40 %. The impedance changes resulting from changes in HYP conductivity show an opposing trend to the impedance change resulting from SC conductivity changes. According to equation (3-20) in the simulation of SC conductivity, the permittivity and frequency in the imaginary part of the impedance had the greatest impact on the impedance results. So the impedance reduces as the SC conductivity increases. In contrast, in the simulation of HYP conductivity, the conductivity in the real part of the impedance had the greatest impact on the impedance result. So the impedance increases as the HYP conductivity increases. Because the values of the SC's conductivity are much smaller than for other layers, it showed a different changing trend in the impedance compared with other layers.

Thirdly, the dielectric constant of skin layer has been analysed at different frequencies. Because the dielectric constant is varied at different frequencies, the dielectric constants at 10 Hz, 100 Hz and 1000 Hz were analysed for the SC and HYP layer. In the simulation, the dielectric constant of SC had the highest impedance difference of approximately 95 % between its lowest and highest dielectric constant (1440 to 6600). Because the dielectric constant of SC at low frequency (less than 10 Hz) is varied and difficult to achieve a constant value, the dielectric constant of the averaged dry skin (1.413×10^3) was applied in further simulation. This average dielectric constant is taken from skin surface and has less variation in the frequency range from 100 Hz to 1000 Hz, so it has been mainly discussed in the literature (Gabriel, Gabriely and Corthout, 1996; Huclova, Erni and Fröhlich, 2012) .

Nevertheless, the dielectric constant variation of the HYP layer was also simulated. The impedance difference resulting from the dielectric constant variation at 100 Hz (3.3×10^5) and 1000 Hz (1.2×10^4) was only approximately 8 %. However, the impedance difference resulting from the dielectric constant at 10 Hz (1.2×10^5) and 100 Hz (3.3×10^5) was approximately 233 %. Similarly, the impedance difference resulting from the dielectric constant of HYP layer at 10 Hz (1.2×10^5) and 100 Hz (1.2×10^4) was also approximately 250 %. Because the simulation is expected to cover the frequency range from low to high,

and the dielectric constant at low frequency is varied across different frequencies, the dielectric constant of HYP at 100 Hz was used in the simulation.

When the electrode simulation is adjusted from a single electrode to a dual electrode, the electrode size has been analysed. In the literature, the only information on an optimum size suggests it should be 1 cm^2. From the simulation results, the electrode size between 1.5 cm^2 to 2 cm^2 showed a balance between material coverage and skin-electrode impedance. When the electrode size is increased from 0.5 cm^2 to 2 cm^2, the skin-electrode impedance is significantly reduces (around 60%); when the electrode size is increased from 2 cm^2 to 3 cm^2, the reduction is about 13 %. Therefore, the optimized or most efficient electrode size is located between 1.5 cm^2 to 2 cm^2.

In next chapter, a textile electrode is introduced and discussed from a manufacturing and materials viewpoint. The 3D skin-electrode simulation is applied to the textile electrode and a comparison is made between the simulation and experimental results.

Chapter 4: Silver electrode design and measurement

4.1 Introduction

Chapter 3 demonstrated that it is essential to identify the relationship between the electrode performance and different parameters (geometry, flexibility of electrode or movement under applied force, skin's electrical/mechanical properties). In this chapter, the textile-based electrode design uses two printing methods. These were inkjet and screen printing. The inkjet printed electrode was fabricated by printing Sun Chemical silver ink on a 75 micron thick polyimide (Kapton) film. This was chosen initially because it is smoother than a textile but still flexible. The screen printed electrode was fabricated using Electrapolymer ELX-30 silver on a polyester cotton textile, which is less smooth than Kapton, but still flexible, plus it is a breathable material. These two methods provide a method to test the parameters and functions of the electrodes modelled in Chapter 3.

4.2 Electrode design and fabrication

Before the electrode was printed on the materials, the electrode structure and pattern was designed by software. In the design, the electrode was drawn by L-edit.

In the schematic shown in Figure 4-1, the circle and rectangle are the printed electrodes and their patterns. The schematic design has three layers. These are the interface layer, the conductive layer and the encapsulation layer. In Figure 4-1, the green area is the interface which provides a smooth surface on the textile for subsequent printing. The red area is the conductive layer which creates electrodes and patterns fabricated using silver ink. The green part is the encapsulation which protects the conductive pattern from physical damage and corrosion. For the three layers, the silver layer and encapsulation layer are printed on the interface layer, meanwhile, the encapsulation layer is used to cover the silver layer (except the electrode and conductive pads, the circles and rectangle in Figure 4-1).

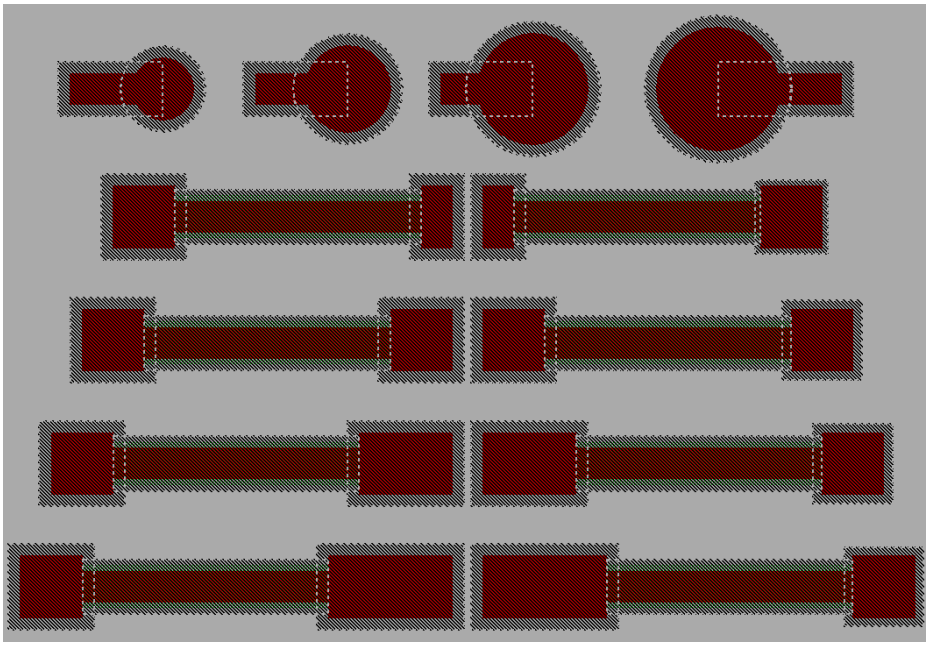

Figure 4-1: Textile electrode layout including electrode with different geometries.

4.3 Inkjet printing

Inkjet printing was used in the 1st design to implement the silver electrode. The electrode can be used to measure the impedance of the skin-electrode interface. For the inkjet printing, the printer used in this work, a Dimatix DMP-2831 Inkjet printer, is shown in Figure 4-3. Sun Chemical Silver ink was selected as the conductive material. The reason is that this silver has been used in previous research at the University of Southampton. The printer printed the layout in Figure 4-1 on Kapton, after the Kapton was cut into 100 mm × 100 mm square for printing. After printing on Kapton, the substrate of Kapton was moved into the oven to dry the silver. The Kapton was placed in a convection oven for 20 minutes at 200 ℃, which was taken from the silver manufacturers' datasheet.

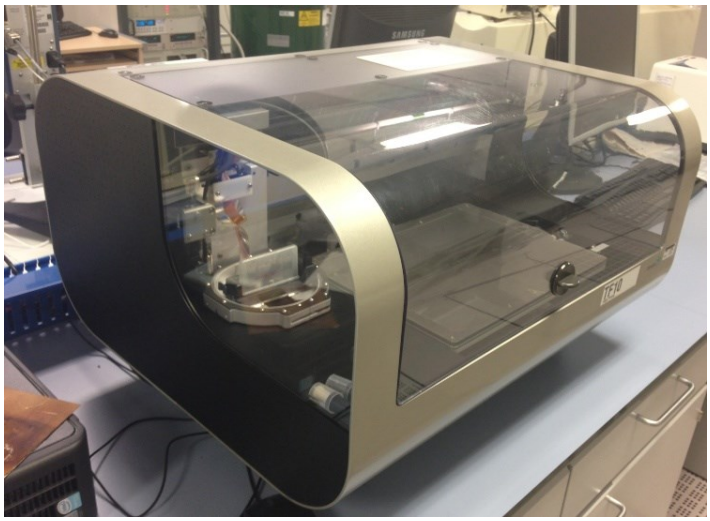

Figure 4-2: Dimatix DMP-2831 inkjet printing machine.

In Figure 4-3, the initial printing results using the design for the passive electrode and accelerometer are shown. Four electrodes were printed, and the fabrication required about 1

hour including the curing time. The bottom two electrodes at the top of Figure 4-3 were used to connect the conventional electrodes and the top two electrodes are the silver electrodes. Each printed pattern was around 20 mm x 15 mm. Although some patterns were printed with good definition, there was some substrate deformation highlighted by the red rectangle. Also, some of the patterns were short-circuited and poorly defined. One possible reason was that the printer settings, especially the resolution and drop speed were not suitable. Because the Dimatix printer only functions correctly when used with only 1 or 2 jets activated, the printer settings needed to be specifically adjusted. Furthermore, some parts of the pattern were too thick and the pattern had also been scraped by the printer head. The printer head moves like a squeegee scraping the printed work when the printer is going to print a new pattern, and thus, some existing patterns would be covered again.

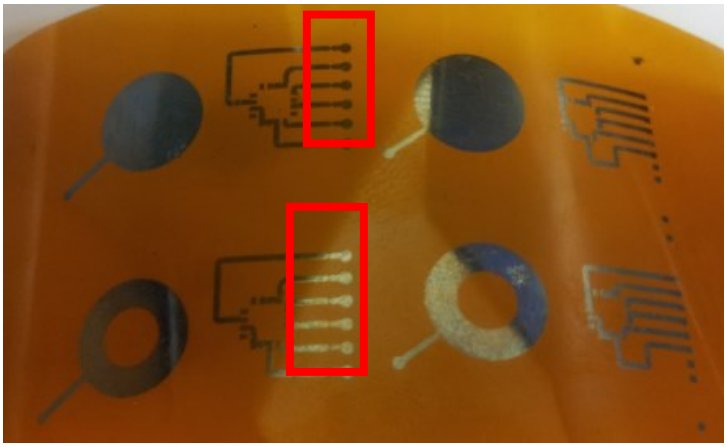

Figure 4-3: Problems in the inkjet printing showing patterns that are blurred (in the red rectangle).

In a further printing trial, a 3-jets activated printer head was used and the temperature of printer changed to 23 ℃, which was higher than the previous two examples which were at 17 ℃. The higher temperature allows the printer head to drop larger ink bubbles. The printing results are shown in Figure 4-4, the most visible change is that there was no substrate deformation at the end of the tracks. The pattern definition was improved. However, scraping of the patterns by the printer head are still observed and some samples were affected by this.

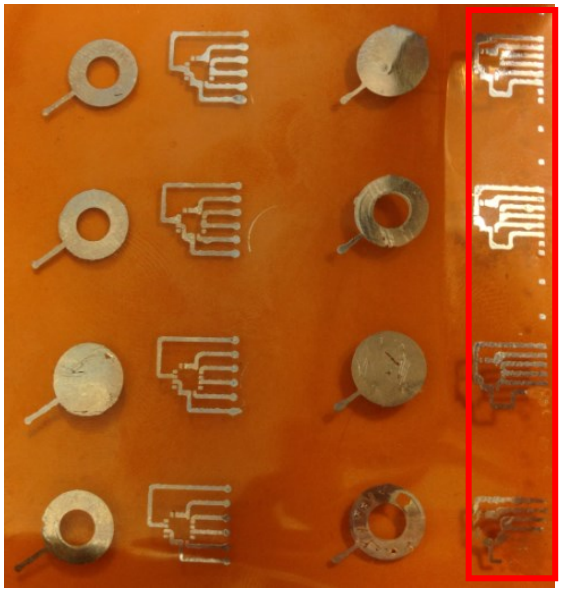

Figure 4-4: 3rd version of Inkjet printing result on Kapton and the improvement on the pattern connection.

Furthermore, inkjet printing is slow. For example, it takes about 2-3 hours to print an area of 100mm ×100mm. If the same size is printed by screen printing, the whole procedure will take about 20 to 30 minutes. Screen printing seems to be a better choice than inkjet printing in this aspect.

4.4 Screen printing

Screen printing can also provide a flexible contact on textile, thus it is worth testing the performance of the screen printed electrode and its modelling. For screen printing design, software called L-edit was used to draw the pattern or electrode, as for inkjet printing. Screen printing uses a DEK 248 semi-automatic flatbed printer as shown in Figure 4-5 with a maximum printable area of printed textile of 280 mm x 280 mm.

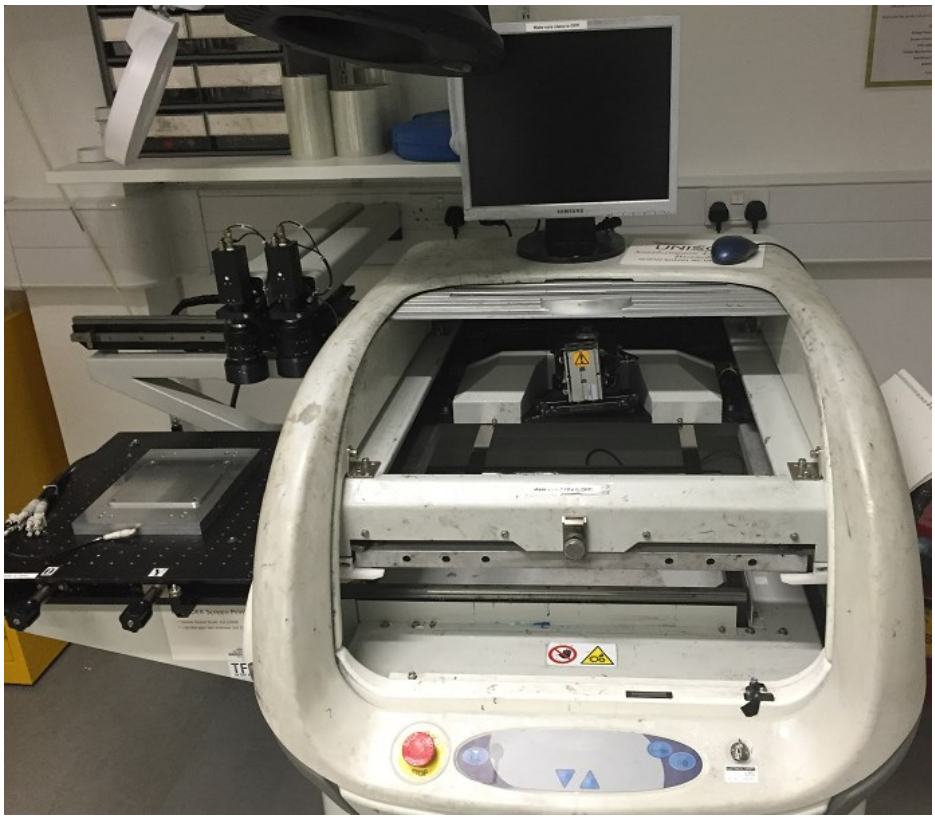

Figure 4-5: DEK 248 semi-automatic flatbed printer.

Screen printing is a printing technique that uses a woven mesh as an ink-blocking stencil to achieve the desired circuit. Thus, the electrode can be implemented in various sizes, geometries, or thicknesses. Shapes like squares, circles or triangles can be defined. Before printing occurs, the layout of the printing screen was drawn using software and sent to the manufacturer. In the printing process, the screen is covered in an emulsion which is then exposed through a mask of the design, and then the unexposed material is removed leaving the desired pattern in the screen. Because the effects of the textile electrode needed to be tested varying different conditions, an existing example from a University of Southampton project (Paul, 2014) was regarded as being fit for this purpose. The project aimed to develop

a wearable electrode on textiles for monitoring human bio-potentials from the skin. This existing design and screens could be used to implement the electrode for different measuring conditions (such as electrode sizes and materials).

4.5 Method of screen printing silver electrodes

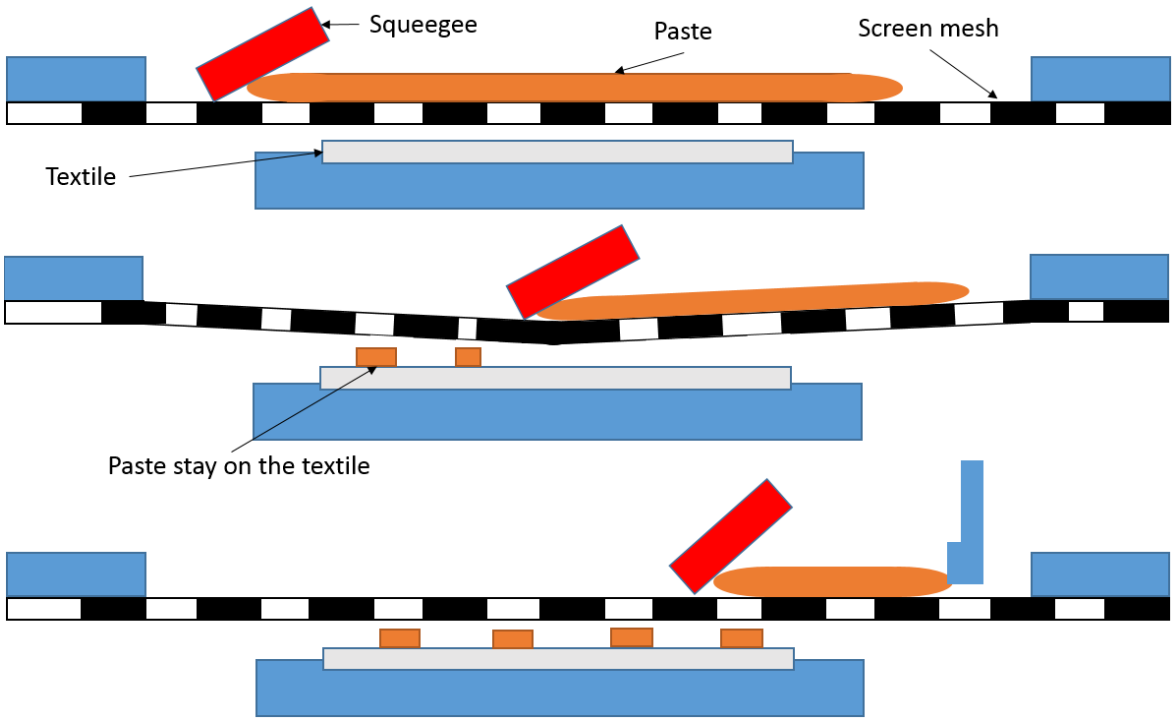

shows each layer of the electrode structure realised by screen printing. In the printing procedure, the polyester/cotton textile (plain weaving, 0.16 mm thick, Bacteriostat fabrics) is placed on a ceramic substrate before printing. The ceramic substrate provides a smooth, easily cleaned plate. The material of interface and encapsulation layer is Fabinks-IF-1004, which is made by University of Southampton. The chosen silver is ELX-30. This silver (ELX-30) has been used in another screen print project (Paul *et al.*, 2014) in University of Southampton . Because the current project is to test the function of the simulation model, the existing material can be used.

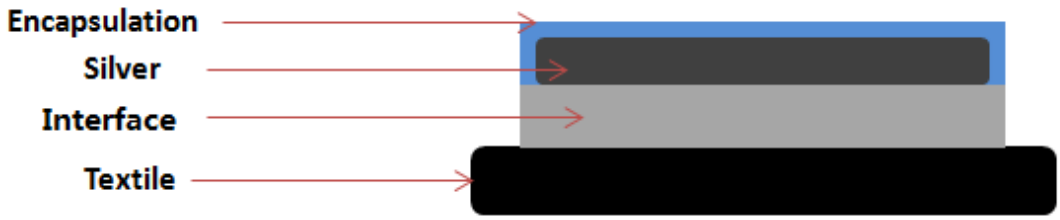

Figure 4-6: Screen printing structure includes each layer.

Figure 4-7 shows the printing procedure for printing one layer, the paste (like silver, interface material) is squeezed by the squeegee through the screen mesh. Subsequently, the paste will stay on the textile.

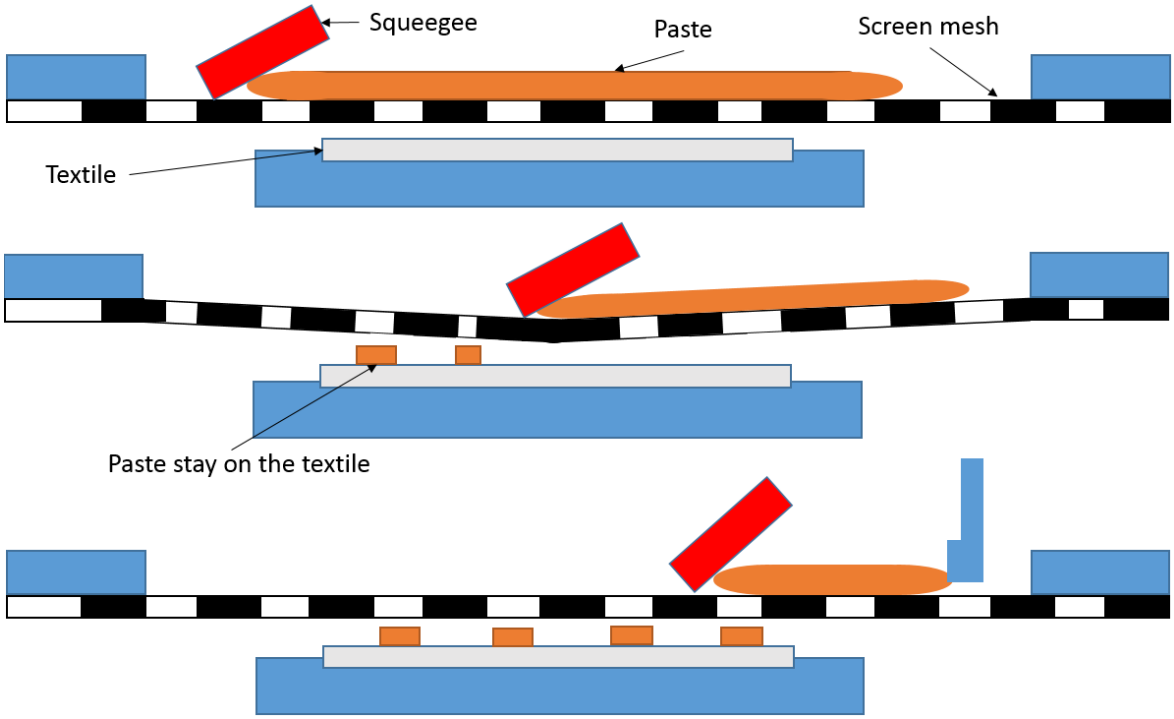

Figure 4-7: Screen printing procedure for printing 1 layer on textile.

Based on Figure 4-7, the printing procedure has the following steps:

- Before printing, the textile needs to be shaved to provide a relatively smooth surface. Then, the textile is cut into the same size as the textile holder, which is a ceramic plate and glued by 3M spray mount adhesive. When the textile is screen printed the textile may be moved by the squeegee so the glue stops textile movement.
- Printing the first layer: interface layer (Fabinks-IF-1004). This layer is used as the base onto which the conductive materials can be printed. If a drop of ink drops on the textile, the ink will diffuse due to the fibrous construction of the textile. As a function, this interface layer is used to prevent diffusion. The screen is supplied by MCI Precision Screen Ltd. It is a 250 thread/inch stainless steel and it has the 40 um emulsion thickness. UV curing is applied to cure the interface layer: each sample is placed into the UV cabinet and cured by a 400 W mercury (Hg) bulb (UV Light Technology Ltd) for 30 s.

  In general, the interface layer is printed twice or three times to make the interface layer smoother. As more layers are printed on the textile, the layer will become much thicker and smoother. However, when the layer becomes thicker and smoother, the thicker layer will have less flexibility. Figure 4-8 shows the interface layers with different numbers of printed layers. It can be seen that the 3-layer interface layer is smoother than the 2-layer interface. The thickness is measured by micrometre (manufacturer: Mitutoyo). The 2-layer interface has a thickness of around 0.17 mm and the 3-layer interface has a thickness of around 0.24 mm, which is an increased 40 % of thickness for a smoother surface for further procedures. A smoother surface will provide better printing conditions and reduce the effect from non-uninform surface. Although the increased number of layers will keep increase the smoothness of the interface surface, the flexibility will be reduced by increasing the number of

layers. Therefore, the 3-layer interface is a balance between smoothness and flexibility.

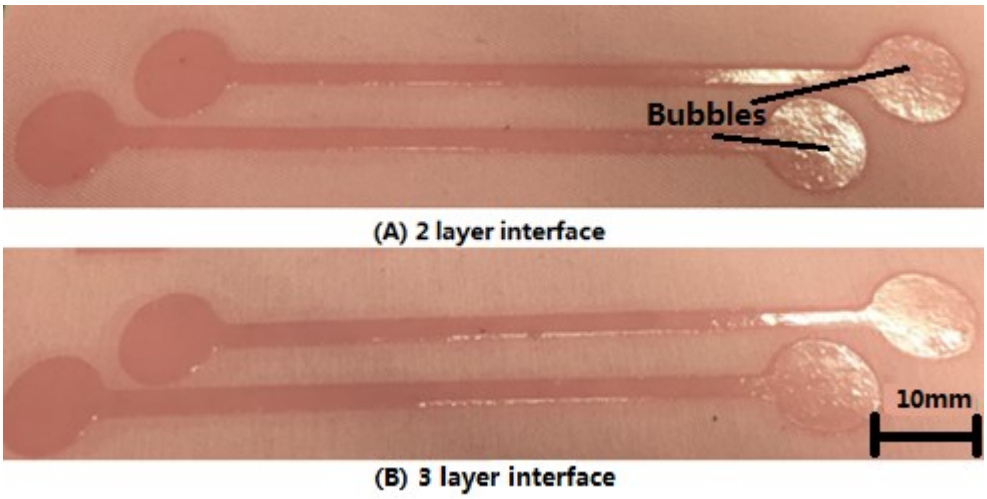

Figure 4-8: The tested screen-printed interface (A) 2-layer interface and (B) 3-layer interface, the 2-layer interface contains some bubbles and the 3-layer interface becomes smoother.

- Printing the second layer: conductive layer. This is the main part of the electrode and pattern and it is made by silver (ELX-30, Electra Polymers). The screen is a 120 thread/cm polyester screen and the thickness of the screen is 10 μm. The silver is cured in a box oven at 120 °C for 10 min. In the printing process, the silver is printed in one layer. Because this thesis is not going to discuss the effect from the thickness of electrode surface and conductive patterns, to reduce the cost of silver, one-layer silver is able to use for measuring the skin-electrode impedance.

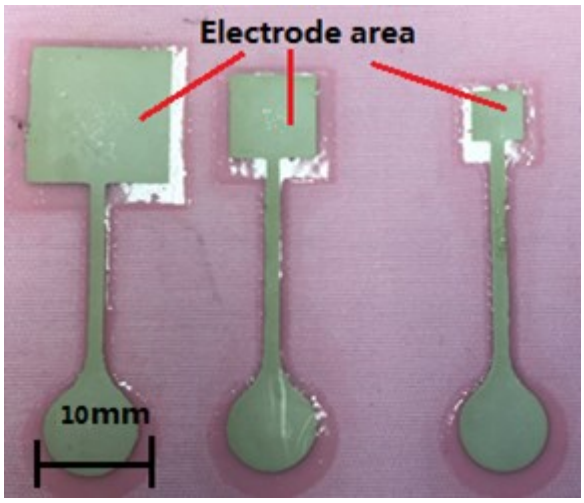

Figure 4-9: Tested screen-printed silver pattern for the electrode.

- Printing the third layer: encapsulation layer (Fabinks-IF-1004). This layer is used to protect the conductive patterns from contact or physical damage. The material is the same as the interface layer. The Fabinks-IF-1004 can be used as encapsulation to produce good production for printed electronics. In addition, the printing and curing conditions are the same as the interface layer. Because this layer is only used to

protect the conductive layer (ELX-30 silver), the smooth surface cannot affect the measured result, to save the cost of material, two layer is able to cover and protect the conductive patterns.

In the following tables (Table 4-1 and Table 4-2), the measured results and printing details are listed. Thickness is measured by micrometre (manufacturer: Mitutoyo). Furthermore, the average thickness is measured 5 times and mean value calculated. The thickness of silver and encapsulation layer are calculated from the following equations:

Thickness of silver layer = total thickness - thickness of interface layer

Thickness of encapsulation = total thickness - thickness of interface layer - thickness of silver layer

Layer	**Material**	**Manufacturer**	**Curing time**	**Curing method**	**Curing temperature (℃)**	**Average thickness (mm)**	**Printing times**
1	Interface (Fabinks-IF-1004)	Fabinks	30 s	UV curing	X	0.24	3
2	Silver (ELX-30)	Electra Polymers	10 min	Box oven	120	0.02	1
3	Encapsulation (Fabinks-IF-1004)	Fabinks	30 s	UV curing	X	0.15	2

Table 4-1: Details of the layer pirnting including manufacturer, curing time and method, average thickness and printing times.

Print setting	**Interface and Encapsulation**	**Silver**
Printing gap	1.0 mm	0.9 mm
pressure	6 kg	5.5 kg
speed	70 mm/s	70 mm/s

Table 4-2: Printing setting for the interface and silver layer.

Figure 4-10 shows the printed silver electrodes from 2.5 cm^2 to 0.5 cm^2.

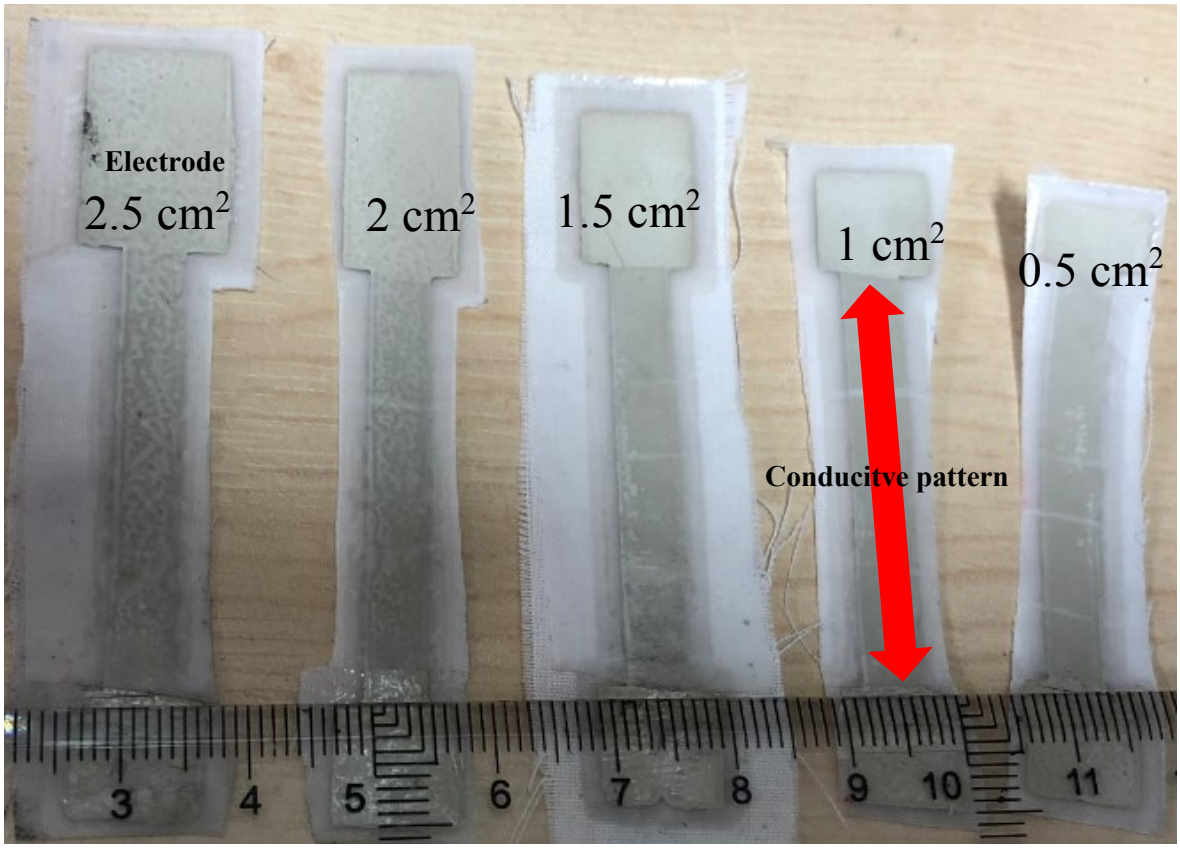

Figure 4-10: Screen printed silver electrodes, where the electrode size is decreased from 2.5 cm^2 to 0.5 cm^2 (left to the right).

4.6 Properties of ELX-30 silver

When the electrode is printed, the resistivity of the conductive patterns as shown in Figure 4-10 has been measured and calculated from the following equation:

$$\rho = \frac{RA}{l} \quad (4\text{-}1)$$

l is the length of conductive pattern (measured by ruler), for an individual sample, the averaged length is 40 mm.

A is the cross sectional area of conductive pattern (thickness of silver × width of the conductive pattern), for an individual sample, the averaged area is approximately 0.01 mm^2.

R is resistor and measured by the multi-meter for the conductive pattern, for an induvial sample, the value of resistor is about 20 Ω.

Each sample is measured 5 times and take the mean value, the mean resistivity of ELX-30 silver electrode is 4.5×10^{-6} Ω.m.

In addition, because the thickness of silver laver is very small (0.02 mm), the mass of silver is calculated from the following equation:

Mass of silver = total mass of (interface + textile + silver) – mass of (interface + textile).

Volume of silver = area of conductive pattern × thickness of silver.

One additional step is added to the printing procedure to measure the mass of silver. In Figure 4-11, half of the electrode area on the screen is blocked by the tape, the other half is printed as normal. After curing the silver, the blocked half contains layers textile and interface, the unblocked part contains layers of textile, interface and silver. Subsequently, the blocked and unblocked parts are overlaid and cut into same size.

The mass of the blocked and unblocked is weighted by electrical weighing scale (Voyagel Pro,OHAUS, minimum scale: 1mg). The mass of one individual silver sample is 0.03 g.

The thickness, width and length of conductive patterns on blocked and unblocked parts are measured by ruler and used to calculate the volume and mass of silver. The volume of one individual sample is 0.0032 cm^3.

Therefore, the average density is approximately 9.1×10^3 kg/m^3.

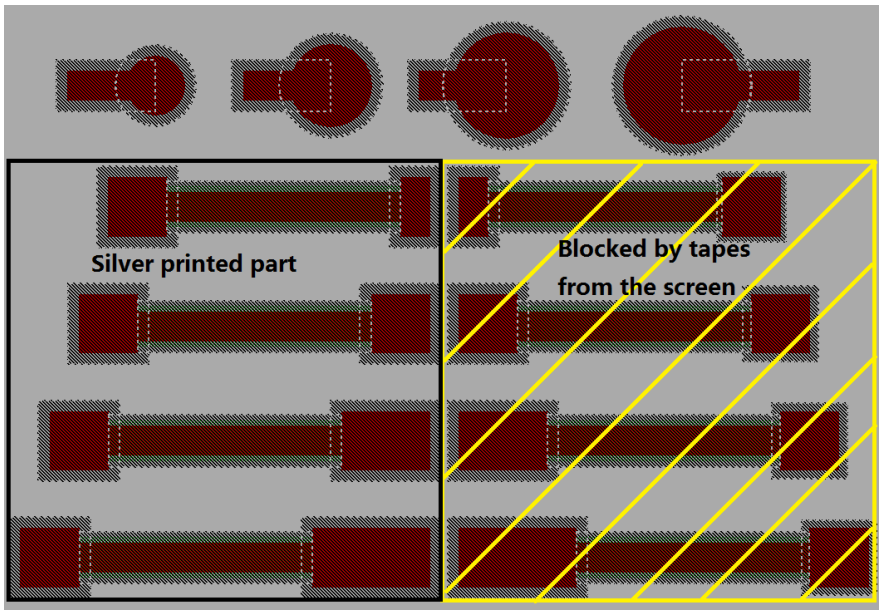

Figure 4-11: Schematic diagram of one print with and without silver layer (yellow part means the pattern are blocked by tape).

4.7 Method of measuring skin electrode impedance

When the skin-electrode impedance is measured, the following measuring conditions are applied to the electrodes.

1. The impedance analyser is a WAYNE KERR 6500B precision impedance analyser.
2. Two identical sized electrodes in a pair and are placed on the inner forearm with a 50 mm separation between them (shown as Figure 4-12). The inner forearm typically has less hair than other areas, hence can provide measurements on a relatively stable and horizontal surface.
3. Before the measurement, the inner forearm needs cleaned up and dried.
4. The two electrodes are covered by tape to limit movement.
5. Each electrode pair is measured 5 times.

6. After each electrode pair measurement, the forearm is cleaned by wet wipes.
7. 3 males and 3 females from university of Southampton have volunteered and their results were measured.
8. Participants have read and signed the ethic form and consent form (see Appendix A and Appendix B): ERGO/FPSE/ 30998.
9. The age of the participants ranges from 20 to 30, and the BMI (body mass index) ranges between18 and 24, all within the range for ideal BMI. Furthermore, limiting BMI in this range will allow relative control of the variable which is the thickness of different skin layers.

Figure 4-12 demonstrates the setting of measurement, the impedance analyser has connected to the electrodes.

Figure 4-12: skin-electrode impedance measurement setting for silver electrode pair (two electrodes are connected impedance analyser).

4.8 Skin-electrode impedance measurement for textile silver electrode

In Chapter 3, the method of simulating skin-electrode impedance has been described. In this section, the impedance curve between skin and electrode is measured and comparison was made with COMSOL simulation in Chapter 3. This comparison is used to find the limitations of the COMSOL simulation and evaluate the performance of the COMSOL simulation. In the following Figures (Figure 4-13 to Figure 4-17), all the electrode pairs with different electrode sizes are shown. They have all been measured 5 times. All the skin-electrode impedances are measured at low frequencies from 20 Hz to 500 Hz. 200 impedance points were measured over the range. 20 Hz was the lowest frequency of the impedance analyser. The simulation in Chapter 3 was simulated from 0.1 Hz to 10 Hz, so the impedance curve was plotted relative to frequency. Therefore, the only change for the simulation was adjusting the frequency to fit the measurement frequency and so the simulation results are

not affected. In the comparison between simulation and measurement (section 4.9), the frequency is changed from 20 to 500 Hz. For the different frequency generator, the simulation is able to provide the same frequency. The first 150 points covered the impedance measurements before 200 Hz. There were more impedance data under 100 Hz since the bio-signals frequencies shown in Figure 2-3 are over the range from 20 to 100 Hz.

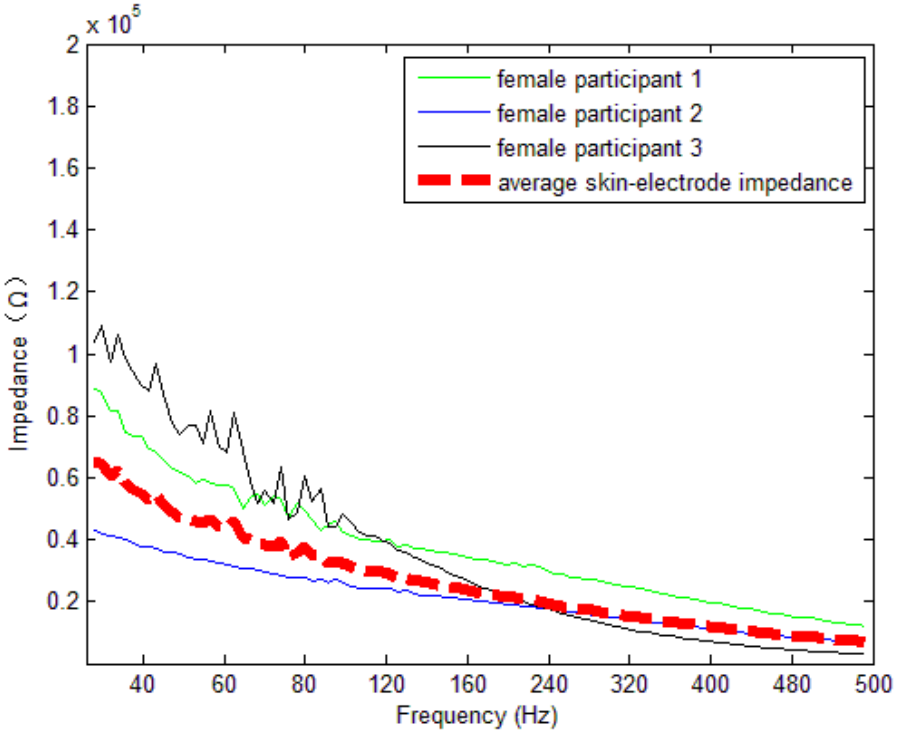

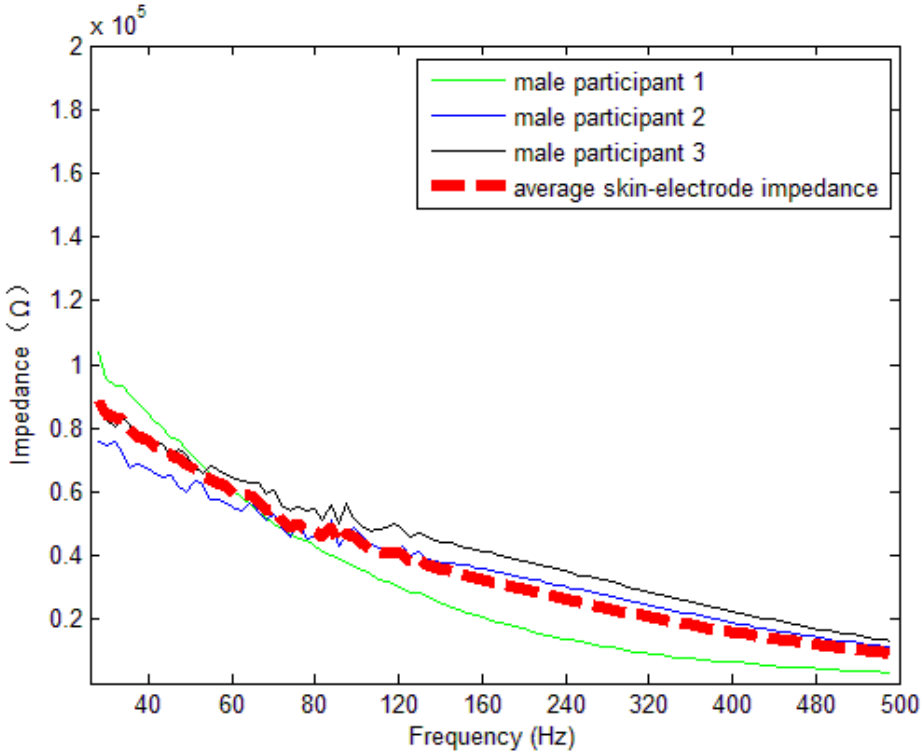

Figure 4-13: Skin-electrode impedance of a 2.5 cm^2 silver electrode pair for (Top): three female participants; and (Bottom): three male participants.

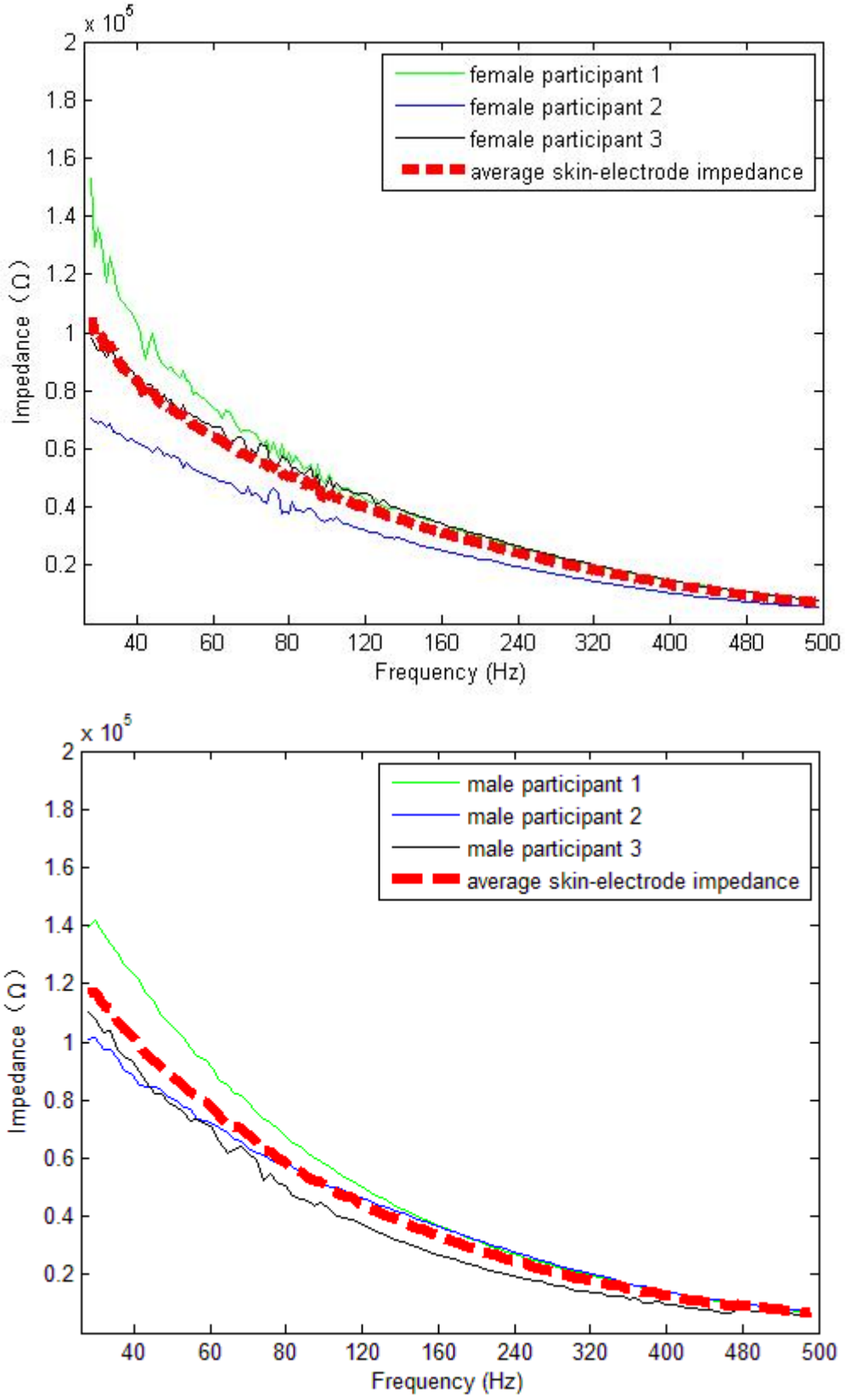

Figure 4-14: Skin-electrode impedance of a 2 cm^2 silver electrode pair for (Top): three female participants; and (Bottom): three male participants.

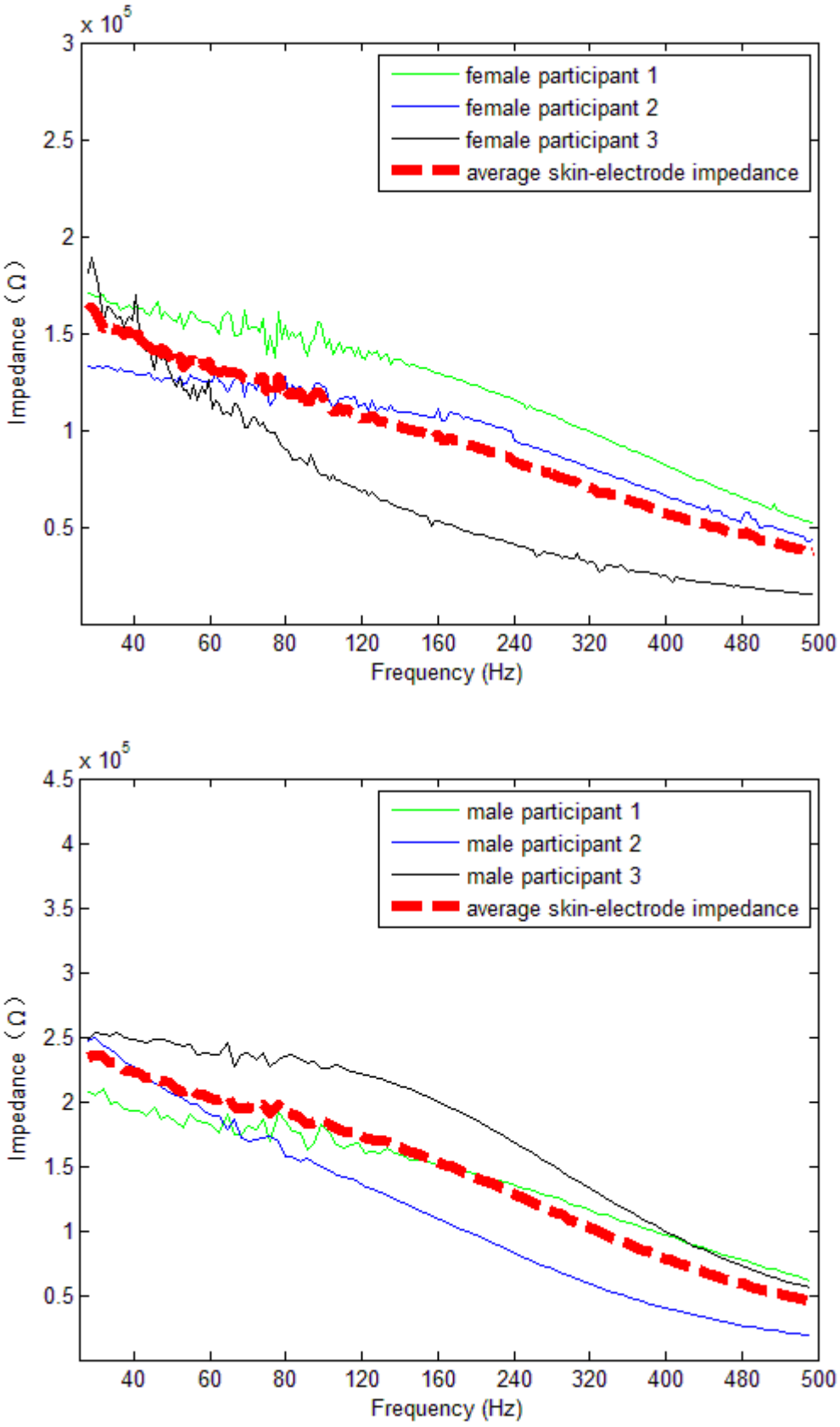

Figure 4-15: Skin-electrode impedance of a 1.5 cm^2 silver electrode pair for (Top): three female participants; and (Bottom): three male participants.

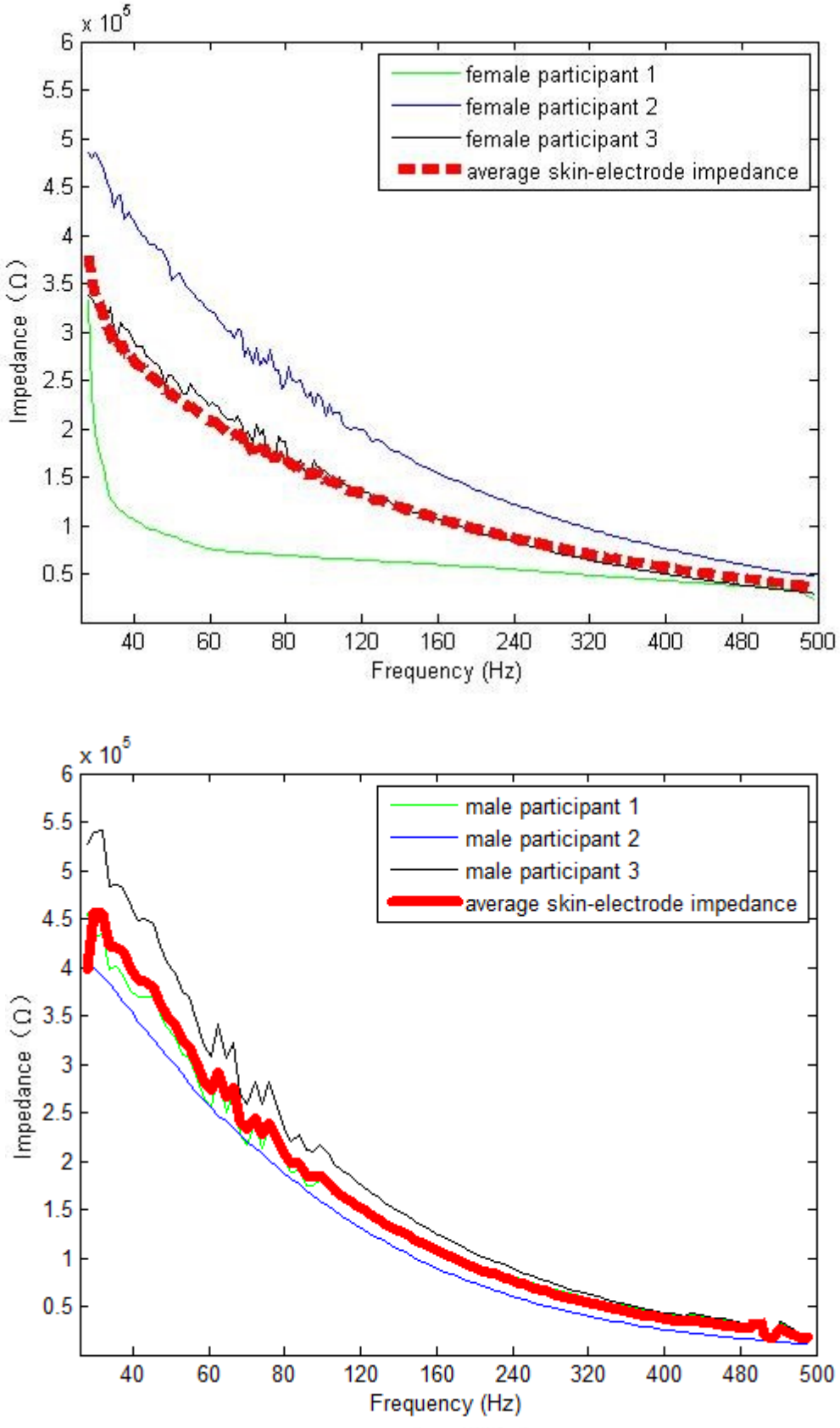

Figure 4-16: Skin-electrode impedance of a 1 cm^2 silver electrode pair for (Top): three female participants; and (Bottom): three male participants.

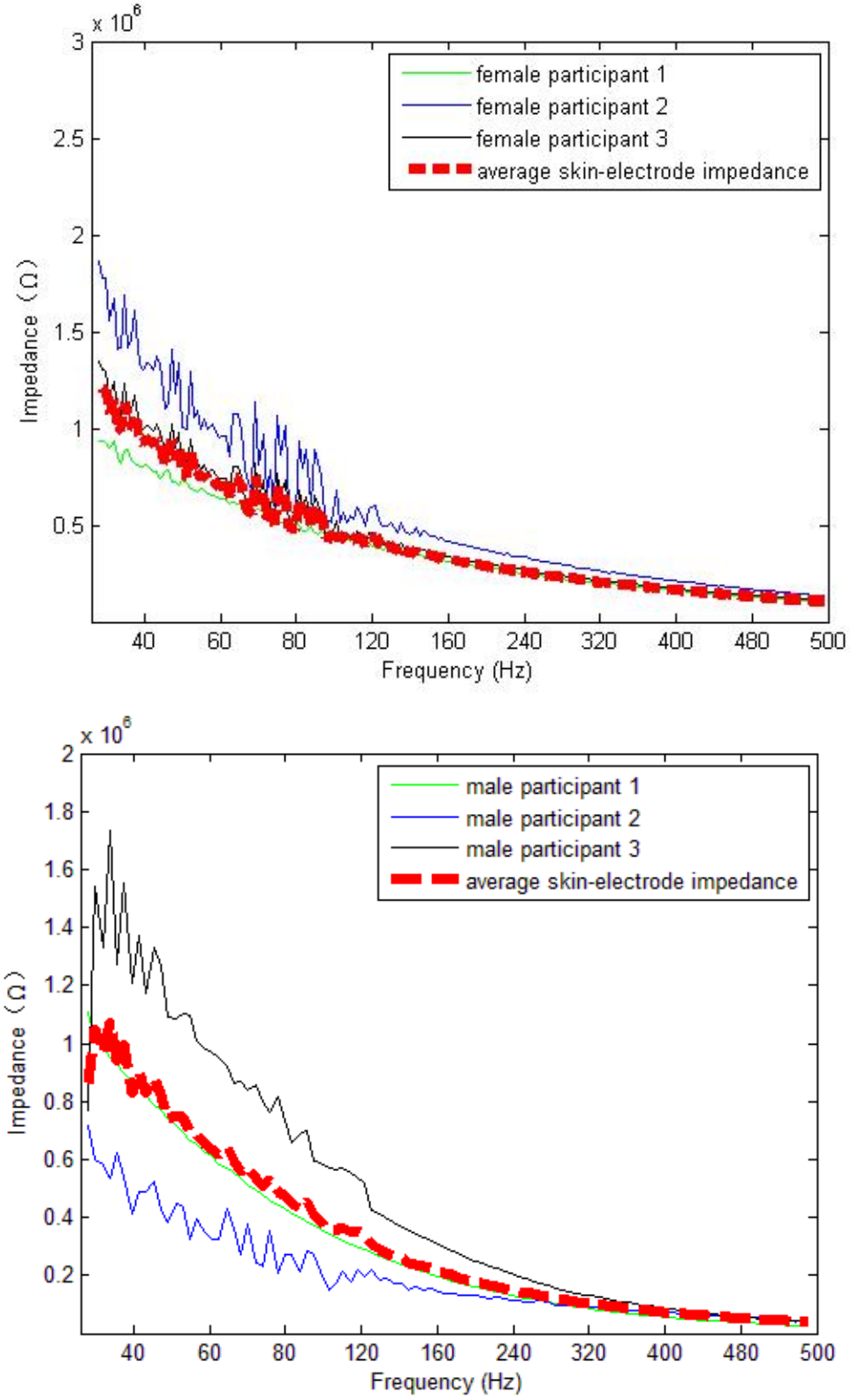

Figure 4-17: Skin-electrode impedance of a 0.5 cm^2 silver electrode pair for (Top): three female participants; and (Bottom): three male participants.

All of the above figures show the skin-electrode impedances for different electrode pairs. In all the figures, the skin-electrode impedances of the silver electrode pairs have been measured from 20 Hz to 500 Hz. The skin-electrode impedances for three male and three female participants were measured.

Moreover, in the measurement of the 1 cm^2 silver electrode for the females, one of the participants' impedance curves was much smoother than the others. The reason is that this particular participant kept the electrode pair stable by applying a small pressure on them by using a hand to hold the electrode pair. But the trend of the impedance curve is similar to before and this did not have a significant impact on the highest and lowest impedance value, so the results have been considered in the measurement. From the measurements, the skin-electrode impedance for the males was higher than that for the females. According to Jovana (Jovana *et al.*, 2012), at a low frequency (less than 5 kHz), male skin impedance will be higher than the female impedance, because a male generally has more muscle than a female.

Furthermore, when the electrode size was reduced from 2.5 cm^2 to 2 cm^2, the highest average skin-electrode impedance of the males increased from 8.9×10^4 Ω to 1.2×10^5 Ω, which is approximately 35 %. If the electrode size was further reduced to 1.5 cm^2, compared with the 2 cm^2 electrode, the highest average skin-electrode impedance increased from 1.2×10^5 Ω to 2.2×10^5 Ω (about 80 %) which is much higher than the impedance changes between 2.5 cm^2 and 2 cm^2 electrode. When the silver electrode size of male was reduced from 1.5 cm^2 to 1 cm^2, the impedance increased to 4.1×10^5 Ω (around 100 %). Nevertheless, when the electrode size of a male was reduced to 0.5 cm^2, the impedance increased to 1.2×10^6 Ω (about 190 %).

Meanwhile, the impedance change for the silver electrode on the females showed the same trend as for the males. When the silver electrode size for the females was reduced from 2.5 cm^2 to 0.5 cm^2 in steps of 0.5 cm^2, the impedances at 20 Hz for females were 6.5×10^4 Ω, 1.1×10^5 Ω, 1.6×10^5 Ω, 3.5×10^5 Ω and 1.2×10^6 Ω, and the impedance differences between each electrode increased approximately 83 %, 45 %, 120 % and 253 % respectively. In the results, there is a less increasing percentage (45 %), when the electrode size was changed from 2 cm^2 to 1.5 cm^2. This lower percentage increase may result from the impedance at low frequency (20 Hz in Figure 4-14 to Figure 4-17). In the measurement, these were the noise in the impedance curve, not the noise in the signal; therefore, they were called impedance noise. When the impedances were taken from low frequencies, there were some impedance noises in the measured results. When the measured results were used to calculate the average values for the impedances, some peak impedance noise may add to the final results. To identify this problem, the averaged total skin-electrode impedances of female and male with different electrode sizes were selected at the highest frequency (500 Hz) and listed in Table 4-3. At this frequency, the skin-electrode impedance was more stable and had less impedance noise during the measurement.

Electrode size (cm^2)	Skin-electrode impedance (Ω)
2.5	6.9×10^3
2	7.1×10^3
1.5	15×10^3
1	38×10^3
0.5	105×10^3

Table 4-3: Skin-electrode impedance of female for different electrode sizes at 500 Hz.

If the impedance differences between each electrode were calculated from Table 4-3, the differences between each electrode were: 3 %, 111 %, 153 % and 176 %. The increased impedance difference showed the similar trend as male's impedance differences. Therefore, the frequency range did not change the percentage of difference. To avoid the effect from impedance noise and analyse the skin-electrode impedance at low frequency, the skin-electrode impedance could be selected from 50 Hz to 100 Hz.

Moreover, these noises impedance in the impedance curves (see Figure 4-13 to Figure 4-17) at low frequency (especially less than 50 Hz) could have been due to:

- The small voltage drop from the muscle being added to the two electrodes and generating these small impedances.
- Noise is defined by a $1/f^{\alpha}$ power spectrum (with $1.5 < \alpha < 2$), which means that the noise decreases inversely with frequency. However, the mechanisms for the generation of this noise are still not clear and the main reasons may come from the skin's properties (Huigen, 2001).
- Nevertheless, when the electrode keeps reducing, noise at low frequencies becomes more obvious. The smaller the electrodes, the worse the situation. From the research of Huigen (2001), this noise (n) is described by the spatial averaging of the uncorrelated noise sources. Forming the following relationship with the electrode size(A):

$$n \propto \frac{1}{\sqrt{A}}$$

From these impedance results, the assumption at the end of Chapter 3 is correct, and there should be a minimum value for the electrode size, and the electrode size needs to be greater than 1 cm^2. For the 1 cm^2 electrode, the noise starts generating in the curve, so if we want to obtain an ideal result for the impedance of the skin-electrode, the electrode size should be greater or equal to 1 cm^2. Figure 4-18 shows the electrode size and skin-electrode impedance for the average male and female. The impedance at low frequency (less than 50 Hz) is the suitable one for the ECG and EMG skin impedance. To avoid the impedance noise's effects at the start of the measurement (20 Hz), the impedance at 50 Hz has been selected to identify the electrode's size effects.

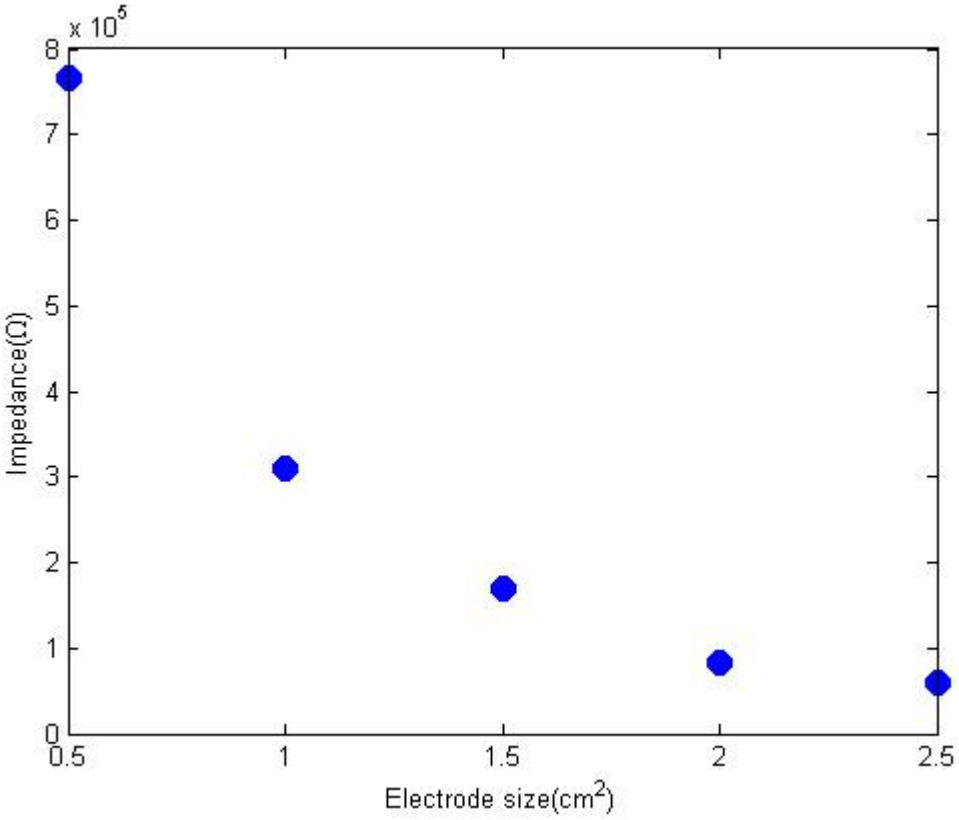

Figure 4-18: Relationship between the silver electrode size and skin-electrode impedance of averaged male and female at 50 Hz.

Figure 4-18 showed that skin-electrode impedance rapidly decreases in two periods, one is the electrode size changed from 0.5 cm^2 to 1 cm^2 and the other one is from 1 cm^2 to 1.5 cm^2 and 1.5 cm^2 to 2 cm^2. When the electrode size was increased from 0.5 to 1 cm^2, the averaged skin-electrode impedance was reduced about 60 % (from 7.7×10^5 Ω to 3.1×10^5 Ω). For the electrode size changed from 1 to 1.5 $cm^2$and 1.5 to 2 cm^2, both changes reduced the skin-electrode impedance (3.1×10^5 Ω to 1.7×10^5 Ω and 1.7×10^5 Ω to 0.83×10^5 Ω) by around 50 %. When the electrode size is increased from 2 to 2.5 cm^2, the impedance change was about 15 %. From this result, it can be concluded that 2 cm^2 is a minimum threshold for the electrode design. The shape of the electrode can be variable, but the area should be around 2 cm^2. Comparing this conclusion with that for the simulated silver electrode, the 2 cm^2 electrode is a typical value for the electrode design.

Nevertheless, comparing the skin-electrode impedance of a textile silver electrode with impedances from the literature showed a similar range of the impedance, which was about 10^5 Ω. In Table 4-4, the skin-electrode impedance on a forearm with a commercial Ag or AgCl electrode were listed, the impedance values were selected at the lowest frequencies in the literature (1 Hz or 10 Hz) and 50 Hz (since 50 Hz was the one used in this thesis). In the literature, the electrode sizes and shapes vary, therefore, the data from the literature enabling the impedance differences to be seen. In Li's research (Li *et al.*, 2017), the electrode had the smallest size (0.36 cm^2) in Table 4-4 and the measured frequency was 10 Hz. In this research, all 6 electrodes were placed in similar places on the forearm. However, the skin impedances on forearm varied significantly ($\pm$ 6.2×10^5 Ω). Because this small electrode had been measured several times at the same position, the reason may be that the small electrode was

very unstable and the impedance may contain the impedance noise like Figure 4-17, and the impedance noise may dominate the total impedance.

Elsewhere in the literature, although the authors applied different measurement methods, like two-electrode or four-electrode measurement in section 2.5.2, the total skin-electrode impedances reduced with increasing electrode size. Specifically, in Rajaraman's research (Rajaraman *et al.*, 2011), when the electrode size was 3.14 cm^2 (circular electrode of 1 cm radius), the total skin-electrode impedance was 0.5×10^5 Ω at 50 Hz. In the measurement of the textile silver electrode, the 2.5 cm^2 electrode had an impedance of 0.7×10^5 Ω; the difference between these two electrodes was about 40 %. The skin-electrode impedance of the textile silver electrode was reduced about 15 %, when the electrode size was increased to 3.14 cm^2. Thus, it could assume that the 3.14 cm^2 skin-electrode impedance of the textile silver electrode was about 0.55×10^5 Ω at 50 Hz (taken the maximum of 20 % difference). Therefore, the difference between the textile silver electrode and commercial silver electrode is about 10 %. Although there were some assumptions to make the comparison between the literature and the textile silver electrode, the skin-electrode impedance difference between textile silver electrode and the electrode in the literature was not too high (about 10 %), the textile silver electrode could be used to test the effects of skin-electrode impedance.

Furthermore, the difference between the experiment and literature may result from:

- In some of the literature (e.g. Rajaraman *et al.* 2011*,* Marcin *et al,* 2016), the silver electrode or commercial electrode contains the electrolyte gel. The gel will reduce the impedance rapidly and improve the quality of the measurement.
- ELX-30 is silver ink, and some solvents (like Acetone or Alcohol based solvents) may be added to ELX-30 to make it easy to print. However, these solvents evaporate during curing, therefore the amount of silver remaining is reduced, this may affect the quality of the skin-electrode impedance measurements.
- The setups for two-electrode measurement or four-electrode measurement were different (like starting frequency, testing source signal for impedance), and the measurement environments were not all the same, therefore, this must result in some mismatches in different measurements.

Author	**Electrode**	**Electrode size (cm^2)**	**Forearm skin impedance (Ω)**	**Year**
Bosnjak *et al*	AgCl	0.8	6×10^5 (at 1 Hz) 4×10^5 (at 50 Hz)	2017
Li *et al*	AgCl	0.36	$5.2 \pm 6.2 \times 10^5$(10 Hz)	2017
Marcin *et al*	Commercial silver	2	3.5×10^5 (at 1 Hz) 1.5×10^5 (at 50 Hz)	2016
Rajaraman *et al*	Commercial	3.14	2×10^5 (at 1 Hz) 0.5×10^5 (at 50 Hz)	2011

Table 4-4: Commercial Ag or AgCl skin-electrode impedance on forearm from the literatures.

In addition, both Li (2016) and Bosnjak (2017) showed the relationship between the electrode size (called electrode contact area in the papers) and the skin-electrode impedance. In Li's research, Li used AgCl electrode and showed that dry electrode impedance reduced when the electrode size was increased. However, there was no information about what electrode size provides the most impedance reduction in the measurement. On the other hand,

Bosnjak (2017)'s research had been discussed in section 3.5.2.2. From the relationship between the stainless-steel electrode size and skin-electrode impedance (Bosnjak *et al.*, 2017), results in a similar conclusion as for the textile silver electrode measurement in this thesis, namely, when the electrode size or contact area was less or equal to 2 cm^2, the change of electrode size give more impact on the skin-electrode impedance. However, when the electrode size or contact area was greater than 2 cm^2, the effect from electrode size was reduced. Therefore, 2 cm^2 is the threshold for designing electrode in both simulation and measurement.

4.9 COMSOL simulation and practical results using silver electrodes

If the 3D COMSOL model described in Chapter 3 is used to represent the results, two methods can be applied to represent the skin-electrode impedance. One is a single electrode model, and the other is to calculate the impedance directly from two electrodes.

The assumptions were similar to Chapter 3 and are listed below.

- The simulation was still built by 'Solid Mechanics' and 'Electric Current'.
- The materials were linear elastic and isotropic for 'Solid Mechanics' and 'Current Conservation' for 'Electric Current'.
- Added the projection part under the electrode. The projection part allows the COMSOL to use intensive mesh to analyse the skin under the electrode.
- In Figure 4-19, 'side boundaries' and 'end boundaries' surface were set to 'fixed constraints'. There will be no movement on these surfaces. When a force is applied to the model, if there are no fixed constants to limit the model movement, the whole model will be pushed under the applied force. In the real-life situation, the far end of the skin (the end of the arm) are connect with body and has less movement in the measurement.
- The 'Model width' was set to 30 mm. The model width has been proved in section 3.5.2.1. For a 1 cm^2 electrode, a model width of 20 mm will not affect the results. The model width set to 30 mm allows for the change of electrode size.
- 'Electrode points' on the centre line and 'Layer surface' in Figure 4-19 were set to 'Prescribed Displacement in z-axes direction '. Therefore, these points and surfaces can only move in the z direction.
- The electrode size was varied from 0.5 cm^2 to 2.5 cm^2 to represent the experiment electrodes.
- The 'symmetry surfaces' in Figure 4-19 were set to 'Symmetry', a function provided by COMSOL to make a symmetrical structure, so only half of the forearm was needed in Figure 4-19.
- Because this model was set to 'Symmetry', the 'Model length' was set to 50 mm to approximate a 100 mm forearm length. This forearm length will have a similar skin-electrode impedance as the full forearm length with about 1.5 % difference and has been shown in section 3.5.1.2.
    - In 'Electric Current', the 'Model boundary' surface were set to 'electric insulation'. The ground was applied to the 'End boundary' (electric potential V

was zero: Dirichlet boundary condition, the boundary equation was a constant voltage).

- A potential of 3 mV (the averaged forearm bio-signal potential (Kareem *et al.*, 2017)) was applied to the 'Bottom surface'. A potential of 10 mV was applied to the top of electrode surface with 'Harmonic Perturbation', which is same as the measurement.
- The impedance was calculated from this bottom surface to the top of the electrode.

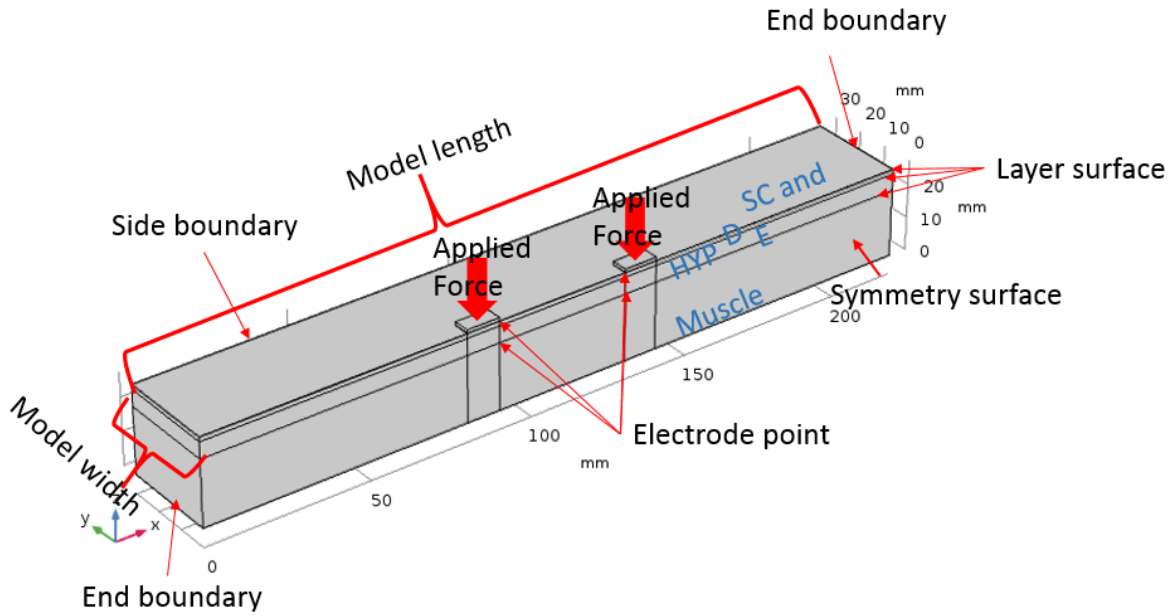

Figure 4-19: Simulated model including the applied signal and symbols/definition for the surfaces, edges and points.

In the simulation, some new assumptions and measured results are added to these to make the calculation more accurate:

- The electrode size was varied but the thickness of electrode is kept at 0.02 mm, which was measured from the textile electrode in section 4.5.
- A small amount of pressure, 1 N, was applied to the tops of the two electrodes and the top of SC layer. This applied force was trying to play the role as the visible tape in and simulating in Figure 4-12. Furthermore, because the visible tape did not cover the whole forearm, the 'fixed constraint' was added to the side boundary showed in Figure 3-33 and gave a zero movement to this boundary.
- The applied frequency changed from 20 Hz to 500 Hz. Although the starting frequency did not like the literatures (starting from 1 Hz or 10 Hz), in the simulation, the results formed a linear relationship and the final results would not be affected by the different starting frequencies. Meanwhile, the 20 Hz frequency was also a small applied frequency and were in ECG, EMG or EEG frequency range, therefore, the starting frequency could start from 20 Hz.

- Total element in the simulation is: 41040.
- The properties of ELX-30 silver electrode:
  - Resistivity is 5×10^{-6} Ω.m and measured in section 4.6
  - Young's Modulus of silver on textile electrode: 220 MPa. This data was selected based on previous work (Komolafe *et al.*, 2018). A previous work has been done in University of Southampton to discuss the Young's modulus of Fabinks-IF-1004 with silver ink. Moreover, from the simulation in chapter 4, the Young's Modulus is not a key parameter in the model, therefore, the results from previous work is able to support this selection. Meanwhile, the Poisson ratio has a pre-tested before simulating. When the Poisson ratio of the electrode was changed from 0.2 to 0.45, the total impedance was change less than 0.1 %, which means the change of Poisson ratio could not change the skin-electrode impedance in the simulation. Therefore, the Poisson ratio of silver defined in COMSOL was used to simulate.
  - Dielectric constant is 1. Because the silver is conductive material and cannot measure its dielectric constant in University of Southampton, the data from online database is used to instead. Because the silver plays the role as conductor in the simulation, the value of the dielectric constant of silver cannot change the simulation results. Therefore, the dielectric constant of silver keeps to the ideal metal value: 1.
  - Density is 9.1×10^3 kg/m^3 and measured in section 4.6.
  - The skin thickness and the properties of materials are shown in Table 4-5.

Electrode and skin	**Thickness (mm)**	**Young's Modulus (MPa)**	**Conductivity (S/m)**	**Poisson ratio**	**Density (kg/m^3)**	**Dielectric Constant/ Relative Permittivity**
Electrode (Ag)	0.02	220	2×10^5	0.4	9100	1
Stratum Corneum(SC)	0.02	2.9	0.0003	0.48	1050	1140
Epidermis(E)	0.1	0.5	0.5	0.48	1020	1140
Dermis(D)	1.42	0.05	3	0.495	1900	1140
Hypodermis and fat (HYP)	5	0.28	0.4	0.48	1800	3.3×10^5
Muscle(M)	25	1.7	0.42	0.45	1120	2.5×10^7

Table 4-5: Different mechanical and electrical properties of the skin and the textile silver electrode. The properties of the silver electrode was measured in section 4.5 and 4.6.

Figure 4-20 shows the textile electrode placed on the skin with a 1 N applied force. The deformation changed in Figure 4-20 direct to electrode centre. The reason is that electrode areas have higher pressure than the SC surface. In section 3.5.1, it has shown that the deformation is relevant to the pressure, when the applied force is applied to SC surface and top surface of electrode, the pressure is not uniform and the pressure will higher on the electrode area, therefore, there is an uniform deformation on the SC surface.

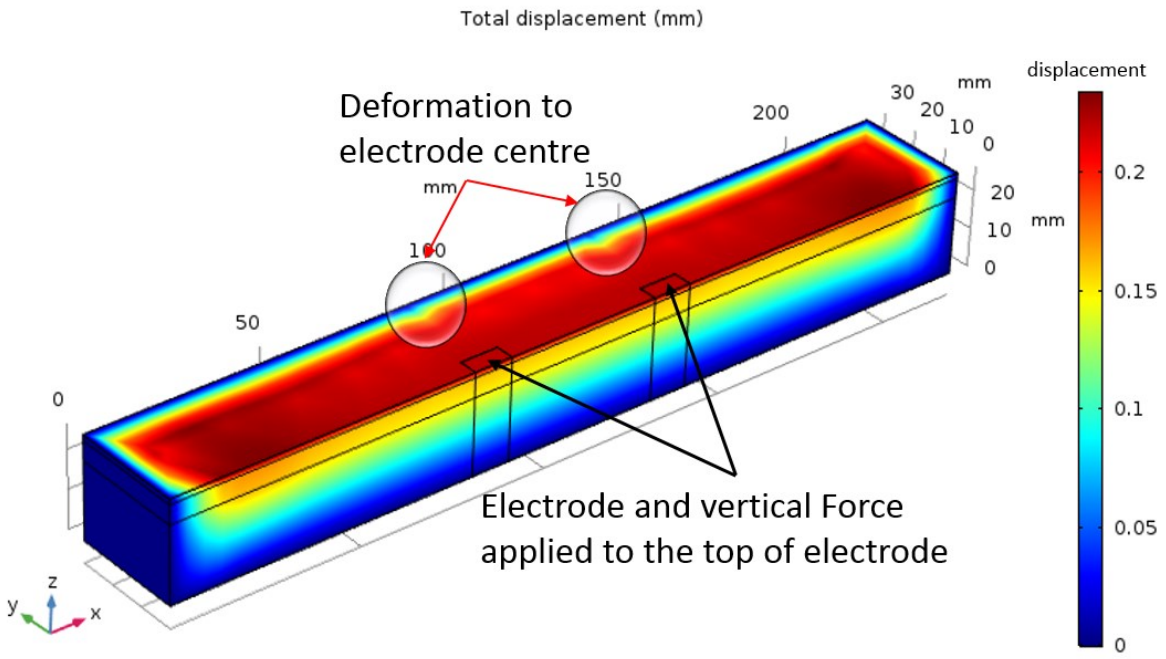

Figure 4-20: COMSOL simulated 1 cm^2 textile silver electrode on the skin model.

After the simulation structure was applied, Figure 4-21 shows an example of the changes in the electrode size to assess the applicability of the COMSOL model and identify the differences between the simulation and measured results. The electrode size was increased from 0.5 cm^2 to 2.5 cm^2. Meanwhile, the simulated changes in the electrodes sizes at 50 Hz are drawn in Figure 4-22. The changes in the electrode sizes at 50 Hz provide a similar conclusion as measured. In Figure 4-22, the threshold of the electrode size was still 2 cm^2. When the electrode size was increased from 0.5 cm^2 to 1 cm^2 and 1 cm^2 to 1.5 cm^2, the impedance changes have the highest decrease of approximately 42 % (from 3.23×10^5 Ω to 1.87×10^5 Ω) and 22 % (1.87×10^5 Ω to 1.46×10^5 Ω). However, when the electrode size was increased from 2 to 2.5 cm^2, the impedance reduction was only approximately 8 % (1.14×10^5 Ω to 1.06×10^5 Ω). Comparing these impedance changes with the electrode sizes, the simulation provided similar conclusions to the measurements.

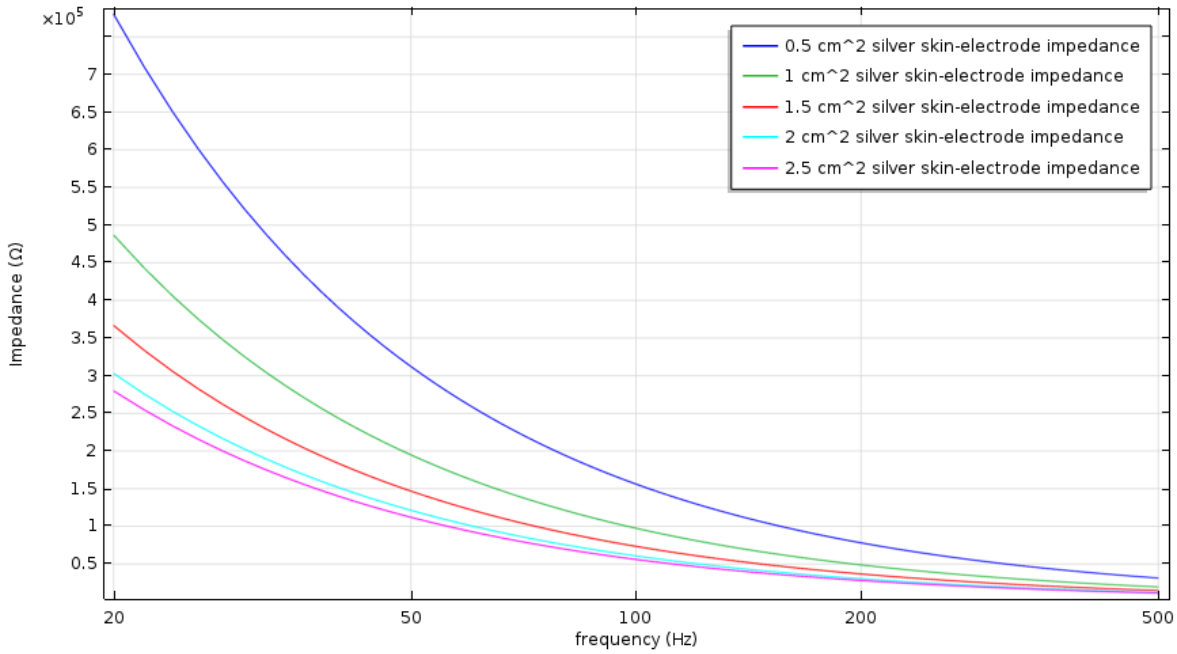

Figure 4-21: COMSOL simulated skin-electrode impedance of the silver textile electrode for different electrode sizes (from 0.5 cm^2 to 2.5 cm^2).

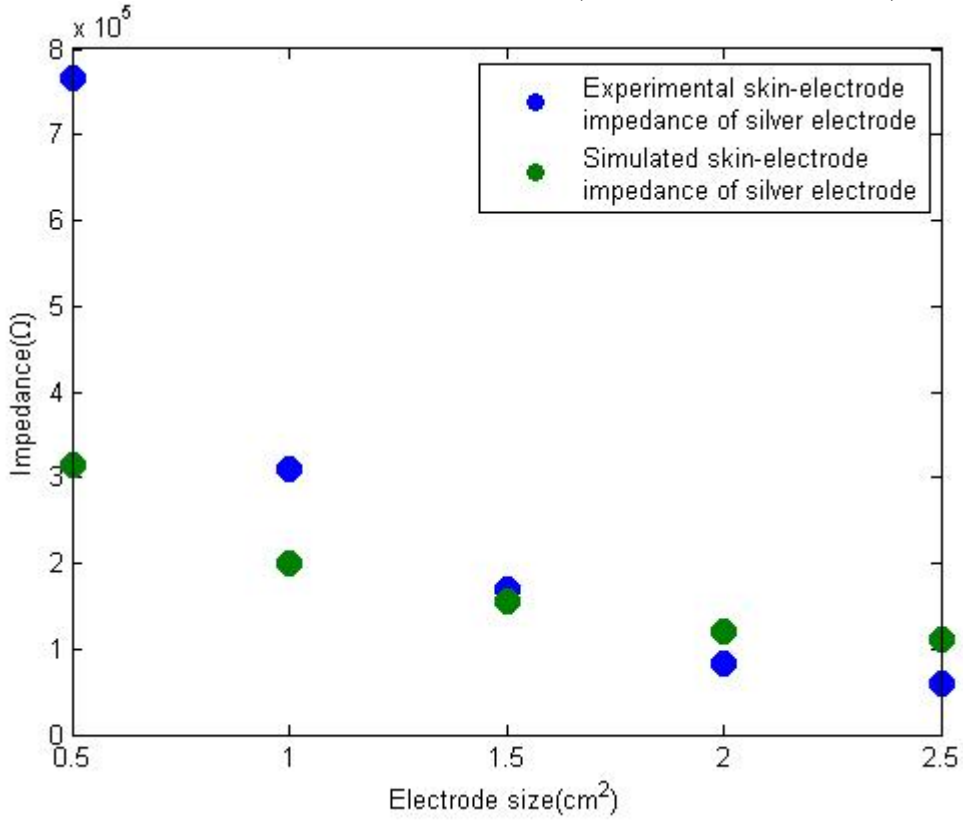

Figure 4-22: Experimental and simulated silver electrode sizes and their skin-electrode impedance at 50 Hz.

Comparing the simulated result with the measured results, the simulated impedance is larger. If the largest and smallest impedances at 50 Hz are selected from the simulations and measurements, it is easier to see the differences between them. At 50 Hz, the 0.5 cm^2 electrode provided the largest impedance for the simulation (3.2×10^5 Ω) and the experimental result averaged for males and females was 7.6×10^5 Ω, so the measurement

was about 58 % greater than the simulated result. Also at 50 Hz, both the 2.5 cm^2 electrode impedances presented the smallest impedances, which were 1.1 × 10^5 Ω for the simulation and 0.6 × 10^5 Ω for the measurement, so the difference between the simulation and measurement was approximately 45 %. Furthermore, the skin-electrode impedance of the simulation decreased by 65 % when changing the electrode size from 0.5 to 2.5 cm^2, however, when the electrode size was increased from 2 to 2.5 cm^2, the impedance was only reduced about 8 %. Therefore, it could say that most of the impedance reduction was from 0.5 to 2 cm^2. Meanwhile, the experiment showed the similar conclusion. When the electrode size was increased from 0.5 to 2.5 cm^2, the averaged male and female skin-electrode impedance was reduced about 90 %. However, when the electrode size was increased from 2 to 2.5 cm^2, the averaged male and female skin-electrode impedance was reduced only 13 %. The simulation and experiment results showed that the 2 cm^2 electrode size was a threshold for reducing skin-electrode impedance. If the skin-electrode impedance of the 2 cm^2 electrode was drawn in Figure 4-23, this could be used to identify the difference between the simulation and experiment.

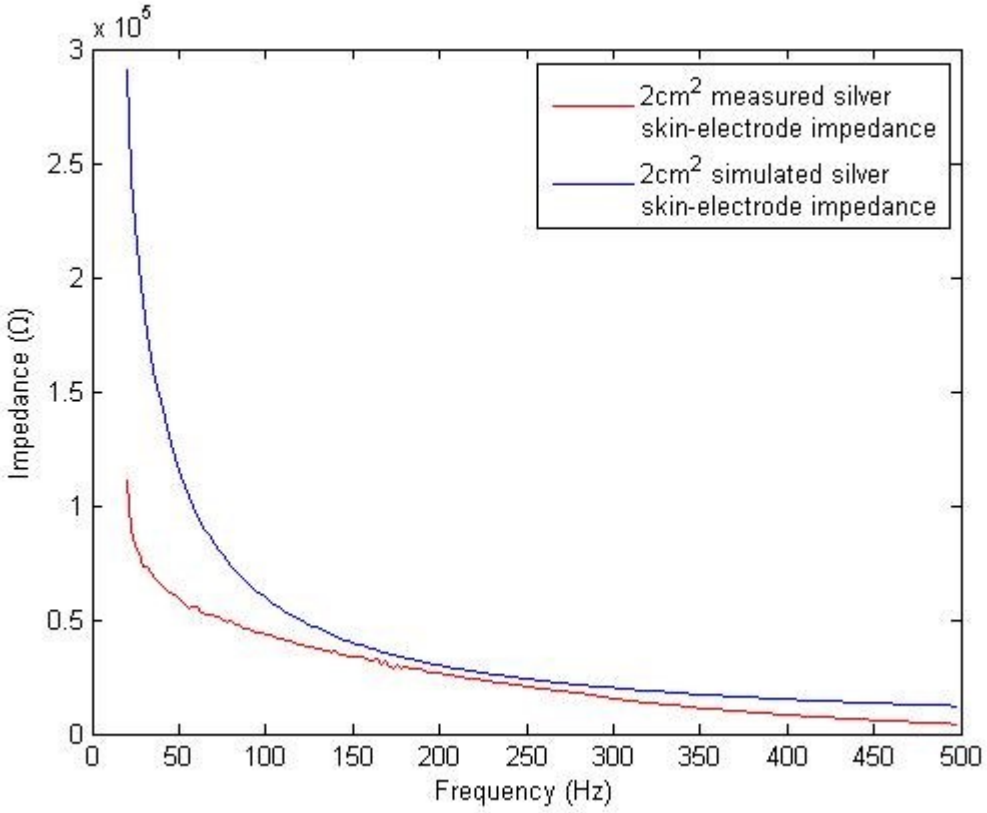

Figure 4-23: Skin-electrode impedance for 2 cm^2 area simulated and measured silver electrode (frequency range: 20 Hz to 500 Hz), the simulation parameters were introduced in Table 4-5.

In Figure 4-23, several certain frequencies (20 Hz, 100 Hz and 500 Hz) were selected to make the result comparisons between simulation and experiment. The lowest frequency 20 Hz had the largest difference (about 60 %), as the frequency was increased to 100 Hz, the difference between the simulation and measurement was reduced to 13 %, after 100 Hz, the difference between the simulation and measurement was around 20 %. Hence, the

differences between the simulated and measured impedance at lower frequency (less than 100 Hz) mean that this was less accurate than at higher frequencies (higher than 100 Hz).

Furthermore, based on Figure 2-53, the low frequency was dominated by the capacitance and showed the imaginary part of the impedance, meanwhile, the dielectric constant was one of the parameters that affect the capacitance. However, the dielectric constants of SC and HYP were based on average values, and both of the average values were at 100 Hz, so the two results are much close over a frequency of 100 Hz. To improve the accuracy of the model, another simulation based on the dielectric constant of SC and HYP at 10 Hz was simulated and shown in Figure 4-24.

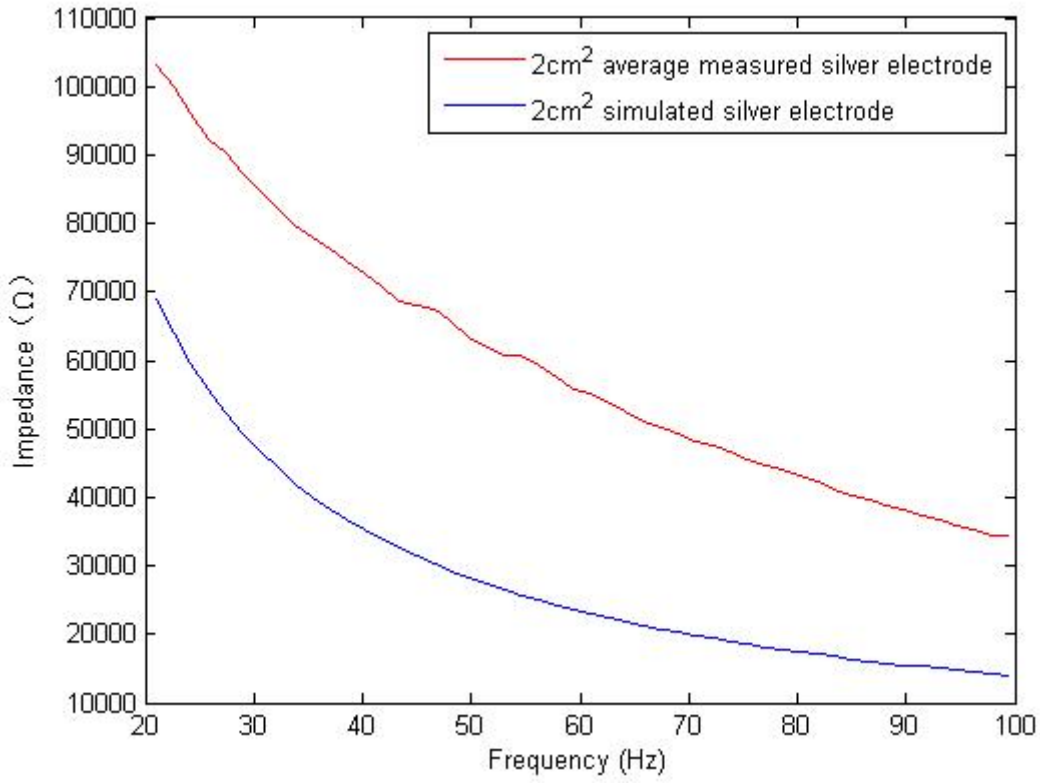

Figure 4-24: Skin-electrode impedance for a 2 cm^2 simulated and measured silver electrode (frequency range: 20 Hz to 100 Hz).

From Figure 4-24, when the dielectric constants of SC and HYP were changed to the values at 10 Hz (SC: 6600, HYP: 1.2×10^7), the difference between the simulated and measured impedance was reduced. If the frequency was 20 Hz, the difference between the simulated (7×10^5 Ω) and measured results (1.01×10^5 Ω) reduced to about 30 %, and thus the difference was reduced by about half. Furthermore, the dielectric constant for the SC and HYP at 10 Hz were not the fitted values. From the literature (Miklavcic *et al.*, 2006), when the SC layer was at frequency of 2 Hz, the dielectric constant was about 10×10^4 Ω. However, if the frequency was increased to 10 Hz, the dielectric constant was reduced to 6600 (reduced about 34 %). Furthermore, from the review by Gabriel et al (1996), the dielectric constant does not form a linear relationship with frequency. Hence, the dielectric constant was difficult to calculate from previous data. From section 2.5.1, the skin and skin cell at different frequencies followed the Cole equation (like Figure 2-52 and Figure 2-53) for the skin impedance, so the dielectric constant of SC and HYP at 10 Hz was still an approximate value in this low frequency range (20 to 100 Hz) simulation.

In section 3.5.2.1.2.2, the effects from dielectric constant for SC and HYP were discussed separately. From the existing data, if the dielectric constant of SC and HYP were used in the simulation to simulate the skin-electrode impedance, the impedance difference between 100 Hz and 1000 Hz was much smaller than the impedance difference between 10 Hz and 100 Hz (over 100 %). Meanwhile, if the skin-electrode impedance simulation is divided into several parts, the skin-electrode impedance curves based on different dielectric constant do not fit. According to dielectric constants at different frequencies, the skin-electrode impedance cannot reduce synchronously. For example, if the dielectric constant of SC at 10 Hz was applied to the frequency range (10 to 100 Hz), the total impedance reduced from 7 $\times 10^5$ Ω to 1.4 $\times 10^5$ Ω. At the same frequency point (like 100 Hz), if the dielectric constant of SC at 100 Hz was applied to a different frequency rage (100 to 500 Hz), the total impedance might reduce from 2.6 $\times 10^5$ Ω to 0.3 $\times 10^5$ Ω, The two impedance curves were not continuous with each other so the two curves cannot be combined together to build a new impedance curve to describe the skin-electrode impedance. Hence, because the change of the dielectric constant for SC and HYP had a significant impact on the simulated results, for a more accurate dielectric constant at certain frequency, the non-linear dielectric constants at different frequencies will provide closer simulated results to the measured results.

Another reason may increase the accuracy of the model is from the thickness of HYP. In the measurement, there were 3 male participant and 3 female participants for measuring the skin-electrode impedance. Meanwhile, from the literature, the female may contain more fat than male (Jovana *et al.*, 2012) and the HYP layer is the main layer to store the fat. Therefore, to identify the effects from HYP thickness, the impedance change of HYP at different thicknesses are shown in Figure 4-25. In Figure 4-25, although the thickness of HYP has been reduced to half (from 5 mm to 2.5 mm), the impedance was reduced by just 4.2 % (from 7 $\times 10^4$ Ω to 6.7 $\times 10^4$ Ω). This showed that the thickness of HYP did not produce significant changes in the simulation results. The reason may come from the calculation of the impedance. When the impedance is calculated in the low frequency, it has the following equation:

$$Z = \frac{d}{2\pi f \varepsilon A} + R_s \quad (4\text{-}2)$$

Where, ε= permittivity, d = thickness of skin, f=frequency, Z = impedance and A = area of electrode, R_s is the constant resistance. However, because the simulated impedance is at low frequency (less than 100 Hz), the R_s could be ignored.

Therefore, the equation becomes:

$$Z = \frac{d}{2\pi f \varepsilon A} \quad (4\text{-}3)$$

In the simulation, the smallest permittivity of the skin layer is less than 10^{-9}, and the thickness of skin is 0.005 m. the ratio between the permittivity and the thickness is over 10^5. According to the equation (4-3), if the HYP thickness was changed from 5 mm to 2.5 mm, although the ratio of thickness was changed 50 % (from 5 $\times 10^5$ to 2.5 $\times 10^5$), but the ratio between the permittivity and the thickness is still over 10^5. Therefore, the thickness cannot give the significant effect on the total impedance.

Because the effects of different HYP layer thickness have been tested, the results suggest that the dielectric constant of the skin layer will have a more significant impact the accuracy for the simulation compared with the thickness.

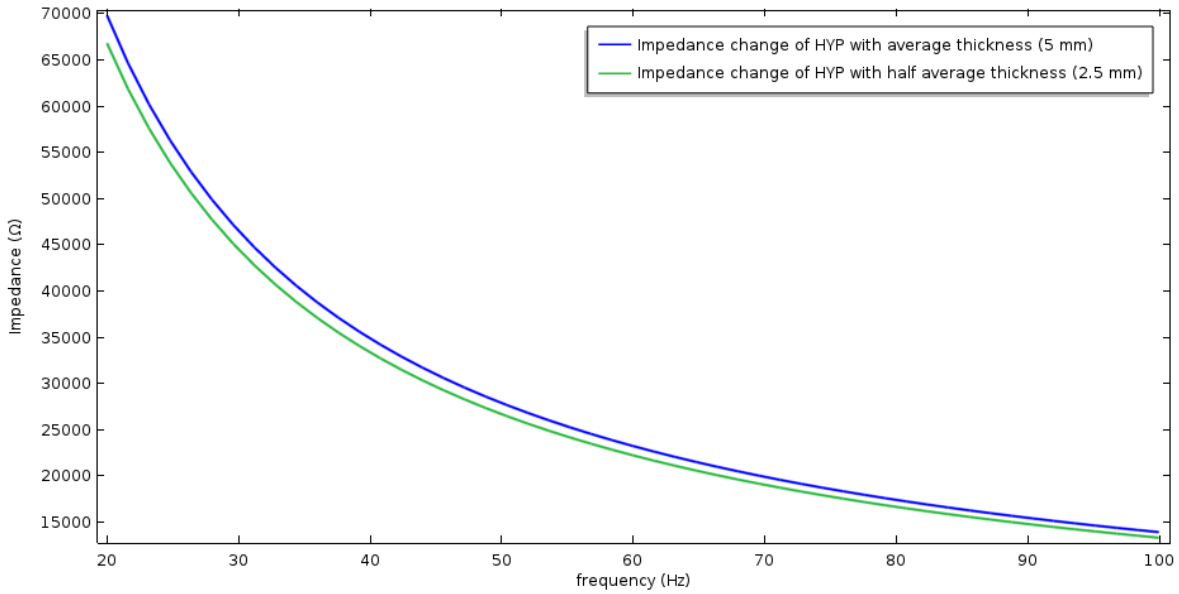

Figure 4-25: Skin-electrode impedance for the HYP at different thicknesses (2.5 mm and 5 mm).

4.10 Conclusions

In this section, printed electrode results are described for inkjet and screen printing. Because inkjet printing produces poorer prints on fabric than screen printing, the test results of screen printing are used to measure the skin-electrode properties and make a comparison between the experimental and COMSOL simulation results.

For the screen printed electrode results, 3 male and 3 female participants were measured. The average skin-electrode impedances for male/female are similar in respect of electrode size. If the electrodes size is larger than or equal to 1.5 cm^2, the result is smoother and clearer skin-electrode impedance curve than when the electrode size is smaller than 1.5 cm^2. Moreover, if the electrode size is reduced to less than 1 cm^2, the results become less accurate compared with those of greater than 1 cm^2. Some noise is generated in the results which is thought to come from the muscle potential.

Comparing the measurement results with the simulation results the simulated skin-electrode impedance decreases as the electrode size is increased, and 2 cm^2 is a threshold for the electrode size design. When the electrode size is increased from 0.5 to 2 cm^2, the impedance reduces rapidly (70 % in measurement and 60 % in simulation). Furthermore, when the electrode size is increased from 2 to 2.5 cm^2, the reduction is less than 20 % in measurement and simulation. Therefore, the 2 cm^2 electrode is the threshold for the electrode design.

Although the simulation is able to show the effect of changes in the electrode size, the simulation cannot fully match the measurement situation. In the experimental measurement, when the electrode size is changed from 0.5 cm^2 to 2.5 cm^2, the skin-electrode impedance

decreases from 9.7×10^5 Ω to 0.5×10^5 Ω at 50 Hz; a change of over 90 %. Under the same change in electrode size, the simulated skin-electrode impedance reduces from 3.23×10^5 Ω to 1×10^5 Ω at 50 Hz; a change of approximately 70 %. Comparing these two changes, the simulation results had a smaller change than the experiment results, and this may have been due to the following limitations of the simulation:

- The skin-electrode model is only half of the reality. Although the model has applied the symmetry to build the skin structure, the model did not contains the bond to the forearm and it was the top half of the forearm. In the experiment, although most of the signal passes though one electrode to another electrode by the shortest distance (which is the top half of the forearm), the impedance is still measured including the muscle of the forearm. If the whole forearm is designed in the simulation, the impedance interference from the bottom may have an effect.
- The skin's dielectric constants were simulated using an average value. In Chapter 3, it was shown that the dielectric constant of skin determines the total impedance of the skin. However, the skin's dielectric constants could not be measured for each person in this research and thus the average value was applied to the simulation. Furthermore, the dielectric constant of skin at low frequency (between 10 to 100 Hz) varies and over a very large interval (10^3 to 10^5), and thus, the accuracy of the simulation was limited by this variable. If the model could utilize data describing the dielectric constant vs frequency, the simulated results would be closer to the measured results. However, from the literature reviews, it cannot find the data about dielectric constant vs frequency at different frequencies. Therefore, the accuracy of the simulation was limited.
- Some material properties (like dielectric constant, Young's Modulus) of ELX-30 used in the simulation are close or ideal values (ideal metal has the dielectric constant of 1). In the simulation, although the silver plays the role as resistor as described in section 2.4, it still needs the value of dielectric constants and this value cannot be measured in University of Southampton, therefore, the dielectric constant has been added from the online database. However, chapter 3 and chapter 4 have shown that the dielectric constant has the significant impact on the simulation result, hence, the ideal dielectric constant of silver limits the performance of simulation.

  Moreover, the Young's Modulus of ELX-30 uses the results from previous work (Komolafe *et al.*, 2018) and the Young's Modulus is relevant to the textile and interface layer (IF-04). Although the model has proved that the Young's modulus has less importance than dielectric constant or conductivity, if Young's Modulus involved ELX-30 can be obtained, simulated results is able to be improved.
- In the measurement, the participant group is 6 people. Therefore, the comparison between the simulation and measurement may limit the validity to be generalized.

Based on the above two reasons, the impedance simulation was simulated for the dielectric constant of SC and HYP at 10 Hz at low frequency less than 100 Hz. When the dielectric constant at 10 Hz was used, the impedance difference between the simulation and measurement reduces from 60 % to 30 % as shown in Figure 4-23 and Figure 4-24. The inconsistent impedance has been reduced to half its original result. From this improvement, if the variation of the dielectric constant with frequency can be identified, the accuracy of the model can be improved.

However, this comparison between the simulation and measurement only showed the limitations of the actual materials used; an alternative soft material may give different results. Therefore, more experiments are needed to provide a more depth performance of the simulation. In the next chapter, a COMSOL skin electrode model is used to model an electrode made of a soft adhesive material.

Chapter 5: Dry electrode implementation and measurement

5.1 Introduction

As described in Chapters 3 and 4, the applied force and displacement on an electrode changes the measured skin-electrode impedance. In this chapter, an alternative dry electrode design using a new carbon loaded rubber material is used to make a comparison with the measured results to assess the simulation performance. This new electrode contains a soft surface and inherently adheres to the skin. This adhesion provides a more stable measuring condition on the skin.

5.2 Paste selection

Before the electrode was implemented, the materials of the electrode were selected. The following material properties were considered:

- Resistivity: the material should have low resistivity to increase the impedance match between the skin and electrode.
- Permittivity (dielectric constant): in the simulation, the impedance is based on the permittivity, so it was necessary to measure this value.
- Mechanical stability: the Electrode sticks to the skin. This helps the electrode to stay on the skin, and avoid the need for an additional conductive glue.
- Printability: the material is available to print by screen printing or other printing methods (like stencil printing).

Based on the above conditions, silicone rubber with carbon black was selected because:

- The silicone with carbon black is flexible.
- Silicone with carbon black is printable like the silver paste used in Chapter 4, which means the silicone with carbon black can be used in the textile electrode.
- Silicone can provide an adhesive surface for the electrode, but silver is not adhesive.

Furthermore, some silicone rubbers have already been used in the medical applications for bio-potential measurements in the literature. The silicone materials described in Table 5-1 were obtained from a relevent project in University of Southampton. These were selected to test their performances with carbon black (ENSACO 250G) which has been used in many projects e.g. Yang et al (2014) and Paul et al (2014) on screen printed electrodes.

Paste	MED-2310	MED-6350
Manufacturer	Nusil	Nusil
Curing time(min)	20	30
Curing temperature(℃)	100	120

Table 5-1: Summary of the silicone rubbers used in these trials.

The resistivity of silicone with carbon black mixture can be modified by considering the ratio between silicone and carbon black. However, initial mixing tests combining the MED-2310 silicone and carbon loading were not conductive. Even if the ratio between carbon and silicone was increased to 50 % and the carbon black particle could not be further mixed into the silicone to saturation, there was no conductivity. Hence, MED-2310 was excluded from this study. To add the material to the simulation model, the conductivity, Young's Modulus and dielectric constants (relative permittivity) of MED-6350 were tested, as described in the following sections.

5.3 Methodology for measuring the properties of MED-6350 silicone carbon rubber

Before testing the properties of MED-6350 silicone carbon rubber it needs to be mixed with carbon black (ENSACO 250G). The mixture of silicone and carbon loading (with different carbon ratios) were mixed using the speed mixer (DAC 150.1 FV-K, Hauschild Engineering) shown in Figure 5-5 with the settings 2500 rpm for 30 seconds.

Figure 5-1: Speed mixer for mixing silicone and carbon black (DAC 150.1 FV-K, Hauschild Engineering).

After the silicone was mixed with carbon black, the mixtures for different carbon loading ratios were cured in a box oven for 30 minutes at 100 ℃. After curing, each sample was cut to a 3 cm × 3 cm square of 1 cm thickness. Because the silicone carbon rubber is flexible, the thickness of each sample was an approximate value. Each sample was placed within two 3 cm × 3 cm cooper plates, pressed by the a weight to make a good contact between the silicone carbon rubber and copper, and connected into a serial circuit to calculate its resistivity, as shown in Figure 5-3.

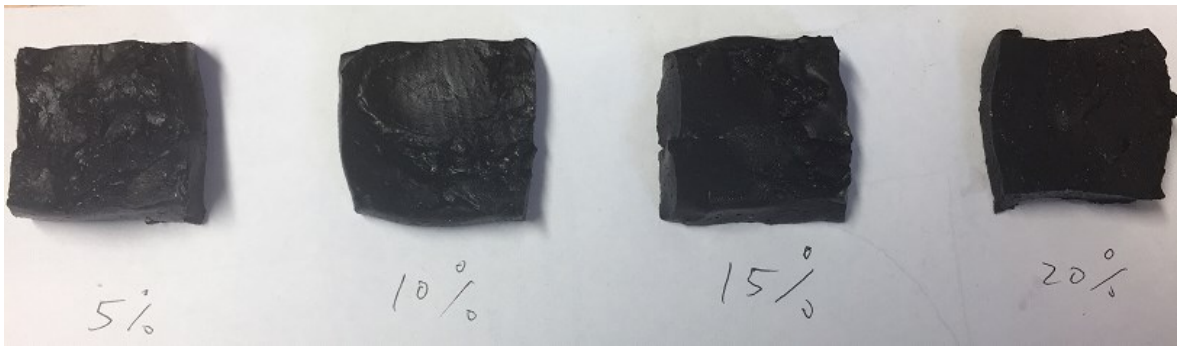

Figure 5-2: 4 MED-6350 silicone carbon mixture with different carbon loading (from left to right to left: 5 % to 20 % of the total mass).

Figure 5-3: MED-6350 placed into copper plates, size of copper plates: 3 cm × 3 cm and size of MED-6350: 3 cm × 3 cm × 1 cm.

5.3.1 Resistivity of MED-6350 silicone carbon rubber

From the above Figure 5-2, it can be seen that the mixture became coarser as the carbon loading increasing. For each silicone carbon rubber mixture, the carbon loading increased from 5 % to 20 % in increments of 5 %. There were 5 samples for each different carbon ratio.

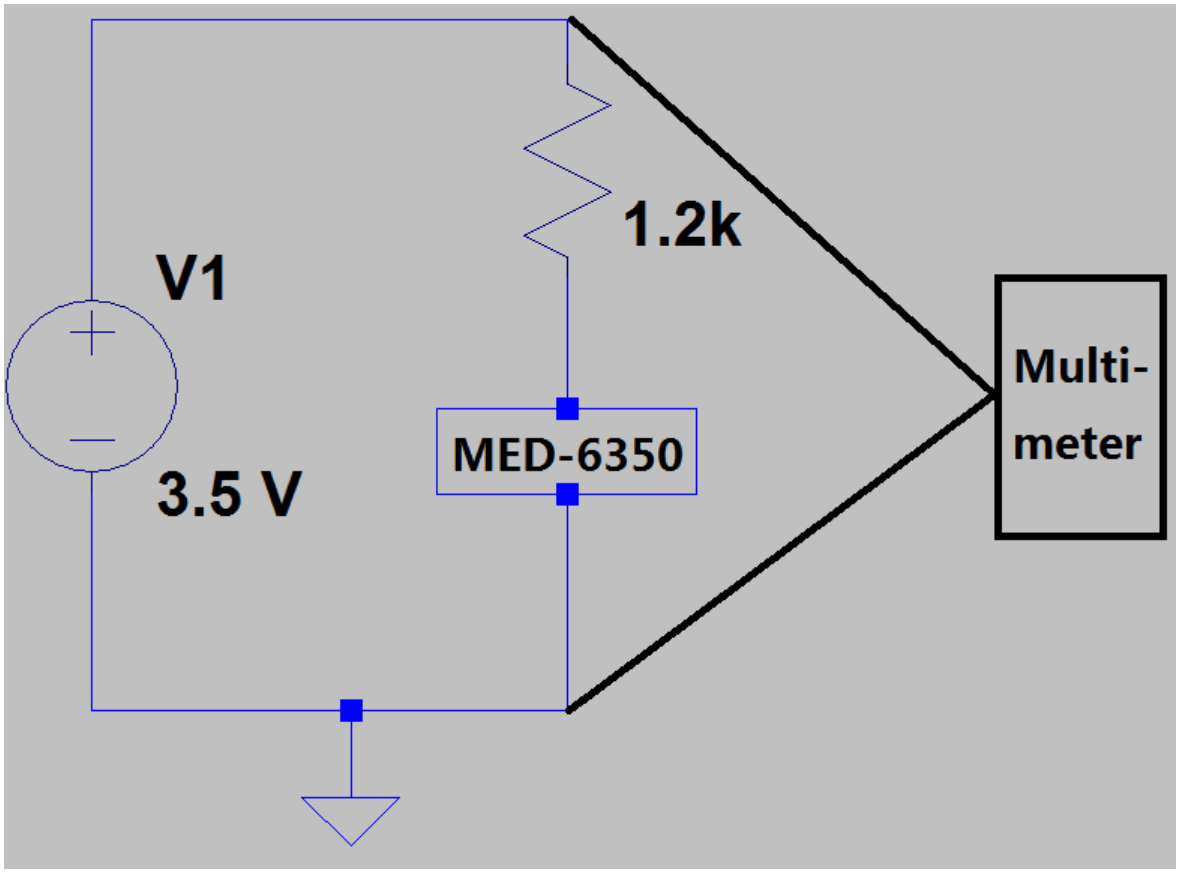

Figure 5-4: Testing circuit for the resistivity of the MED-6350.

Based on the voltage and current reading from the multi-meter, the resistance could be calculated. Each silicone-carbon cube's resistor was measured 5 times and the average value taken. The resistivity was then calculated using the following equation:

$$\rho = \frac{RA}{l} \quad (5\text{-}1)$$

Where, l is the height (10 mm) of the silicone-carbon cube, A is the area (20 mm x 20 mm) and R is the measured resistor. The resistivity of MED-6350 for different carbon ratios is shown in Figure 5-5.

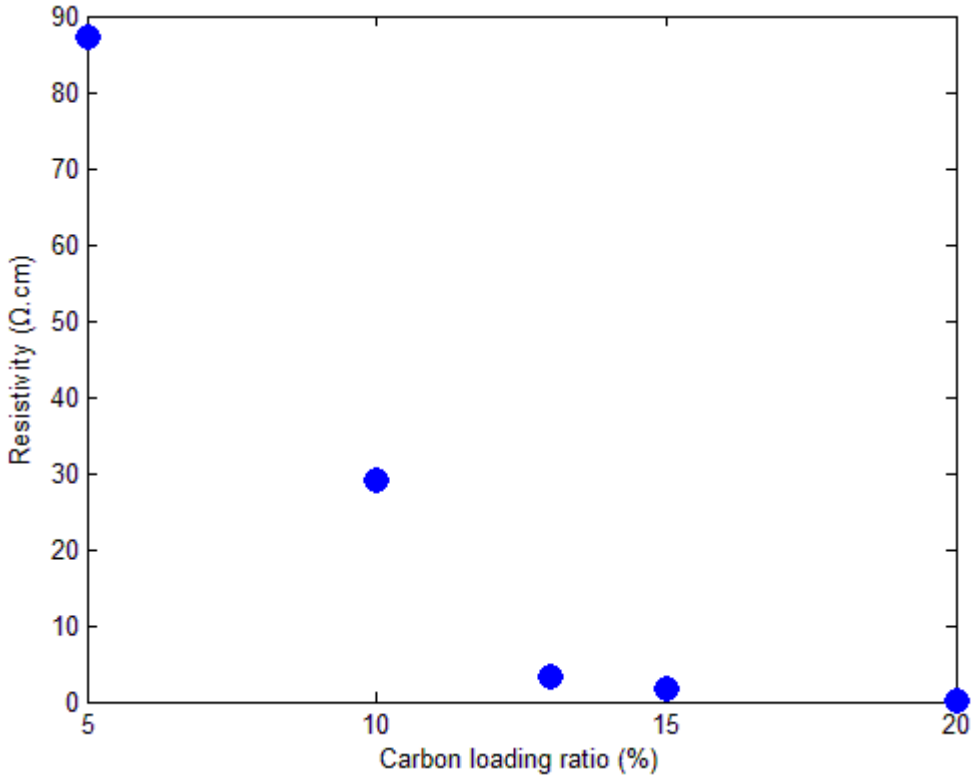

Figure 5-5: Resistivity of MED-6350 silicone-carbon rubber across different carbon loadings ratio (each silicone-carbon cube's resistor was measured 5 times and the average value taken).

In Figure 5-5, the resistivity of MED-6350 silicone rubber was reduced by approximately 99.8 % (from 87.1 Ω.cm to 0.142 Ω.cm). From the results, when the carbon loading was increased from 5 to 15 %, the resistivity of silicone carbon rubber decreased by around 93 % (from 87.1 Ω.cm to 1.79 Ω.cm), subsequently, the resistivity of silicone carbon rubber decreased from 1.79 Ω.cm to 0.142 Ω.cm, when the carbon loading increased from 15 to 20 %. Therefore, the increment of the carbon loading from 5 to 15 % exerts a significant impact, and the 15 % carbon loading was used to implement the electrode.

5.3.2 Permittivity of MED-6350 silicone carbon rubber

For the permittivity, because the permittivity was very small (x 10^{-12}), the impedance analyzer had to be used to provide an approximate value. In the impedance analyzer, the silicone carbon rubber was connected into series, and the impedance formed the following equations:

$$Z = R + \frac{1}{2\pi f c} \quad (5\text{-}2)$$

$$\text{And } C = \varepsilon \frac{A}{d} \quad (5\text{-}3)$$

At low frequency (20 Hz), the impedance from the capacitor dominates the main function, which means R can be ignored. So the impedance Z can be presented as:

$$Z = \frac{1}{2\pi fc} \quad (5\text{-}4)$$

So the permittivity can be represented as:

$$\varepsilon = \frac{d}{2\pi fZA} \quad (5\text{-}5)$$

Where, ε= permittivity, d = height of the silicone-carbon cube, f=frequency, Z= measured impedance and A= area of the silicone-carbon cube.

Because there was no equipment at the University of Southampton that could measure the material's permittivity, a fitting tube for a capacitor from Sheng's design (Yong *et al.*, 2015) as shown in Figure 5-6 and Figure 5-7, was used to measure the permittivity. The fitting tube diameter was half an inch (1.27 cm) and the distance between the two copper electrodes could be adjusted. Each end was connected to the impedance analyzer. From the impedance analyzer, both the capacitance and impedance are able to be measured. When the impedance was measured, each silicone-carbon cube was measured 5 times and the average value calculated.

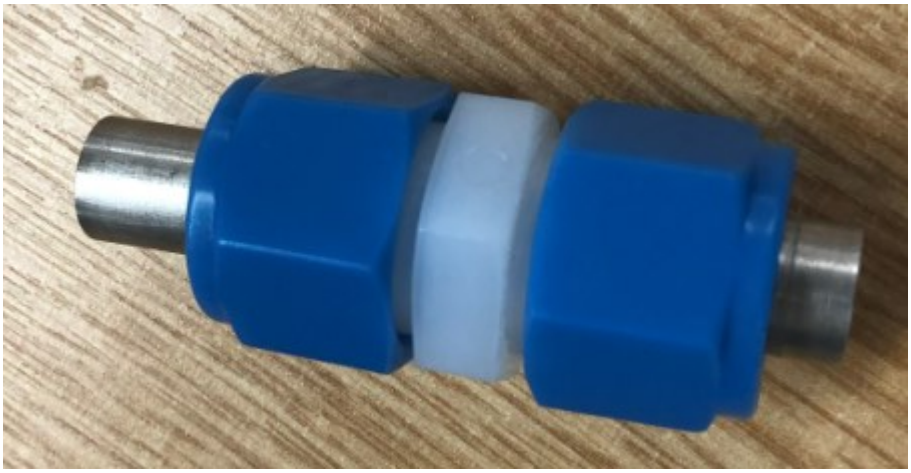

Figure 5-6: Fitting tube for measuring the permittivity of MED-6350.

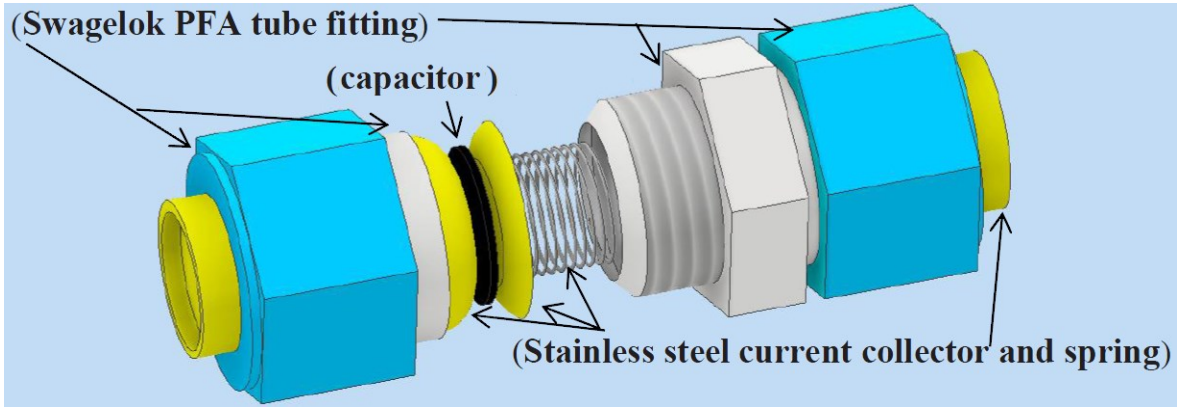

Figure 5-7: Tube fitting used to test the capacitor before closing the two fitting caps (Yong *et al.*, 2015).

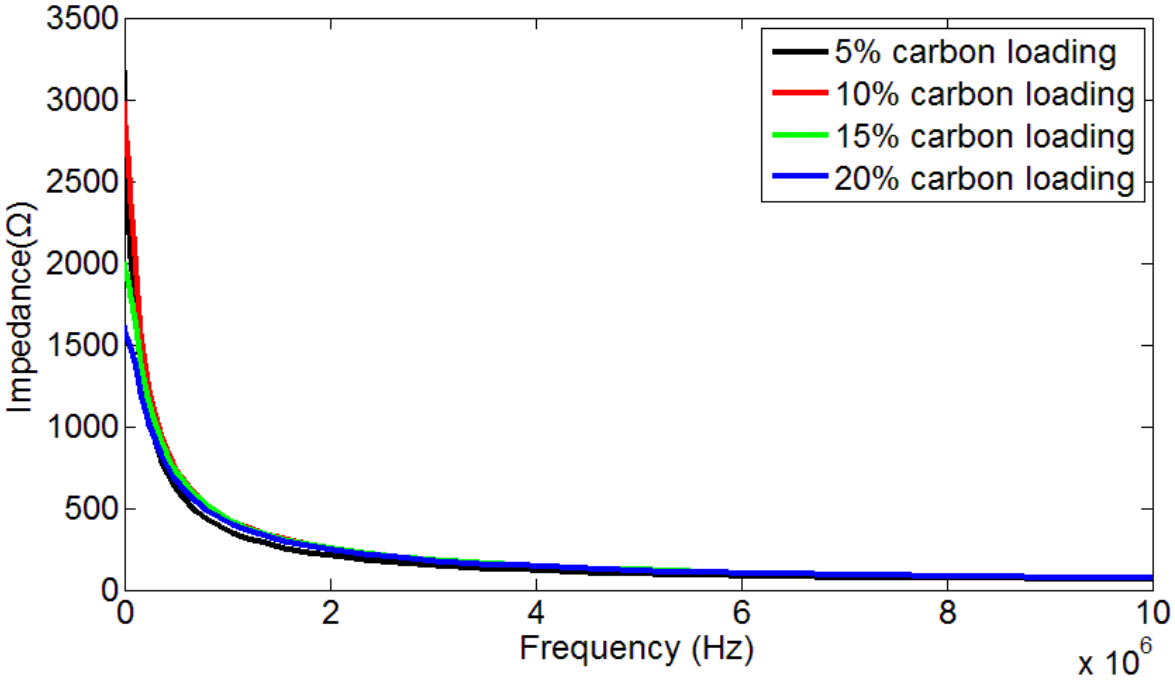

Figure 5-8: Impedance measurement for calculating permittivity of MED-6350.

From Figure 5-8, the impedance could be calculated using the equation 5-2 to 5-5. Although the silicone with different carbon ratios have different impedance values, however, all the permitivities for different carbon ratios are about 1×10^{-14} F/m. This is because the permittivity is a very small value, so the resultant impedance change is small. If this the permitivity is translated into dielectric constant:

$$\varepsilon_r = \frac{\varepsilon}{\varepsilon_0}$$

Where ε_r is the dielectric constant, ε is the abosolute permitivity and ε_0 is the vacumm permittivity (8.85×10^{-12} F/m).

However, the dielectric constant of MED-6350 is about 10^{-3}. However, from the online database of silicone rubber (AzoMaterials, 2018), the relative permitivities should be between 2 to 4.

This difference may be due to the following reasons: this measurement equipment was not a perfect capacitor structure. In a capacitor, the structure should be packaged and under a vacuum, but this fitting tube could not achieve this.

However, from the equations, the resistivity and permittivity are independent. For the resistivity, its equation is (5-1) and the permittivity has equation (5-2 and 5-3). Theoretically, the resistivity dominates the results in the real part of the impedance, at the same time, the permittivity dominates the results in the imaginary part of the impedance and is affected by the frequency. Although they will have some interaction due to the polarization in the electrical field, these relationships are different for different formulation and materials. Furthermore, from the literature (Barzegar *et al.*, 2015), the addition of carbon black to an electrolyte demonstrated the capacitance remained stable, which means the permittivity is stable.

Furthermore, because of the limitations of the measuring equipment for the dielectric constant, there is a dramatic difference between the measuring results (10^{-3}) and the results from the literature database (3.5). So the dielectric constant of silicone rubber of 3.5 from the database (AzoMaterials, 2018) is used in the simulation.

5.3.3 Young's modulus of MED-6350 silicone carbon rubber

The Young's modulus of the MED-6350 sample was measured using an Instron Electropuls E1000 as shown in Figure 5-9. The size of the MED-6350 sample was measured using a ruler before testing (size of MED-6350: 3 cm × 3 cm × 1 cm, the same as section 5.3.1), after measuring the size of MED-6350, the E1000 was used to record the tensile stress and tensile strain. Figure 5-10 was used to calculate Young's modulus. To avoid over stretching, the cross sectional area of the MED- 6350 sample was measured under the first 40 mm extension.

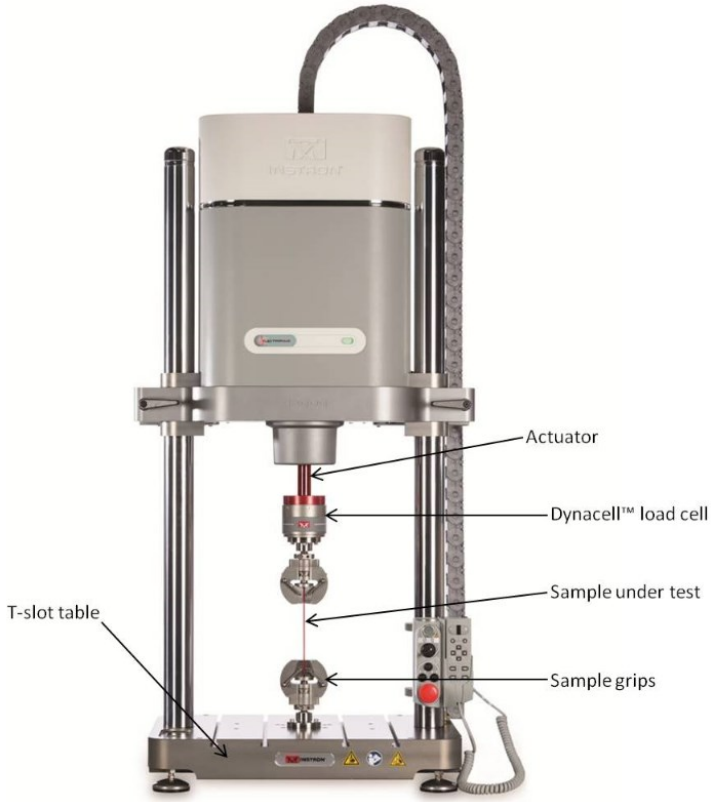

Figure 5-9: The Young's Modulus is measured using Instron Electropuls E1000.

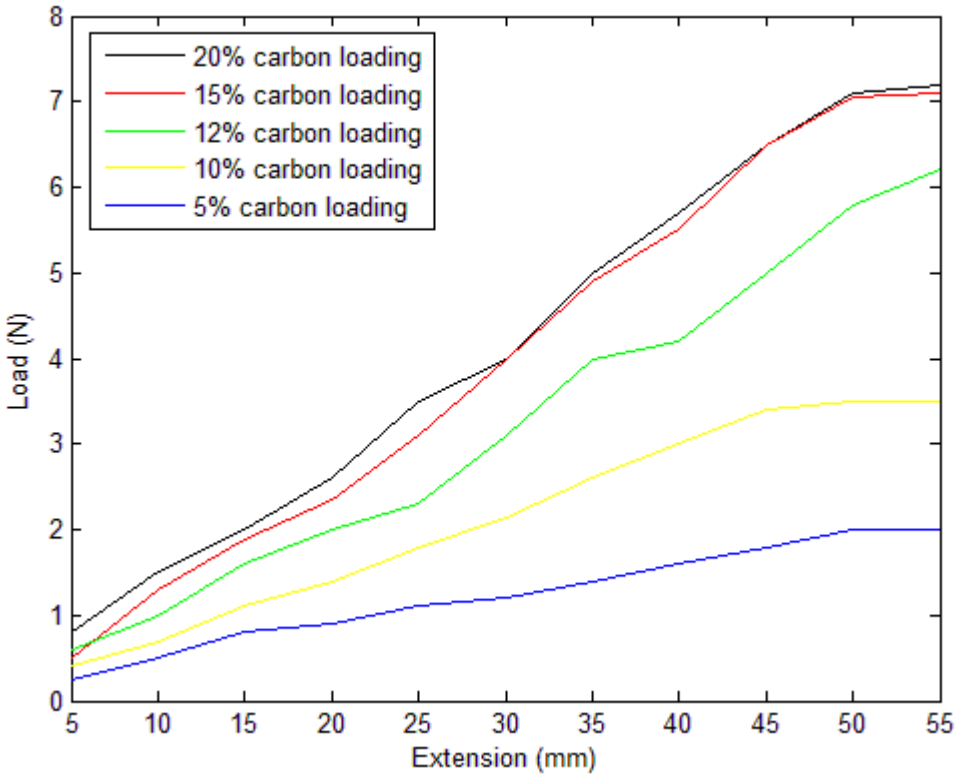

Figure 5-10: Extension of the MED-6350 with different carbon loading ratios under different loads and measured by Instron Electropuls E1000.

According to the equation for calculating Young's Modulus:

$$F = \frac{EA\Delta L}{L_0} \quad (5\text{-}6)$$

Where F= load applied to the material, A = the cross section area, ΔL=extension and L_0=origin length, and E= Young's Modulus.

In Figure 5-10, the gradient is$\frac{F}{\Delta L}$, is used to obtain Young's Modulus. The gradients of different carbon loading ratios were calculated from the average value of the extension (before 50 mm extension which is the breaking points in Figure 5-10). The average value of the extension was calculated from each 5 mm extension. Young's Modulus was calculated for different carbon loading ratios with the results shown in Figure 5-11.

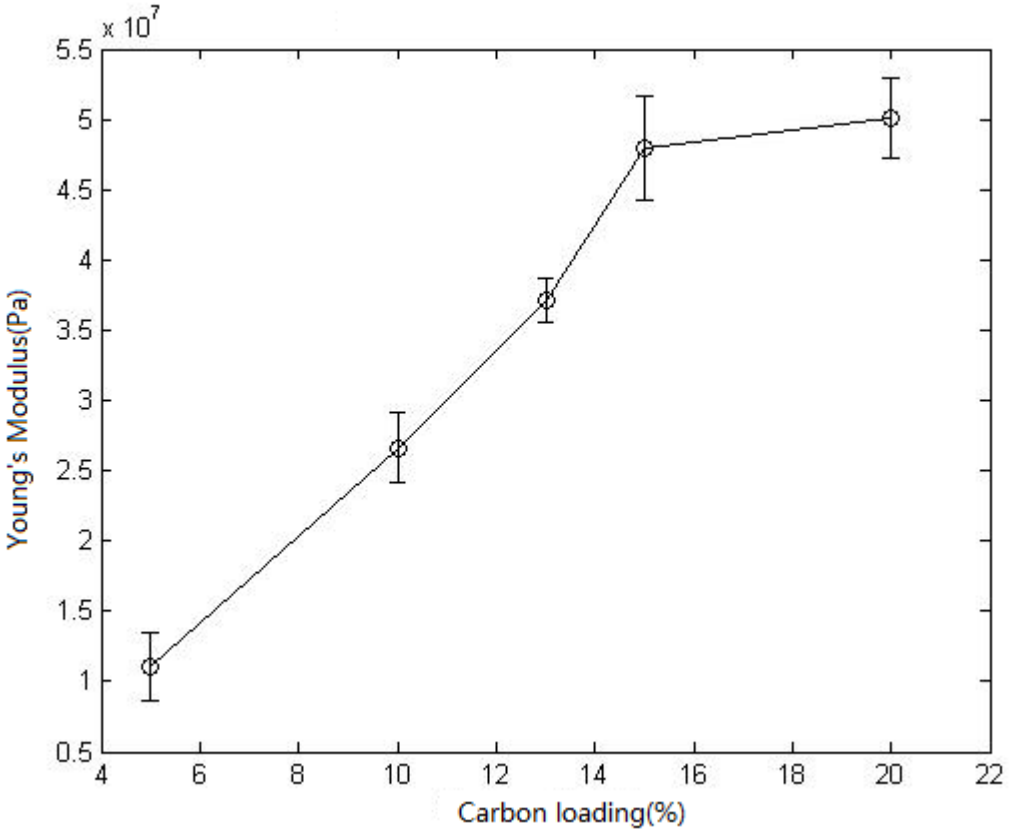

Figure 5-11: Young's modulus of MED-6350 silicone rubber with variation in carbon loading, the error bar is for standard deviation.

As the carbon loading increases, Young's modulus increases. When the carbon loading is 5 %, the silicone rubber has the lowest Young's modulus, which is 1.11×10^7 Pa. As the carbon loading increases, Young's modulus increases to 4.9×10^7 Pa. The Young's modulus of silicone rubber increases by around 350 % between 5 and 15 % carbon loading. Furthermore, when the carbon loading is increased from 15 to 20 %, Young's modulus increases to its highest value and remains around 5.1×10^7 Pa, an increase of around 4 %. From Figure 5-5 and Figure 5-11, it can be concluded that the carbon particles became saturated in the silicone, the saturation means there are only minor changes and differences in the impedance and Young's modulus after this point. Therefore, in the further implementation, the mixed proportion of carbon and silicone is approximately 15 %.

From all the above testing results, the carbon loading at 15 % will give the most efficient results for printing the electrode. When the carbon loading is 15 %, the resistivity of silicone carbon rubber is around 0.142 Ω.cm with a 50 MPa Young's Modulus and an adhesive surface. All of these properties mean the electrode will stay on the skin with a comfortable contact surface.

5.3.4 Density of MED-6350 silicone carbon rubber

When the silicone with 15 % carbon loading is selected, the density could be measured and calculated. Because the silicone carbon rubber has been cut to a 3 cm × 3 cm square of 1 cm thickness from the start of section 5.3, the volume is approximately 9 cm^3. In addition, the

mass is weighted by electrical weighing scale (Voyagel Pro,OHAUS, minimum scale: 1mg). For an individual sample, it has the weight of 6.24 g.

There are 3 samples to be measured and the averaged value is calculated from these 3 samples. Therefore, the averaged density of MED-6350 silicone carbon rubber is 6.9×10^3 kg/m^3.

5.4 Method of printing MED-6350 silicone carbon electrode

The MED-6350 silicone electrode was printed using two separate methods: one was screen printing and the other stencil printing. The schematic diagram in Figure 5-12 shows the printing structure with different materials. Screen printing was used to print the first and second layers and stencil print was used to print the last electrode layer on the top. The first three steps are the same as those described in Chapter 4, but there was one more step which was to stencil print to print silicone carbon rubber. Stencil printing as shown in Figure 5-13 is a method to print the electrode in a fixed mould. The stencil is fixed by the clamp, and a squeegee is used to print the material where needed. This method was applied for some materials which could not be printed by the screen printer. The viscosity of paste for screen print should be in the range of 9000 - 15000 cP (Cao *et al.*, 2016), When the viscosity is over 15000 cP, the printer meshes do not allow the material to pass through it, so it cannot be screen printed. However, for the MED-6350, the viscosity is 20,750 cP, therefore, the stencil printing was applied to print MED-6350.

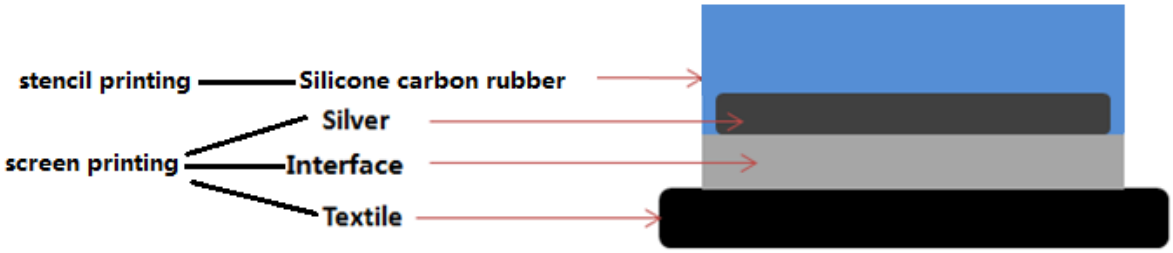

Figure 5-12: Printing electrode structure including each layer.

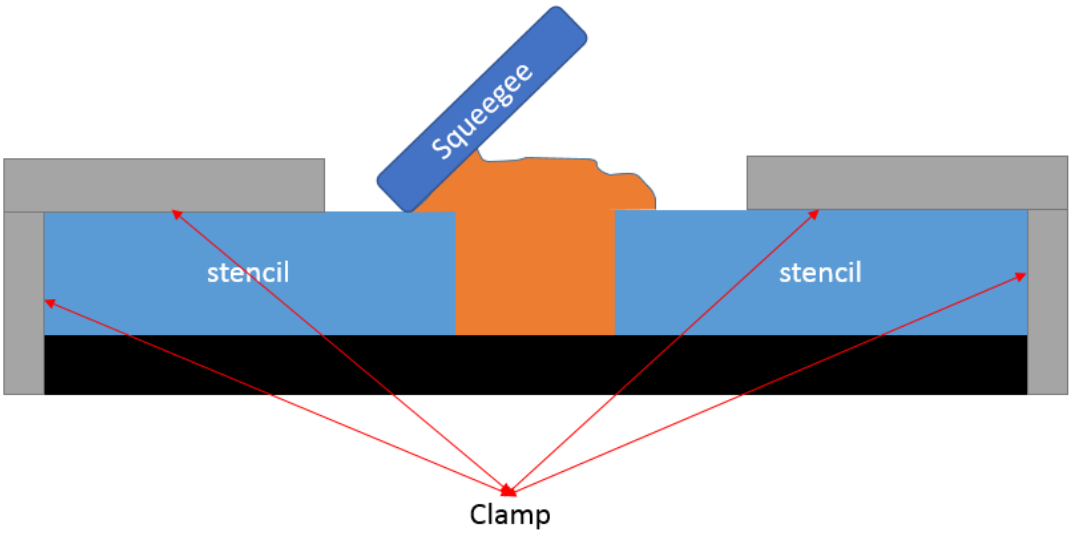

Figure 5-13: Stencil printing schematics diagram for printing silicone carbon rubber on textile.

To summarise, the printing procedure have the following steps, the first three steps were same as for ELX-30 silver electrode and shown in section 4.5, the last step is applied the stencil printing for silicone carbon layer, which is different to ELX-30 silver electrode.

- Before printing, the textile needs to be shaved to provide a relatively smooth surface. Then, the textile is cut into the same size as the textile holder, which is a ceramic plate and glued by 3M spray mount adhesive.
- Printing the first layer: interface layer. The material was still Fabinks-IF-1004, which is made by University of Southampton and provided a smooth surface for conductive patterns.
- Printing the second layer: conductive layer. This is the main part of the conductive patterns and made by silver (ELX-30).
- Printing the third layer: encapsulation layer (Fabinks-IF-1004). This layer is used to protect the conductive patterns from contact or physical damage. The material and screen were the same as the interface layer.
- Printing the fourth layer: silicone carbon rubber (printed by stencil printing in Figure 5-13). The moulds of the electrode are shown in Figure 5-14. The aluminium mould was obtained from a previous project in University of Southampton (G.M.Paul, 2014) and the polytetrafluoroethylene (PTFE) mould was designed at a University of Southampton workshop for this thesis. Compared with these two moulds, the PTFE can provide an easier to remove mould than aluminium. If the silicone carbon mixture was printed on the silver layer (as described in Figure 5-13), the silicone carbon mixture would stick to the aluminium mould, and the mixture could not printed on the silver pad, and the material would stay on the mould. After curing, the aluminium mould would destroy the electrode surface, as in Figure 5-15 (A). However, if the PTFE mould was designed to the stencil print, the result is shown in Figure 5-15 (B). Comparing these two printed results in Figure 5-15, the PTFE mould provides a smoother electrode surface, and the electrode will stay on the silver pattern.

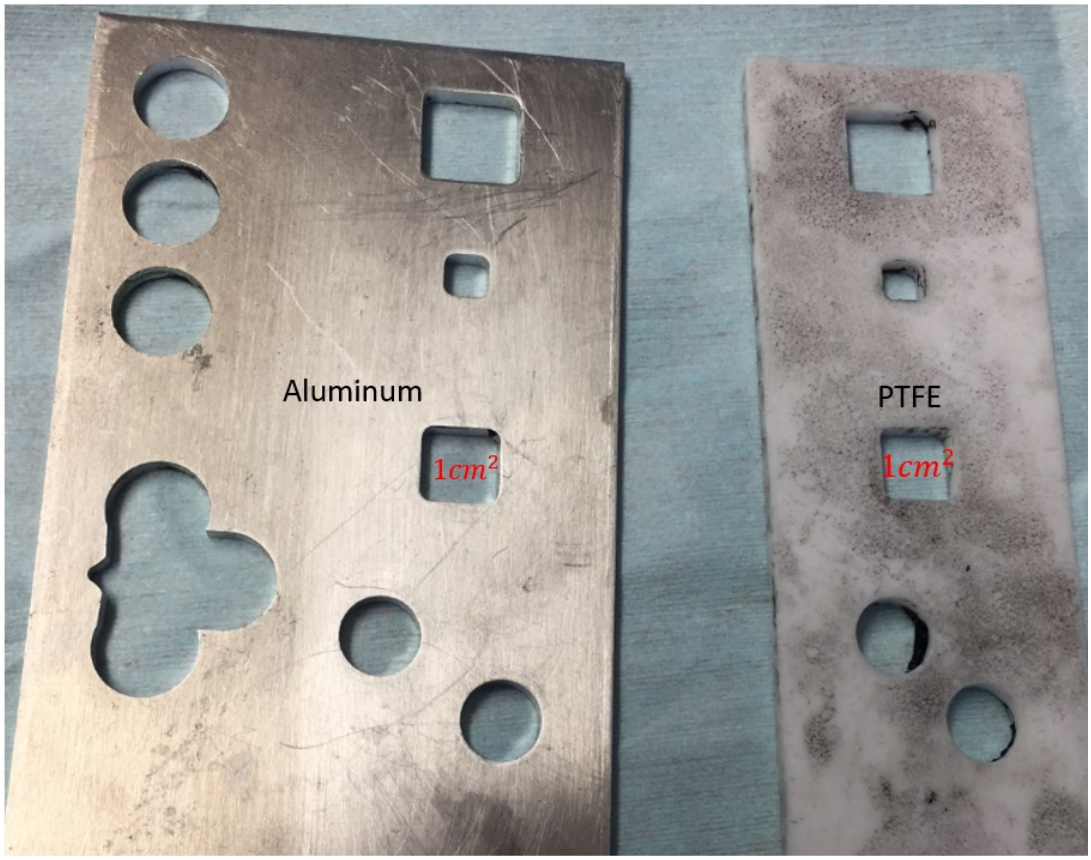

Figure 5-14: Aluminium and PTFE mould.

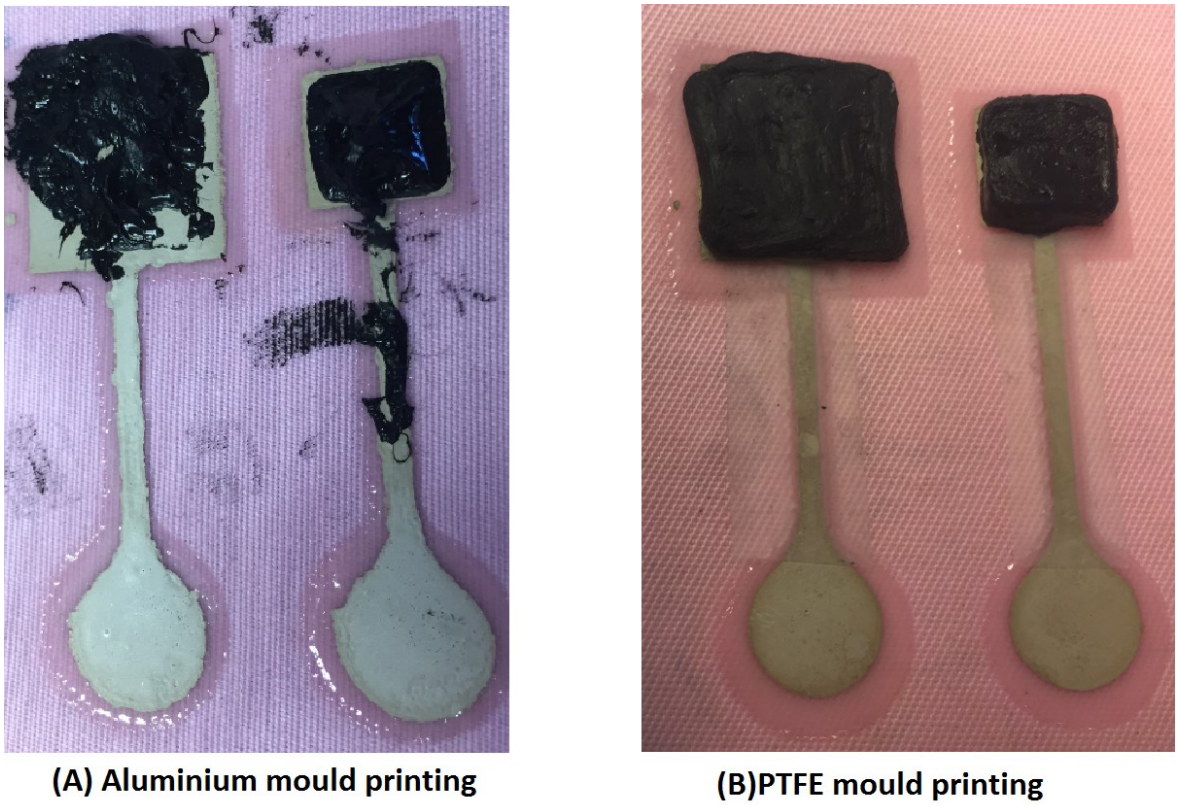

Figure 5-15: Silicone-carbon electrode – where the silicone carbon rubber covers the electrode areas in Figure 5-5.

Table 5-2 and Table 5-3 show the printing and curing conditions for each layer. The 1st and 2nd layer had the same conditions as described in Chapter 4, the only difference being the 3rd layer. When the MED-6350 silicone rubber was printed by stencil print, the mould remained in place during curing for the initial 25 minutes, after 25 minutes, the mould was removed for the remaining 5 minutes of curing. The initial 25 minutes were used to dry the material in the mould and make it easier to remove the material from the mould. The remaining 5 minutes were used to cure the material on the silver.

The thickness of each layer was measured same as chapter 4, each sample was measured 5 times and take the average value. However, because the silicone-carbon layer is flexible, the thickness of this layer is varied.

Layer	**Material**	**Curing time**	**Curing method**	**Curing temperature(℃)**	**Average Thickness (mm)**
1	Interface (Fabinks-IF-1004)	30 s	UV curing	X	0.24
2	Silver (ELX-30)	10 min	Box oven	120	0.02
3	Encapsulation (Fabinks-IF-1004)	30 s	UV curing	X	0.15
4	Silicone rubber + carbon black (MED-6350 and ENSACO 250G)	25 min + 5 min	Box oven	100	4.3-3.2

Table 5-2: Layer printing detail including curing time, method and temperature.

	Interface	**Silver**
Printing gap	1.0 mm	0.9 mm
pressure	6 kg	5.5 kg
speed	70mm/s	70mm/s

Table 5-3: Print settings for the interface and silver layer.

The printed electrode was shown in Figure 5-16. The electrode size was decreased from 2.5 cm^2 to 1 cm^2, which was used to make the further comparison with simulated electrode. Because the electrode was made by silicone rubber with carbon black and soft, the eletrode gemeotries are not regular squres or rectangles.

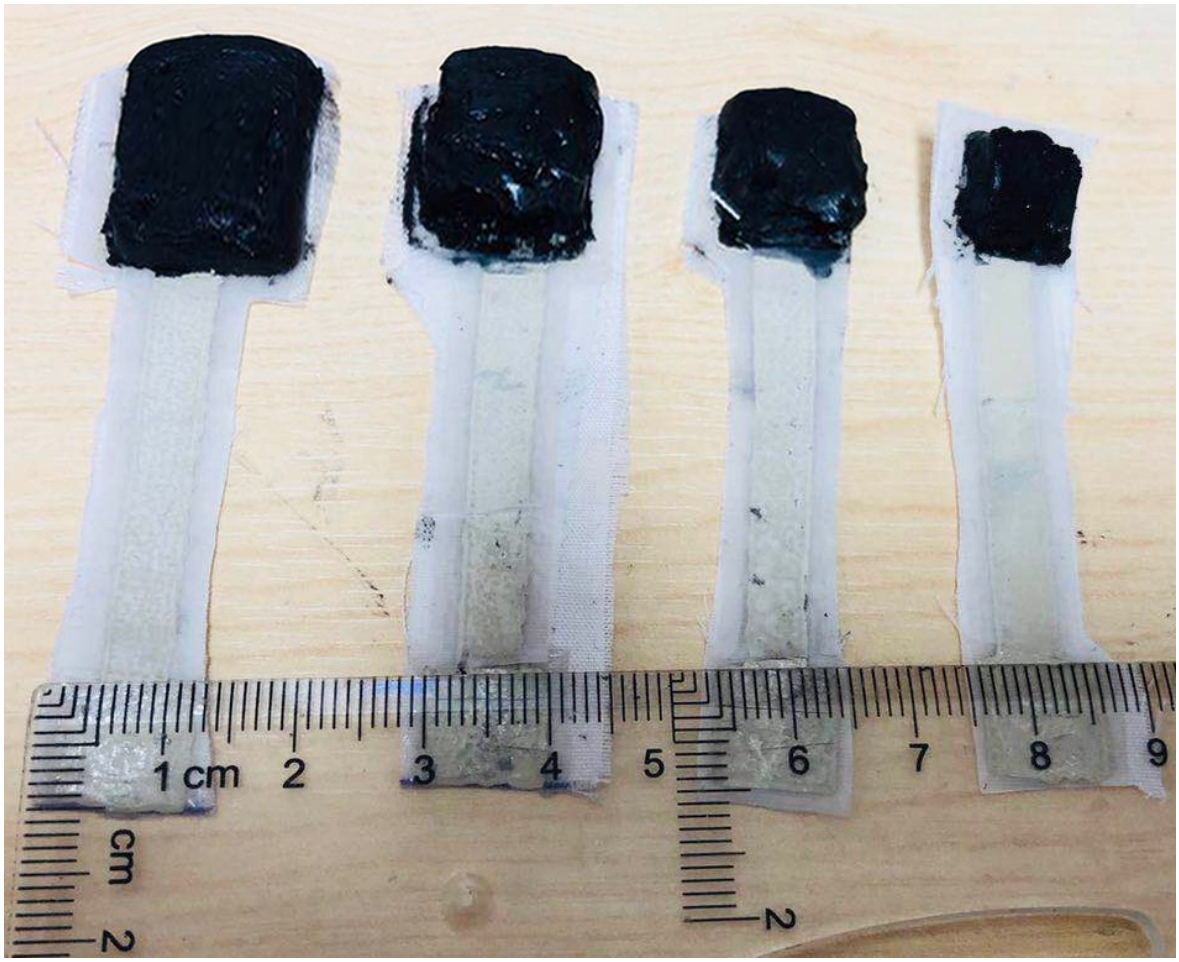

Figure 5-16: MED-6350 silicone-carbon electrode, electrode size was decreased from 2.5 cm^2 to 1 cm^2 (left to the right).

5.5 Adhesive silicone carbon electrode results and analysis

From the findings of the previous material tests, there are some advantages (adhesion and flexible) from this material. In this section, the adhesion, and the skin-electrode impedance of silicone carbon electrode are measured. The impedance is used to identify the difference between the measurements and COMSOL simulations. The difference between measurement and simulation is used to evaluate the performance of the simulation model.

5.5.1 Adhesion test for the silicone carbon electrode

Because MED-6350 the silicone carbon electrode has adhesive property, the electrode does not need gel and stays on the skin naturally. Thus the adhesive stress was tested to find the limit of this electrode. Because these kinds of electrodes are for an ECG or EMG, the measuring conditions may be on the chest, or there will be an angle between the electrode and the horizontal ground. To test this force, a simple measurement was designed to test the adhesion of the silicone carbon electrode. In the test, the situation is the electrode is on the chest and the patient stands, which means the angle between the electrode and the ground is 90°. The force to remove the electrode was from weights which hung on the electrode as in

Figure 5-17. The electrode was banded with tape to provide a uniform vertical force. The weights were used to adjust the applied forces.

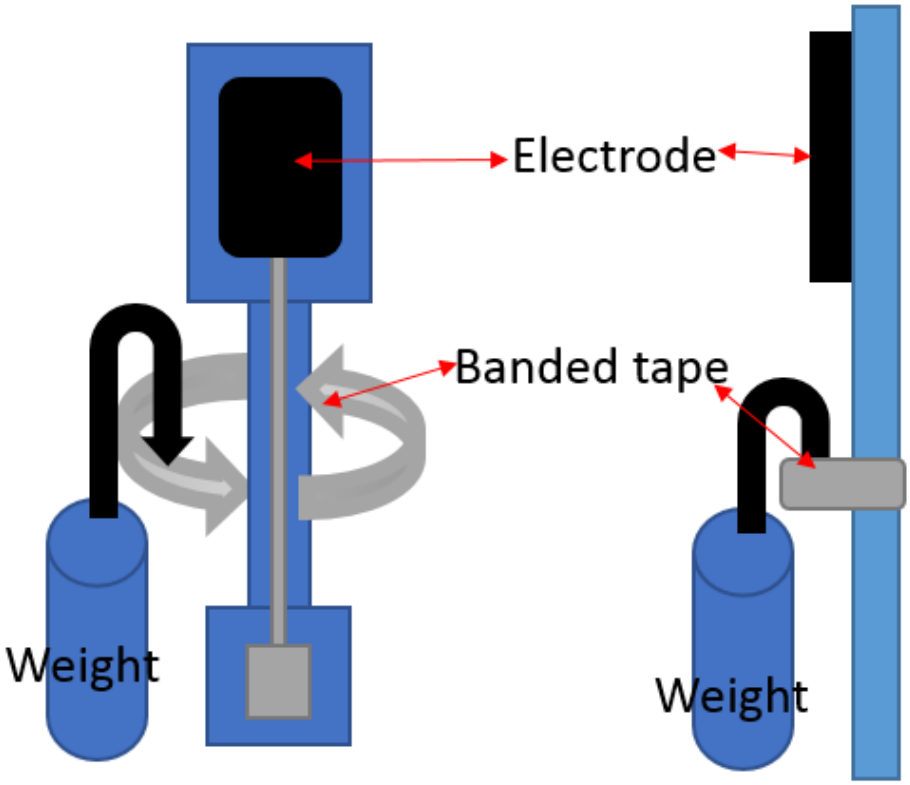

Figure 5-17: Adhesive testing for MED-6350, the tape is banded around the electrode pattern.

When the electrode was set up, the following steps were applied to estimate the adhesive force:

1. Before each single test, the electrodes were placed on the inner forearm horizontally and pressed by a 1 KG weight for 1 minute as shown in
2. Figure 5-18 (A). This step allows the electrode to completely contact the surface.
3. The inner forearm was placed vertically shown as
4. Figure 5-18 (B) (90° to the horizontal direction). This step simulated the ECG electrode measurement on the chest (90° to ground horizontal line).
5. Each applied force remained for 1 minute. If the electrode was still on the forearm, this meant the applied force had passed the test. Each applied force needed to be tested for 3 times to ensure stability.
6. The applied force was increased until the electrode pulled off.
7. Between each applied force test, the electrode surface was cleaned to reduce the effect from sweat or oil.
8. The results in Figure 5-19 showed the limitation of the adhesive force on the electrode.

However, some limitations limited the accuracy of the measurement, which were:

- This method can only measure the adhesion force in the vertical direction, if the force was over 90°, the result would be different.
- The weight was controlled and managed manually, the results were not accurate like the equipment used to test young's modulus.
- Although the skin surface was cleaned up before each single test, the results may be effected by the different skin conditions (unexpected oil, etc.).

Figure 5-19 shows the results of the electrode adhesion, where each sample test was repeated 5 times and the standard deviation calculated to estimate the error. The electrode size was increased from 1 cm^2 to 2.5 cm^2 and the adhesion force increased by 183 % (from 0.6 N to 1.5 N). It can be seen that the electrode adhesion increased as the electrode size increases. Improved adhesion means the electrode remains more stable under movement. However, after several uses, the electrode adhesion reduced. This may have resulted from the sweat and oil on the skin. When the electrode was cleaned using IPA (Isopropyl alcohol, a cleaning fluid in laboratory, especially for dissolving oils), the results are shown in Figure 5-20. The threshold size of 2 cm^2 printed electrode was selected as an example.

Figure 5-18: Adhesion test for MED-6350 electrode. (A) Before testing, applying force to provide a full contact. and (B) Testing the adhesive force in the vertical direction.

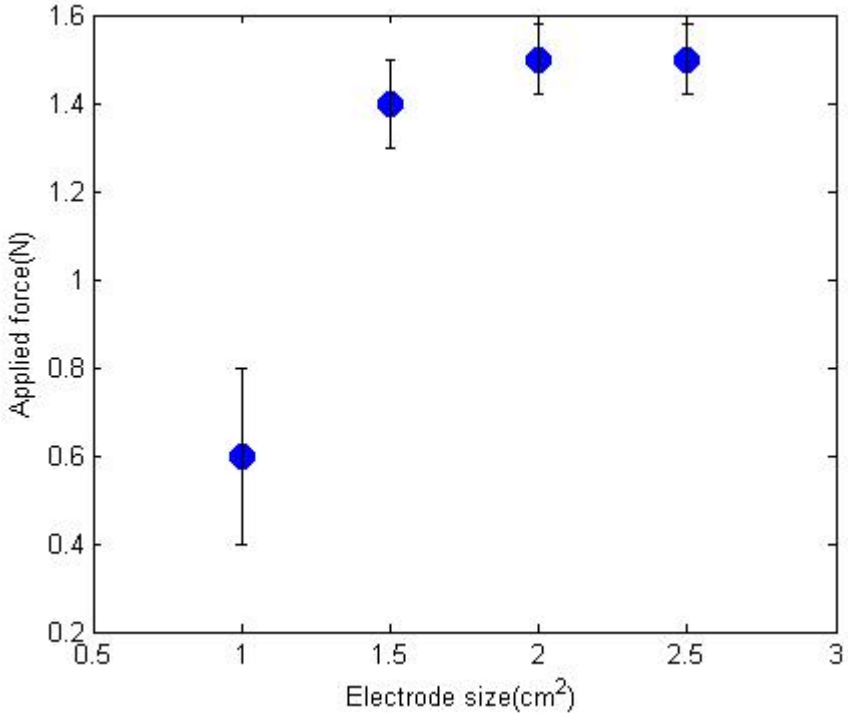

Figure 5-19: Electrode adhesive surface testing for varying electrode sizes from 1 cm^2 to 2.5 cm^2, there are 3 samples are measured in the test, the error bar described the standard derivation.

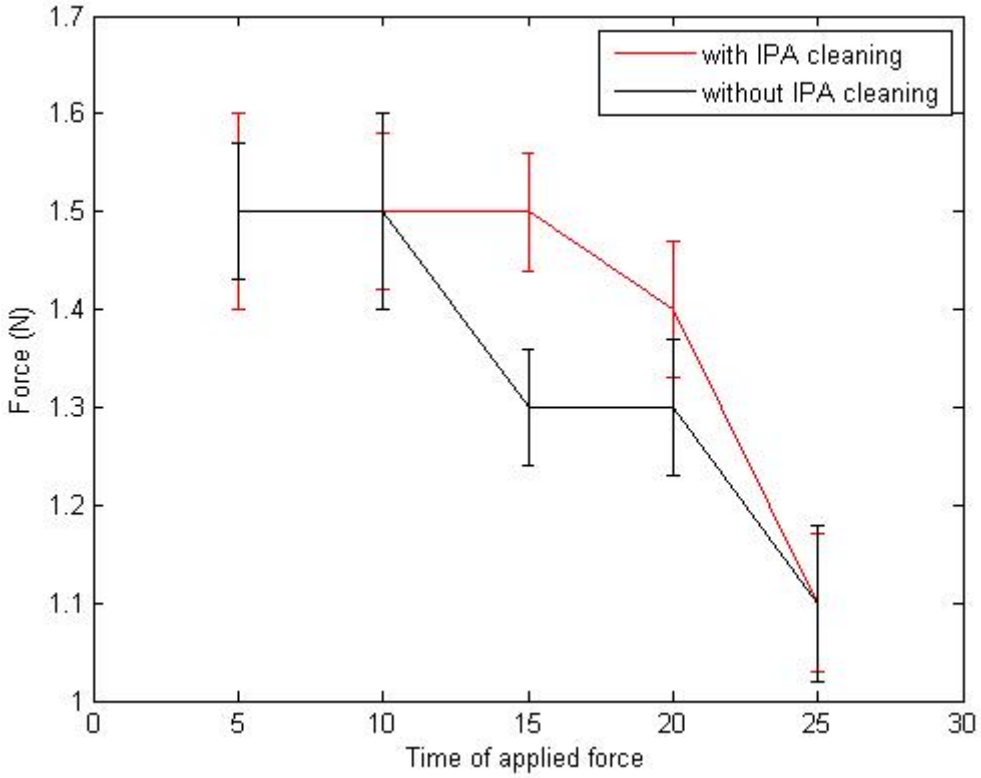

Figure 5-20: Adhesion testing for 1 cm^2 MED-6350 electrode, pulling force changes varied with different use times (from 0 to 25 times), the error bar described the standard derivation.

In Figure 5-20, the adhesion of a 1 cm^2 electrode was shown for different use times from 5 to 20 times. If the electrode had never been used before, the electrode had a higher adhesion/stickiness. When the electrode was used 5 times, the adhesion started to decrease. When the electrode had been used 25 times, the adhesion was around 90% less than a new electrode. Moreover, if the electrode was cleaned after each use, and the adhesion surface remained adhesive for longer.

5.5.2 Skin-electrode impedance measurement for MED-6350 silicone electrode

In section 4.6, the measurement for skin-electrode impedance was discussed and the same method was applied to measure the skin-electrode impedance for the silicone carbon electrode as shown in Figure 4-12. From the analysis of the electrode size in Chapter 4, electrodes of four sizes were selected, which were 1 cm^2, 1.5 cm^2, 2 cm^2 and 2.5 cm^2. Figure 5-21 demonstrates the setting of measurement, where the impedance analyser is connected to the electrodes.

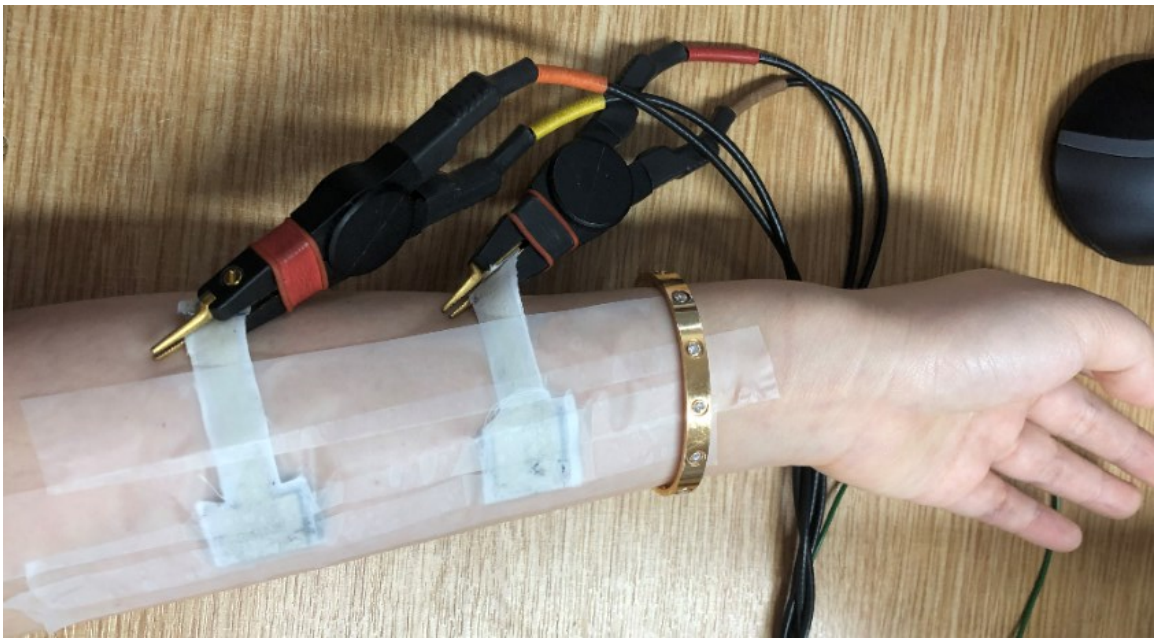

Figure 5-21: Skin-electrode impedance measurement setting for silicone carbon electrode pair (two electrodes are connected to the impedance analyser).

In the following figures (Figure 5-21 to Figure 5-22), all the electrode pairs with different electrode sizes were measured 5 times. All the data were obtained using the same method described in section 4.8, Chapter 4.

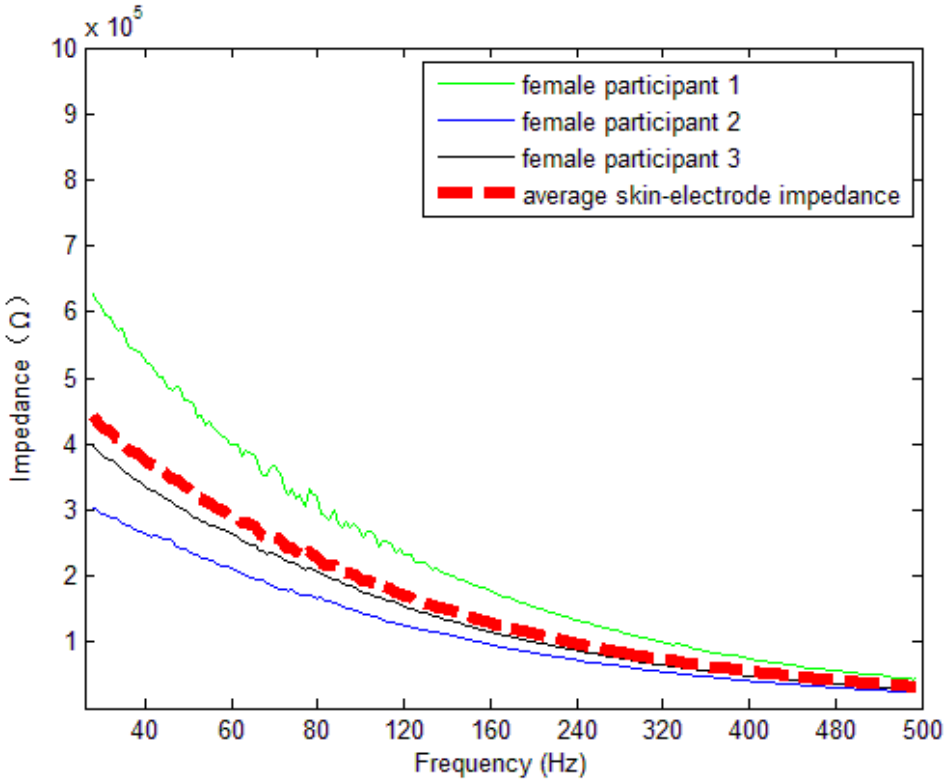

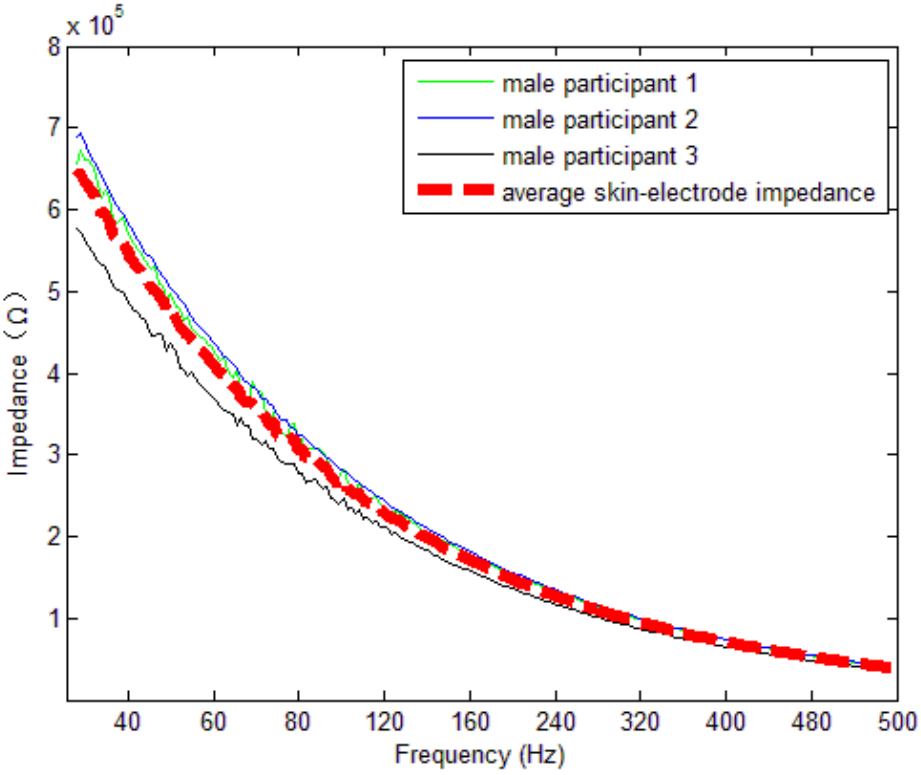

Figure 5-22: Skin-electrode impedance of a 2.5 cm^2 silicone carbon electrode pair for: (Top): three female participants; and (Bottom): three male participants.

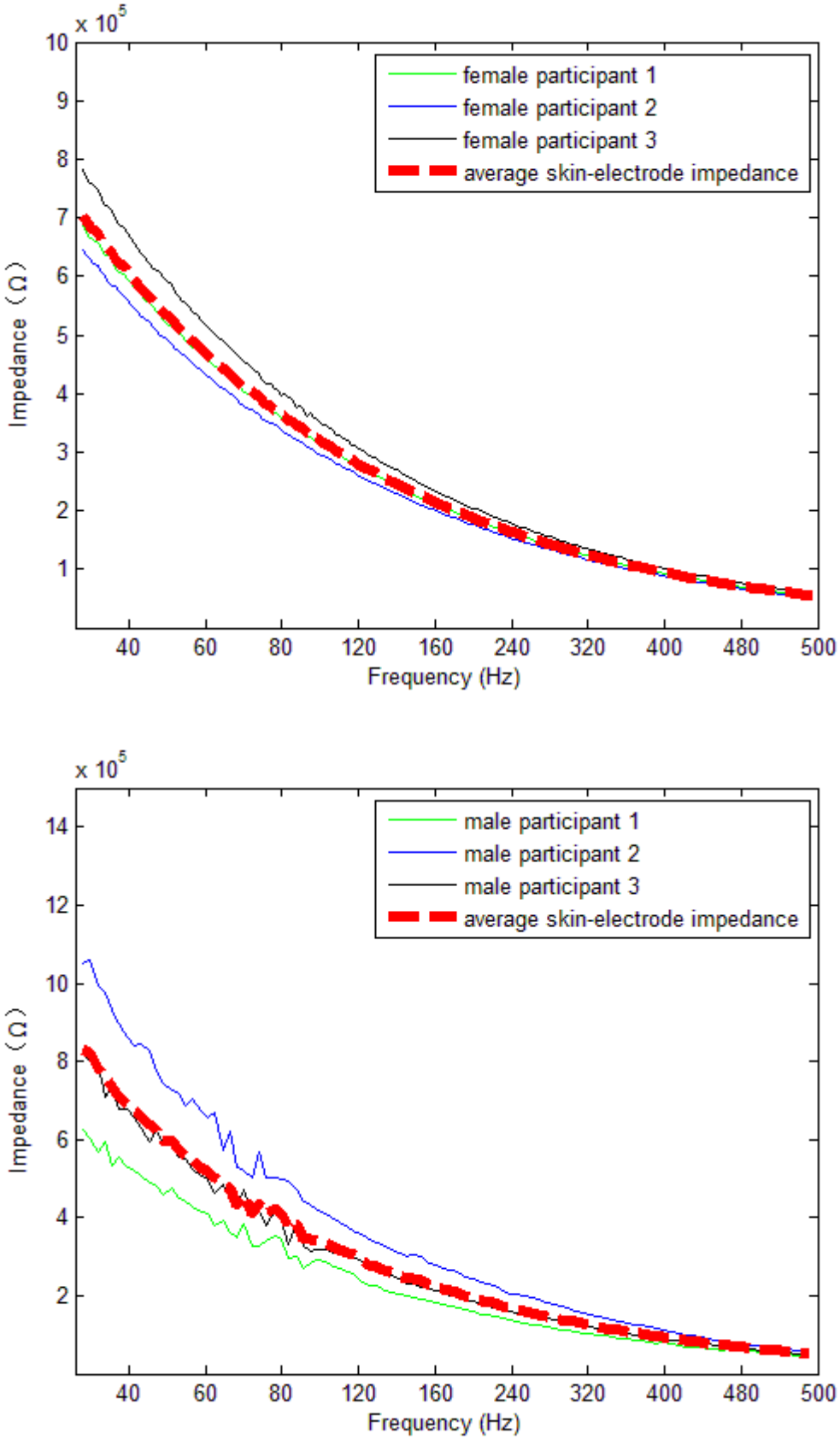

Figure 5-23: Skin-electrode impedance of a 2 cm^2 silicone carbon electrode pair for: (Top): three female participants; and (Bottom): three male participants.

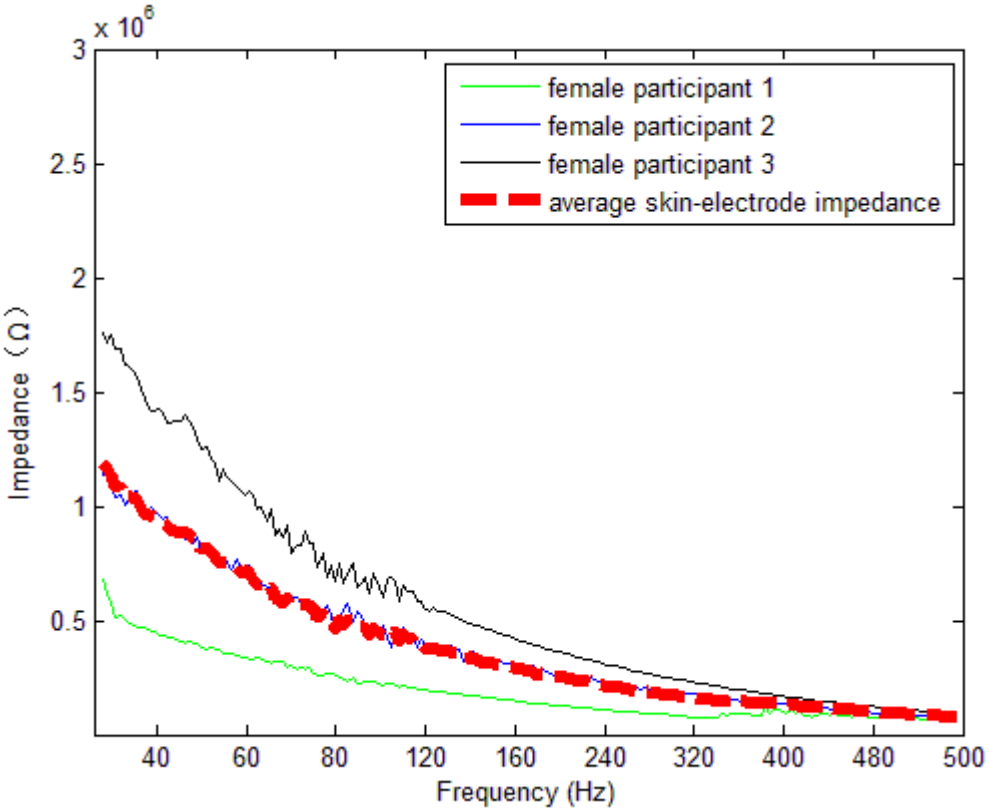

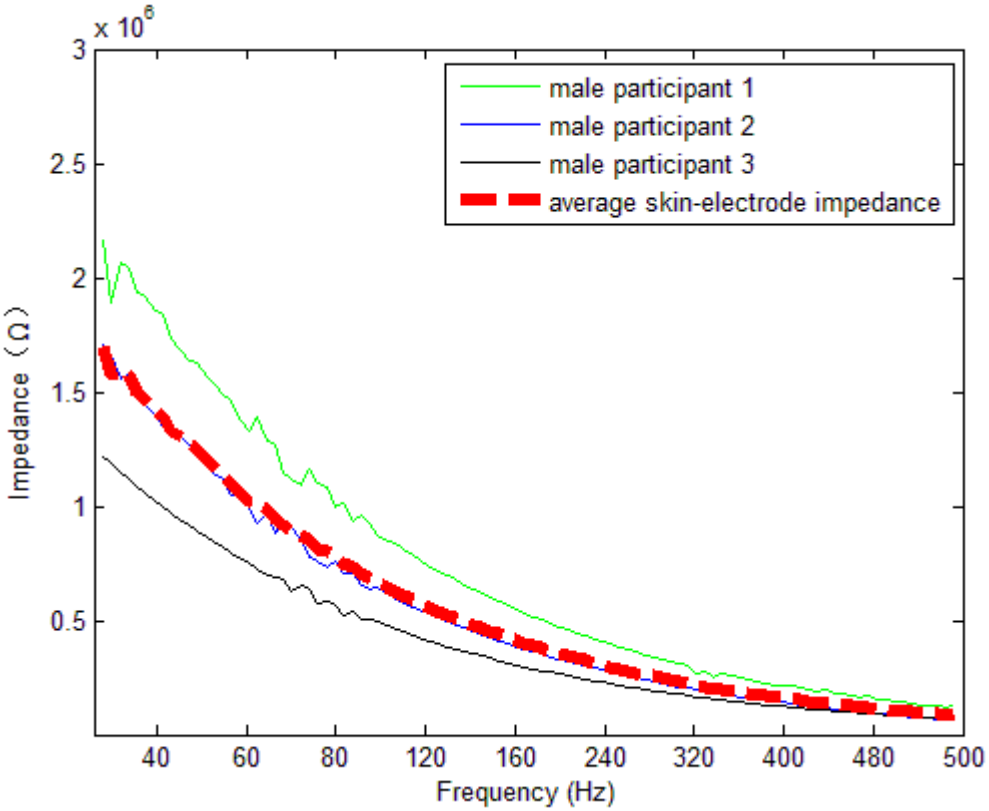

(B)

Figure 5-24: Skin-electrode impedance of a 1.5 cm^2 silicone carbon electrode pair for: (Top): three female participants; and (Bottom): three male participants.

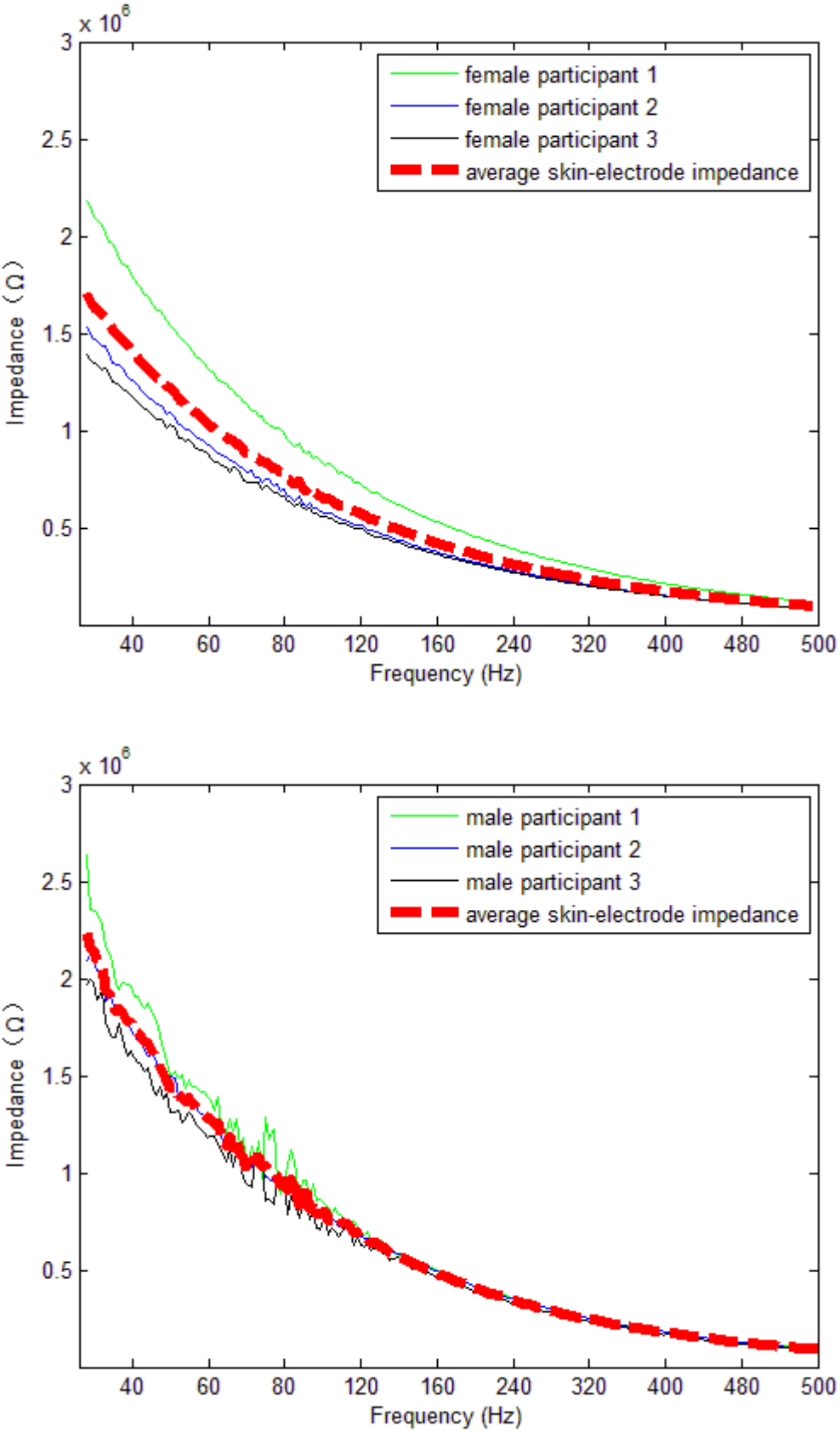

Figure 5-25: Skin-electrode impedance of a 1 cm^2 silicone carbon electrode pair for: (Top): three female participants; and (Bottom): three male participants.

All of the above figures show the skin-electrode impedances for different silicone-carbon electrode pairs with different sizes. Three male and three female participants' skin-electrode impedances were measured. For the measurements, the same results appeared: the males' skin-electrode impedance was higher than for the females. Moreover, compared with the silver skin-electrode impedance at lower frequency (less than 50 Hz), the impedance noise of the silicone-carbon electrode at lower frequency (less than 50 Hz) was reduced and the silicone-carbon electrode impedance curves became smoother than the skin-electrode impedance curves for the silver electrodes. Comparing all the MED-6350 silicone carbon electrode impedances with the ELX-30 silver electrode impedance (Figure 4-13 to Figure 4-17 and Figure 5-25 to Figure 5-22), there are two significant differences with the MED-6350:

1. The impedance noise at lower frequency (less than 50 Hz) was cancelled by the electrode itself because the skin-electrode impedance of the silicone-carbon electrode was higher than the silver electrode. For example, when the electrode size was 2 cm^2 and frequency was 50 Hz, the impedance of silicone-carbon electrode was 5.6×10^5 Ω and the impedance of silver electrode was 5.4×10^4 Ω, thus, the impedance of the silicone-carbon electrode was 10 times higher than the silver electrode. Hence, the same level of impedance noise will be dominated by this larger impedance range.
2. The silicone-carbon electrode provided a better contact than the silver electrode. Based on the research about skin noise (Huigen, Peper and Grimbergen, 2001), the main reason for the low impedance noise level at low frequency in the MED-6350 electrode may be better contact than the silver electrode. In Huigen's research (Huigen, Peper and Grimbergen, 2001), the wet-gel electrodes had a lower impedance noise level compared to the Hydrogel electrodes, because the saturation of the skin from the gel (electrolyte) effectively increased the contact area. Similarly, although both silicone-carbon and silver electrodes were attached using tape, the silicone-carbon electrode had a more adhesive surface, which provided an improved surface contact with the skin. However, the silver electrode had a smooth surface and may have less skin contact than the MED-6350 electrode.

Furthermore, if the averaged female and male skin-electrode impedance of silicone-carbon electrode was made at 50 Hz and a comparison made with the silver electrode, both silver and silicone carbon electrodes showed similar conclusion. In Figure 5-26, when the silicone-carbon electrode size was reduced from 2.5 cm^2 to 2 cm^2, the average skin-electrode impedance increased from 5.2×10^5 Ω to 4.2×10^5 Ω, which is approximately 24 %. If the silicone-carbon electrode size was further reduced to 1.5 cm^2, comparing the impedance with 2 cm^2 silicone-carbon electrode, the average skin-electrode impedance increased by about 80 % (increase to 9.3×10^5 Ω). Furthermore, if the highest impedance of a further smaller sized (1 cm^2) electrode was calculated, the impedance of this smaller electrodes increased by 50 % (13.5×10^5 Ω).

Comparing the skin electrode impedance of the silver and MED-6350 electrode at 50 Hz in Figure 5-26, both of these two results provided the same conclusion as the measurement results in Chapter 4, section 4.8. When the electrode size was increased from 1 cm^2 to 2 cm^2, the skin-electrode impedance rapidly decreases (from 13.5×10^5 Ω to 5.2×10^5 Ω, about 62 %). Meanwhile, when the electrode size was increased from 2 cm^2 to 2.5 cm^2, the skin-

electrode impedance was only reduced by about a further 17 % (from 5.2 × 10^5 Ω to 4.3 × 10^5 Ω). According to the skin-electrode impedance for a stainless-steel electrode at different electrode sizes (Bosnjak *et a*l., 2017), when the electrode size was increased from 1 to 2 cm^2, the skin-electrode impedance at 10 Hz had the highest impedance reduction (from 9 × 10^5 Ω to 1.5 × 10^5 Ω, about 80 %). If the electrode size is further increased to 3.2 cm^2, the skin-electrode impedance only reduces by about 30 % (from 1.5 × 10^5 Ω to 1 × 10^5 Ω). Furthermore, when the electrode area was increased from 3.2 to 6.72 cm^2 (electrode size had been doubled), the skin-electrode impedance at 10 Hz reduced only by about 40 %. From Bosnjak's results, the total skin-electrode impedance of 6.72 cm^2 and 9.6 cm^2 were almost the same. Therefore, it can be concluded that the 2 cm^2 area had the maximum ratio of impedance reduction to electrode area increase. Furthermore, changing the electrode material cannot affect this electrode size of 2 cm^2 as the ideal dimensions.

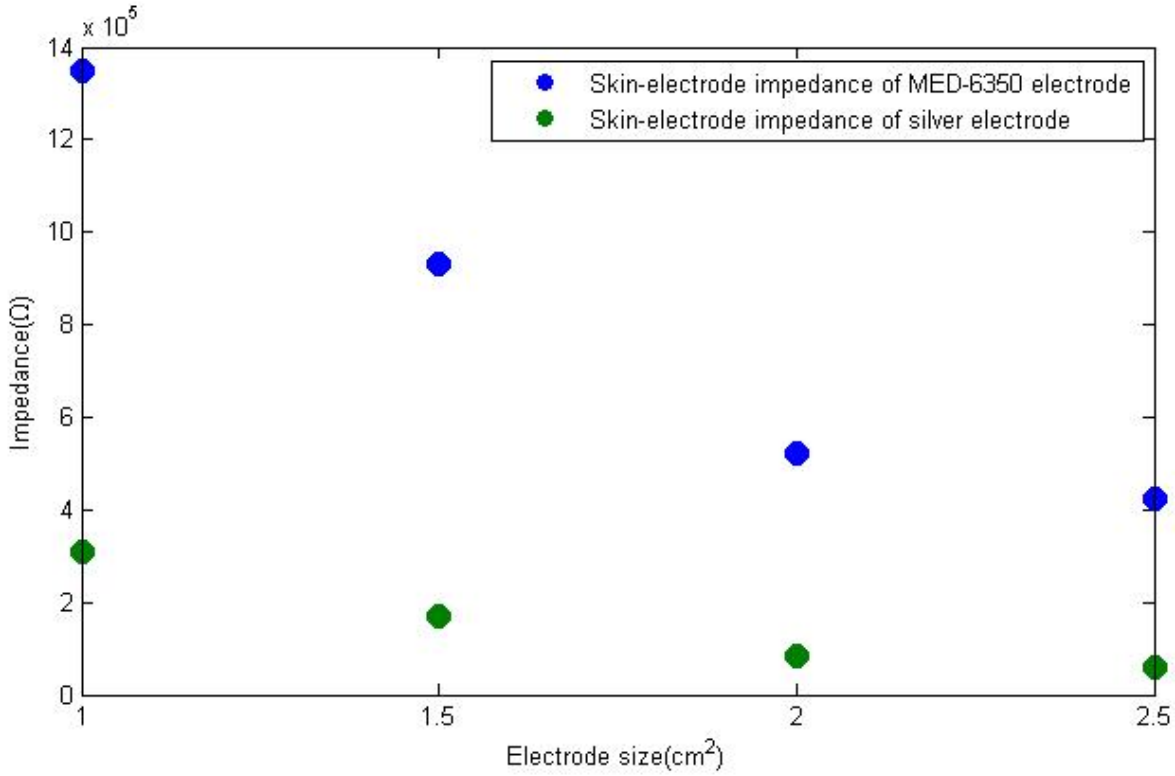

Figure 5-26: The experimental silver and MED-6350 skin-electrode impedance of averaged male and female at 50 Hz for different electrode sizes.

To make a better comparison with the existing polymer or rubber electrodes from the literature, Table 5-4 shows several relevant reviews. In all of these 4 literature results, although the electrodes made by carbon nanotube (CNT) and polydimethylsiloxane (PDMS) had the smallest electrode size (Peng *et al.,* 2012), it had almost the lowest skin-electrode impedance at 50 Hz. Meanwhile, another printed electrode was fabricated from PDMS and multi-wall carbon nanotube (MWCNT) (Chlaihawi *et al.,* 2018), but the 3 cm^2 electrode at 50 Hz had a similar skin-electrode impedance as Peng's results. The reasons may come from the fabrication, additives and the recipe of the electrode.

In Peng's design, the mixture of PDMS and CNT was fabricated on a silicon wafer, but Chlaihawi's electrode was printed PDMS and MWCNT mixture on the flexible polyethylene terephthalate (PET) substrate. However, both of them had a problem about the dispersion of

MWCNTs in PDMS. Therefore, Chlaihawi used magnetic stirring and sonication to optimize the dispersion of MWCNTs in PDMS, and Peng used the ultrasonic dispersion process to overcome the problem. After mixing the two materials, the weight ratio of PDMS and MWCNT providing the highest conductivity was used as the final formula. The final mixture had 8 % MWCNT in PDMS for Chlaihawi, meanwhile, Peng's final mixture had 10 % CNT in PDMS. Although the increasing weight ratio of MWCNT could increase the conductivity of the PDMS mixture, both of these two papers faced a different problems. In Chlaihawi's research, because the MWCNT/PDMS was printed on the substrate, if the ratio was over 8 %, there would result in peel-off effect. In Peng's research, if the ratio of MWCNT and PDMS was over 10 %, the amount of MWCNTs saturated in the PDMS, the MWCNTs aggregated again and this led to a reduction of the electrical conductivity. Therefore, although both of these two papers used PDMS with carbon nanotubes, the different additive percentages, mixing and fabrication processes cause a difference in the final skin-electrode impedance.

Another research paper used different additives in EPDM (propylene diene monomer) rubber to find the best additives (Chen *et al.,* 2014). Chen added carbon, stainless steel fibres and carbon nanotubes into polymer to achieve low contact impedance and better skin contact. The polymer electrodes containing 45 % of carbon were selected as the optimum electrode. From the comparison between the EPDM electrode with other electrodes in the literature, if the lowest value is selected, although the size of EPDM electrode is not the largest one, the EPDM rubber at 10 Hz has the lowest skin-electrode impedance of the four reviewed electrodes.

In all the literature, the skin-electrode impedance had a wider impedance range than the impedance of a silver electrode, with an impedance range from $2 \times 10^5\ \Omega$ to $5 \times 10^5\ \Omega$ at 50 Hz. Comparing the skin-electrode impedance of MED-6350 with the impedances from the literature, the skin-electrode impedance of MED-6350 was still an acceptable value. Furthermore, in the literature, the electrode sizes were varied from 0.78 to 3.14 cm^2; therefore, the skin-electrode impedances were varied at different electrode sizes, which makes difficult to identify the absolute cause of this impedance change.

Author	Electrode material	Electrode size (cm^2)	Forearm skin impedance (Ω)	Year
Peng *et al*	Carbon nanotube and PDMS	0.78	10×10^5 (at 10 Hz) 2×10^5 (at 50 Hz)	2015
Chen *et al*	EPDM rubber with conductive additives	1.5	5 to 0.5×10^7 (at 10 Hz for different ratio of conductive additives)	2014
Chlaihawi *et al*	Printed electrode PDMS with multi-wall carbon nanotube	3.14	8×10^5 (at 10 Hz) 3×10^5 (at 50 Hz)	2013
Rahal *et al*	Commercial Numetriex Textile electrode	1.6	1.2×10^6 (at 10 Hz) 1.05×10^6 (at 50 Hz)	2009

Table 5-4: Skin-electrode impedance of flexible electrode from the literatures.

5.5.3 COMSOL simulation for skin-electrode impedance

For the simulation, the properties of the adhesive electrode were added to the simulation and a comparison made between the experimental and simulation results. In the simulation, the boundary conditions were the same as in section 4.9. Furthermore, the electrode material

properties (Young's Modulus, conductivity and permittivity) were replaced by the silicone-carbon electrode properties from previous measurements. The Poisson ratio had the similar situation as section 4.9 which was. When the Poisson's ratio of the silicone-carbon electrode was changed from 0.2 to 0.45, the total impedance changed by less than 0.1 %, which mean the change of Poisson's ratio could not change the skin-electrode impedance in the simulation. Therefore, the Poisson's ratio of silicone rubber defined in COMSOL was used in the simulation and is shown in Figure 5-27. Meanwhile, the differences were shown below:

- The electrode part contains two layers: one is silver, another was MED-6350. Silver part was the same as in Chapter 4 (0.02 mm thickness and ELX-30 silver), MED-6350 was the main layer (4 mm).
- The electrode size was varied from 1 cm^2 to 2.5 cm^2 and the thickness is 4 mm to represent the experiment electrode sizes.
- A small amount of pressure, 1 N, is applied to the tops of the two electrodes and the top of SC layer. This applied force is trying to play the role as the visible tape in and simulating in Figure 5-21. Furthermore, because the visible tape did not cover the whole forearm, the 'fixed constraint' is added to the side boundary showed in Figure 3-33 and gives a zero movement to this boundary.
- The applied frequency changed from 20 Hz to 500 Hz, which was same as section 4.9. Although the starting frequency did not like the literatures (starting from 1 Hz or 10 Hz), in the simulation, the results formed a linear relationship and the final results would not be affected by the different starting frequencies. Meanwhile, the 20 Hz frequency was also a small applied frequency and were in ECG, EMG or EEG frequency range, therefore, the starting frequency could start from 20 Hz.
- The properties of ELX-30 silver and MED-6350 are shown in Table 5-5.
- Total element in the simulation was: 43308.

Electrode and skin	**Thickness (mm)**	**Young's Modulus (MPa)**	**Conductivity (S/m)**	**Poisson ratio**	**Density (kg/m^3)**	**Dielectric Constant/ Relative Permittivity**
silver (Ag)	0.02	220	2×10^5	0.43	9100	1
MED-6350 silicone-carbon mixture	4	49	704	0.3	6900	3.5
Stratum Corneum(SC)	0.02	2.9	0.0003	0.48	1050	1140
Epidermis(E)	0.1	0.5	0.5	0.48	1020	1140
Dermis(D)	1.42	0.05	3	0.495	1900	1140
Hypodermis and fat (HYP)	5	0.28	0.4	0.48	1800	1.2×10^7
Muscle(M)	25	1.7	0.42	0.45	1120	2.5×10^7

Table 5-5: Different mechanical and electrical properties of the skin and textile silicone-carbon electrode. The properties of silver was measured in section 4.5 and 4.6 and the properties of silicone-carbon electrode was measured in section 5.3.

The deformation diagram is shown in Figure 5-27.

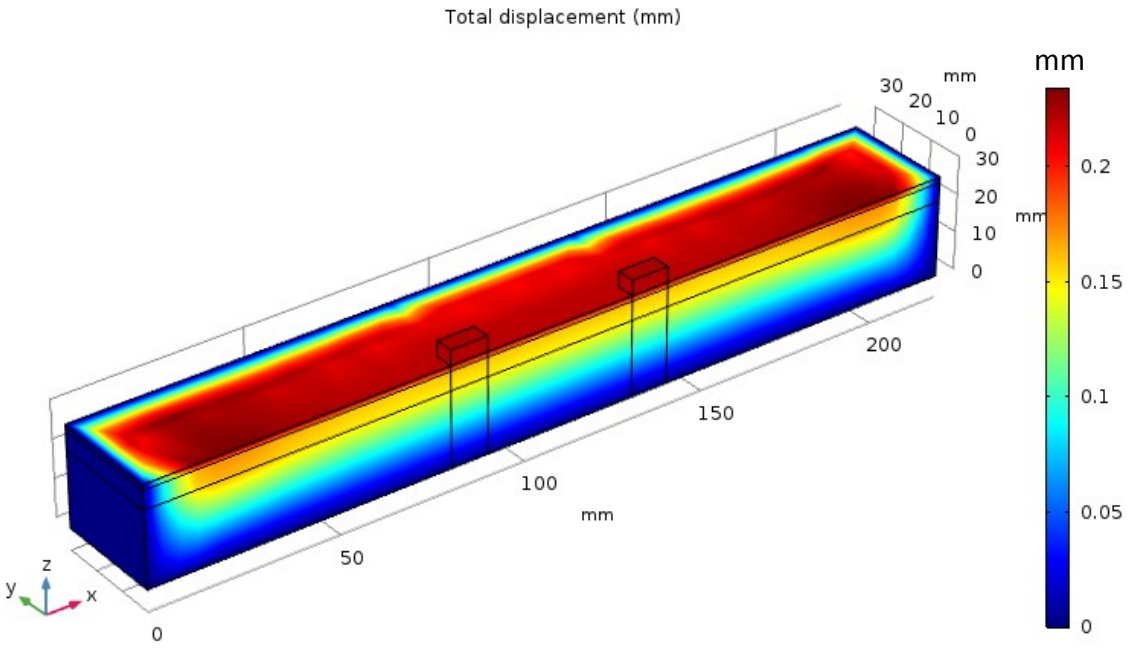

Figure 5-27: COMSOL simulated 1 cm^2 silicone carbon textile electrode on the skin model with a 1 N applied force.

In Figure 5-27, it has the similar deformation as the silver electrode like Figure 4-20. If the average displacement at the electrode bottom is calculated before and after deformation, the average displacement of the silver electrode is 3.07 mm and the average displacement of the silicone electrode is 1.37 mm giving a 1.7 mm difference. If the geometry of electrode is analysed in the software, the silver electrode has almost zero deformation (0.01 mm), but the adhesive silicone electrode has a 1.5 mm deformation. This is because the adhesive silicone electrode is thicker and more flexible than the silver electrode, when the pressure was applied to the electrodes, the electrode would have more movement than the thinner silver electrode.

After analysing the electrode deformation, the skin-electrode impedances of MED-6350 for different electrode sizes are shown in Figure 5-28. In the simulation, the highest skin-electrode impedance was 9×10^5 Ω for a 1 cm^2 electrode at 20 Hz. Comparing the measured average male and female skin-electrode impedance (17×10^5 Ω),the simulated skin-electrode impedance was half that of the measured impedance. When the electrode size is increased to 2.5 cm^2, the simulated skin-electrode impedance becomes 4.5×10^5 Ω, which is similar to the measured skin-electrode impedance (5.5×10^5 Ω). To avoid the noise in the measurement, if the skin-electrode impedance at 50 Hz is selected as an example, Figure 5-28, Figure 5-29 and Table 5-6 showed the differences of electrode sizes between the simulation and measurements.

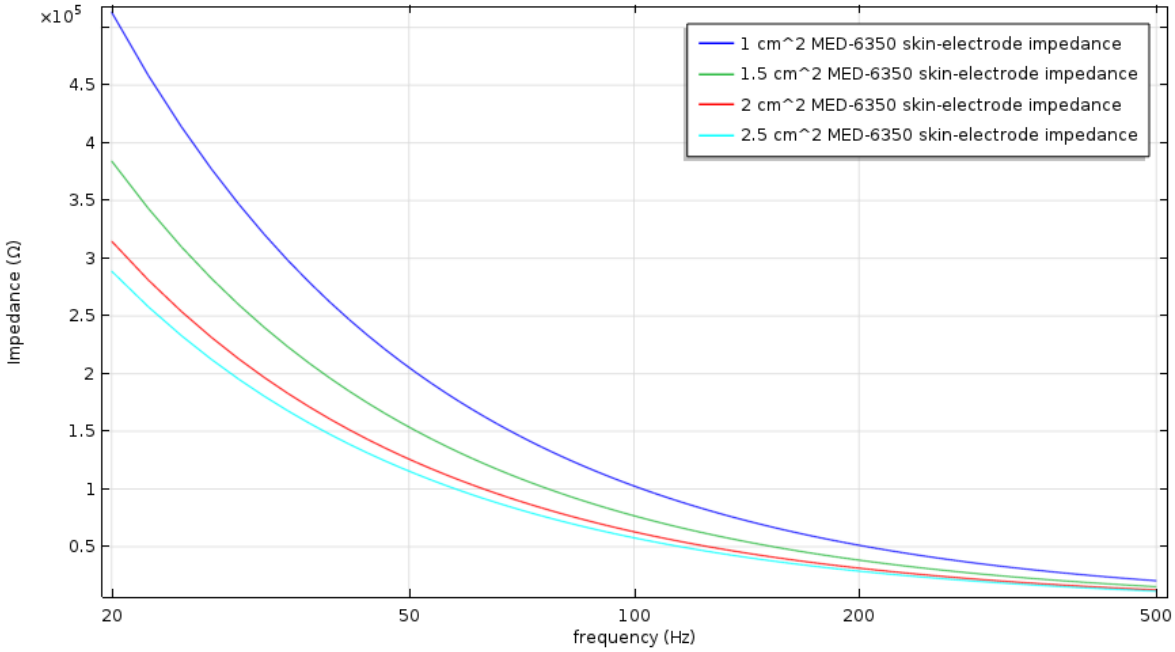

Figure 5-28: COMSOL simulated MED-6350 electrode (electrode sizes have been increased from 1 cm^2 to 2.5 cm^2 and frequency is increased from 20 to 500 Hz).

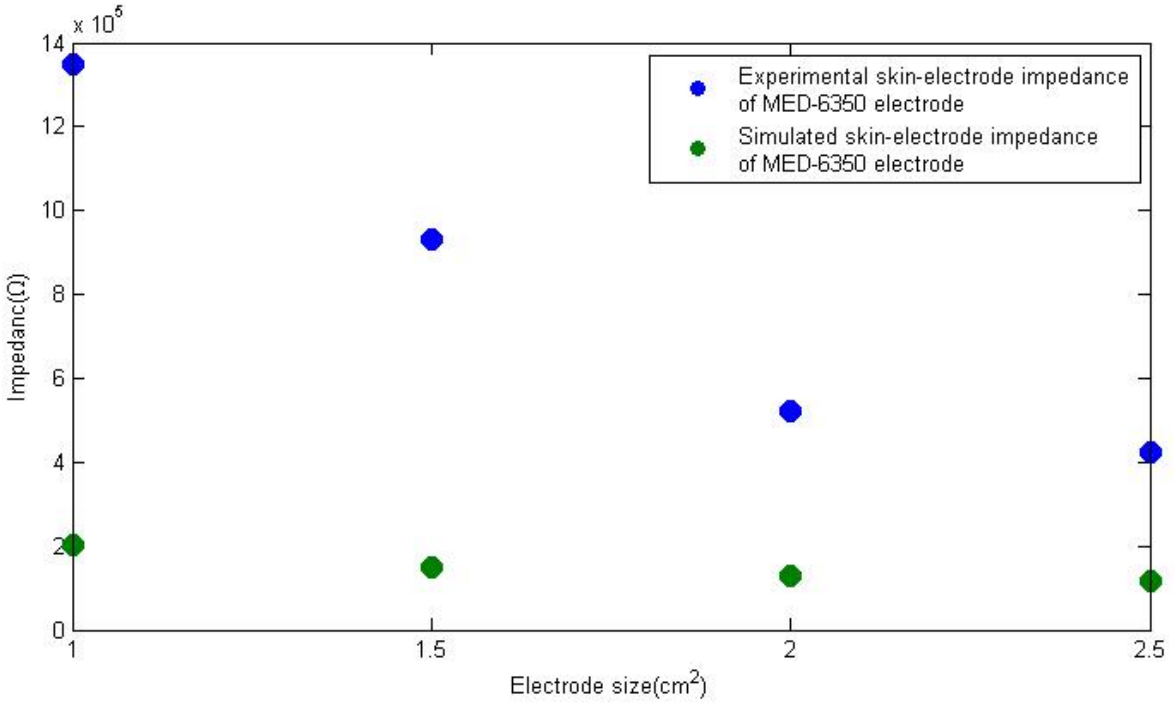

Figure 5-29: Relationship between the experimental and simulated MED-6350 silicone carbon electrode for different sizes and their skin-electrode impedances at 50 Hz.

In Figure 5-29, the experiment and simulated MED-6350 silicone-carbon electrode impedance at 50 Hz were drawn. Because the experiment skin-electrode impedance of MED-6350 was much higher than the simulation, for 2 cm^2 electrode size at 50 Hz, the difference between the experiment result (5.2×10^5 Ω) and simulation result (1.4×10^5 Ω) was about 73 %. Therefore, two certain electrode size and impedance were selected in Table 5-6 and made a comparison between simulation and experiment results.

Electrode size	Silver impedance (Ω)		MED-6350 impedance(Ω)	
	measurement	simulation	measurement	simulation
1 cm^2	7.6×10^5	1.6×10^5	13.5×10^5	2.2×10^5
2 cm^2	0.8×10^5	1.1×10^5	5.2×10^5	1.3×10^5

Table 5-6: 1 cm^2 and 2 cm^2 skin-electrode impedance for simulated and measured silver/MED-6350 electrode at 50 Hz.

Comparing the data in Table 5-6, Figure 5-26 and Figure 5-29, the measured impedances were always smaller than the simulated impedances. Furthermore, when the electrode size was increased, the measured impedance reduced proportionately more than the simulated results. Moreover, for each electrode material, the measured and simulated impedances gave different changes.

- Simulated impedance of the material change from silver to MED-6350 silicone carbon: 1 cm^2: changed 37.5 %; 2 cm^2: 18 %
- Measured impedance of the material change from silver to MED-6350 silicone carbon: 1 cm^2: changed 77 %; 2 cm^2: 550 %.

Although the material change occurs, the simulation effects were not as large as in the measurements (over 50 %). Except for the dielectric constant of skin, the following factors may exist with the simulation.

- In the simulation, the structure was a capacitor structure, the electrodes were two plates of this capacitor and the main medium between the two capacitor plates was the skin layer which was approximately 30 mm thick (including the muscle). The electrode material and electrode thickness could not change the medium too much. From the calculation for the capacitor, this has the equation:

$$C = \varepsilon_r \varepsilon_0 \frac{A}{d} \quad (5\text{-}7)$$

  Where, ε_r is the dielectric constant, ε_0 is the electric constant, A is the area of the $\varepsilon r \varepsilon 0 A d$, it can be seen that the capacitor is defined by the distance between two plates (skin's thickness), the dielectric constant and plate area (electrode size). In these two simulations, the plate area (electrode size) is the same and changed from 1 cm to 2.5 cm^2, so the distance between two plates (thickness of skin and electrode) and dielectric constant are key factors.
  - For the thickness, in the silver electrode model, the thickness of the electrode is 0.05 mm and the ratio between the electrode and skin layer was 5:3000. For the MED-6350 silicone carbon electrode, the thickness was about 4 mm and the ratio between the electrode and skin layer was 1:75. Furthermore, the distance between two plates was defined by the thickness of skin, both of the electrodes had no or very little effect on the distance between two plates (less than 1.3 %). Therefore, the distance between two plates is defined by the skin.
  - For the dielectric constant in these two simulations, the silver electrode was -15 and the MED-6350 was 3.5. Comparing with the dielectric constant of the skin (10^3 to 10^5), the effect of the electrode material was much less (less than 0.5 %).

The skin's material plays the most import role in this capacitor simulation, so the dielectric constant of this capacitor structure is also defined by the skin's dielectric constant.

Therefore, it can say the skin's effects are much more significant than the electrode's effects in the simulation.

Moreover, in the simulation, the Young's modulus and dielectric constant of ELX-30 silver electrode were chosen as the close or ideal values, meanwhile, the dielectric constant of MED-6350 silicone-carbon electrode was chosen from the online database (AzoMaterials, 2018). Although these values cannot be measured in University of Southampton, the difference between the ideal and measured value will affect the comparison between simulation and measurement. Therefore, the impedance of ELX-30 and MED-6350 electrodes are measured to see the effects from materials.

Nevertheless, from Table 5-6, because the skin-electrode impedance of MED-6350 is as approximately 1.5 times the skin-electrode impedance of silver, the impedance of the electrode itself is measured by the same impedance analyser to see the effects on electrode impedance. In the example, two 1 cm^2 electrodes are selected to measure the impedance, each sample is measured 5 times and an average value taken. The results are shown in Table 5-7.

Electrode type	**Impedance (Ω)**
Silver (ELX-30)	1.2 ± 0.2
MED-6350	545 ± 3

Table 5-7: Impedance measurement for one single electrode from 20 Hz to 500 Hz.

In Table 5-7, the impedance measurements of the electrodes were almost a constant value. For the silver, the impedance was 1.2 ± 0.2 Ω; for the MED-6350, the impedance was 545 ± 3 Ω. The impedance of MED-6350 electrode was about 520 times higher than the impedance of silver electrode. The resistance value did not vary with frequency and therefore the analyser showed that the electrodes were pure resistors. Although the 1cm^2 electrode impedance difference between MED-6350 electrode and silver electrode was over 500 %, the skin-electrode impedance difference between MED-6350 electrode and silver electrode is around 150 % as shown in Table 5-6. The effects from skin or the skin impedance produced this significant reduction. Therefore, the results showed that the skin impedance was more significant than the electrode impedance, this conclusion matched the simulation results.

In addition, the COMSOL simulation is able to generate a data set about skin impedance versus frequency. The data from COMSOL can be exported into the SPICE circuit software and the SPICE software provides the interface to input these data. In Figure 5-30 (A), the COMSOL simulated impedance (2 cm^2 MED-6350 electrode at low frequency (1 to 10 Hz)) has been imported into a SPICE software (Micro-Cap 12.0.1.0, Evaluation Version, Spectrum software). In this SPICE circuit software, because this is a demo version, the impedance data need to be imported by manually typed into the software. Hence, the data is selected with the frequency step of 1 Hz to reduce the input time. Moreover, because less

impedance data is imported into SPICE software, the impedance curve of SPICE simulation does not match exactly the COMSOL simulated impedance curve in Figure 5-30 (B). In COMSOL simulation, the impedance is calculated with the frequency step of 0.1 Hz. However, both simulation showed the highest impedance is about 2.3×10^6 Ω and the lowest impedance is around 0.2×10^6 Ω. Therefore, the COMSOL simulated impedance data can be used in the SPICE circuit simulation, and the COMSOL skin model can be used to replace the skin's equivalent circuit in section 3.2 and Figure 3-2. In addition, if the COMSOL model have more accurate data about the skin details, like the dielectric constants of skin at different frequencies, the data set about skin impedance versus frequency can be used to provide closer skin impedance information than the equivalent circuit.

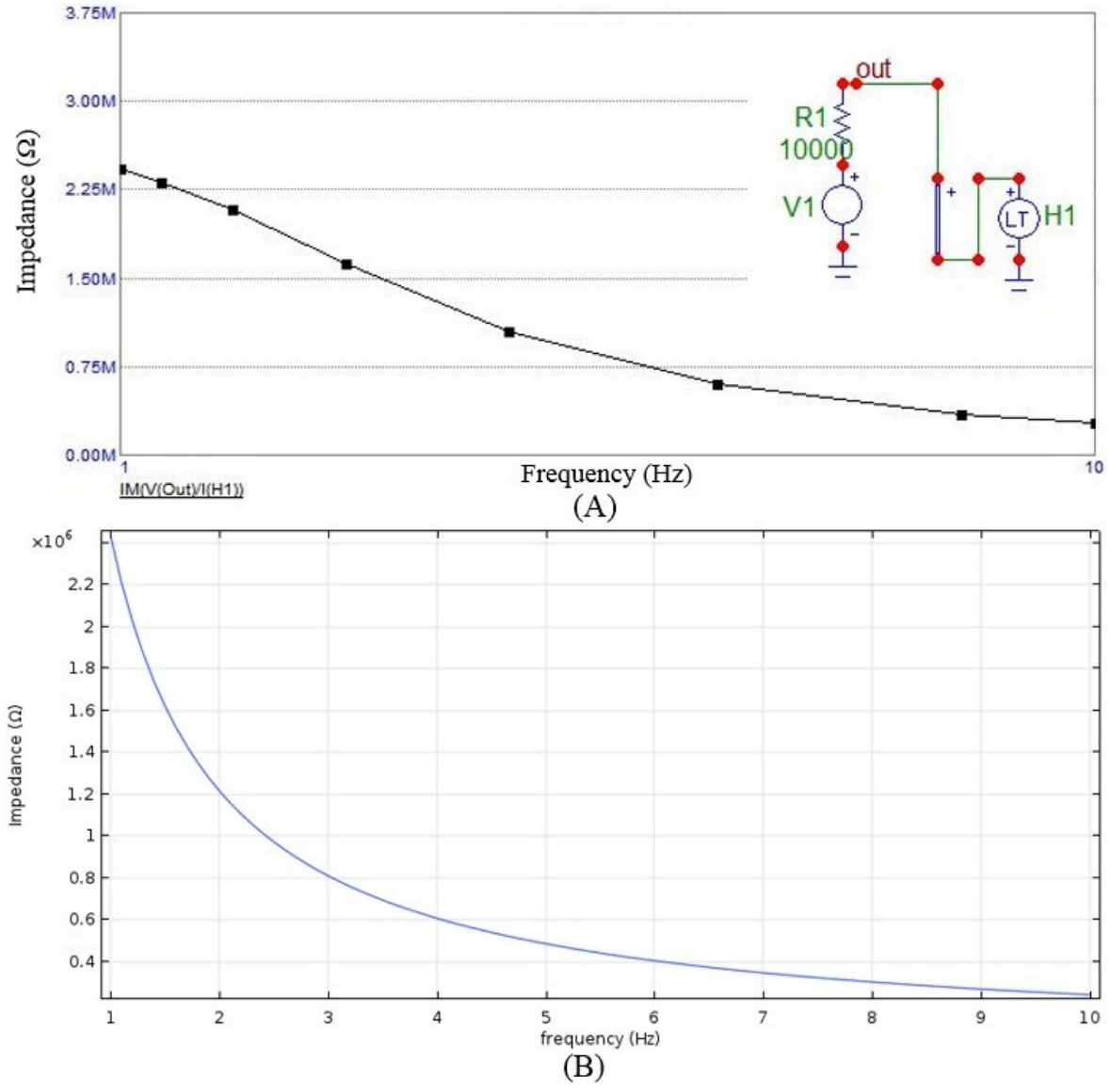

Figure 5-30: Converting the skin-electrode impedance from COMSOL to SPICE circuit software. (A) The component in the top right is the converted components, this component contains the impedance vs frequency data generated by COMSOL. (B) Original COMSOL output for just the skin and electrode.

5.6 Conclusion

An adhesive flexible printed electrode was implemented. The electrode was made by MED-6350 silicone rubber combined with carbon black powder (ENSACO 250G). The best formulation uses 15 % carbon black providing a balance between the cost of materials and resistivity. The resistivity of MED-6350 with 15 % carbon black was able to reach 0.142 Ω.cm. When the percentage of carbon black increased from 5 % to 15 %, the resistivity of the material materials showed an obvious decrease of approximately 98 %. When the carbon percentage was over 15 %, the material resistivity showed similar results to the 15 % carbon black. Moreover, Young's Modulus of MED-6350 with 15 % carbon loading gave the highest value (5.1×10^7 Pa), and a further increase of the percentage of the carbon loading did not increase it. Hence the MED-6350 with 15 % carbon loading was used as the formulation.

Furthermore, when the MED-6350 silicone rubber with carbon black was procured to the electrode, the adhesion was tested for different electrode sizes. The 2 cm^2 silicone carbon electrode provided an adhesive force of around 1.5 N when adhering to the skin. This adhesive force provides a more stable measuring condition than the textile silver electrode without gel. Although the resistivity of textile silicone carbon electrode was approximately 30 % higher than the textile silver electrode, the MED-6350 electrode is softer and more flexible than the silver electrode and adhesive.

Comparing the COMSOL simulated results with the measured results for MED-6350 silicone carbon electrodes gives a similar conclusion as for the silver electrodes. When the electrode size is increased from 1 cm^2 to 2.5 cm^2, the simulated impedance results have been reduced by around 70 % and the measured results have been reduced by 90 %. These two results show the significant impact on impedance arising from the electrode size.

Although the model showed the effects of electrode size, the model does not obviously demonstrate the effects from the electrode material. When a 1 cm^2 electrode material is printed with another material (MED-6350) on the top of the silver electrode, the simulated impedance has increased by about 10 %. However, in the measurement, when the MED-6350 with 15 % carbon loading is printed on the silver electrode, the measured results increased by approximately 50 %. The difference between simulation and measurement is significant. Except the effect from the dielectric constant which has been discussed in section 4.9, this is a significant difference. In the simulation, the impedance is calculated from a capacitor structure, which means the main medium material for the capacitor is the skin layer, and the electrode plays a less important role. Meanwhile, in the measurement, the skin is a much more complex than a multi-layer capacitor structure. When the skin-electrode impedance is measured, although the tapes are applied to improve the communication between the skin and electrode, the inner forearm is chosen to avoid the effects from hairs, there are still some air or holes may exist in the skin-electrode interface. These air or holes can generate the capacitive effects and result the final skin-electrode impedance. Furthermore, the body tissues and skin layers are not layered like the simulation, some blood vessels or glands are in multi layers, these unstructured elements may generate the

differences between the simulation and measurement, hence the simulated and measured results differ.

Furthermore, when the impedances are measured for 1 cm^2 silver and MED-6350 electrode, the impedance between silver and MED-6350 is increased by 520 %. The electrode impedance difference between two different electrode materials is much higher than the skin-electrode impedance difference between the two different material electrodes, approximately 10 times. Therefore, in the measurement, the effect from the electrode is much smaller than the effect from skin, the skin's effect is much more significant than the electrode's effect. Meanwhile, the effects from skin prove why the simulation results between two different materials is close and only 10 % difference.

However, the COMSOL simulation showed the possibility to replace the skin-electrode equivalent circuit model. Because the COMSOL or FE model is able to generate a data set about impedance versus frequency, meanwhile, the SPICE software provides the interface to import the impedance data in the circuit. Therefore, the skin is able to be analysed by COMSOL and connected into electrode amplifying circuit, the electrode circuit will have more accurate and detailed skin information for designing the amplifying circuit.

Moreover, comparing these two measured results, the MED-6350 silicone carbon electrode has less impedance noise across all electrode sizes. According to Huigen's noise research, the MED-6350 silicone-carbon rubber provides a larger contact area with the skin than the silver electrode which reduces noise in the impedance measurement. Moreover, based on the simulation, if the dielectric constant of the material is much less than the average dielectric constant of the skin, it may not increase the measured impedance level sufficiently (over 2 times), and if the measurement requires a more stable impedance curve, the electrode with low noise is a better choice than the electrode with low impedance.

Chapter 6: Conclusions and Future Work

6.1 Introduction

This chapter summaries the work undertaken and results from the research in this thesis. Recommendations are made for further work.

6.2 Literature review

The literature review in this thesis overviewed the existing electrode technologies these being the conventional, dry, and the non-contact electrode. The advantages and disadvantages are described. The conventional Ag/AgCl electrode with conductive gel provides the best signal acquisition, but the patients' hair or skin contaminates the electrode and the gel dries with time so the electrodes have to be replaced daily. The other types of electrode are implemented using different materials or electrode geometries, when compared to the conventional Ag/AgCl electrode aiming to achieve more comfort and a better stable long-term measurement than the Ag/AgCl electrode. Moreover, since the dry and non-contact electrodes do not apply any gel, the measurement will not effected by as gel drying. In general, before the electrode is implemented, the performance and effects of different electrode materials and geometries cannot be simulated by using a conventional skin-electrode equivalent circuit. In particular, for the printed electrode on fabric, since flexibility is another electrode property, the skin-electrode equivalent circuit has a limited simulation performance. FE model can potentially provide more insight into electrode performance before electrode implementation.

For the FE simulation in terms of applying the FE model to replace the equivalent circuit simulation, the electrode properties and skin properties are key factors in the skin-electrode model. From the review of skin-electrode models, the electrode properties include: electrode size, electrode thickness and materials. The skin is divided into 5 layers: stratum corneum (SC), epidermis (E), dermis (D), hypodermis (HYP) and muscle (M). The key properties are layer thickness, dielectric constant, conductivity, Young's Modulus and Poisson's ratio. Furthermore, as the parameters or properties converge to the measurement situation, the modelling results will become closer to the measured results.

6.3 Performance of the skin-electrode impedance model

In terms of the simulation of the skin and skin-electrode model, the results shown in Table 6-1 are focused on the effects of the model's electrical and mechanical properties. In the table, the most significant differences are listed and weighted by their importance.

Skin layer's property	**Importance**	
Dielectric constant	Strong	Highest impedance change is over 95 % in SC layer's interval between 1140 and 6600. Change is based on frequency.
Conductivity	Average/Strong	Highest impedance change is about 70 % in SC layer's interval between 0.000125 and 0.000455 S/m.
Young's Modulus	Less	Highest impedance change is about 5 % in HYP layer's interval between 1.3 to 2.2 MPa.
Thickness	Less	The thickness of the thickest layer (HYP) has been reduced 50 %, impedance changed about 4 %.
External condition		
Electrode size	Average	Electrode size is increased from 0.5 cm^2 to 2 cm^2, the impedance is reduced about 60 %. After 2 cm^2, the impedance reduced less than 20 % for each 0.5 cm^2 reduction. The threshold is 2 cm^2.
External applied force	Average/Less	Decide by the pressure. Decide by the placement from electrode centre to the boundary.
Electrode material	Less	The highest impedance of the material replacement from silver to MED-6350 is about 8 %. Limited by the simulation software.

Table 6-1: Importance of skin and external conditions (electrode size, force), weighted from most to least importance.

From the summary of the influence of the properties of the skin layer in Table 6-1 it can be seen that its electrical properties play a more important role than the mechanical properties in the simulation. In the simulation, the effects of the electrical properties produce a change in impedance of ~90 % (e.g. dielectric constant on SC layer). However, the mechanical properties have less impact on the skin-electrode impedance, the most significant impact occurred with the applied external force causing a change of impedance ~10 %. The main reason may be due to the simulation mechanism. The simulation was fundamentally based on a capacitor structure, which means the electrical properties related to a capacitor will be shown in the results. From the Table 6-1, the properties that reached average or above average are relevant to build a capacitor structure. The only exception is the thickness. This is because the thickness in the simulation was too thick for a capacitor structure. According to equation (4-1), the thickness of the skin layer cannot have a significant effect on the impedance results.

Each single property has a different key layer to assess its effects. Firstly, the dielectric constant of the skin layer was analysed at different frequencies. Because the dielectric

constant was varied at different frequencies, the dielectric constants at 10 Hz, 100 Hz and 1000 Hz were analysed for the SC and HYP layers. In the simulation, the dielectric constant of SC had the highest impedance difference of approximately 95 % between its lowest and highest dielectric constant (1440 to 6600). Because the dielectric constant of SC at low frequency (less than 10 Hz) is varied and difficult to have a constant value, the dielectric constant of average dry skin (1.413×10^3) was applied in further simulation. This average dielectric constant was taken from the skin surface and has less change in the frequency range from 100 Hz to 1000 Hz, so has mainly been used in the literature.

Nevertheless, the dielectric constant variation of the HYP layer was also simulated. The impedance difference resulting from the dielectric constant variation at 100 Hz (3.3×10^5) and 1000 Hz (1.2×10^4) was only approximately 8 %. However, the impedance difference resulting from the dielectric constant at 10 Hz (1.2×10^5) and 100 Hz (3.3×10^5) was approximately 233 %. Similarly, the impedance difference resulting from the dielectric constant of HYP layer at 10 Hz (1.2×10^5) and 100 Hz (1.2×10^4) was also approximately 250 %. Because the simulation was expected to cover the frequency range from low to high, and the dielectric constant at low frequency is varied at different frequencies, the dielectric constant of HYP at 100 Hz was used in the simulation.

Secondly, for the conductivity, for these four layers, the SC layer showed the most significant impedance difference in the simulation. When the conductivity of SC increased from 0.000125 S/m to 0.000455 S/m (about 256 %, based on the interval chosen from the literature), the impedance reduced by 70 %. The second most significant layer was the HYP layer. When the conductivity of HYP layer increased in its interval from 0.02 S/m to 0.04 S/m (increased 100 %), the overall impedance increased by about 40 %. The impedance changes resulting from changes in HYP conductivity showed an opposite trend to the impedance change resulting from SC conductivity changes. According to equation (3-20), in the simulation of SC conductivity, the permittivity and frequency in the imaginary part of the impedance drive the impedance results. So the impedance reduces as the SC conductivity increases. In contrast, in the simulation of HYP conductivity, the conductivity in the real part of the impedance drives the impedance result. So the impedance increases as the HYP conductivity increases. Because the values of the SC's conductivity are much smaller than other layers, this showed a different changing trend in the impedance compared with the other layers.

Thirdly, from the simulation of Young's Modulus, because the HYP is the thickest layer across all four layers, the HYP layer provided the most significant effect for the skin-electrode impedance (about 5 %) based on the interval chosen from the literature (0.2 to 2 MPa) for the variation in Young's Modulus. Moreover, when the thickness of the thickest layer (HYP) for all layers was reduced by 50 %, the skin-electrode impedance only changed by approximately 4 %. Comparing the impedance change in Young's Modulus with the impedance change in conductivity and dielectric constant, the effect from Young's Modulus and the thickness of the layer were significant parameters in the simulation.

The effect of electrode size was also analysed and compared with literature. In the literature, Bosnjak (2017) showed that the electrode size or contact area equalled to 2 cm^2, the change of electrode size had more impact on the skin-electrode impedance. From the simulation

results, an electrode size of between 1.5 cm^2 to 2 cm^2 showed a balance between material coverage and skin-electrode impedance. When the electrode size increased from 0.5 cm^2 to 2 cm^2, the skin-electrode impedance significantly reduced (around 60 %); when the electrode size increased from 2 cm^2 to 3 cm^2, the reduction was approximately 13 %. Comparing the simulated skin-electrode impedance of different electrode sizes with the skin-electrode impedance of different electrode sizes in the literature, showed a similar conclusion. The most efficient electrode size or the threshold for designing an electrode is located between 1.5 cm^2 to 2 cm^2.

In the model, the simulation was based on a linear model in the mechanical and electrical characteristics of the skin-electrode interface. Compared with the non-linear mechanical and electrical characteristics, the non-linear model may have more accurate results than the linear model, but the linear model has its own advantages and disadvantages.

- In the mechanical simulation, the skin was divided into several layers and assumed as a linear elastic material for each layer. However, real skin contains hair follicles, nerve fibres or sebaceous glands. Therefore, the linearity characteristics in the simulation only can show average results. In some literature, if the skin simulation or model was applied using the non-linear parameters (like Young's modulus (Hendriks, *et.al, 2002*)), the author measured the first and second invariant (I_1 and I_2) of the Finger strain tensor, C_{10} and C_{11} for non-linear Young's Modulus matrix (C_{10} and C_{11} were used to create Young's Modulus matrix). However, from the skin-electrode model in this thesis showed that the Young's Modulus was not a key factor (less than 5 %) in the skin-electrode impedance. Even if the non-linear Young's Modulus is added to the simulation, the results should not have a huge impact after updating linear to non-linear Young's Modulus.
- In the electrical simulation, the dielectric constants and electric conductivities vary with frequency, which means that each dielectric constant and electric conductivity at one frequency will have a constant skin-electrode impedance. If the non-linear model is applied to the simulation, the model will be more close to the real-life situation. The current linear model can work for the dielectric constant and conductivity at a specific frequency. It means that if the skin simulation is going simulate the skin-electrode impedance at a fixed known frequency (like 10 Hz or 100 Hz), the model in the thesis has the potential to simulate the results (like making the comparison with the literature simulation in section 3.5.2.1.2.3). Furthermore, if the skin-electrode model aims to find the electrode or skin properties (like effect of electrode contact area or the thickness of skin tissue) at a fixed frequency and the dielectric constant and conductivity has been measured, the linear model can give acceptable results. However, when the electric model aims to cover the skin-electrode impedance from low frequency to high frequency, the linear constant dielectric constant and conductivity cannot provide a reasonable results.
- Furthermore, there is no database or measuring equipment currently available to support the measurement of non-linear dielectric constants and conductivities. In the reviewed literature and databases, the dielectric constants and conductivities are given only for several fixed frequencies (e.g. 10 Hz, 100 Hz and 1000 Hz), most of the data of dielectric constants of skin were at very high frequencies (higher than 10,

000 Hz), these points at lower frequencies cannot support a non-linear parameter. Therefore the average dielectric constant and conductivity have to be applied in the model. Section 3.5.2.1.2.3 has shown that each increment of dielectric constant (10^3) would reduce the total skin-electrode impedance by about 15 %. Because this model used the average dielectric constants or conductivities in the simulation, the total skin-electrode impedance is different between the simulation and experiment.

Therefore, this linear skin-electrode impedance model could be used to simulate the electrical properties for the skin or electrode at a fixed frequency, like the electrode size, the importance of different skin layers or the effect of the thickness of the different skin layers. Because the comparison for these parameters (electrode size, electrical or mechanical properties of skin, thickness of skin, etc) could be simulated at a fixed frequency, the relationships between these parameters and frequency will not be changed at a different frequency range. For example, if the dielectric constant of one skin layer gives a huge impact on skin-electrode impedance at low frequency, the dielectric constant of this skin layer will change the skin-electrode impedance more at high frequency. However, if this skin-electrode model would be used to simulate the skin-electrode impedance from low to high frequency, this linear skin-electrode model cannot work and this is the weakest point in this model. However, because the lack of data for the non-linear dielectric constant and conductivity, the average value has been used in the simulation.

The electrode material has been discussed for this model in section 5.5.3. For the electrode material, because of limitations in the model, when the new material (MED-6350 based carbon electrode) combined with the silver electrode in the model, the skin-electrode impedance has only increased by about 10 %, which is much less than the measured results in Chapter 4 and 5, 150 %. This is another weak point for this skin-electrode model. In this skin-electrode model, the impedance is calculated from a capacitor structure, which means the skin is the main medium material for the capacitor, and the electrodes are the two plates for this capacitor structure. When the electrode material was changed, the medium between this capacitor is still the skin material. Comparing the thickness between the skin and electrode, the change of electrode material was much less than the main materials in the skin-electrode model (less than 1.3 %, see section 5.5.3). Therefore, the change of electrode materials cannot be shown from the simulated skin-electrode impedance. However, from the measurements for electrode impedance without skin, when the material was changed from silver to MED-6350, the electrode impedance without skin would change over 500 %. The change of material from silver to MED-6350 silicone electrode causes a change of skin-electrode impedance results of approximately 50 % for a 1 cm^2 electrode. Comparing the change of electrode impedance and the change of skin-electrode impedance, it can be seen that the skin has a more significant effect on the skin-electrode impedance. Although the increased simulated skin-electrode impedance was much less than the measured increased skin-electrode impedance, both simulation and measurement showed that the effects from skin impedance was more significant than the effects from electrode impedance. This is because the practical measurement of skin-electrode impedance uses an amplifier, therefore does not measure directly at the electrode like the simulation does. Therefore, the measurement gave the same conclusion as the simulation; the skin plays more important role than the electrode.

Furthermore, the COMSOL model provides the ability to import FE simulation results into the SPICE circuit design. When the MED-6350 simulated electrode results from COMSOL for impedance versus frequency are imported into the SPICE circuit, the COMSOL simulation provides more accurate results than the equivalent circuit design based on skin's properties and improves the amplifying circuit design in electrode circuit.

6.4 Textile Electrode design and material selection

For the electrode implementation, three printing methods have been evaluated: inkjet and screen printing in chapter 4, stencil printing in chapter 5. When the electrodes are printed, inkjet printing does not provide acceptable results in terms of electrode quality or the time required to manufacture. However, screen printing is a faster printing procedure and the screen printed electrode has better quality. To achieve characteristics not achievable using screen printing, stencil printing is used in addition to screen printing. The stencil print is therefore used to deposit high viscosity pastes that screen printing cannot print like silicones. Therefore, the combination of screen and stencil printing is used to make the textile electrode.

According to the simulation and reviews, the electrodes made using silver (ELX-30 with the resistivity of 4.5×10^{-5} Ω.m) have the most effective performance in the area range from 1.5 cm^2 to 2 cm^2. In this range, the electrode balances electrode impedance and the measured bio-signal when EMG is recorded on the forearm. Furthermore, the MED-6350 with 15 % carbon loading provided the best combination of tensile strength with the Young's modulus of 50 MPa and the lowest resistivity of around 1.79 Ω.cm. Nevertheless, the MED-6350 provided an adhesive force of around 0.8 to 0.9 N on 1 cm^2 electrode; this adhesion helps the electrode reject movement during the measurement and increases the conductive area.

6.5 Recommendations for future work

This thesis have provided a possible method to investigate the key parameters in a skin-electrode model. In this model, the effects of different skin layers (SC, E, D and HYP) and external conditions (electrode size, applied force and electrode material) are simulated. Due to the limitations of the model, the electrical properties of the skin have a more significant impact than the mechanical properties. However, a threshold of the electrode size was identified using the simulation which is close to the measured results. However, there are still opportunities for further research that could be implemented to examine the electrode and its modelling.

In the simulation, some further investigations could be undertaken:

- In the current model, the skin's dielectric constants were modelled using average values. However, the dielectric constant at low frequency varies for different skin layers, especially below 20 Hz. Hence, if the dielectric constant vs. frequency could be identified and substituted into the model, the accuracy of the model could be improved.
- The model could be developed to analyze the results for different electrode materials. Currently, because of the limitations in building the model, the electrode material has

an impact on the skin-electrode impedance, but this is not the key impact. If the electrode materials are to be analyzed, the capacitor structure is not the best simulation option.

- Details of skin geometries could be further developed. In the present simulation the skin on the forearm has been selected for test and simulation. Compared to other areas on the body, the skin on the forearm is relatively flat, and is easy to measure the impedance. It has less hair, and so hair will not be a problem for measuring the impedance from the forearm. However, the hair on the skin and skin of different geometries will become important parameters when measuring EEG.
- Different functions should be further studied for the skin, such as skin sweat or temperature. In the simulation, the sweat was not been used as a function as the model is based on a capacitor structure. An improved key function may be required in the simulation for sweat. The sweat may change the electrolyte in the modelled structure. Furthermore, the skin impedance may change with temperature.

Printed materials have many combinations for the implementation of electrodes. The silicone carbon rubber studied in this thesis was optimized for the electrode testing, but some other materials may have lower resistivity, higher adhesive force and be more flexible than MED-6350 with carbon black. In order to improve the performance of the electrode, further investigation of the formulations of different materials may be required. When the materials' properties have been identified, they could be implemented in the simulation library to assess if this material provides a more comfortable, flexible and stable electrode.

Appendix A: Forms and sheets

UNIVERSITY OF Southampton

Participant Information Sheet

Study Title: **Analysing the Effects on Electrode Design and Simulation for Bio-signal Recording on Textile**

Researcher: Zihao Li
ERGO number: ERGO/FPSE/ 30998

Please read this information carefully before deciding to take part in this research. It is up to you to decide whether or not to take part. If you are happy to participate you will be asked to sign a consent form.

What is the research about?
This project involves measuring the skin impedance from the forearm over a certain frequencies.
The participants will wear an armband which is made of fabric and printed carbon electrodes. The impedance will be collected by an impedance analyser and stored in a USB memory.
The purpose of this research is used to estimate the performance of the electrode and make the comparison between the simulation and experiment results.

Why have I been asked to participate?
You have been asked BEFORE the experiment because you:

- Can understand/speak English;
- have no disease, headache, dizziness affecting their action of response;
- have no contagious skin infections;
- have no any cardiovascular problems, for example, heart disease, breathlessness, high blood pressure, etc.
- no other skin conditions, such as eczema;
- no skin allergies;

We are hoping to find 20 people who are interested in taking part in this research study. It is up to you to decide whether to take part. If you decide to take part, you will be given this information sheet to keep and be asked to sign a consent form. Even if you have been involved, you are still free to withdraw at any time and without giving a reason.

What will happen to me if I take part?
If you would like to discuss taking part, please contact me in the next fortnight (zl1e08@soton.ac.uk). Please feel free to discuss this research study with other people. Once you decide to take part in, you will be given a copy of participant information, consent form and risk assessment form to read and sign.
The study will take place in a quiet private room in which are an impedance analyser, a printed smart fabric armband and electronics. Participants will be asked to sit on a chair and switch off their mobile phones, tablets, laptops and other electronic devices.
The functionality of the armband, including each component, will be described to the participants and any potential discomfort will be explained prior to the experiment (e.g armband too tight). The experimental procedure will also be explained.
Two electrodes from arm band are placed on the forearm, and the leads from impedance analyser are connected to the electrodes. The frequency of impedance analyser is increased from 0 Hz to 1 kHz, and the impedance will be recorded under different frequencies from the arm band. The electrode size is increased from 0.5 cm^2 to 2.5 cm^2 with the step of 0.5 cm^2. The impedance for each electrode size will be recorded 5 times.

When the study is completed, the participants will be asked to leave the room and the anonymity will be maintained as no photographs will be taken and no names/contact details will be shared. All data recorded during the study will be encrypted in a password protected PC in a locked office. No other person, except the investigators, can access the data.

UNIVERSITY OF Southampton

Are there any benefits in my taking part?
There is unlikely to be any direct benefit to you from taking part in this study. It might be fun and you might learn about the skin's information from the electronic side. We hope the results will have a beneficial impact on the medical application in the future.

Are there any risks involved?
There is no risk during this study since all electronics work at a low voltage of 1 V and a current less than 80 mA.

Will my participation be confidential?
All information collected about you during the course of the research will be kept strictly confidential. Any information about you which is used in research reports or publications will have your name and contact details removed so that you cannot be recognised from it.

What should I do if I want to take part?
All information collected about you during the course of the research will be kept strictly confidential. Any information about you which is used in research reports or publications will have your name and contact details removed so that you cannot be recognised from it.

What happens if I change my mind?
You continued participation is completely voluntary. You are free to withdraw at any time and for any reason, without your legal rights being affected. In this case, any data captured will be deleted without being reviewed by any of the researchers. You retain control over your data after the end of the study, and can request that your data be deleted at any time.

What will happen to the results of the research?
The results will be used to investigate the difference between the simulation and experiment results. When the results is collected by the researcher, it will be used to analyse with simulation results which is built by researcher. All the results will be written and analysed in researcher's PhD thesis.

Where can I get more information?
You are very welcome to get in touch with one of the investigators, whose details are given at the top of this document. They will be happy to answer any questions.

What happens if something goes wrong?
You are first invited to contact one of the investigators involved in the study if you have any problems. Their contact details are listed at the top of this document. In the case of concern or complaint, you should contact the Research Integrity and Governance Manager (023 8059 5058, rgoinfo@soton.ac.uk).

Thank you.
Thank the individual for taking the time to read the information sheet and considering taking part in the research.

Appendix

FPSE Ethics Committee
FPSE EC Application Form

Ver 6.6e

Reference number: **ERGO/**FPSE**/ 30998**	Submission version: 2.0	Date: 2017-11-15
Name of **investigator**(s): Zihao Li		
Name of supervisor(s) (if student **investigator**(s)): Dr Joh Tudor, Dr Russel Torah		
Title of study: **Analysing the Effects on Electrode Design and Simulation for Bio-signal Recording on Textile**		
Expected study start date: 15/01/2018	Expected study end date: 30/06/2018	

Note that the dates requested on the "IRGA" form refer to the start and end of *data collection*. These are *not* the same as the start and end dates of the study, above, for which approval is sought. (A study may be considered to end when its final report is submitted.)

Note that ethics approval must be obtained before the expected study start date as given above; retrospective approval cannot be given.

Note that failure to follow the University's policy on Ethics may lead to disciplinary action concerning Misconduct or a breach of Academic Integrity.

By submitting this application, the investigator(s) undertake to:

- Conduct the study in accordance with University policies governing:
  Ethics (http://www.southampton.ac.uk/ris/policies/ethics.html);
  Data management (http://www.southampton.ac.uk/library/research/researchdata/);
  Health and Safety (http://www.southampton.ac.uk/healthandsafety);
  Academic Integrity (http://www.calendar.soton.ac.uk/sectionIV/academic-integrity-statement.html.
- Ensure the study Reference number ERGO/FPSE/30998 is prominently displayed on all advertising and study materials, and is reported on all media and in all publications;
- Conduct the study in accordance with the information provided in the application, its appendices, and any other documents submitted;
- Submit the study for re-review (as an amendment through ERGO) or seek FPSE EC advice if any changes, circumstances, or outcomes materially affect the study or the information given;
- Promptly advise an appropriate authority (Research Governance Office) of any adverse study outcomes (via an adverse event notification through ERGO);
- Submit an end-of-study form if required to do so.

REFER TO THE INSTRUCTIONS AND GUIDE DOCUMENTS WHEN COMPLETING THIS FORM AND THE TEMPLATES DOCUMENT WHEN PREPARING THE REQUIRED APPENDICES.

PRE-STUDY

Characterise the proposed **participants**
A sample of 20 participants (50% male and 50% female) will be recruited by word of mouth from the investigators ''s lab and emails within ECS.

Describe how **participants** will be approached
A sample of 20 participants will be recruited from within Electronics and Computer Science (ECS) at the University of Southampton. Email will be sent only to the member of Electronics and Computer Science with the criteria described in the next section. The investigators will identify the most suitable 20 participants with equal gender distributions. Participants will be contacted only by blind copied emails such that the confidentiality of each participant can be persevered. If they agree, they will be provided with the following information sheets: - A copy of the participant information - A copy of the consent form - A copy of the risk assessment Once all 20 participants have read and signed above document, the study schedule (e.g. location and time) will be sent. If any non-FPSE e-mail lists are used, justify their use: they won't be.

Describe how inclusion and/or exclusion criteria will be applied (if any)
Participants will be included in the study if they are able to read/communicate in English. Participants will be asked BEFORE the experiment if they have: - Any contagious skin infections - Any cardiovascular problems (e.g. heart disease, breathlessness, high blood pressure) - Any skin condition (e.g. eczema) - Any known allergy - Any disease, headache, dizziness affecting their response If the participants have any of the above, they will not be allowed to attend the experiment.

Describe how **participants** will decide whether to take part
Prospective participants will be invited to attend a short session in the demo room (room 4235 building 59) at Electronics and Computer Science. Participants will be shown the printed arm band and explained about it, and how the study will take place in detail. Safety consideration will be covered. Participants will be given the opportunity to ask any questions and will make the decision whether they are willing to be involved in the study. Additionally, participants will be informed that they can withdraw at any time during the study.

Participant Information (Appendix (i))

Provide the **Participant Information** in the form that it will be given to **participants** as Appendix (i). All studies must provide **participant information.**

Consent Form/Information (Appendix (iii))

Provide the **Consent Form** (or the request for consent) in the form that it will be given to **participants** as Appendix (iii). All studies must obtain **participant** consent. Some studies may obtain verbal consent (and only present consent information), other studies will require written consent, as explained in the *Instructions, Guide,* and *Templates* documents.

DURING THE STUDY

Describe the study procedures as they will be experienced by the **participant**
The study will take place in a quiet private room in which are an impedance analyser, a printed smart fabric arm band and electronics. Participants will be asked to sit on a chair and switch off their mobile phones, tablets, laptops and other electronic devices. The functionality of the arm band, including each component, will be described to the participants and any potential discomfort will be explained prior to the experiment (e.g arm band too tight or uncomfortable). The experimental procedure will also be explained. If the participants agree to the study, the arm band will be instrumented and adjusted with Impedance analyser. Signal acquisition cables of the arm band will be connected to the impedance analyser for data collection. A small 1 V voltage and 0.8 mA current from impedance analyser are applied to the participants during the study. Two electrodes from arm band are placed on the forearm, and the leads from impedance analyser are connected to the electrodes. The frequency of impedance analyser is increased from20 Hz to 500 kHz, and the impedance will be recorded under different frequencies from the arm band. The electrode size is increased from 0.5 cm^2 to 2.5 cm^2 with the step of 0.5 cm^2. The impedance for each electrode size will be recorded 5 times. When the study is completed, the participants will be asked to leave the room and the anonymity will be maintained as no photographs will be taken and no names/contact details will be shared. All data recorded during the study will be encrypted in a password protected PC in a locked office. No other person, except the investigators, can access the data.

Identify how, when, where, and what kind of data will be recorded (not just the formal research data, but including all other study data such as e-mail addresses and signed consent forms)
All participant data files collected through the investigation will be encrypted on a password protected PC in a locked office. Any paper records will be kept in a locked filing cabinet and published reports at the end of the study will contain no person sensitive information. No other person, except the investigators, can access the personal data. If the participant would like to see their own data, they can ask the investigators after their own testing, and the investigators will give a copy of their own data.

Participant questionnaire/data gathering methods (Appendix (ii))

As Appendix (ii), reproduce any and all **participant** questionnaires or data gathering instruments in the exact forms that they will be given to or experienced by **participants.** If conducting less formal data collection, or data collection that does not involve direct questioning or observation of participants (eg secondary data or "big data"), provide specific information concerning the methods that will be used to obtain the data of the study.

POST-STUDY

Identify how, when, and where data will be stored, processed, and destroyed
If Study Characteristic M.1 applies, provide this information in the **DPA Plan** as Appendix (iv) instead and do *not* provide explanation or information on this matter here.

STUDY CHARACTERISTICS

(L.1) The study is funded by a commercial organisation: **No** If 'Yes', provide details of the funder or funding agency *here.*

(L.2) There are **restrictions** upon the study: **No** If 'Yes', explain the nature and necessity of the **restrictions** *here.*

(L.3) Access to **participants** is through a third party: **No** If 'Yes', provide evidence of your permission to contact them as Appendix (v). Do *not* provide explanation or information on this matter here.

(M.1) **Personal data** is or *may be collected or processed: **Yes** Data will be processed outside the UK: **No** If 'Yes' to either question, provide the **DPA Plan** as Appendix (iv). Do *not* provide information or explanation on this matter here. Note that using or recording e-mail addresses, telephone numbers, signed consent forms, or similar study-related **personal data** requires M.1 to be "Yes". (* Secondary data / "big data" may be *de*-anonymised, or may contain **personal data.** If so, answer 'Yes'.)

(M.2) There is **inducement** to **participants**: **No** If 'Yes', explain the nature and necessity of the inducement *here.*

(M.3) The study is **intrusive**: **No** If 'Yes', provide the **Risk Management Plan,** the **Debrief Plan,** and Technical Details as Appendices (vi), (vii), and (ix), and explain *here* the nature and necessity of the intrusion(s).

(M.4) There is **risk of harm** during the study: **No** If 'Yes', provide the **Risk Management Plan**, the **Contact Information**, the **Debrief Plan**, and Technical Details as Appendices (vi), (vii), (viii), and (ix), and explain *here* the necessity of the risks.

(M.5) The true purpose of the study will be hidden from **participants**: **No** The study involves **deception** of **participants**: **No** If 'Yes' to either question, provide the **Debrief Plan** and Technical Details as Appendices (vii) and (ix), and explain *here* the necessity of the deception.

(M.6) **Participants** may be minors or otherwise have **diminished capacity**: **No** If 'Yes', AND if one or more Study Characteristics in categories M or H applies, provide the **Risk Management Plan,** the **Contact Information**, and Technical Details as Appendices (vi), (vii), & (ix), and explain *here* the special arrangements that will ensure informed consent.

(M.7) **Sensitive data** is collected or processed: **No** If 'Yes', provide the **DPA Plan** and Technical Details as Appendices (iv) and (ix). Do *not* provide explanation or information on this matter here.

(H.1) The study involves: **invasive** equipment, material(s), or process(es); or **participants** who are not able to withdraw at any time and for any reason; or animals; or human tissue; or biological samples: **No** If 'Yes', provide Technical Details and further justifications as Appendices (ix) and (x). Do *not* provide explanation or information on these matters here. Note that the study will require separate approval by the Research Governance Office.

Appendix

DPA Plan

Ethics reference number: **ERGO/FPSE/ 30998**	Version: 2.0	Date: 2017-11-15
Study Title: **Analysing the Effects on Electrode Design and Simulation for Bio-signal Recording on Textile**		
Investigator: Zihao Li		

The only people with access to the participants' information are the investigators (Zihao Li, Dr John Tudor and Dr Russel Torah). They will know names, gender and contact details as data is collected before the study. No one else needs to know this information and therefore any information shared with the collaborators will be replaced by an identification number replacing a name. For example, each participant will be named by P1, P2, and P3 and so on. Only the researchers and collaborators within the University of Southampton will have access to the data for analysis and presentation.

The data is relevant to the study purposes because the data will be collected only for the skin-electrode impedance analysing. The data is adequate because each participant will be asked to be tested 5 times per each electrode.

The data will be processed fairly because the participants will have given explicit consent.

The data's accuracy is ensured because A sample of 20 participants (50% male and 50% female) will be recruited by word of mouth from the investigators `s lab and emails within ECS.

Data will be stored on University server, the data will be held in accordance with University policy on data retention.

Before the study, participants will be shown the printed arm band and explained about it, and how the study will take place in detail. Safety consideration will be covered. Participants will be given the opportunity to ask any questions and will make the decision whether they are willing to be involved in the study. Additionally, participants will be informed that they can withdraw at any time during the study. Once participants are agreed, they need to sign the consent form.

During the study, the researcher will retain and encrypt each participant's data on password protected PC in a locked office. Any paper-based data, the researchers will be stored in a locked office during the study. Any collaborators will also store the anonymised data in a similarly secure fashion to that used in Southampton.

The data will be processed in accordance with the rights of the participants because they will have the right to access, correct, and/or withdraw their data at any time and for any reason. Participants will be able to exercise their rights by contacting the investigator (e-mail: zl1e08@soton.ac.uk) or the project supervisor (e-mail:mjt@ecs.soton.ac.uk).

The data will be anonymised by the researcher, consent forms will be linked to the data by University of Southampton.

Bibliography

Abe, T. and Loenneke, J. (2015). Handgrip strength dominance is associated with difference in forearm muscle size. *Journal of Physical Therapy Science*, 27(7), pp.2147-2149.

Agache, P., Monneur, C., Leveque, J. and De Rigal, J. (1980). Mechanical properties and Young's modulus of human skin in vivo. *Archives of Dermatological Research*, 269(3), pp.221-232.

Agilent, T.B. (1976). *Proper Cable Shielding Avoids RF Interference Problems in Precision Data Acquisition Systems*. [Online] Keysight.com. Available at: https://www.keysight.com/upload/cmc_upload/All/EPSG084828.pdf.

Albet Torres, B. and Bragós Bardia, R. (2011). *Wireless system for the measurement of bioelectric signals using capacitive electrodes* [Online]. Available at: https://upcommons.upc.edu/bitstream/handle/2099.1/12267/PFC.pdf

Alba, N. A., Sclabassi, R. J., Sun, M. and Cui, X. T. (2010). Novel Hydrogel-Based Preparation-Free EEG Electrode. *IEEE Transactions on Neural Systems and Rehabilitation Engineering*, 18(4), 415-423. Available at: http://ieeexplore.ieee.org/stamp/stamp.jsp?tp=&arnumber=5454276&isnumber=5545713 [Accessed 9 March, 2019].

Anas, A. and Chan, A. (2012). Electrode-skin impedance changes due to an externally applied force. In: *2012 IEEE International Symposium on Medical Measurements and Applications Proceedings*. [Online] Budapest, Hungary: IEEE. Available at: http://10.1109/MeMeA.2012.6226628 [Accessed 28 Jun. 2012].

Assambo, C., Baba, A., Dozio. R. and Burke. M.J. (2007). Determination of the Parameters of the Skin-Electrode Impedance Model for ECG Measurement, *6th WSEAS Int. Conf. on Electronics, Hardware, Wireless and Optical Communications*. pp. 90-95.

AZoM.com. (2018). Silicone Rubber. *Materials Science Articles | Latest Science Articles | Scientific Development*. [Online] Available at: https://www.azom.com/properties.aspx?ArticleID=920. [Accessed 17 Oct. 2018].

Baek, H., Lee, H., Lim, Y. and Park, K. (2012). Conductive Polymer Foam Surface Improves the Performance of a Capacitive EEG Electrode. *IEEE Transactions on Biomedical Engineering*, 59(12), pp.3422-3431.

Baek, J., An, J., Choi, J., Park, K. and Lee, S. (2008). Flexible polymeric dry electrodes for the long-term monitoring of ECG. *Sensors and Actuators A: Physical*, 143(2), pp.423-429.

Barzegar, F., Dangbegnon, J., Bello, A., Momodu, D., Charlie Johnson Jr, A. and Manyala, N. (2015). *Effect of conductive additives to gel electrolytes on activated carbon-based supercapacitors*. [Online] AIP Advances 5. Available at: https://doi.org/10.1063/1.4931956 [Accessed 2015].

Bazzazi, F. and Sadr, A. (2010). Finite-element simulation of effects of laser parameters on laser generated ultrasonic waves in human skin. In: *2010 IEEE EMBS Conference on*

Biomedical Engineering and Sciences (IECBES). [Online] Kuala Lumpur, Malaysia: IEEE, pp.1-4. Available at: http://10.1109/IECBES.2010.5742100 [Accessed 5 Apr. 2011].

Bischoff, J.E., Arruda, E.M. and Grosh, K. (2000). Finite element modeling of human skin using an isotropic, nonlinear elastic constitutive model, *Journal of Biomechanics*, 33(6), pp.645-652.

Bronzino, J. (2018). Biopotential Electrode Section V Biomedical Sensors. In: J. Bronzino, ed., *The Biomedical Engineering Handbook*, 2nd ed. Florida: CRC Press, pp. 48-1-48-4.

Bosnjak, A., Kenneddy, A., Linares, P., Borges, M., McLaughlin, J. and Escalona, O. (2017). Performance assessment of dry electrodes for wearable long term cardiac rhythm monitoring: skin-electrode impedance spectroscopy. *Proc. 39th Annual International Conference of the IEEE Engineering and Medicine Biology Society*, July 2017.

Boone, K. and Holder, D. (1996). Effect of skin impedance on image quality and variability in electrical impedance tomography: a model study. *Medical & Biological Engineering & Computing*, 34(5), pp.351-354.

Cao, Z., Tudor, M., Torah, R. and Beeby, S. (2016). Screen Printable Flexible BiTe–SbTe-Based Composite Thermoelectric Materials on Textiles for Wearable Applications. *IEEE Transactions on Electron Devices*, 63(10), pp.4024-4030.

Cardu, R., Leong, P.H.W., Jin, C.T. and McEwan, A. (2012). Electrode contact impedance sensitivity to variations in geometry Physiol. Meas, 33(1), pp.817–30.

Chen, E., Novakofski, J., Jenkins, W. and O'Brien, W. (1996). Young's modulus measurements of soft tissues with application to elasticity imaging. *IEEE Transactions on Ultrasonics, Ferroelectrics and Frequency Control*, 43(1), pp.191-195.

Chen, Y.H., DeBeeck, M.O., Vanderheyden, L., Carrette, E., Mihajlovic, V., Vanstreels, K., Grundlehner, B., Gadeyne, S., Boon, P. and VanHoof, C., Soft, comfortable polymer dry electrodes for high quality ECG and EEG recording. *Sensors. 2014*, 14(12), pp.23758–23780.

Chi, Y., Jung, T. and Cauwenberghs, G. (2010). Dry-Contact and Noncontact Biopotential Electrodes: Methodological Review. *IEEE Reviews in Biomedical Engineering*, 3, pp.106-119.

Chi, Y., Ng, P., Kang, E., Kang, J. and Fang, J. (2010). *Wireless non-contact cardiac and neural monitoring*. [Online] Isn.ucsd.edu. Available at: http://isn.ucsd.edu/pubs/wh2010.pdf [Accessed 17 Oct. 2018].

Chin-Teng Lin, Lun-De Liao, Yu-Hang Liu, I-Jan Wang, Bor-Shyh Lin and Jyh-Yeong Chang (2011). Novel Dry Polymer Foam Electrodes for Long-Term EEG Measurement. *IEEE Transactions on Biomedical Engineering*, 58(5), pp.1200-1207.

Chiou, J. C., Ko, L. W., Lin, C. T., Hong, C. T., Jung, T. P., Liang, S. F., & Jeng, J. L. (2006). Using novel MEMS EEG sensors in detecting drowsiness application. In *Biomedical Circuits and Systems Conference, 2006. BioCAS 2006. IEEE*. pp. 33-36.

Cömert, A. and Hyttinen, J. (2014). Impedance spectroscopy of changes in skin-electrode impedance induced by motion. *BioMedical Engineering OnLine*. Available at:

https://biomedical-engineering-online.biomedcentral.com/articles/10.1186/1475-925X-13-149 [Accessed 18 Nov. 2014].

Flynn, C. and McCormack, B. (2008). Finite element modelling of forearm skin wrinkling. *Skin Research and Technology*, 14(3), pp.261-269.

Gabriel, C., Gabriel, S. and Corthout, E. (1996). The dielectric properties of biological tissues: I. Literature survey. *Physics in Medicine and Biology*, 41(11), pp.2231-2249.

Gabriel, S., Lau, R.W. and Gabriel, C., (1996), The dielectric properties of biological tissues: II. Measurements in the frequency range 10 Hz to 20 GHz, *Physics in Medicine and Biology*, 41(11), pp. 2251-2269.

Gaetano, G., Paolo, B., Rafael, A. Calvo, M.C., Craig, J., Alistair, M. and André, S. (2010). Non-invasive Electronic Biosensor Circuits and Systems, *Intelligent and Biosensors Vernon S. Somerset, Intech Open*, DOI: 10.5772/7027. Available at: https://www.intechopen.com/books/intelligent-and-biosensors/non-invasive-electronic-biosensor-circuits-and-systems/

Gerligs, M. (2009). *Skin layer mechanics*. [Online] Mate.tue.nl. Available at: http://www.mate.tue.nl/mate/pdfs/11390.pdf.

Grimnes, S. and Martinsen, O. (2008). *Bioelectricity and bioimpedance basics*. London: Academic.

Gruetzmann, A., Hansen, S. and Müller, J. (2007). Novel dry electrodes for ECG monitoring. *Physiological Measurement*, 28(11), pp.1375-1390.

Hara, Y., Masuda, Y., Hirao, T. and Yoshikawa, N. (2013). The relationship between the Young's modulus of the stratum corneum and age: a pilot study. *Skin Research and Technology*, 19(3), pp.339-345.

Hao, Q. and Hu, Fei. (2010). A compressive eletroencephalography (EEG) sensor design. *2010 IEEE Sensors*. Kona, September 2010.

Harland, C., Clark, T. and Prance, R. (2002). Electric potential probes - new directions in the remote sensing of the human body. *Measurement Science and Technology*, 13(2), pp.163-169.

Hendriks, F. (1969). Mechanical behaviour of human skin in vivo. *Bio-medical. Eng.*, *4*, 322-327.

Hendriks, F., Brokken, D., Eemeren, J.V., Oomens, C., Baaijens, F. and Horsten, J. (2003).A numerical-experimental method to characterize the non-linear mechanical behaviour of human skin. *Skin Res Technol* .9(3), pp. 274–283.

Huclova, S., Erni, D. and Fröhlich, J. (2011). Modelling and validation of dielectric properties of human skin in the MHz region focusing on skin layer morphology and material composition. *Journal of Physics D: Applied Physics*, 45(2), pp.025301-025318.

Bibliography

Huigen, E. (2001). *Noise characteristics of surface electrodes*. [Online] University of Amsterdam Section Medical Physics. Available at: http://www.angelfire.com/planet/ehuigen/scriptie.pdf.

Huigen, E., Peper, A. and Grimbergen, C. (2001). Investigation into the origin of the noise of surface electrodes. *Medical & Biological Engineering & Computing*, 40(3), pp.332-338.

Hume, P., Png, W., Aziz, A. and Razali, M. (2009). Differences in world badminton players' physical and proportionality characteristics between singles and doubles players. In: *Kinanthropometry XI: 2008 Pre-Olympic Congress Anthropometry Research*. New Zealand, Auckland: Auckland: Sport Performance Research Institute New Zealand, Auckland University of Technology, pp.78-89.

Institute of Electrical and Electronics Engineers (2007). *IEEE Biomedical Circuits and Systems Conference 2007 BIOCAS - Technische Informationsbibliothek (TIB)*. [Online] Tib.eu. Available at: https://www.tib.eu/de/suchen/id/TIBKAT%3A593998286/.

Itis.swiss. (2018). *Dielectric Properties » IT'IS Foundation*. [Online] Available at: https://itis.swiss/virtual-population/tissue-properties/database/dielectric-properties/ [Accessed 18 Oct. 2018].

Gomez-Clapers, J. , Serrano-Finetti, J. , Casanella,R. and Pallas-Areny,R. (2018). Can driven-right-leg circuits increase interference in ECG amplifiers? , *IEEE Conference Publication*.
Ieeexplore.ieee.org. Available at: https://ieeexplore.ieee.org/document/6091184.

James, W., Berger, T. and Elston, D. (2005). *Andrews' Diseases of the Skin: Clinical Dermatology (10th ed.)*. Saunders. Pages 1, 11–12.

Johnson, P. and Christy, R. (1972). *Optical Constants of the Noble Metals*.

Kang, T., Merritt, C., Grant, E., Pourdeyhimi, B. and Nagle, H. (2008). Nonwoven Fabric Active Electrodes for Biopotential Measurement During Normal Daily Activity. *IEEE Transactions on Biomedical Engineering*, 55(1), pp.188-196.

Kato, T., Ueno, A., Kataoka, S., Hoshino, H. and Ishiyama, Y. (2006). An Application of Capacitive Electrode for Detecting Electrocardiogram of Neonates and Infants. *2006 International Conference of the IEEE Engineering in Medicine and Biology Society*.

Kareem, F.R., Azeem, M.H, Mohamehgenedy and Sameh, A.M. (2017). Classification of EMG Signals of Lower Arm (Forearm\Hand) Motion Patterns Used To Control Robot Hand Movement. In: *89th ISERD International Conference*. [Online]
Available at: http://www.worldresearchlibrary.org/up_proc/pdf/1134-151151520140-45.pdf.

Kita, N. (2019). *The Hypodermis Layer of the Skin Structure and Function*. [Online] Available at: https://www.verywellhealth.com/the-hypodermis-is-the-lowermost-layer-of-skin-2710144

Komolafe, A., Torah, R., Tudor, M. and Beeby, S. (2018). Modelling and experimental validation of the effect of the elastic properties of fabrics on the durability of screen printed e-textiles. *Smart Materials and Structures*, 27(7), pp.075046-075058.

Lee, J., Pearce, F., Hibbs, A., Matthews, R. and Morrissette, C. (2004). *Evaluation of a Capacitively-Coupled, Non-Contact (through Clothing) Electrode or ECG Monitoring and Life Signs Detection for the Objective Force Warfighter*. [Online] Citeseerx.ist.psu.edu. Available at: http://citeseerx.ist.psu.edu/viewdoc/summary?doi=10.1.1.215.5527.

Li,G. Wang,Y. and Duan,Y. Towards gel-free electrodes: a systematic study of electrode-skin impedance, *Sens. Actuators B Chem.*, 241 (2017), pp. 1244-1255.

Liao, L., Wang, I., Chen, S., Chang, J. and Lin, C. (2011). Design, Fabrication and Experimental Validation of a Novel Dry-Contact Sensor for Measuring Electroencephalography Signals without Skin Preparation. *Sensors*, 11(6), pp.5819-5834.

López, R. (2011). *Model based enhancement of bioimpedance spectroscopy analysis: towards textile enabled applications*. Degree of Licentiate of Technology. KTH – Royal Institute of Technology.

Lourtioz, J.M. et al. (2005). *Photonic Crystals: Towards Nanoscale Photonic Devices*. Springer. pp. 121–122.

Lun-De Liao, Chin-Teng Lin, McDowell, K., Wickenden, A., Gramann, K., Tzyy-Ping Jung, Li-Wei Ko and Jyh-Yeong Chang (2012). Biosensor Technologies for Augmented Brain–Computer Interfaces in the Next Decades. *Proceedings of the IEEE*, 100 (Special Centennial Issue), pp.1553-1566.

Lymberis, A. Smart wearable systems for personalised health management: current R&D and future challenges. *Proceedings of the 25th Annual International Conference of the IEEE Engineering in Medicine and Biology Society (IEEE Cat. No.03CH37439)*. Cancun, 2003, pp. 3716-3719 Vol.4.

Marks, J.G. and Miller, J. (2006). *Lookingbill and Marks' Principles of Dermatology* (4th ed). Elsevier. pp. 1–7.

Merritt, C., Nagle, H. and Grant, E. (2009). Fabric-Based Active Electrode Design and Fabrication for Health Monitoring Clothing. *IEEE Transactions on Information Technology in Biomedicine*, 13(2), pp.274-280.

Miklavcic, D., Pavselj, N., and Hart, F. X. (2006). Electric properties of tissues. *Wiley Encyclopedia of Biomedical Engineering*.

Mohanty, B., Agrawal, D., Mishra, K., Samantsinghar, P. and Chinara, P. (2013). Estimation of height of an individual from forearm length on the population of Eastern India. *Journal of Medical & Allied Sciences*, [Online] pp.72-75. Available at: http://jmas.in/sites/default/files/articles/Estimation%20of%20height%20of%20an%20individual%20from%20forearm%20length%20on%20the%20population%20of%20Eastern%20India.pdf.

Mojarradi, M., Binkley, D., Blalock, B., Andersen, R., Ulshoefer, N., Johnson, T. and Castillo, L. (2003). A miniaturized neuroprosthesis suitable for implantation into the brain. *IEEE Transactions on Neural Systems and Rehabilitation Engineering*, 11(1), pp.38-42.

Bibliography

Neuman, M. (2000). Biopotential Electrodes. In: J. Bronzino, ed., *The Biomedical Engineering Handbook*, 2nd ed. [Online] Boca Raton: CRC Press LLC. Available at: *http://www.fis.uc.pt/data/20062007/apontamentos/apnt_134_5.pdf*.

Paul, G. (2014). Screen printed textile based wearable biopotential monitoring. *University of Southampton, Physical Sciences and Engineering, Doctoral Thesis*, pp. 236-240.

Paul, G., Fan Cao, Torah, R., Kai Yang, Beeby, S. and Tudor, J. (2014). A Smart Textile Based Facial EMG and EOG Computer Interface. *IEEE Sensors Journal*, 14(2), pp.393-400.

Paul, G., Torah, R., Yang, K., Beeby, S. and Tudor, J. (2014). *An investigation into the durability of screen-printed conductive tracks on textiles*. [Online]. Avalable at: http://iopscience.iop.org/article/10.1088/0957-0233/25/2/025006/meta.

Peng, H.L. et al., Flexible dry electrode based on carbon nanotube/polymer hybrid micropillars for biopotential recording, *Sens. Actuators A Phys.*, vol. 235, pp. 48-56, Nov. 2015.

Pola, T. and Vanhala, J. (2007). *Textile electrodes in ECG measurement*. in ISSNIP -07 Third International Conference of Intelligent Sensors, Sensor Networks an Information Processing, December 3-6 2007, Melbourne, Australia. pp. 5-7.

Ponec, M,Weerheim, A., Lankhorst, P. and Wertz, P. (2003). New acylceramide in native and reconstructed epidermis. *J Invest Dermatol*, 120 (4), pp.581-588.

Prutchi, D. and Norrid, M. (2005a). Chapter 2: Bandpass selection for biopotential amplifiers. In: *Design and development of medical electronic instrumentation: a practical perspective of the design, construction, and test of medical devices*. [Online]. Canada: John Wiley & Sons, Inc., Hoboken, New Jersey, p.5. Available at: http://www.kelm.ftn.uns.ac.rs/literatura/pbmums/pdf/MedicalElectronicInstrumentation.pdf.

Pursiainen, S., Lucka, F. and Wolters, C. (2012). Corrigendum: Complete electrode model in EEG: relationship and differences to the point electrode model. *Physics in Medicine and Biology*, 58(1), pp.185-185.

Rahal, M., Khor, J.M., Demosthenous, A., Tizzard, A. and Bayford, R. (2009). A comparison of electrodes for neonate electrocal impedance tomography. *Physiol. Meas*, 30 (1), pp.73-84.

Rajaraman, S., Bragg, J.A., Ross, J.D. and Allen, M.G., Micromachined three-dimensional electrode arrays for transcutaneous nerve tracking. *Journal of Micromechanics and Microengineering*, 21 (2011), pp. 085014-085027.

Saadi, H. and Attari, M. (2013). Electrode-gel-skin interface characterization and modeling for surface biopotential recording: Impedance measurements and noise. *2013 2nd International Conference on Advances in Biomedical Engineering*.

Sawan, M. (2011). *Electrodes – Part I*. [ebook] Available at: http://www.groupes.polymtl.ca/gbm8320/Ch8_P1_Electrodes_web.pdf.

Bibliography

Serteyn, A., Vullings, R., Meftah, M. and Bergmans, J. (2015). Motion Artifacts in Capacitive ECG Measurements: Reducing the Combined Effect of DC Voltages and Capacitance Changes Using an Injection Signal. *IEEE Transactions on Biomedical Engineering*, 62(1), pp.264-273.

Simic-Krstic, J., Kalauzi, A., Ribar, S., Lazovic, G. and Radojicic, R. (2012). Electrical characteristics of female and male human skin. *Archives of Biological Sciences*, 64(3), pp.1165-1171.

Taji, B., Shirmohammadi School of Electrical Engineering and Computer Science, University of Ottawa, Ottawa, ON, Canada, S., Groza, V. and Batkin, I. (2018). *Impact of Skin–Electrode Interface on Electrocardiogram Measurements Using Conductive Textile Electrodes - IEEE Journals & Magazine*. [Online] Ieeexplore.ieee.org. Available at: https://ieeexplore.ieee.org/document/6670113 [Accessed 19 Nov. 2013].

Tavernier, A., Dierickx, M. and Hinsenkamp, M. (1992). Conductivity and dielectric permittivity of dermis and epidermis in nutrient liquid saturation. In: *14th Annual International Conference of the IEEE Engineering in Medicine and Biology Society.* Paris. pp. 274-275.

Teklemariam, A., Hodson-Tole, E., Reeves, N., Costen, N. and Cooper, G. (2016). A Finite Element Model Approach to Determine the Influence of Electrode Design and Muscle Architecture on Myoelectric Signal Properties. *PLOS ONE*, 11(2), p.e0148275.

Todorow, V. (2018). *Impedance Matching and Matching Networks. Valentin Todorow, December, PDF*. [online] Docplayer.net. Available at: https://docplayer.net/19018041-Impedance-matching-and-matching-networks-valentin-todorow-december-2009.html [Accessed 17 Oct. 2018].

Webster, J. (1984). Reducing Motion Artifacts and Interference in Biopotential Recording, *IEEE Journals & Magazine*. [Online] Ieeexplore.ieee.org. Available at: https://ieeexplore.ieee.org/document/4121779.

Webster, J. (2006). *Encyclopedia of medical devices and instrumentation*. 2nd ed. New York: Wiley.

Yang, C.M., Kao, T., Yang, T.L. and Wu, C.C. (2012). Performance assessment of active electrode applied in wearable physiological monitoring system. *Proceedings of 2012 IEEE-EMBS International Conference on Biomedical and Health Informatics*.

Yang, K., Freeman, C., Torah, R., Beeby, S. and Tudor, J. (2014). Screen printed fabric electrode array for wearable functional electrical stimulation. *Sensors and Actuators A: Physical*, 213, pp.108-115.

Yong, S., Owen, J., Tudor, M. and Beeby, S. (2016). Integrated Flexible Solid-State Supercapacitor Fabricated In A Single Fabric Layer. *Journal of Physics: Conference Series*, 773, pp.012086-012090.